Phenomenology of Little Higgs Models and Quantum Leptogenesis

---

Dissertation

zur

Erlangung der naturwissenschaftlichen Doktorwürde
(Dr. sc. nat.)

vorgelegt der

Mathematisch-naturwissenschaftlichen Fakultät

der

Universität Zürich

von

Pedro Schwaller

aus

Deutschland

Promotionskomitee:

Prof. Dr. Daniel Wyler (Vorsitz und Leitung)
Prof. Dr. Thomas Gehrmann
Prof. Dr. Babis Anastasiou
Prof. Dr. Ben Moore

Zürich, 2010

Zusammenfassung

In den letzten Jahren wurden zahlreiche Neue Physik Modelle vorgeschlagen, um Beobachtungen zu erklären, die nicht mit dem Standardmodell der Teilchenphysik in Einklang zu bringen sind, oder um dessen theoretische Probleme zu lösen.

Der erste Teil dieser Arbeit widmet sich einer Klasse von Erweiterungen des Standardmodells, die als "little Higgs" Modelle bekannt sind. Diese Modelle lösen das Hierarchieproblem des Standardmodells indem sie zusätzliche globale Symmetrien einführen. Eine Paritäts-Symmetrie liefert zudem ein stabiles massives Teilchen, welches ein möglicher Kandidat für dunkle Materie ist. In den meisten little Higgs Modellen wird diese Parität jedoch durch topologische Anomalien gebrochen.

In dieser Arbeit werden zunächst die Wechselwirkungen untersucht, welche durch die paritätsverletzenden Operatoren induziert werden. Einschränkungen an die Parameter des Modells werden unter diesen Aspekten neu bewertet, und neue Signale für den Large Hadron Collider (LHC) werden vorhergesagt. Dannach wird ein neues little Higgs Modell mit ungebrochener Dunkle Materie Parität vorgestellt. Die Paritäts-Symmetrie wird als Austauschsymmetrie zwischen verschiedenen Sektoren des Modells implementiert. Dies garantiert dass keine paritätsverletzenden Operatoren durch topologische Anomalien erzeugt werden können. Das Teilchenspektrum des Modells wird bestimmt und Einschränkungen von Präzisionsobservablen werden berechnet. Desweiteren wird ein Überblick über die möglichen Signale an Hadron Beschleunigern gegeben. Ein hervorzuhebendes Merkmal des neuen Modells ist die Existenz eines leichten Skalarfeldes, welches Signale mit mehreren Photonen im Endzustand am LHC vorhersagt. Dieses Signal wird im Detail untersucht. Die Hintergründe für das Signal durch Standardmodell Prozesse werden analysiert. Am LHC kann das Signal über einen grossen Bereich des erlaubten Parameterraums hinweg beobachtet und die Masse der neuen Teilchen mit hoher Präzision bestimmt werden.

Der zweite Teil der Arbeit behandelt die Leptogenese. In diesem Szenario wird die beobachtete Baryonasymmetrie im Universum über eine Leptonasymmetrie erzeugt. Leptogenese geschieht im frühen Universum durch Zerfälle von schweren rechtshändigen Neutrinos. Die theoretische Beschreibung erfolgt im Rahmen der Nichtgleichgewichts-Quantenfeldtheorie (NEQFT), welche insbesondere die Wechselwirkungen der Felder mit dem heissen thermischen Plasma ein-

schliesst. Die Schwierigkeit besteht darin ein geeignetes Näherungsschema zu finden, welches das Herleiten analytischer Resultate erlaubt.

In dieser Arbeit werden die kinetischen Gleichungen, welche die Zeitentwicklung der Neutrinodichten und der Leptonasymmetrie beschreiben, mit Hilfe einer Gradientenentwicklung hergeleitet. Insbesondere wird aufgezeigt dass dieser Zugang frei von Doppelzählproblemen ist, und die Korrekturen zur erzeugten Asymmetrie durch Wechselwirkungen mit dem Plasma werden berechnet. Eine numerische Analyse zeigt dass diese Korrekturen in Szenarien mit schwacher Auswaschung erheblich sein können. Im einem nächsten Schritt werden die Effekte von Wechselwirkungen hinzugefügt, welche die verschiedenen Lepton "flavors" unterscheiden. Die Bewegungsgleichungen für die flavorabhängigen Asymmetrien werden hergeleitet. Es wird gezeigt dass flavor-unabhängige Wechselwirkungen die flavor-Oszillationen über-dämpfen und dass die Dekohärenz im flavor-Raum hauptsächlich durch flavor-sensitive Streuprozesse induziert wird. Numerisch wird gezeigt dass die gefundenen Bewegungsgleichungen erfolgreich den Parameterbereich beschreiben, in dem weder eine flavor-unabhaengige noch eine voll geflavorte Behandlung zulässig ist.

Abstract

Several new physics models have been proposed in recent years to explain observations that disagree with predictions of the standard model of particle physics, or to cure some of its theoretical problems.

In the first part of this thesis a class of extensions of the standard model known as little Higgs models are discussed. Little Higgs models solve the standard model hierarchy problem by introducing additional global symmetries and provide a stable candidate for dark matter through a parity symmetry. In most little Higgs models this parity symmetry is violated by topological anomalies.

In this work the interactions that are induced by the parity breaking operators are studied in detail. Existing constraints on the parameter space of little Higgs models are reevaluated under these aspects, and new signals at the Large Hadron Collider (LHC) are predicted. Next, a new little Higgs model with unbroken dark matter parity is presented. The parity symmetry is implemented as an exchange symmetry between two different sectors, such that parity breaking operators can not be generated through topological anomalies. The particle spectrum and electroweak precision constraints on this model are studied, and an overview over the phenomenology at hadron colliders is given. A peculiar new feature are light scalar fields that predict multi photon signals at the LHC. These new signals and their standard model backgrounds are studied in detail. The signal is found to be in reach of the LHC over a large range of parameters, and the particle masses can be determined with high accuracy.

The second part of this thesis is on Leptogenesis, a scenario where the baryon asymmetry of the universe is produced through a lepton asymmetry. Leptogenesis takes place in the early universe through out of equilibrium decays of heavy righthanded neutrinos. The proper theoretical formulation of this is in terms of nonequilibrium quantum field theory that encompasses the interactions of the fields with the hot thermal plasma they propagate in. The difficulty here is to find a suitable approximation scheme that allows one to derive analytic results.

In this work the kinetic equations, that describe the time evolution of the neutrino densities and of the lepton asymmetry, are derived using a gradient expansion. It is emphasized how this approach is free of the double counting problem, and the corrections to the generated lepton asymmetry due to plasma interactions are given. A numerical analysis shows that the corrections can be

large in scenarios with weak washout. In a next step, the effects of lepton flavor interactions are included. The quantum kinetic equations for the flavoured lepton asymmetries are derived. It is shown that flavor blind interactions overdamp flavor oscillations and that flavor decoherence is mostly induced by flavor sensitive scatterings. It is demonstrated numerically that the kinetic equations properly describe the intermediate regime where neither an unflavoured nor a fully flavoured treatment is justified.

Acknowledgements

The work presented in this thesis was carried out over a period of three years at the University of Zurich. This would not have been possible without the continuous support and help of a large number of people, and I want to take this opportunity to express my gratitude to them.

First of all, I want to thank my advisor Daniel Wyler for offering me this opportunity, for freedom in the choice of research topics, for continuous support, encouragement an endless amount of confidence in me. Thank you.

I want to thank Ayres Freitas for collaborating with me all these years, for answering all my questions and helping me to transform ideas into results. Further I want to thank Martin Beneke for inviting me to work on Leptogenesis with the group at the RWTH Aachen University. A big thank you also goes to Thomas Gehrmann for numerous insights into particle physics and for ongoing support.

I want to thank all my collaborators. Thomas and Nico, for an interesting and funny adventure into the physics of cosmic ray showers. Martin Beneke, Bjoern Garbrecht, Matti Herranen and Christian Fidler for successful collaboration on the Leptogenesis projects. Daniel, Ayres, Marc and Andreas for all that little Higgs stuff.

My officemates, Hana, Nico and Rikkert, for three pleasant years and for numerous discussions of physics and non-physics topics. The Doppelkopf crew, in particular Daniel M., Beat and Cedric for making it happen almost every week. Uli Haisch, for introducing me to the joys of self-made Latte Macchiato.

Thanks go to all the past and present members of the ITP in Zurich for a great working atmosphere and for all the parties, excursions and cheese fondues. Another big hug to all of you who joined us on our trips to Abart and other nightly excursions. Katja and I will miss you! Thanks also to the group at ETH for the joint seminars and for organizing a journal club, to Zoltan for introducing me to the exciting field of beyond standard model physics and to Babis for encouragement and helpful advice. Thanks to the groups in Aachen and Pittsburgh for creating a congenial atmosphere during my visits.

I want to thank my family for supporting me for all those years and for always believing in me.

Finally I can't even say how much I want to thank Katja for supporting me, for sharing my weird life as a theoretical physicist and for just being there.

Contents

1 Introduction **1**

1.1 The Standard Model of Particle Physics 3

1.1.1 Particles and their Interactions 3

1.1.2 The Higgs Mechanism 6

1.2 Motivations to go Beyond the Standard Model 7

1.2.1 Hierarchy Problem 7

1.2.2 Neutrino Masses 8

1.2.3 Matter-Antimatter Asymmetry 9

1.2.4 Dark Matter and Dark Energy 9

1.3 Beyond the Standard Model 10

1.3.1 Little Higgs: Dark Matter from a Solution to the Hierarchy Problem 10

1.3.2 Leptogenesis: The Baryon Asymmetry from a Model of Neutrino Masses 12

I Little Higgs Models **15**

2 T-Parity Breaking in the Littlest Higgs Model **17**

2.1 Introduction 17

2.2 The LHT Model 18

2.3 The WZW term in the LHT Model 21

2.3.1 The Wess Zumino Witten term 21

2.3.2 Gauge invariance 22

2.3.3 Divergences and counterterms 24

2.4 Phenomenology of T-parity breaking effects 27

2.4.1 Decays of A_H 27

2.4.2 Bounds from electroweak precision tests and direct detection at LEP 29

2.4.3 Bounds from Tevatron 29

2.4.4 LHC phenomenology 33

2.4.5 The Case of a fermionic LTOP 38

2.5 Conclusion 39

2.6 Appendix: T-odd gauge invariant counterterms 40
2.7 Appendix: Feynman rules for the LHT with WZW term 41

3 A Little Higgs Model with Exact Dark Matter Parity 49
3.1 Introduction 49
3.2 The model 50
3.2.1 Scalar and gauge sector 51
3.2.2 Fermion sector 53
3.3 Mass spectrum 56
3.3.1 Top quark sector 56
3.3.2 Scalar masses 58
3.3.3 Electroweak symmetry breaking 60
3.4 Phenomenology 62
3.4.1 Electroweak precision constraints 63
3.4.2 Decays of heavy particles 67
3.4.3 Collider phenomenology 71
3.5 Summary 73

4 Multi-Photon Signals from Composite Models at LHC 75
4.1 Introduction 75
4.2 Pseudoscalar Triplets in Extensions of the Standard Model 76
4.3 Signals and Backgrounds 79
4.3.1 The signal 79
4.3.2 Real Backgrounds 80
4.3.3 Fake Backgrounds 81
4.3.4 LHC Sensitivity 82
4.4 Measuring Particle Properties 85
4.4.1 Mass Measurements 85
4.4.2 Spin and CP Properties 86
4.4.3 Extracting Model Information 87
4.5 Conclusions 87

II Leptogenesis 89

5 Finite Number Density Corrections to Leptogenesis 91
5.1 Introduction 91
5.2 CTP Approach to Leptogenesis 94
5.2.1 Propagators 94
5.2.2 One-loop self-energies 96
5.3 Tree-Level Contributions to the Kinetic Equations 97
5.3.1 Tree-level collision terms 98
5.3.2 Expansion of the Universe 99

5.3.3 Boltzmann equations . . . 101
5.4 Self-Energy Contribution to the CP Asymmetry . . . 103
5.4.1 Wave-Function Correction to $\mathcal{C}_\ell$ . . . 103
5.4.2 KMS and Real Intermediate State Subtraction . . . 104
5.4.3 CP Source . . . 106
5.5 Vertex Contribution to the CP Asymmetry . . . 108
5.5.1 Vertex Correction to $\mathcal{C}_\ell$ . . . 108
5.5.2 KMS and Real Intermediate State Subtraction . . . 109
5.5.3 CP Source . . . 111
5.5.4 Source term in the strongly hierarchical limit . . . 112
5.6 Numerical Estimates of Finite Density Effects . . . 113
5.6.1 Effective CP-violating parameter . . . 113
5.6.2 Numerical solution of the Boltzmann equations . . . 115
5.7 Conclusions . . . 118
5.8 Appendix: Calculation of the Self Energies . . . 119

6 Closed Time Path Approach to Flavor Effects in Leptogenesis 121
6.1 Introduction . . . 121
6.2 Flavoured Leptons . . . 123
6.2.1 Schwinger-Dyson Equations . . . 123
6.2.2 Thermal Self Energies . . . 126
6.2.3 Kinetic and Constraint Equations . . . 128
6.3 Kinetic Equations for Lepton Number Densities . . . 131
6.3.1 Matrices for Lepton Number Densities . . . 132
6.3.2 Source and Washout Term . . . 134
6.3.3 Flavour Blind Interactions . . . 135
6.3.4 Flavour Sensitive Interactions . . . 137
6.3.5 Suppression of Flavour Oscillations . . . 138
6.3.6 Kinetic Equations for Left and Right Handed Number Densities . . . 141
6.4 Solutions to the Flavoured Kinetic Equations . . . 142
6.5 Conclusions . . . 150
6.6 Appendix: Pole-Mass Equation and Finite Width Propagators . . . 152

A Nonequilibrium Quantum Field Theory 155
A.1 Fermions . . . 155
A.1.1 Definition of Greens functions . . . 155
A.1.2 Fermion Equations of Motion . . . 156
A.1.3 Spin decomposition . . . 158
A.1.4 (Free) Fermionic Equilibrium Solutions . . . 159
A.1.5 Close to Equilibrium Forms . . . 160
A.2 Boltzmann Equations in an Expanding Universe . . . 160
A.2.1 Physical Quantities in Conformal Coordinates . . . 160

A.2.2 Solving the flavored evolution equations 162

References **165**

Chapter 1

Introduction

Dass ich erkenne, was die Welt
Im Innersten zusammenhält.

J. W. von Goethe, Faust I, 1808

Much progress has been made in understanding the forces that hold the world together since the days of Goethe. The standard model of electroweak interactions [6], developed in the 1960s, has been successfully established as model of the electromagnetic and weak interactions. Experiments at CERN have observed neutral current interactions [7] and later discovered the W and Z bosons [8, 9] predicted by the model. Subsequent measurements performed at the LEP1 and LEP2 experiments at CERN have determined the parameters of the standard model to a high accuracy, leaving very little room for effects of physics that go beyond the standard model [10]. The standard model is the correct description of nature up to energies of a few 100 GeV.

Very recently, after many years of construction, the CERN Large Hadron Collider (LHC), one of the largest experiment ever built, has begun operating with the aim to find the Higgs boson [11], the last missing ingredient of the standard model, and to explore physics at the TeV scale.

Despite its success, there are several important observations that can not be explained within the standard model of particle physics. Among them are the amount of visible matter in the universe, the existence of dark matter and the masses of neutrinos. Also theoretically the standard model is not fully satisfactory, since the mass of the Higgs boson is not protected against large radiative corrections. This is the so called hierarchy problem.

The LHC for the first time opens the window to physics at the TeV scale and beyond, with collisions at center of mass energies of $7 - 14$ TeV. If new physics is hiding in the electroweak symmetry breaking sector, the LHC is almost bound to discover it. At the same time, numerous other experiments, ground based and in the sky, search for traces of dark matter, the unknown particles that are believed

to make up more than three quarters of the matter density in the universe. In addition, a large number of experiments are being conducted to determine the masses and mixing parameters of neutrinos. In the next few years, we might accomplish a major step in the understanding of nature.

This thesis deals with extensions of the standard model that aim to improve some of the theoretical obstacles and to explain the observations that are not understood within the standard model. In the rest of this chapter, I give a brief introduction to the standard model and its shortcomings and I introduce two extensions of the standard model that provide the basis for the work presented in this thesis.

The topic of part I is a class of extensions of the standard model known as little Higgs models. Chapter 2 discusses consequences of parity violation in little Higgs models, with an emphasis on phenomenology at hadron colliders like the LHC. In chapter 3 I present a little Higgs model with an exact internal parity symmetry that allows for a stable dark matter candidate. Precision constraints on the model and it's phenomenology are discussed. The model predicts new signatures at LHC with three or more photons in the final state. These signals that can also appear in other models of electroweak symmetry breaking are analyzed in chapter 4 with a detailed simulation of backgrounds and detector effects.

The second part of my thesis aims towards a rigorous analysis of the Leptogenesis mechanism using methods of nonequilibrium quantum field theory. In chapter 5 finite number density corrections are derived that arise from corrections to the particles propagating in the thermal plasma in the early universe. In chapter 6 the analysis is extended to a scenario with multiple active flavors. This leads to flavor oscillations and effects of time dependent mass eigenstates in the evolution equations. Appendix A gives a brief introduction to nonequilibrium techniques in quantum field theory and appendix A.2 provides additional details on the results obtained in chapters 5 and 6.

The work presented in chapters 2 and 3 is based on the publications [1, 2] written together with A. Freitas and D. Wyler. Chapter 5 is based on [3] written in collaboration with M. Beneke, B. Garbrecht and M. Herranen. The work presented in chapter 4 (in collaboration with A. Freitas) and chapter 6 (in collaboration with M. Beneke, C. Fidler, B. Garbrecht and M. Herranen) was published after completion of this thesis, as Refs. [4, 5].

force	**gauge bosons**	**coupling**	**phenomena**
electromagnetism	A_μ	e	electricity, atomic spectra
weak force	$W_\mu^\pm$, Z_μ	G_F	β-decay
strong force	G_μ^a	g_s	binding energy of atoms

Table 1.1: Known gauge bosons, couplings, and the forces they describe in nature. The boson that is assumed to mediate gravitational forces, the graviton, has not yet been discovered.

1.1 The Standard Model of Particle Physics

The structure of the standard model of particle physics is strongly guided by symmetry principles. The Lagrangian contains all terms that are consistent with Poincaré invariance and invariant under local gauge transformations of the standard model gauge group $G_{\text{SM}} = \text{SU}(3) \times \text{SU}(2) \times \text{U}(1)$. An immediate consequence is that all matter fields are arranged in irreducible representations of the gauge group and interactions are only allowed if the corresponding term can be written as a gauge singlet in the Lagrangian.

1.1.1 Particles and their Interactions

A SU(N) gauge theory contains $\text{N}^2 - 1$ vector fields V_μ^a, $a = 1, \ldots, \text{N}^2 - 1$, the gauge bosons, corresponding to the $\text{N}^2 - 1$ generators of the group. The gauge fields corresponding to the SU(3) gauge symmetry of the standard model are called gluons, G_μ^a. They mediate the strong force that is responsible for binding together protons and neutrons in nuclei. The remaining $\text{SU}(2) \times \text{U}(1)$ gauge symmetry describes the electromagnetic and weak interactions, giving rise to four gauge bosons. After electroweak symmetry breaking they decompose into the massless photon A_μ and three massive gauge bosons, $W_\mu^\pm$ and Z. The gauge bosons and the forces they mediate are summarized in table 1.1.

The gauge field Lagrangian is completely fixed by the gauge symmetry and given by

$$\mathcal{L}_{\text{SM,gauge}} = -\frac{1}{4}\left(G_{\mu\nu}^a G^{a,\mu,\nu} + W_{\mu\nu}^i W^{i,\mu,\nu} + B_{\mu\nu} B^{\mu\nu}\right) \tag{1.1}$$

where

$$V_{\mu\nu}^a = \partial_\mu V_\nu^a - \partial_\nu V_\mu^a - i g_V f^{abc} V_\mu^b V_\nu^c \tag{1.2}$$

is the field strength tensor for the gauge field V_μ^a and g_V the corresponding gauge coupling. The f^{abc} are the structure constants of the corresponding gauge group.

type	**field**	SU(3)	SU(2)	U(1)
quarks	q_L^i	3	2	+1/6
	u_R^i	3	1	+2/3
	d_R^i	3	1	-1/3
leptons	ℓ_L^i	1	2	+1/2
	e_R^i	1	1	1

Table 1.2: Matter fields in the standard model and their quantum numbers. The numbers denote the dimension of the representation for the nonabelian groups and the charge Y under the abelian U(1). The index $i = 1, 2, 3$ denotes is the family index.

The fields W_μ^i and B_μ correspond to the SU(2) and U(1) gauge groups, with couplings $g_W = g$ and $g_B = g'$. Their relations to the physical fields listed in table 1.1 will be explained in the next section.

As mentioned above, the matter fields are classified into irreducible representations of $G_{\rm SM}$. All known matter fields are fermions. Matter fields that feel the strong force are called quarks, while matter fields that only have electroweak interactions are known as leptons. The known particles and their quantum numbers under the standard model gauge group are listed in table 1.2.

A few comments are in order. First, note that the left and right handed components of the matter fields transform in different representations of SU(2). The left handed fields $q_L = (d_L, u_L)$ and $\ell_L = (\nu_L, e_L)$ are doublets, while the right handed fields transform as singlets. This property that left and right handed fields transform separately is usually referred to as chiral symmetry.

The electric charge Q of a field is obtained from $Q = T_3 + Y$, where T_3 is denotes the diagonal generator of $SU(2)$. In this way we obtain the conventional charges for quarks and leptons. Finally note that there are no right handed neutrinos in the standard model, a fact that will become important in the discussion of neutrino masses.

The kinetic terms for the matter fields have the form

$$\mathcal{L}_{\rm SM,fermion} = \bar{\psi}_A \gamma^\mu D_\mu \psi_A \,, \tag{1.3}$$

where ψ_A denotes any of the fields in table 1.2 and $\bar{\psi} = \psi^\dagger \gamma^0$. The form of the covariant derivative $D_\mu \psi_A$ is dictated by gauge invariance and depends on the representations of the fields under $G_{\rm SM}$. As an example, for the left handed quark

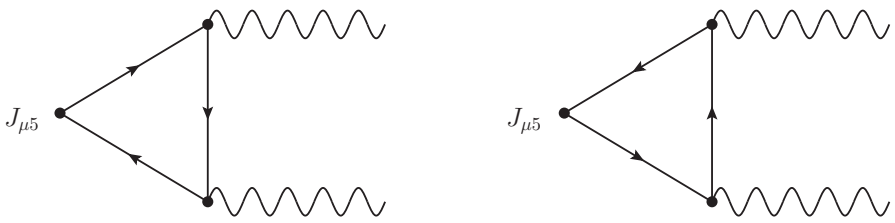

Figure 1.1: Coupling of an axial current to two vector bosons through a closed fermion loop.

fields, we have

$$D_\mu q_L = \left(\partial_\mu - ig_s G^a_\mu \lambda^a - igW^i_\mu \sigma^i - igYB_\mu\right) q_L \tag{1.4}$$

where λ^a and σ^i denote the generators of SU(3) and SU(2) in the fundamental representation. There terms describe the interactions between the matter fields and the gauge fields in the standard model. Note that no other interactions between the fermion fields can be written down with dimension four or less without violating some of the gauge symmetries. In particular no explicit Dirac mass term can be written for the fermions because it would mix left and right handed fields and thus violate $\mathrm{SU}(2) \times \mathrm{U}(1)$ invariance. The same applies to the gauge fields where an explicit mass term $m_V^2 V_\mu V^\mu$ is not gauge invariant.[1] The generation of gauge boson as well as fermion masses through the Higgs mechanism will be discussed in the next section.

The matter fields in the standard model come in three families, each one consisting of an up and a down type quark and a corresponding charged and neutral lepton. In table 1.2 this is denoted by the family index i. While there is no compelling explanation for the number of families observed, there is a deeper meaning behind the fact that all families are complete. The reason is that gauge theories need to maintain gauge invariance not only at the Lagrangian level but also when going to higher order corrections in perturbation theory.

The potential problem arises already at the one loop level, through graphs where an axial current couples to two gauge bosons through a closed fermion loop, as depicted in figure 1.1. In a chiral theory the sum of these two graphs can be linearly divergent. This implies that

$$\partial^\mu J_{\mu 5} \neq 0\,, \tag{1.5}$$

i.e. that the axial current is not conserved and the corresponding Ward identity is not satisfied. Since Ward identities are essential in proving renormalizability of gauge theories, this would spoil the consistency of the theory. Luckily this does

[1] Note that for U(1) gauge fields it is possible to write a gauge invariant mass term by introducing a Stueckelberg field [12] to compensate for the gauge variation of the mass term.

not happen in the standard model. Explicit calculation of the above diagrams shows that the divergent piece of these diagrams are proportional to

$$-Q_e^2 + Q_{\nu_e}^2 + 3(Q_u^2 - Q_d^2) = 0\,, \tag{1.6}$$

where the sum is over the electric charges of all left handed matter fields in the SM, in one generation. This cancellation would not happen if incomplete families were present in the theory. In this sense, the discovery of the top quark [13] was a nontrivial consistency check for the standard model.

Note that anomalies can also appear in global symmetry currents. This does not pose a conceptual problem, it just shows that a given symmetry is not a symmetry of the full theory at the quantum level.

1.1.2 The Higgs Mechanism

Consider a complex scalar field, the Higgs doublet $H = (h^+, h^0)^T$, with $Y = 1/2$ and with Lagrangian [14]

$$\mathcal{L}_{\rm SM,H} = E_{\rm kin} - V = D_\mu H^\dagger D^\mu H - \mu^2 H^\dagger H - \frac{\lambda}{4}(H^\dagger H)^2\,. \tag{1.7}$$

When the parameter μ^2 is positive this describes a scalar particle with mass μ and the ground state of the theory is at $H = 0$. On the other hand, if $\mu^2 < 0$ the minimum of the potential V is not at $H = 0$ but at

$$\langle H^\dagger H\rangle = -\frac{2\mu^2}{\lambda} \equiv \frac{v^2}{2}\,. \tag{1.8}$$

The gauge symmetry allows us to rotate the field such that the minimum occurs at $H = (0, v)^T/\sqrt{2}$, with v real. Note that the vacuum state is no longer gauge invariant. The gauge symmetry was broken spontaneously.

We can now expand the Higgs field around the vacuum state. In unitary gauge, where unphysical degrees of freedom are absent, this amounts to setting $H = (0, v + h)^T/\sqrt{2}$. Inserting this into the Lagrangian (1.7) we obtain

$$\mathcal{L}_{\rm SM,H} = \frac{1}{2}(\partial_\mu h)^2 + \frac{g^2 v^2}{4}\left[(W_\mu^1)^2 + (W_\mu^2)^2\right] + \frac{v^2}{4}\left(gW_\mu^3 - g'B_\mu\right)^2 + \ldots \tag{1.9}$$

where the dots represent cubic and quartic terms. We can now define the physical Z-boson and photon fields as

$$Z_\mu = \frac{gW_\mu^3 - g'B_\mu}{\sqrt{g^2 + g'^2}} \equiv \cos\theta_w W_\mu^3 - \sin\theta_w B_\mu\,, \tag{1.10}$$

$$A_\mu = \sin\theta_w W_\mu^3 + \cos\theta_w B_\mu\,, \tag{1.11}$$

defining the Weinberg angle θ_w. It follows immediately that the photon remains massless, while the W and Z-bosons pick up masses

$$M_W^2 = \frac{g^2 v^2}{2}, \qquad M_Z^2 = \frac{g^2 v^2}{2\cos^2\theta_w} = \frac{M_W^2}{\cos^2\theta_w}\,. \tag{1.12}$$

Working out the coupling of the photon field A_μ to the electron using (1.3) we note that we can identify

$$e = g\sin\theta_w\,. \tag{1.13}$$

It is also possible to express the Fermi coupling G_F in terms of fundamental parameters:

$$G_F = \frac{\sqrt{2}g^2}{8M_W^2}\,. \tag{1.14}$$

In the fermion sector one can now write down renormalizable gauge invariant (Yukawa) couplings of the Higgs field to the fermions. In particular, for the quarks, one can write

$$\mathcal{L}_{\mathrm{SM,Y}} = \bar{q}_L^i Y_{ij}^u u_R^j H + \bar{q}_L^i Y_{ij}^d d_R^j \tilde{H} \tag{1.15}$$

where Y^u, Y^d are the Yukawa coupling matrices and $\tilde{H} = \sigma_2 H^*$. Upon electroweak symmetry breaking, these couplings give masses to the up and down type quarks. A similar term can be written down to give masses to the charged leptons, while the neutrinos remain massless in the standard model.

The neutral scalar h, the elusive Higgs field, obtains a mass that depends on the unknown parameter μ^2. Despite ongoing searches at the Tevatron and at the LHC, it has so far evaded detection. Revealing the true nature of the physics that underlies electroweak symmetry breaking is one of the biggest goals of 21st century particle physics.

1.2 Motivations to go Beyond the Standard Model

Most reasons to extend the standard model are in some way connected to the Higgs sector. Here I will present some of the experimental observations and theoretical obstacles that require extensions of the standard model.

1.2.1 Hierarchy Problem

The Higgs mass, like any other physical quantity, receives radiative corrections from loop diagrams. As an example, we can consider the insertion of a top quark loop into the Higgs propagator, depicted in figure 1.2. The diagram is

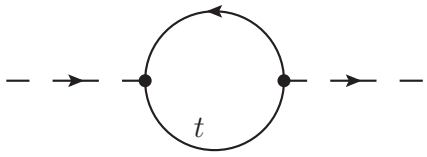

Figure 1.2: One-loop contribution of the top quark to the Higgs mass.

quadratically divergent. Regularizing the divergence with a cutoff Λ yields a contribution to the Higgs mass of

$$\delta m_H^2 = -\frac{3}{8\pi^2}\lambda_t^2\Lambda^2\,, \tag{1.16}$$

where λ_t is the top quark Yukawa coupling. Similar contributions come from gauge loops and Higgs loops, and to a lesser extent also from the lighter fermions in the standard model. The cutoff scale Λ represents any scale where new physics enters the model, for example in the context of grand unified theories ($\Lambda \sim 10^{15}$ GeV) or theories of quantum gravity ($\Lambda \sim 10^{19}$ GeV).

To obtain a light Higgs, as required by unitarity and indirect experimental constraints, one would need to tune the bare mass parameter m_H to an extremely high degree of accuracy, making the theory appear unnatural. This is the hierarchy problem.

The most commonly adopted solution is to assume that new particles are present in the theory that cut off the contribution to the Higgs mass at a sufficiently low scale. Equation (1.16) implies that these new particles must be lighter than a few TeV, in reach of the LHC. The possible discovery of these new particles motivate building models that implement this ideas and studies their collider signatures. A class of such models called *little Higgs models* will be introduced in section 1.3.1.

1.2.2 Neutrino Masses

Observation of neutrino oscillations in solar and atmospheric neutrinos provide clear evidence that at least two of the three known neutrinos are massive.[2] The most stringent upper bound on masses comes from Cosmology [15], constraining the sum of the three neutrino masses to be less than 0.5 eV. The mass splittings measured in the oscillation experiments on the other hand implies that at least one neutrino has a mass above 10^{-3} eV.

In the standard model neutrinos are exactly massless due to the absence of a righthanded component ν_R. One could in principle add a righthanded partner for each neutrino and introduce a mass term similar to the mass term for down type quarks. The problem however is that the mass scale for neutrinos is at least a

[2]Evidence for neutrino masses is reviewed in [15].

million times smaller than that of the lightest massive standard model field, the electron. There is no reason why the Yukawa couplings of the neutrinos should be so many orders of magnitude smaller than those of any other fields.

An extension of the standard model that leads to small neutrino masses in a natural way, the see-saw mechanism, will be presented in section 1.3.2.

1.2.3 Matter-Antimatter Asymmetry

The thermal history of the early universe is well described by the standard model of big bang cosmology, ΛCDM. In a CP symmetric universe, after the big bang an equal amount of matter and antimatter would be generated from radiation and later annihilate as the universe cools down, leaving an almost empty universe with tiny but equal amounts of matter and antimatter. This contradicts observations in two ways: the universe is not empty and we do not observe large amounts of antimatter. The currently best measurement of the entropy normalized matter-antimatter or Baryon asymmetry is [92]

$$Y_{\Delta B} = \frac{n_B - n_{\bar{B}}}{s} = (8.75 \pm 0.23) \times 10^{-11} \,. \tag{1.17}$$

In 1967 Sakharov [16] identified three necessary conditions to generate a Baryon asymmetry in the early universe:

- CP (or time reversal) violation,
- Baryon number violation,
- Departure from thermal equilibrium.

In the standard model, two of the three conditions are fulfilled. CP is violated in the quark sector through a complex phase in the CKM matrix. Furthermore Baryon number B is violated by electroweak sphaleron processes that can be fast in the early universe. However departure from equilibrium does not happen during the electroweak phase transition: the lower bound on the Higgs mass of $m_H > 114$ GeV implies that the phase transition is only second order and thus no significant departure from thermal equilibrium does appear.

An explanation of the observed Baryon asymmetry clearly requires an extension of the standard model, either to modify the electroweak phase transition or to provide a different source for departure from equilibrium. One such possibility arises in the context of the see-saw mechanism.

1.2.4 Dark Matter and Dark Energy

To obtain correct predictions for galaxy rotation curves, the cosmic microwave background and to understand the accelerated expansion of the universe, the

ΛCDM cosmological model assumes that about 75% of the energy density in the universe is in the form of dark energy, additional 20% consist of some unknown particles called dark matter, while only about 5% of the energy density is due to ordinary, visible matter, i.e. atoms and molekules.

Neither dark energy nor dark matter can be understood within the standard model of particle physics. While the solution to the dark energy problem is possibly related to a theory of quantum gravity and thus well out of reach of current experiments, there is some evidence that dark matter is connected to the electroweak scale.

The reason for this is the so called *WIMP miracle*. Assume that there is a neutral stable particle χ with a mass m_χ that is in thermal equilibrium in the early universe ($T > m_\chi$) due to processes $\chi\chi \leftrightarrow \psi\psi$ with cross section σ, where ψ is any standard model particle. At some temperature T_F the annihilation rate drops below the expansion rate of the universe and the (entropy normalized) density of χ, Ω_χ, becomes constant. This process is known as freeze-out. An order of magnitude estimate for the resulting Ω_χ yields [17]:

$$\Omega h^2 \approx \frac{3 \times 10^{-27} cm^3 s^{-1}}{\langle v\sigma \rangle} = \frac{2.5 \times 10^{-10} \text{ GeV}^2}{\langle v\sigma \rangle} \approx \frac{0.1 \text{ pb}}{\langle v\sigma \rangle} \tag{1.18}$$

where h is the Hubble rate. The interaction rate in the numerator is that of a particle with a mass of the order of the electroweak scale interacting with the strength of the weak interactions. While this could be a coincidence, it motivates the possibility that dark matter is connected to the mechanism of electroweak symmetry breaking. Indeed it has been shown that many extensions of the standard model that aim to solve the hierarchy problem also provide a viable dark matter candidate.

1.3 Beyond the Standard Model

In this section I provide a basic introduction to two extensions of the standard model on which the research presented in this thesis is based.

1.3.1 Little Higgs: Dark Matter from a Solution to the Hierarchy Problem

Little Higgs models attempt to solve the hierarchy problem by implementing the Higgs boson as a Goldstone boson of a spontaneously broken global symmetry. According to Goldstones theorem, when a global symmetry group G is broken spontaneously to a subgroup H one obtains one massless Goldstone boson for each broken symmetry generator. The broken symmetry generators act non linearly on the Goldstone bosons, in particular under an infinitesimal transformation $e^{i\epsilon}$ the fields shift as $\phi \to \phi + \epsilon$. It follows that a Lagrangian that respects the global

symmetries can only contain derivative terms. In particular a mass term is not allowed.

If the global symmetry G is weakly broken, for example by gauge interactions, the fields become pseudo Goldstone bosons. The fields corresponding to the explicitly broken symmetry generators will acquire a mass term through radiative corrections that is controlled by the small symmetry breaking parameter, e.g. the gauge coupling g, and therefore protected from large corrections.

Models with pseudo Goldstone Higgs bosons are effective theories characterized by one scale, the global symmetry breaking scale f. At a scale $\Lambda = 4\pi f$ the models become non-perturbative and require a ultraviolet (UV) completion. The problem with the simplest possible construction now arises when one tries to decouple the unknown UV physics by increasing Λ to the 10 TeV scale or above, i.e. $f \geq 1$ TeV, to avoid conflicts with electroweak precision observables. The masses generated by one loop radiative corrections are proportional to

$$\Delta m^2 \sim \frac{g^2}{16\pi^2}\Lambda^2 = g^2 f^2 \,, \tag{1.19}$$

again requiring a large amount of fine tuning to obtain a light Higgs. A solution to this problem was developed in [18] and goes by the name of *collective symmetry breaking*. The idea behind collective symmetry breaking is to use more than one global symmetry to protect the Higgs mass from radiative corrections. To achieve this one enlarges the global symmetry group G such that it contains two subgroups, G_1 and G_2, that act nonlinearly on the Higgs, i.e. each group separately forbids a mass term for the Higgs. An interaction that leaves any of the G_i unbroken can not alone generate a contribution to the Higgs mass.

The electroweak gauge interactions are implemented by gauging two copies of $G_{\rm ew} = {\rm SU}(2) \times {\rm U}(1)$ such that $G_{\rm ew,1}$ respects G_1 and $G_{\rm ew,2}$ respects the G_2 subgroup of G. Any diagram that gives a contribution to the Higgs mass must then involve contributions from both $G_{\rm ew,1}$ and $G_{\rm ew,2}$. Diagrams of this type that are quadratic divergent can only appear at the two loop level and are thus suppressed by an additional loop factor:

$$\Delta m^2_{\rm collective} \sim \frac{g^2}{(16\pi^2)}\Lambda^2 = g^2\frac{f^2}{16\pi^2} \,. \tag{1.20}$$

With this setup, the scale f can be of order of the electroweak scale without causing an unnaturally large contribution to the Higgs mass.

The extended gauge group $G_{\rm ew,1} \times G_{\rm ew,2}$ is typically broken to the standard model gauge group at the scale f, so this mechanism predicts new heavy gauge bosons at that scale. When evaluated in the mass basis, the one loop corrections to the Higgs mass from standard model gauge boson loops are cancelled by diagrams involving the new heavy gauge bosons.

A similar procedure must be used to control the contribution from top quark loops and from Higgs loops, which can be achieved by adding a partner for the

top quark and additional scalar fields to the model. Since we are only interested in raising the cutoff to $\Lambda \geq 10$ TeV, contributions to the Higgs mass from the light quarks and leptons can typically be neglected. Models that implement this mechanism go by the name of little Higgs models [19].

In [30] a parity symmetry was implemented in little Higgs models. This *T-parity* essentially exchanges $G_{\text{ew},1} \leftrightarrow G_{\text{ew},2}$ and ensures that all new particles that are introduced at the TeV scale are parity odd and can not be exchanged between standard model fields at the tree level. This not only improves the agreement of little Higgs models with electroweak precision data, but also provides a dark matter candidate since the lightest T-odd particle can be stable.

In section 2 of chapter 2 I introduce the Littlest Higgs model with T-parity [27,30] and then discuss the phenomenological consequences of T-parity breaking by nonperturbative effects. In chapter 3 I present a little Higgs model that implements a new parity symmetry, X-parity, that is not broken by nonperturbative effects and provides a robust dark matter candidate.

1.3.2 Leptogenesis: The Baryon Asymmetry from a Model of Neutrino Masses

The (indirect) observation of neutrino masses clearly indicates that right handed neutrinos need to be added to the standard model. Right handed neutrinos are different from other standard model fields in that they are singlets under all interactions and therefore are their own anti-particles:

$$N_R^c = C\bar{N}_R^T = N_R\,, \tag{1.21}$$

where $C$is the charge conjugation matrix. It is then possible to write down a Majorana mass term for N_R. To illustrate the effect consider a toy model with a single flavor and one righthanded neutrino, with Lagrangian

$$\mathcal{L} = \frac{1}{2}\bar{N}_R(\mathrm{i}\partial\!\!\!/ - M)N_R + \bar{\ell}_L \mathrm{i}\partial\!\!\!/\ell_L + \bar{e}_R \ell \mathrm{i}\partial\!\!\!/ e_R - Y\bar{\ell}_L H^\dagger N_R - Y\bar{N}_R H\ell_L\,, \tag{1.22}$$

where ℓ_L is the lefthanded lepton doublet and Y is the neutrino Yukawa coupling. After electroweak symmetry breaking this leads to a mass matrix for the neutrinos of the form

$$\begin{pmatrix} 0 & -m \\ m & M \end{pmatrix} \tag{1.23}$$

where $m = Y\langle H\rangle = Yv/\sqrt{2}$. For $M \gg m$ this matrix has one large and one small Eigenvalue,

$$M_N = M + \mathcal{O}\left(\frac{m^2}{M}\right) \qquad m_\nu \approx \frac{m^2}{2M} = Y^2 v\frac{v}{2M}\,. \tag{1.24}$$

This is the see-saw mechanism [20]. The masses of the light neutrinos are suppressed by a factor of (v/M). With Y of order one, small enough neutrino masses are obtained with $M \sim 10^{10}$ GeV $- 10^{15}$ GeV. Such large Majorana masses appear naturally in the context of SO(10) grand unified theories [21].

To extend this mechanism to a realistic model of neutrino masses one needs to include at least two righthanded neutrinos $N_{1,2}$. The Yukawa couplings then become matrices in flavor space and can will in general include CP violating phases. In particular, CP violation can apprear in the decay of the righthanded neutrinos into lepton and Higgs boson, $N_i \to \ell H, \bar{\ell} H^\dagger$, thus satisfying the first of Sakharov's conditions for successful Baryogenesis.

Departure from thermal equilibrium appears when the universe cools down below the temperature $T \sim M_1$, where M_1 denotes the mass of the lightest righthanded neutrino. The interactions mediated by the Yukawa coupling Y are in general too slow to keep the N_1 in thermal equilibrium so that an asymmetry can actually be generated without being washed out immediately.

The last condition, baryon number violation, is a bit more tricky. The Majorana mass term in (1.22) violates lepton number L, so it is possible to generate a lepton asymmetry. As mentioned in section 1.2.3, baryon number is violated in the standard model by sphaleron processes, and the same is true for lepton number. Only the combined $B - L$ number is a conserved quantity in the standard model. Since the Majorana mass term violates both L and $B - L$, out of equilibrium decays of N_1 will generate a net $B - L$ charge by generating a nonzero L. This lepton number asymmetry is then partially converted into a baryon number asymmetry through the sphaleron processes.

In the simplest scenario where only the righthanded Majorana neutrinos N_i are added to the standard model, the relation between the generated lepton asymmetry Y_ℓ and the resulting baryon asymmetry is given by

$$Y_B \approx \frac{1}{3} Y_\ell \,. \tag{1.25}$$

Leptogenesis takes place in the early universe in a relativistic thermal plasma consisting of gauge bosons and matter fields. Conventional approaches neglect this complications and use a set of semi classical Boltzmann equations to describe the evolution of the number density n_{N_1} and of the lepton asymmetry Y_ℓ. While this approach leads to correct qualitative results in most cases, a systematic treatment is desireable to obtain reliable quantitative predictions. This was the motivation for the research presented in part II of this thesis.

Part I

Little Higgs Models

Chapter 2

Consequences of T-Parity Breaking in the Littlest Higgs Model

2.1 Introduction

Little Higgs models provide a mechanism to explain a hierarchy between the electroweak scale and a larger, fundamental scale where symmetry breaking occurs through strong dynamics. In this scheme, the Higgs scalar doublet is a composite particle of the strong dynamics, a pseudo-Goldstone boson stemming from the spontaneously broken symmetry at a scale f. The Goldstone mechanism protects the Higgs boson from acquiring a large mass term, with one-loop quadratic corrections being cancelled by new gauge bosons and partners of the top quark.

A simple implementation of the Little Higgs concept with a single global symmetry group is the *Littlest* Higgs model [27]. However, owing to tree-level contributions of the new particles to the oblique electroweak parameters, electroweak precision data requires f to be above 5 TeV [28]. On the other hand a scale as low as 1 TeV is required to avoid fine-tuning of the Higgs mass.

This problem can be circumvented by imposing a discrete symmetry, called *T-parity* [29,30]. Under this symmetry, the Standard Model (SM) fields are T-even, while the new TeV-scale particles are odd, effectively forbidding all tree-level interactions between one of the new heavy degrees of freedom and SM particles. Therefore, the new particles can only be generated in pairs, which is reminiscent of R-parity in supersymmetric theories. Besides satisfying the electroweak constraints even for $f < 1$ TeV, an exactly realized T-parity also leads to the lightest T-odd particle being stable and, if neutral, a good candidate for (cold) dark matter.

However, it was pointed out by Hill and Hill [31, 32] that typical models of strongly interacting symmetry breaking would lead to a Wess-Zumino-Witten

(WZW) term [33] which is odd under T-parity[1]. The structure of the WZW term can be derived from topological considerations and depends only on the pattern of the global and gauged symmetry groups. The breaking of T-parity by the WZW term, though suppressed by the large symmetry breaking scale, rules out the lightest T-odd particle as a dark matter candidate, since this particle would decay promptly into gauge bosons [36]. Nevertheless, if the WZW term is a priori the only source of T-parity breaking, the electroweak precision constraints could still be satisfied.

In this chapter, we analyze the effect of the WZW term in the Littlest Higgs model with T-parity (LHT) further. The relevant interactions induced by this term are derived, and their gauge invariance is shown. Furthermore, it is demonstrated that the WZW term cannot be the only T-parity violating operator, but that other T-odd terms are needed in the Lagrangian to make the theory consistent. Equipped with these results, we discuss the constraints on the model from LEP and Tevatron data and comment on the surprisingly rich phenomenological prospects for LHC.

After reviewing the LHT model and specifying the notations in section 2.2, the T-odd interactions induced by the WZW term are studied in section 2.3. In section 2.4 the T-parity violating signals at LEP and hadron colliders are investigated. Finally, conclusions are given in section 2.5.

2.2 The Littlest Higgs model with T-parity

Here the main aspects of the model are reviewed, following the detailed description in Refs. [37, 38].

The Littlest Higgs model is based on a SU(5)/SO(5) symmetry breaking pattern. A global SU(5) symmetry is broken down to SO(5) by a vacuum expectation value of the form

$$\langle\Sigma\rangle = \Sigma_0 = \begin{pmatrix} & & 1 & & \\ & & & 1 & \\ & 1 & & & \\ 1 & & & & \\ & 1 & & & \end{pmatrix} \tag{2.1}$$

for a field Σ transforming in the two-index symmetric representation of SU(5). The generators of SU(5) are split up into a set of ten unbroken generators T^a that generate the unbroken SO(5) subgroup and a set of 14 broken generators X^a.

[1] It is possible to construct models which do not have WZW terms or where T-parity is not broken by these terms [34, 35]. This avenue will not be explored further here.

The Goldstone modes of the broken generators are implemented in a non-linear sigma model with a breaking scale f,

$$\mathcal{L}_\Sigma = \frac{f^2}{4}\mathrm{Tr}|D_\mu \Sigma|^2, \tag{2.2}$$

with

$$\Sigma = e^{i\Pi/f}\Sigma_0 e^{i\Pi^\top/f} = e^{2i\Pi/f}\Sigma_0, \tag{2.3}$$

where $\Pi = \pi_a X^a$ is the Goldstone matrix. A $[\mathrm{SU}(2)\times\mathrm{U}(1)]^2$ subgroup of SU(5) is gauged [27], with associated gauge bosons $W^a_{1,2}$ and $B_{1,2}$, respectively. In terms of 2×2, 1×1 and 2×2 blocks, the gauge group generators are given by

$$Q_1^a = \begin{pmatrix} \sigma^a/2 & 0 & 0 \\ 0 & 0 & 0 \\ 0 & 0 & 0 \end{pmatrix}, \qquad Y_1 = \frac{1}{10}\begin{pmatrix} 3 & 0 & 0 \\ 0 & -2 & 0 \\ 0 & 0 & -2 \end{pmatrix}, \tag{2.4}$$

$$Q_2^a = \begin{pmatrix} 0 & 0 & 0 \\ 0 & 0 & 0 \\ 0 & 0 & -\sigma^{a*}/2 \end{pmatrix}, \qquad Y_2 = \frac{1}{10}\begin{pmatrix} 2 & 0 & 0 \\ 0 & 2 & 0 \\ 0 & 0 & -3 \end{pmatrix}, \tag{2.5}$$

where σ^a, $a = 1, 2, 3$ are the Pauli matrices. The covariant derivative reads

$$D_\mu\Sigma \equiv \partial_\mu\Sigma - \sum_{k=1,2}\left[g_k W^a_{k,\mu}(Q^a_k\Sigma + \Sigma Q^{aT}_k) + g'_k B_{k,\mu}(Y_k\Sigma + \Sigma Y_k)\right]. \tag{2.6}$$

The vacuum Σ_0 breaks the gauge symmetry $[\mathrm{SU}(2)\times\mathrm{U}(1)]^2$ down to the diagonal subgroup, giving one set of gauge bosons with masses of order f, while the other set remains massless at this stage and is identified with the Standard Model gauge bosons. The Goldstone matrix Π is explicitly given by

$$\Pi = \begin{pmatrix} \omega/2 - \eta/\sqrt{20}\,\mathbb{1} & H/\sqrt{2} & \Phi \\ H^\dagger/\sqrt{2} & \sqrt{4/5}\eta & H^\top/\sqrt{2} \\ \Phi^\dagger & H^*/\sqrt{2} & \omega^\dagger/2 - \eta/\sqrt{20}\,\mathbb{1} \end{pmatrix}, \tag{2.7}$$

where H is the Little Higgs doublet, Φ is a complex triplet under $(\mathrm{SU}(2)\times\mathrm{U}(1))_{SM}$, which receives a mass of $\mathcal{O}(f)$, and the real triplet field $\omega = \omega^a\sigma^a$ and the real singlet η are eaten by the heavy gauge bosons ($\mathbb{1}$ is the 2×2 identity matrix).

The Littlest Higgs model can be supplemented by a discrete Z_2 symmetry called T-parity [30], with SM particles being even ($T = +1$), and non-SM particles odd ($T = -1$) under this symmetry. Their couplings to the non-linear sigma fields

generate masses of order f for the T-odd particles. In the gauge sector, T-parity is realized by the automorphism $T^a \to T^a$ and $X^a \to -X^a$. As a result, T-parity interchanges the two sets of gauge bosons,

$$W_1^a \leftrightarrow W_2^a, \qquad B_1 \leftrightarrow B_2. \tag{2.8}$$

T-parity requires the two sets of gauge couplings to be identical: $g_1 = g_2 = \sqrt{2}g$ and $g_1' = g_2' = \sqrt{2}g'$. The gauge bosons form a light and a heavy linear combination:

$$W_L^a = \tfrac{1}{\sqrt{2}}(W_1^a + W_2^a), \qquad \text{(T-even)} \tag{2.9}$$

$$B_L = \tfrac{1}{\sqrt{2}}(B_1 + B_2), \tag{2.10}$$

with masses from usual electroweak symmetry breaking, and

$$W_H^a = \tfrac{1}{\sqrt{2}}(W_1^a - W_2^a), \qquad \text{(T-odd)} \tag{2.11}$$

$$B_H = \tfrac{1}{\sqrt{2}}(B_1 - B_2), \tag{2.12}$$

with masses of order f generated from the kinetic term of the non-linear sigma model. After electroweak symmetry breaking, the light gauge bosons mix to form the usual physical states of the SM, $A_L = c_{\rm W}B_L - s_{\rm W}W_L^3$, $Z_L = s_{\rm W}B_L + c_{\rm W}W_L^3$ and $W_L^\pm = (W_L^1 \mp W_L^2)/\sqrt{2}$. Here, as usual, $s_{\rm W}$ and $c_{\rm W}$ denote the sine and cosine of the weak mixing angle. Similarly, a small mixing of order $\mathcal{O}(v^2/f^2)$ is introduced between B_H and W_H^3 through electroweak symmetry breaking, yielding

$$A_H = \cos\theta_H\, B_H - \sin\theta_H W_H^3, \qquad M_{A_H}^2 = \frac{g'^2}{5}f^2 - \frac{g'^2}{4}v^2 + \mathcal{O}\Big(\frac{v^4}{f^2}\Big), \tag{2.13}$$

$$Z_H = \sin\theta_H\, B_H + \cos\theta_H W_H^3, \qquad M_{Z_H}^2 = g^2 f^2 - \frac{g^2}{4}v^2 + \mathcal{O}\Big(\frac{v^4}{f^2}\Big), \tag{2.14}$$

$$\sin\theta_H = \frac{gg'}{4g^2 - \frac{4}{5}g'^2}\,\frac{v^2}{f^2} + \mathcal{O}\Big(\frac{v^4}{f^4}\Big), \tag{2.15}$$

and

$$W_H^\pm = (W_H^1 \mp W_H^2)/\sqrt{2}, \qquad M_{W_H^\pm}^2 = g^2 f^2 - \frac{g^2}{4}v^2. \tag{2.16}$$

The A_H will be referred to as heavy photon throughout this text. It is always lighter than the other T-odd gauge bosons and thus a good candidate for the LTP (lightest T-odd particle) and dark matter, if T-parity is an exact symmetry. Note that the mixing between the heavy photon and Z_H, is numerically small and leads to corrections at the 1% level at most.

In the scalar sector, T parity is defined as

$$\Pi \to -\Omega\Pi\Omega, \qquad \Omega = \mathrm{diag}(1,1,-1,1,1), \tag{2.17}$$

such that H is T-even while Φ, ω and η are T-odd.

The kinetic term (2.2) is not the full non-linear sigma model Lagrangian but just the first term in an expansion in external momenta p. The higher order terms that have to be added to (2.2) to cancel divergencies that appear in perturbation theory are suppressed by powers of (p/Λ), where Λ is the intrinsic cutoff of the theory beyond which ordinary perturbation theory breaks down.

In Little Higgs models $\Lambda = 4\pi f$ is typically of the order of 10 TeV, and the phenomenology at the TeV scale is well described by (2.2). Exceptions are possible if the lowest order Lagrangian possesses more symmetries than the full model. In that case higher order terms have to be taken into account and may change the phenomenology significantly.

T-parity also requires a doubling of the left-chiral fermion sector. Each left-handed T-even (SM) fermion is accompanied by a T-odd partner f_H (mirror fermion) with mass [39]

$$m_{f_{H,i}} = \sqrt{2}\kappa_i f + \mathcal{O}\Big(\frac{v^2}{f}\Big), \tag{2.18}$$

where the Yukawa couplings κ_i can in general depend on the fermion species i.

The implementation of the mass terms for the mirror fermions also introduces T-odd SU(2)-singlet fermions, which may receive large masses and do not mix with the SU(2)-doublets f_H. Here it is therefore assumed that these extra singlet fermions are too heavy to be observable at current or next-generation collider experiments.

The top sector requires an additional T-even fermion t'_+ and one T-odd fermion t'_- to cancel quadratic divergencies to the Higgs mass. Both particles obtain order f masses. We will not discuss the top sector of the Littlest Higgs model here, but refer the reader to Refs. [37,38] for further details. The Feynman rules of the Littlest Higgs model with T-parity are summarized in Ref. [38].

2.3 The WZW term in the Littlest Higgs model

2.3.1 The Wess Zumino Witten term

The nontrivial vacuum structure of the Littlest Higgs leads one to include the Wess Zumino Witten term [33] in the effective Lagrangian [31]. It consists of two parts,

$$\Gamma_{WZW} = \frac{N}{48\pi^2}\left(\Gamma_0(\Sigma) + \Gamma(\Sigma, A_l, A_r)\right). \tag{2.19}$$

Here Γ_0 is the ungauged WZW term that can be expressed as integral over a five-dimensional manifold with spacetime as its boundary [33], whereas $\Gamma(\Sigma, A_l, A_r)$

is the gauged part of the WZW action that can be written as an ordinary four-dimensional spacetime integral. The explicit form of $\Gamma(\Sigma, A_l, A_r)$ and a prescription how to relate the gauge fields A_l, A_r to those appearing in the Littlest Higgs are given in Ref. [31]:

$$A_{l,r} = \sqrt{2}\big[g(W_L^a Q_L^a \mp W_H^a Q_H^a) + g'(B_L Y_L \mp B_H Y_H)\big]. \tag{2.20}$$

The Integer N depends on the UV completion of the Littlest Higgs model. In strongly coupled UV-completions, where the Little Higgs is a composite particle of some underlying Ultracolor theory [40], N will equal the number of ultracolors, $N = N_{uc}$.

The WZW term is T-odd by construction, i.e. it changes sign under a T-parity transformation. The fact that Γ_{WZW} violates T-parity and that its coefficient N can not be chosen arbitrarily make the WZW term stand out from other higher order terms in the expansion of the non-linear sigma model lagrangian.

In those cases where the UV completion demands a nonzero N, T-parity cannot be a fundamental symmetry of the full theory, instead it has to be seen as accidental symmetry of the lowest order effective Lagrangian. This is the point of view we want to adopt in this work.

2.3.2 Gauge invariance

The WZW term is not manifestly gauge invariant, rather under a gauge transformation

$$\Sigma \to e^{i\epsilon_l}\Sigma e^{-i\epsilon_r}, \qquad A_l^\mu \to A_l^\mu + \partial^\mu \epsilon_l + i[\epsilon_l, A_l^\mu], \qquad A_r^\mu \to A_r^\mu + \partial^\mu \epsilon_r + i[\epsilon_r, A_r^\mu], \tag{2.21}$$

it transforms as $\Gamma_{WZW} \to \Gamma_{WZW} + \delta\Gamma_{WZW}$, with $\delta\Gamma_{WZW}$ given by

$$\delta\Gamma_{WZW} = -\frac{N}{24\pi^2}\int d^4x\, \epsilon_{\mu\nu\rho\sigma}\mathrm{Tr}\left[\epsilon_l\left(\partial^\mu A_l^\nu \partial^\rho A_l^\sigma - \tfrac{i}{2}\partial^\mu(A_l^\nu A_l^\rho A_l^\sigma)\right) - (L \to R)\right], \tag{2.22}$$

reproducing the well-known nonabelian chiral anomaly [33]. In order to restore gauge invariance, a sector must be added to the theory whose gauge variation cancels (2.22) exactly. Various options to cancel the anomaly are discussed in [32].

One possible way to to cancel the anomaly directly at the level of the underlying ultracolor theory is by introducing a set of spectator leptons with $U(1)_1$ and $U(1)_2$ charges chosen such that they directly cancel the anomalies from the ultrafermions. Making the spectator leptons sufficiently heavy allows one to neglect their contributions to physical observables, without affecting the anomaly cancellation.

The anomalous couplings in Γ_{WZW} are the terms with three or four gauge bosons, with an odd number of T-odd gauge bosons. For example the three

gauge boson terms with one T-odd gauge boson are of the form $\epsilon_{\mu\nu\rho\sigma} V_H^\mu V^\nu \partial^\rho V^\sigma$, where V_H is any T-odd gauge boson and V denote SM gauge bosons. Independent of the actual implementation, any anomaly canceling sector does at least cancel all these terms.

There could be additional effects from the anomaly canceling sector that do depend on the details of its implementation. We will here assume that these effects can be decoupled, as in the example above, or at least are suppressed by some sufficiently large scale, and leave the details to further studies.

With the anomalous couplings cancelled, the leading T-odd interactions now appear at order $(1/f^2)$ in the expansion of Γ_{WZW}. For example three gauge boson interactions with two SM gauge bosons and one T-odd gauge boson are generated by $\epsilon_{\mu\nu\rho\sigma} H^\dagger H/f^2 V_H^\mu V^\nu \partial^\rho V^\sigma$ once electroweak symmetry is broken.

The systematic expansion of Γ_{WZW} leads to a large number of T-parity violating interactions. To leading order in $(1/f)$ the part of the WZW term containing one neutral T-odd gauge boson is given by

$$\begin{aligned}\Gamma_n =& \frac{Ng^2g'}{48\pi^2 f^2}\int d^4x\,(v+h)^2\epsilon_{\mu\nu\rho\sigma}\times \\ & \big[-\tfrac{6}{5}A_H^\mu\left(c_w^{-2}Z^\nu\partial^\rho Z^\sigma + W^{+\nu}D_A^\rho W^{-\sigma} + W^{-\nu}D_A^\rho W^{+\sigma}\right. \\ & \left. + i\,(3gc_w + g's_w)W^{+\nu}W^{-\rho}Z^\sigma\right) \\ & + t_w^{-1}Z_H^\mu\left(2c_w^{-2}Z^\nu\partial^\rho Z^\sigma + W^{+\nu}D_A^\rho W^{-\sigma} + W^{-\nu}D_A^\rho W^{+\sigma}\right. \\ & \left. -2i(2gc_w + g's_w)W^{+\nu}W^{-\rho}Z^\sigma\right)\big]\end{aligned} \tag{2.23}$$

while the part containing one charged T-odd gauge boson reads

$$\begin{aligned}\Gamma_c =& \frac{Ng^2g'}{48\pi^2 f^2}\int d^4x\,(v+h)^2\epsilon_{\mu\nu\rho\sigma}\times \\ & \big[2W_H^{+\mu}W^{-\nu}(-c_w\partial^\rho A^\sigma + s_w\partial^\rho Z^\sigma) + c_w W_H^{+\mu}D_A^\nu W^{-\rho}(-A^\sigma + (2t_w + t_w^{-1})Z^\sigma) \\ & + c_w D_A^\mu W_H^{+\nu}W^{-\rho}(A^\sigma + t_w^{-1}Z^\sigma)\big] + h.c.,\end{aligned} \tag{2.24}$$

written in unitary gauge. The vacuum expectation value of the Higgs field is denoted by v, h is the physical Higgs boson and we defined $D_A^\mu W^{\pm\nu} = (\partial^\mu \mp ieA^\mu)W^{\pm\nu}$. Furthermore s_w, c_w and t_w denote the sine, cosine and tangent of the weak mixing angle, respectively.

We do not write other parts of the WZW term here, instead all T-violating vertices with up to four legs have been tabulated in appendix 2.7, including the interactions of the complex triplet Φ. These Feynman rules have further been implemented into a model file for CalcHEP 2.5 [41, 42].

Because of (2.23) the heavy photon can decay either into a pair of Z-bosons or into a W^+W^- pair, with a decay width of order $\mathcal{O}$(eV) [36]. This clearly rules out the A_H as dark matter candidate. A more detailed analysis, in particular for

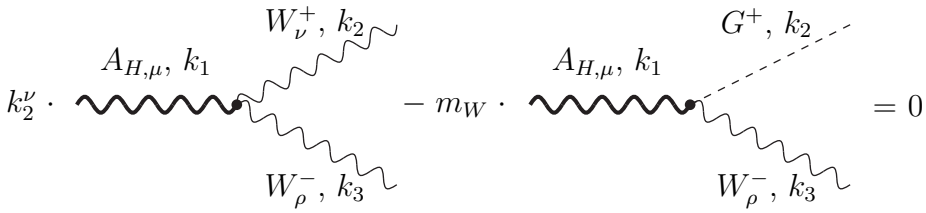

Figure 2.1: *Tree level Ward identity for the $A_H W^+ W^-$ vertex, all momenta incoming*

the case where the decay into real SM gauge bosons is kinematically forbidden, will be performed in section 2.4.

The gauge invariance of the WZW term can be verified using Ward identities for the three-point functions involving massive gauge bosons. These identities can be derived in a similar way as the Ward identities for three-boson vertices in the SM [43]. For example vertices involving the heavy photon A_H have to satisfy

$$k_2^\nu \Gamma^{A_H ZZ}_{\mu\nu\rho}(k_1,k_2,k_3) - i m_Z \Gamma^{A_H G^0 Z}_{\mu\rho}(k_1,k_2,k_3) = 0, \tag{2.25}$$

$$k_2^\nu \Gamma^{A_H W^+W^-}_{\mu\nu\rho}(k_1,k_2,k_3) - m_W \Gamma^{A_H G^+W^-}_{\mu\rho}(k_1,k_2,k_3) = 0. \tag{2.26}$$

At the tree level these identities have simple interpretations in terms of Feynman graphs, as shown in Fig. 2.1. Using the gauge boson-Goldstone boson vertices of Tab. 2.10 we have checked explicitly that $[SU(2) \times U(1)]_{SM}$ gauge invariance is respected by all interactions coming from equations (2.23) and (2.24).

2.3.3 Divergences and counterterms

Apart from the tree level interactions additional T-parity violating processes are induced at the loop level. These are especially important when corresponding tree level processes are kinematically forbidden. In particular, when $M_{A_H} < 2M_W$, the heavy photon cannot decay into real SM gauge bosons, and decays induced by one-loop processes have to be taken into account.

The most important processes are of the type shown in Fig. 2.2, where the heavy photon couples to two light T-even fermions via a triangle loop. A similar set of graphs also couple Z_H and $W_H^\pm$ to SM fermions. Since the three-boson vertex involves one power of the loop momentum, graphs of this type are logarithmically divergent.

The counterterms needed to cancel these divergencies are of the form

$$\mathcal{L}_{ct} = \bar{f}\gamma_\mu \left(c_L^f P_L + c_R^f P_R \right) f A_H^\mu, \tag{2.27}$$

$$c_i^f = c_{i,\epsilon}^f \left(\frac{1}{\epsilon} + \log \mu^2 + \mathcal{O}(1) \right). \tag{2.28}$$

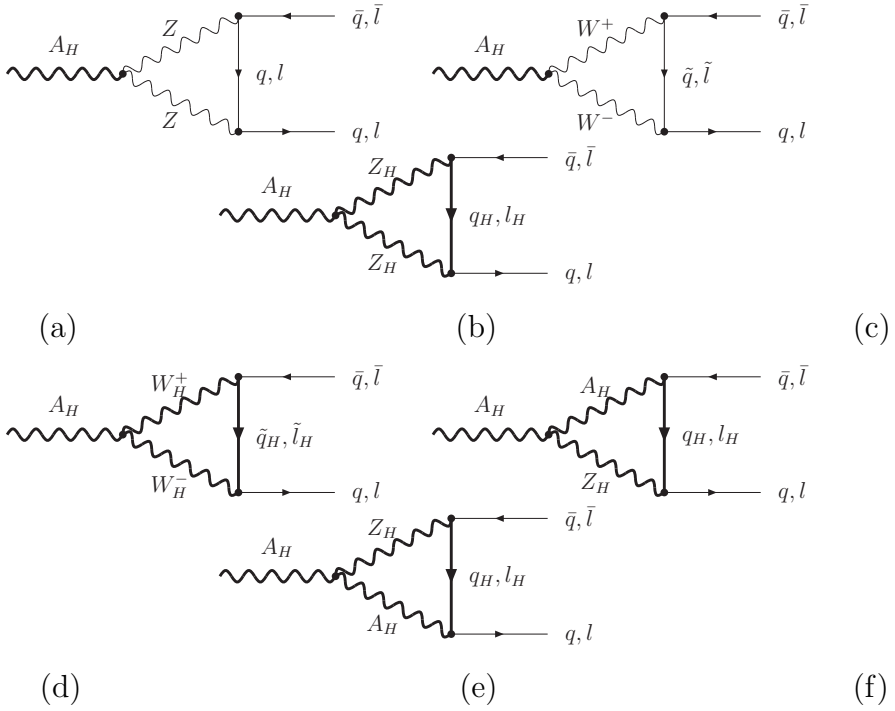

Figure 2.2: *Loop induced decay of A_H into SM quarks/leptons. Thick lines indicate T-odd propagators. $q = (u, d, c, s, b)$, $\tilde{q} = (d, u, s, c, t)$, and similar for l, $\tilde{l}$.*

The coefficients $c_i(\mu)$ of the counterterms are determined as follows. The scale dependence of the above loop processes must be cancelled by the scale dependence of the $c_i(\mu)$. Naturalness arguments then suggest that an $\mathcal{O}(1)$ change in the renormalization scale should be compensated by an $\mathcal{O}(1)$ change in the $c_i(\mu)$. Therefore these coefficients are given, up to $\mathcal{O}(1)$ factors, by the coefficients of the leading $1/\epsilon$ divergence in dimensional regularization of the above loop diagrams. The resulting coefficients are given in Tab. 2.1. Since the A_H only couples very weakly to fermions, the contributions of diagrams (e) and (f) in Fig. 2.2 have been neglected. An alternative, gauge invariant formulation of the counterterms (2.27) is discussed in appendix 2.6.

Another important set of diagrams arises from those in Fig. 2.2 by replacing the A_H with a Z boson and one of the fermions with its mirror partner. These diagrams, as well as the corresponding diagrams where the Z is replaced by $W^\pm$, are again logarithmically divergent and require T-violating counterterms.[2] These may become important in scenarios where one of the mirror fermions is the LTP.

Other T-violating counterterms induced at the one loop level are not relevant for phenomenology for almost all reasonable choices of parameters in the Littlest

[2]The loop that couples the photon to a fermion-mirror fermion pair is finite, as required by gauge invariance.

Particles	$c^f_{L,\epsilon}$	$c^f_{R,\epsilon}$
$A_H e^+ e^-$	$\frac{9\hat{N}}{160\pi^2}\frac{v^2}{f^2}g^4 g'\,(4+(c_w^{-2}-2t_w^2)^2)$	$-\frac{9\hat{N}}{40\pi^2}\frac{v^2}{f^2}g'^5$
$A_H \bar{\nu}\nu$	$\frac{9\hat{N}}{160\pi^2}\frac{v^2}{f^2}g^4 g'\,(4+c_w^{-4})$	0
$A_H \bar{u}_a u_b$	$-\frac{\hat{N}}{160\pi^2}\frac{v^2}{f^2}g^4 g'\,(36+(3c_w^{-2}-4t_w^2)^2)\,\delta_{ab}$	$-\frac{\hat{N}}{10\pi^2}\frac{v^2}{f^2}g'^5\delta_{ab}$
$A_H \bar{d}_a d_b$	$-\frac{\hat{N}}{160\pi^2}\frac{v^2}{f^2}g^4 g'\,(36+(3c_w^{-2}-2t_w^2)^2)\,\delta_{ab}$	$-\frac{\hat{N}}{40\pi^2}\frac{v^2}{f^2}g'^5\delta_{ab}$

Table 2.1: *Coefficients for the counterterm (2.27). Here* $\hat{N}=\frac{N}{48\pi^2}$ *denotes the coefficient of the WZW term, while* a,b *indicate the color indices of the external quarks.*

Higgs model.

Mixing between T-even and T-odd gauge bosons is also induced by loop diagrams and may affect electroweak precision observables. The existing one loop graphs vanish due to the antisymmetry of the ϵ-tensor, so the first contributions come only at the two loop level. The nonvanishing two loop diagrams are shown in Fig. 2.3.

The relevant counterterms are of the form

$$\mathcal{L}_{ct} = \frac{c^{V_L V_H}}{4}(\partial_\mu V_{L,\nu} - \partial_\nu V_{L,\mu})(\partial^\mu V_H^\nu - \partial^\nu V_H^\mu), \tag{2.29}$$

$$c^{V_L V_H} = c_\epsilon^{V_L V_H}\left(\frac{1}{\epsilon} + \log\mu^2 + \mathcal{O}(1)\right), \tag{2.30}$$

where $V_L \in \{A_L, Z_L, W_L^\pm\}$ and $V_H \in \{A_H, Z_H, W_H^\pm\}$. For the gauge boson mixing terms, the leading $1/\epsilon$ divergence is not completely determined in the LHT model. The reason is that the LHT model as a low-energy effective theory has an "incomplete" fermion content whose $[\mathrm{U}(1)_i\times\mathrm{SU}(2)_j\times\mathrm{SU}(2)_j]$ gauge anomalies $(i,j=1,2)$ must be cancelled (see above) by an interacting UV completion. If not specified, the $\mathcal{O}(1)$ uncertainty remains for the $1/\epsilon$ coefficients of the T-violating gauge boson mixing counterterms. For this reason we only list the parametric dependence of the coefficients $c_\epsilon^{V_L V_H}$ with an undetermined prefactor which is expected to be close to one:

$$c_\epsilon^{V_L V_H} = \text{const.}\times\frac{\hat{N}}{(4\pi)^4}\frac{v^2}{f^2}\,g^5 g'\Big(B_0(k^2,0,0) + 2\tfrac{m_t^2}{k^2}\,B_0(0,m_t^2,m_t^2) - (1+2\tfrac{m_t^2}{k^2})\,B_0(k^2,m_t^2,m_t^2)\Big),\quad V_i = A_i, Z_i, \tag{2.31}$$

$$c_\epsilon^{W_L^\pm W_H^\pm} = \text{const.}\times\frac{\hat{N}}{(4\pi)^4}\frac{v^2}{f^2}\,g^5 g'\Big(B_0(k^2,0,0) + \tfrac{m_t^2}{k^2}(1-2\tfrac{m_t^2}{k^2})\,B_0(0,0,m_t^2) - \tfrac{(k^2-m_t^2)(k^2+2m_t^2)}{k^4}\,B_0(k^2,0,m_t^2) - \tfrac{m_t^2}{k^2}\Big), \tag{2.32}$$

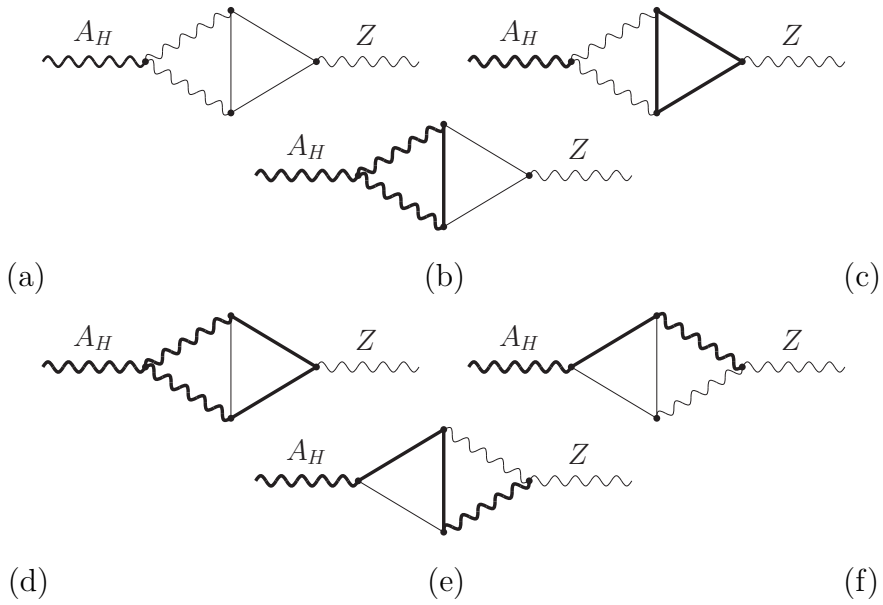

Figure 2.3: *Two loop diagrams that contribute to A_H-Z boson mixing. As above thick lines indicate T-odd propagators. All types of fermions and mirror-fermions are allowed.*

where all SM Yukawa couplings except the top Yukawa coupling have been set to zero, $\hat{N} = \frac{N}{48\pi^2}$ and "const." stands for a complex $\mathcal{O}(1)$ constant, which depends on V_L and V_H. Here B_0 is the usual standard one-loop self-energy function and k is the external gauge boson momentum. The mixing between T-even and T-odd gauge bosons induced by the WZW term is very small due to the two-loop suppression and does not lead to observable effects in electroweak precision observables. For $m_t \to 0$ the gauge boson mixing terms have to vanish owing to gauge anomaly cancellation.

2.4 Phenomenology of T-parity breaking effects

2.4.1 Decays of A_H

The leading decays of A_H are induced by the $A_H W^+ W^-$ and $A_H ZZ$ terms in (2.23). For large enough f the decay into real gauge bosons is allowed and the corresponding partial widths are

$$\Gamma(A_H \to ZZ) = \frac{1}{2\pi}\left(\frac{Ng'}{40\sqrt{3}\pi^2}\right)^2 \frac{m_{A_H}^3 m_Z^2}{f^4}\left(1-\frac{4m_Z^2}{m_{A_H}^2}\right)^{\frac{5}{2}}, \tag{2.33}$$

$$\Gamma(A_H \to W^+W^-) = \frac{1}{\pi}\left(\frac{Ng'}{40\sqrt{3}\pi^2}\right)^2 \frac{m_{A_H}^3 m_W^2}{f^4}\left(1-\frac{4m_W^2}{m_{A_H}^2}\right)^{\frac{5}{2}}. \tag{2.34}$$

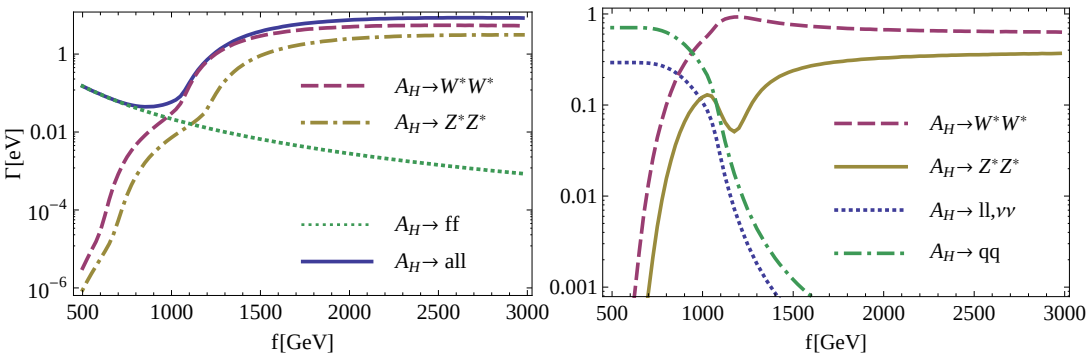

Figure 2.4: *Left: Decay widths of A_H into Z^*Z^* (solid, red line), into W^*W^* (dashed, blue) and into fermion pairs (dotted, green) as well as the total width (thick black line), for $N = 3$. Right: Corresponding branching fractions. These are independent of N.*

To leading order in $(1/f)$ this agrees with the result of Ref. [36] if we set $K = 6\sqrt{5/3}$.

The threshold for the decay into real gauge bosons, $m_{A_H} > 2m_W$, corresponds to a value of $f = 1070$ GeV. However previous studies have shown that values of f as low as 500 GeV are consistent with electroweak precision data [37, 44]. In this region of parameter space, three-body decays via $A_H \to VV^*$ are dominant, where V^* indicates an off-shell SM gauge boson. For $f < 600$ GeV the mass of A_H even drops below M_W and four-body decays via two virtual intermediate gauge bosons have to be considered.

Below $f \sim 1200$ GeV the loop induced two body decays shown in Fig. 2.2 become relevant. A reliable estimate of the decay widths can be obtained by just using the finite, scale independent part of the counterterms and setting to one the undetermined $\mathcal{O}(1)$ coefficient that enters the results through the counterterms (2.27) (see section 2.3).

The partial width of a massive gauge boson V into a pair of fermions with couplings

$$\mathcal{L}_{Vff} = \bar{f}\gamma_\mu \left(\frac{r+l}{2} + \frac{r-l}{2}\gamma_5 \right) f V^\mu, \tag{2.35}$$

where l and r are the coefficients of the left and right chiral projectors, is given by

$$\Gamma_{V\to ff} = \frac{N_{C_f} M_V}{48\pi} \sqrt{1 - \frac{4m_f^2}{M_V^2}} \left[(r-l)^2 \left(1 - \frac{4m_f^2}{M_V^2} \right) + (r+l)^2 \left(1 + \frac{2m_f^2}{M_V^2} \right) \right], \tag{2.36}$$

N_{C_f} denoting the number of colors of fermion species f.

The total width of A_H for $N = 3$, including the loop induced two body decays, is shown in Fig. 2.4 together with the corresponding branching fractions. Above

$f = 1500$ GeV, A_H dominantly decays into two on-shell gauge bosons, with a total width of $\Gamma_{A_H} \sim 1 - 2$ eV. The fermionic decay channels are negligible in this region.

Beneath the threshold for real W production, $M_{A_H} < 2m_W$, the decay phenomenology of A_H changes dramatically. For f below ~ 1000 GeV the decay into a light fermion pair becomes dominant; in approximately 10% of all cases, the decay is into a pair of charged leptons with an invariant mass m_{A_H} and an extremely small width of $\mathcal{O}$(eV).

The uncertainty in the fermionic widths due to the unknown $\mathcal{O}(1)$ coefficients in the counterterms (2.27) may slightly change the value of f where the fermionic decays become dominant, however the overall picture does not change.

2.4.2 Bounds from electroweak precision tests and direct detection at LEP

T-parity in Little Higgs models evades the tension between a low value of f and electroweak precision tests (EWPT). Models without T-parity are typically only compatible with EWPT for $f \geq 5$ TeV [28], while lower values of f are favored by naturalness.

However, if T-parity is broken by the WZW term, the situation is different and we do not expect disagreement with electroweak precision data, even for values of f lower than 1 TeV. One reason is that the coefficient of Γ_{WZW}, $N/48\pi^2$, is very small for reasonable values of N. Furthermore, the T-odd operators affecting electroweak precision observables are suppressed by loops, as discussed in section 2.3, so that their contribution is smaller than the experimental error of those observables. We conclude that the Littlest Higgs model with anomalous T parity is not constrained by electroweak precision data; in particular values of f as low as 500 GeV are allowed. In addition the stringent bounds from dark matter overproduction are evaded.

While most of the T-odd particles are quite heavy, the A_H is rather light and could in principle have been produced and detected by the LEP experiments. However, the cross section for pair production of A_H in e^+e^- collisions is smaller than 10^{-6} pb for all allowed values of f, and thus invisible at LEP. T-violating single A_H production is further suppressed by $N/48\pi^2$ and therefore also out of reach of the LEP experiments.

2.4.3 Bounds from Tevatron

The rates for pair production of heavy gauge bosons are relatively small also at Tevatron. While the $A_H A_H$ production is suppressed due to its small couplings, other combinations like $A_H Z_H$ or $W_H^+ W_H^-$ are too heavy to be produced in noticeable amounts.

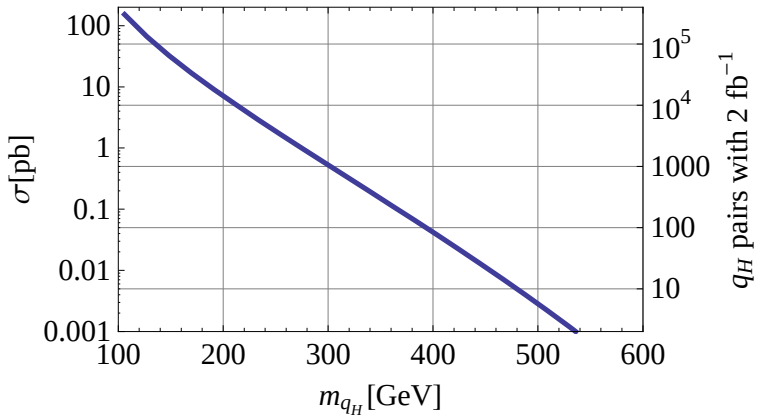

Figure 2.5: *Cross section for first and second family mirror-quark pair production at Tevatron as a function of m_{q_H}. Right edge: Number of expected $q_H q_H$ pairs with 2 fb^{-1} of integrated luminosity.*

The situation is slightly different for the production of T-odd quark pairs. In the LHT, their mass is essentially a free parameter, only bound to lie between 100 GeV and a few TeV, so they can in principle be light enough to be produced in sizable amounts even at Tevatron.

The phenomenology of T-odd quarks at Tevatron has been studied in Ref. [45], assuming a common mass m_{q_H} for the first two families of T-odd quarks and exact T-parity. It was found that T-odd quarks are produced in sizeable numbers for $m_{q_H} < 500$ GeV and are excluded for $m_{q_H} < 350$ GeV in the $2j + \not{E}_T$ channel.[3]

After including the WZW term the collider signatures of a T-odd quark change completely. The main decay mode is still $q_H \to qA_H$, but the heavy photon A_H subsequently decays either into a pair of light fermions for small f or into a pair of (Standard Model) gauge bosons for larger values of f.

The cross section for the production of a $q_H \bar{q}_H$ pair in $p\bar{p}$ collisions depends strongly on their mass m_{q_H} and is nearly independent of f. It is therefore sufficient to analyse the phenomenology for two characteristic values of f, namely $f = 750$ GeV where A_H decays into fermion pairs in more than 90% of the cases, and $f = 1500$ GeV where essentially all A_H decay into gauge boson pairs. The results of this section furthermore do not depend on the actual value of N, as long as it is nonzero (see below).

The cross section for the pair production of mirror quarks at Tevatron is shown in Fig. 2.5, along with the number of expected $q_H q_H$ pairs produced with 2 fb^{-1} of integrated luminosity, as computed with CalcHEP. The renormalization and factorization scales μ were chosen to be the invariant mass of the incoming partons. This is a conservative choice as lower values of μ can increase the cross sections by up to 30%. To reduce this scale dependence a full next-to-leading

[3]For small T-odd masses m_{q_H} the dominant decay is $q_H \to qA_H$ which yields a $j + \not{E}_T$ signal if T-parity is unbroken.

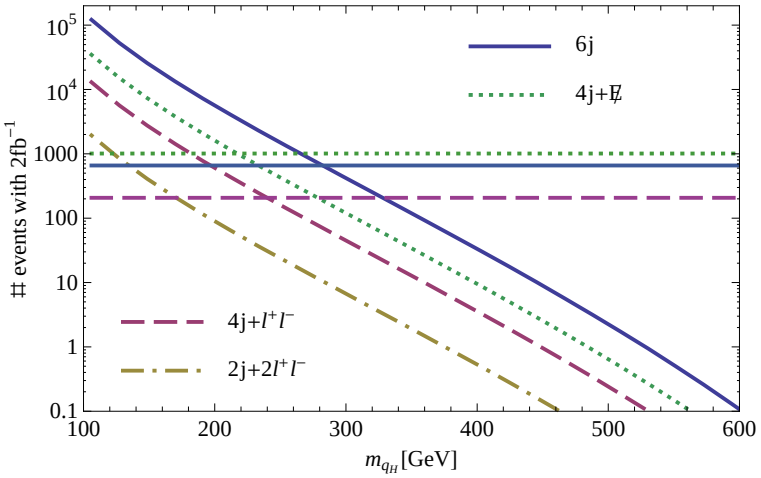

Figure 2.6: *Event rates for the different decay channels of $q_H q_H$ pairs for $f = 750$ GeV with 2 fb^{-1} at Tevatron, together with the corresponding SM backgrounds (horizontal lines). No cuts have been applied to the signals.*

order calculation of this process would be required.

We will first consider the case $f = 750$ GeV as a representative value for values of f below 1000 GeV, corresponding to A_H masses of 80–150 GeV. Here we assume that q_H is much heavier that A_H. The case where m_{q_H} is close to M_{A_H} is treated at the end of this section, while the case where (some of) the mirror fermions are lighter than A_H is discussed in section 2.4.5.

With A_H decaying, there are various possible final states originating from a $q_H \bar{q}_H$ pair. The highest rate results for the channel where both heavy photons decay into quark pairs, leading to six jets. Further there are events with four jets plus one lepton pair and events with two jets and two lepton pairs with the same invariant mass. Finally also four jets plus missing energy, two jets plus lepton pair plus missing energy and two jets plus missing energy are possible, since one or both A_H's can decay into neutrinos. Figure 2.6 shows the expected number of events in the most promising channels together with the corresponding SM backgrounds (as listed in Ref. [46]) for 2 fb^{-1}, as a function of m_{q_H}. Note that we did not include detector acceptance effects in the computation of the signal, so that the experimentally observable rates could be slightly lower than the numbers in the figure.

The most stringent bounds on m_{q_H} could be derived from the six jet channel. Using the preliminary data from the CDF Vista global search [46] at 2 fb^{-1} we find that

$$m_{q_H} > 350 \text{ GeV}. \tag{2.37}$$

As mentioned, this bound could be improved by including NLO order corrections and appropriate cuts.

Final State	BF [%]	m_{q_H} [GeV]	Final State	BF [%]	m_{q_H} [GeV]
$8j + l + \nu_l$	22.5	335	$8j + l^+l^-$	4.4	270
$6j + 2\,(l\nu_l)$	13.9	315	$4j + 3\,l\nu_l$	4.1	265
$6j + 2\,(l^+l^-)$	0.4	185	$10j$	21.9	330

Table 2.2: *Possible final states from the decay of a $q_H\bar{q}_H$-pair for $f > 1000$ GeV, together with their branching fractions (second column) and the value of m_{q_H} where the expected number of events with 2 fb^{-1} at Tevatron drops below 100 (third column), assuming $B(A_H \to W^+W^-) = 66\%$. Here l denotes any of e, μ, τ.*

Due to their smaller background and cleaner signatures, the channels with leptonic final states could in principle provide stronger bounds than the one derived from purely hadronic decays. However in the interesting region above $m_{q_H} \gtrsim 300$ GeV their statistical significance drops quickly. A dedicated study of these final states still could yield more reliable the bounds, but this is not possible with the Vista data alone.

The analysis is more involved in the second case, $f > 1000$ GeV, where A_H dominantly decays into two gauge bosons. As can be seen in Fig. 2.4, or from equations (2.33) and (2.34), the branching $B(A_H \to W^+W^-)$ is larger than 60% in that region, with a peak value of $\sim 95\%$ around the W-boson pair production threshold.

The final states originating from the decay of a $q_H\bar{q}_H$ pair will consist of at least ten particles. Events with eight quarks and two leptons are the most common final state, followed by ten jet events and events with six quarks and four leptons in the final state. In most cases some or all of the leptons are neutrinos and escape detection, while the fraction of events where all leptons come in charged pairs is rather small.

To give an idea of the range of m_{q_H} that can be tested at Tevatron in this case, in Tab. 2.2 we list all final states with at least one charged lepton together with the value of m_{q_H} above which less than 100 events are to be expected with 2 fb^{-1}.

There are at least three channels where we expect a significant signal for $m_{q_H} < 300$ GeV, even after experimental cuts have been applied. The current data from Tevatron therefore strongly suggests that $m_{q_H} > 300$ GeV. It should be possible to derive more stringent bounds with a detailed analysis and refinement of some of the final states listed above. For instance, a fraction of the $6j + 2\,(l\nu_l)$ final state will have both leptons with the same-sign charge.

Finally we can discuss the case where q_H is only slightly heavier than A_H.

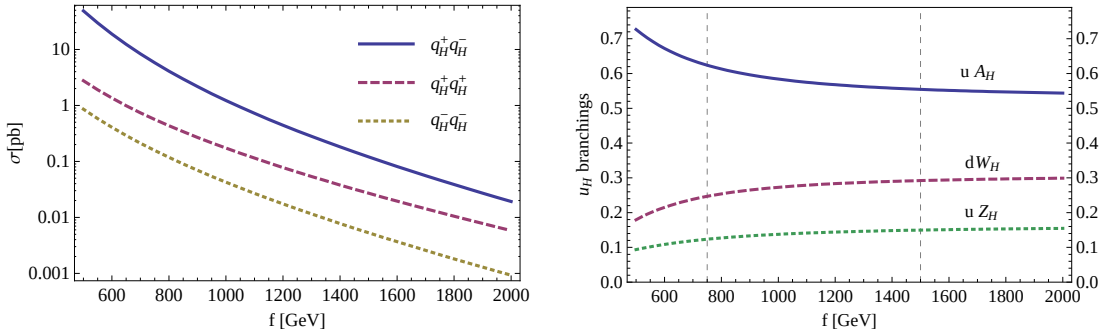

Figure 2.7: *Left: Production of T-odd quark pairs, where* $q^+ = \{u_H, \bar{d}_H, c_H, \bar{s}_H\}$ *and* $q^- = \{\bar{u}_H, d_H, \bar{c}_H, s_H\}$*, as a function of* f *for* $\kappa = 0.5$ *Right: Branching fractions for the decay of* u_H *with* $\kappa = 0.5$*. The dashed vertical lines indicate our two reference scenarios with* $f = 750$ *GeV and* $f = 1500$ *GeV. The branching fractions for down-type mirror quarks* d_H *are similar, although there are small differences due to* $\mathcal{O}(v^2/f^2)$ *mass corrections [38, 49].*

This is possible only for somewhat larger values of f where we need to consider A_H decaying into SM gauge bosons. The quarks from the decay $q_H \to A_H + q$ are too soft to be observable in this case. Apart from this, the phenomenology is the same as in the previous analysis, in particular the results from Tab. 2.2 can be adopted by reducing the number of jets by two for each final state. With the same arguments as above we conclude that current experimental data strongly suggest $m_{q_H} > 300$ GeV also in this case.

2.4.4 LHC phenomenology

Single production of T-odd particles is possible in principle at LHC, however the T-violating partial widths are too small for these processes to be observable. Therefore pair production remains the dominant source of T-odd particles. For LHC, the pair production rates, including the effects of the mirror fermions, have been studied in Refs. [47] and [48]. It turns out that not only the T-odd quark production but also the pair production rates for T-odd gauge bosons depend on the mass m_{q_H} of the mirror quarks.

For definiteness, we will take $\kappa = 0.5$ throughout this chapter and comment on other choices later. In this case the mirror quarks are always somewhat heavier than W_H and Z_H. As above we will consider two cases, case 1 with $f = 750$ GeV and case 2 with $f = 1500$ GeV. The corresponding particle masses are:

Case 1: $M_{W_H^\pm} = M_{Z_H} = 482$ GeV, $M_{A_H} = 111$ GeV, $m_{u_H} = 523$ GeV and $m_{d_H} = 530$ GeV for the first and second generation mirror quarks.

Case 2: $M_{W_H^\pm} = M_{Z_H} = 975$ GeV, $M_{A_H} = 235$ GeV, $m_{u_H} = 1057$ GeV and $m_{d_H} = 1061$ GeV for the first and second generation mirror quarks.

Signal rates for $f = 750$ GeV				
$q_H^+ q_H^- \to$	$q^+q^-A_HA_H$ (BF: 39%)		$q^+q^+A_HW_H^-$ (BF: 15%)	
	Final State	σ[fb]	Final State	σ[fb]
	$6j$	994	$6j + l_*^- + \not{E}$	124
	$4j + \not{E}$	568	$4j + l_*^- + \not{E}$	71
	$4j + ll$	319	$4j + l_*^- + ll + \not{E}$	40
	$2j + 2\,ll$	26	$2j + l_*^- + 2\,ll + \not{E}$	3.2
$q_H^+ q_H^- \to$	$q^-q^+W_H^-W_H^+$ (BF: 6%)		$q^+q^-Z_HA_H$ (BF: 15%)	
	Final State	σ[fb]	Final State	σ[fb]
	$6j + l_*^+l_*^- + \not{E}$	16.0	$6j + h$	306
	$4j + ll + l_*^+l_*^- + \not{E}$	5.2	$4j + ll + h$	98
			$4j + h + \not{E}$	175

Table 2.3: *Signal rates without cuts, from $q_H^+q_H^-$ pair decays. Leptons $l = \{e, \mu, \tau\}$, and ll always denotes a charged lepton pair l^+l^- of the same flavor, while a hard charged lepton coming from a decay $W_H \to WA_H \to l\nu_l A_H$ is denoted by l_*.*

For the chosen value of κ the most important source of T-odd particles at LHC is the pair production of mirror quarks q_H. The left plot in Fig. 2.7 shows the cross sections for the production of equally charged and opposite charged mirror quark pairs, for the first two quark families. For moderate values of f the cross section for $q_H^+q_H^-$ is of the order of one picobarn. The cross section for positively charged mirror quark pairs is larger than the one for quark pairs of negative charge and approaches the $q_H^+q_H^-$ cross section for increasing values of f. As for the Tevatron calculation, the renormalization and factorization scales μ were chosen to be the invariant mass of the incoming partons. The scale uncertainty is again around 30%.

The right plot in Fig. 2.7 shows the branching fractions for the two-body decays of an up-type mirror quark u_H as a function of f. While the decay into A_H and a SM quark dominates, the branching ratios for the other channels are sizeable, leading to a large variety of phenomenological signatures. Note that the mass of the mirror quarks always lies above the Tevatron bounds of section 2.4.3 for the considered range of parameters.

We will first discuss the signals stemming from the decay of opposite charge

Signal rates for $f = 1500$ GeV				
$q_H^+ q_H^- \to$	$q^+q^-A_HA_H$ (BF: 31%)		$q^+q^+A_HW_H^-$ (BF: 16%)	
	Final State	σ[fb]	Final State	σ[fb]
	$10j$	8.2	$10j + l_*^- + \not{E}$	1.37
	$8j + l + \not{E}$	8.4	$8j + l_*^- + l + \not{E}$	1.40
	$6j + ll + \not{E}$	5.2	$8j + l_*^- + l^- + \not{E}$	0.70
	$6j + l^\pm l^\pm + \not{E}$	1.6	$l_*^- + ll + \not{E} +$ jets	1.14
$q_H^+ q_H^- \to$	$q^-q^+W_H^-W_H^+$ (BF: 9%)		$q^+q^-Z_HA_H$ (BF: 17%)	
	Final State	σ[fb]	Final State	σ[fb]
	$10j + l_*^+ l_*^- + \not{E}$	0.25	$10j + h$	3.16
	$l_*^+ l_*^- + l + l + \not{E} +$ jets	0.21	$6j + h + l^\pm l^\pm + \not{E}$	1.15

Table 2.4: *Signal rates without cuts, from $q_H^+ q_H^-$ pair decays. Notation as in Tab. 2.3.*

mirror quark pairs, $q_H^+ q_H^-$. When both q_H decay into $A_H + q$, the final states are the same as those discussed for Tevatron. The results for case 1 are shown in the upper left block of Tab. 2.3. The cross sections are large, in particular for the six jet channel, but also the channels with two or four charged leptons in the final states are well populated. For case 2 the cross sections, shown in Tab. 2.4, are significantly lower. A detailed analysis would be needed to extract a signal from the background in this case. However we expect very low SM background for the four-lepton channel, suggesting this signature as a promising discovery channel.

Consider now the case where one of the mirror quarks decays into $W_H + q$, and the other one into $A_H + q$. For the values of f considered here the branching fraction $B(W_H \to WA_H)$ is above 90% [36], so we will here neglect other decays. We then get

$$q_H^+ q_H^- \longrightarrow q^+q^+W^-A_HA_H \tag{2.38}$$

as intermediate decay product. We will focus on channels where the W^- decays leptonically, and denote the corresponding lepton by l_*^-. The results for both cases can be found in the upper right blocks of Tab. 2.3 and Tab. 2.4, respectively. For case 1, the interesting channels are the same as before, just with the l_*^- added. Since the W^- from the W_H decay is strongly boosted, a rather strong cut can be imposed on the transverse energy of l_*^- as well as on the missing transverse energy. This will effectively reduce the SM background, making these channels suitable

for new physics searches, despite their somewhat smaller signal cross sections. Also for case 2 the cross sections are somewhat smaller than above. However due to the additional lepton, the same sign dilepton channel is enhanced, and furthermore the trilepton channel gets a sizeable cross section. In addition to the processes in the upper right block of Tab. 2.3 and Tab. 2.4 also the corresponding charge conjugate final states appear with the same cross sections. Combining both channels further increases the discovery reach in these decay modes.

Even more distinctive final states appear when both mirror quarks decay into $W_H + q$. Here we only consider channels where both W bosons originating from W_H's decay leptonically. Thus every final state contains two oppositely charged leptons with uncorrelated flavor. For case 1 the cross sections are rather small compared to those of the channels considered above, so we only list the two strongest ones, in the lower left block of Tab. 2.3. Note that the channel with four leptons in the final state only has a slightly larger cross section than the five lepton channel from the $A_H W_H$ decay modes. We therefore do not expect these two channels to be particularly important for the discovery of the model. For case 2 the situation is similar. The cross sections for the two most interesting channels are shown in Tab. 2.4. The second channel has four uncorrelated leptons, and could for example lead to $e^+e^+\mu^+\tau^-$ final states. While this channel is quite distinctive, it would require a higher luminosity than presently forseen.

Finally we consider the case where the mirror quark pair decays into two quarks and $A_H Z_H$. The novel feature here is that Z_H decays into the Higgs boson and A_H with a branching fraction of ~ 80 % [36]. We thus have processes of the form

$$q_H^+ q_H^- \longrightarrow q^+ q^- h A_H A_H. \tag{2.39}$$

The actual value of $B(Z_H \to h A_H)$ depends on the Higgs boson mass, but lies above $\sim 80\%$ as long as the Z_H is somewhat heavier than the decay products, i.e. $M_{Z_H} > m_h + M_{A_H}$. The number of Higgs bosons produced in this channel can be sizeable as illustrated in Tab. 2.3 and Tab. 2.4, respectively. Depending on the Higgs boson mass, the (very) final states vary and a more detailed analysis would be required if a signal would surface. In Tab. 2.3 we list the three channels with the largest cross section. The production rates for $h +$ jets and for $h +$ jets $+ \not{E}$ are sizeable, in total around 0.5 pb. This is similar to tth production in the SM, especially for larger values of the Higgs mass. The channel with a charged lepton pair produced along with the Higgs boson is particularly interesting. The signal is comparable to the SM background coming from Zh production, but can be distinguished by requiring additional jets from the q_H decays and by the fact that the lepton pair has an invariant mass M_{A_H}.

As expected, the cross sections are much smaller for case 2. We were still able to identify an interesting channel where the Higgs is produced along with two equally charged leptons. While the signal is rather small, the same is true for the

Same Sign Multilepton Rates			
$f = 750$ GeV		$f = 1500$ GeV	
Final State	σ[fb]	Final State	σ[fb]
$6j + l_*^+ l_*^+$	1.56	$l_*^+ l_*^+ +$ anything	0.256
$4j + l_*^+ l_*^+ + \not{E}$	0.89	$l_*^+ l_*^+ + l^+ +$ anything	0.115
$4j + l_*^+ l_*^+ + ll$	0.50		

Table 2.5: *Rates for same sign lepton signals, from $q_H^+ q_H^+$ pair decays. Notation as in Tab. 2.3 and "*anything*" stands for additional jets, leptons and/or missing energy from neutrinos.*

SM background. The results for this channel and for $h + 10$ jets production are shown in the lower right block of Tab. 2.4.

Next we will discuss the signals from decays of positively charged mirror quark pairs, $q_H^+ q_H^+$. Since the production rate for same sign mirror quark pairs is almost one order of magnitude smaller than the one for opposite sign mirror quarks, we will only consider decay modes that lead to a distinctive final state. These mainly come from processes where both mirror quarks decay into W_H^+ and a quark, leading to

$$q_H^+ q_H^+ \longrightarrow q^- q^- W^+ W^+ A_H A_H. \tag{2.40}$$

To be sensitive to the charges we only consider leptonic decays of the W bosons, leading to two positively charged hard leptons which we will again denote by l_*^+.

The signal rates for both case 1 and case 2 can be found in Tab. 2.5. Since we require leptonic decays of at least two W bosons, the signal rates for both cases are rather small. With suitable cuts on the transverse momentum of the two hard leptons it should still be possible to efficiently remove the SM background.

T-odd gauge bosons in general provide a cleaner signature, since less particles are produced in their decay. However the cross section for T-odd gauge boson pair production is rather small. For the values of f and κ chosen here at least ten times more T-odd gauge bosons are produced in the decays of mirror quarks.

Furthermore it is hard to distinguish directly produced T-odd gauge bosons from those coming from mirror quark decays. The reason is that while the possible final states differ in the total number of jets, that number is rather large for most processes and thus would require a full reconstruction of all events to be measured.

A comment on the effects of a variation of the free parameters is in order.

If f is increased further, all T-odd particle masses are increased and the cross sections for all processes go down, while the final states and their branching fractions remain essentially unchanged.

Changing κ, on the contrary, changes the results more significantly because it affects the mirror quark mass m_{q_H} while leaving the heavy gauge boson masses unchanged . If κ goes below 0.45, the decays into most T-odd gauge bosons become inaccessible, leaving $A_H + q$ as the only two-body final state. In that case direct T-odd gauge boson pair production becomes important, since W_H and Z_H are not obtained from q_H decays anymore. The extreme case where the mirror quarks are also lighter than A_H will be discussed in the next chapter. On the other hand, if κ is increased, the cross section for $q_H q_H$ pair production decreases while at the same time most cross sections for T-odd gauge boson pair production increase, as has been shown in [47]. A further effect is that the branching fractions of q_H change, with the branching fraction $B(q_H \to qW_H)$ reaching around 60%, while $B(q_H \to qA_H)$ drops below the 10% level.

The T-odd gauge boson pair production rates are affected differently by increasing κ. While the cross section for $pp \to W_H^+ Z_H$ increases, the one for $pp \to W_H^+ A_H$ is reduced [47]. If the mirror quarks are very heavy and only the T-odd gauge bosons are accessible, the ratio of these cross sections provides a possibility to measure m_{q_H} indirectly.

While inclusion of the WZW term leads to many new signatures of the Littlest Higgs model at LHC, none of the processes discussed above is actually sensitive to its integer parameter N. The reason is that vertices containing the WZW term only appear in decays, and all partial width are multiplied by the same power of N. Measuring the total width of A_H could in principle give access to N, however in practice a width of the order of one eV is not measurable. The same problem appears if one tries to measure the T-violating partial widths in the decays of other T-odd particles like W_H. T-violating decays into two gauge bosons can be distinguished from T-conserving decays by measuring the distribution of the angle between the outgoing gauge bosons and the polarization axis of W_H [34]. In practice however the T-violating partial width is too small for this analysis to be feasible.

Single T-odd gauge boson production via gauge boson fusion would give direct access to N. This process is not in the reach of LHC, but might be detectable at a very luminous linear collider.

2.4.5 The Case of a fermionic LTOP

The masses of the mirror fermions are free parameters in the LHT, determined by the parameters κ_i. Thus in principle some of them could be lighter than the lightest T-odd gauge boson A_H. With T-parity broken these fermions are unstable, so any of them could be the lightest T-odd particle (LTOP).

Since the WZW term breaks T-parity directly only in the gauge sector, the simplest decay process is a three body decay mediated by a virtual T-odd gauge boson. Loop induced two body decays can be of similar importance. The most relevant diagrams are similar to those shown in Fig. 2.2, with the A_H replaced by a Z or W boson and one of the external fermions replaced by the fermionic LTOP f_H. Major decay channels therefore are $f_H \to Zf$, $f_H \to W\tilde{f}$ and $f_H \to A_H^* f$. The last channel will either yield a three fermion final state $f'\bar{f}'f$ or a VVf final state with two SM gauge bosons, depending on the mass of f_H and A_H and the kinematics of the decay.

We will now briefly discuss how this could affect the phenomenology at hadron colliders. If f_H is a T-odd quark, it will be pair produced directly in sizeable amounts and decay as discussed above. Furthermore most of the directly produced T-odd gauge bosons will decay into $f_H f$ pairs, since the direct decay into SM particles via the WZW term is suppressed in general. If the mirror quark masses are somewhat hierarchical, one could also imagine longer decay chains, with the branching fractions depending on the flavor structure of the mirror quark sector.

Even more appealing is the case where f_H is a lepton. While their direct production rate is small in that case, the pair produced mirror quarks will now decay via long chains:

$$q_H \longrightarrow A_H q \longrightarrow l_H^{\pm} l^{\mp} q \longrightarrow \ldots, \tag{2.41}$$

$$q_H \longrightarrow W_H q \longrightarrow A_H W q \longrightarrow l_H^{\pm} f^{\mp} W q \longrightarrow \ldots \tag{2.42}$$

Studying these novel collider signatures of the Littlest Higgs model in more detail would certainly be interesting.

2.5 Conclusion

In this chapter we have considered some phenomenological consequences of the natural T-parity breaking Wess-Zumino-Witten term in the effective Lagrangian of the classically T-parity invariant Littlest Higgs model. In particular we have calculated the loop induced decays of the heavy photon A_H into normal fermion pairs, assuming A_H to be the lightest T-odd particle. These complement the known tree level decays into normal gauge bosons [36] and are the dominant modes for breaking scales below 1 TeV. For these values, the effect is quite distinct and changes the phenomenology of the model substantially, because A_H appears as a decay product of any other T-odd particle. Due to its small prefactor the Wess-Zumino-Witten term only makes a negligible contribution to electroweak precision observables.

The new decay modes typically give rise to final states with many jets. Comparing with published data from other new physics searches at the Tevatron, this leads to improved bounds on the mass of the heavy quarks q_H for values of the

breaking scale below 1 TeV. If q_H is heavier than A_H, the new decays of the latter induce new decays of q_H. In particular, as illustrated in Figure 2.6, six jet events give rise to a quite strict limit on m_{q_H} of 350 GeV for $f = 750$ GeV. But the present study gives only a rough picture and a refined analysis would be necessary for more accurate results.

At the LHC, the situation is even better. For $q_H\bar{q}_H$ pairs , their decays into light quarks (antiquarks) and A_H would lead to the same final states as discussed above. But because of the higher energy, larger heavy quark masses can be probed, where decays of the form $q_H \to q + W_H$ are possible, leading to very distinctive finale states which may be distinguished from SM background. Of particular interest in this respect are final states with four leptons. Even more tantalizing are processes involving a Z_H boson decaying through a Higgs boson. The production rate for h+jets (and missing energy) from these processes is sizeable, possibly comparable to the SM top associated Higgs boson production rate, although highly dependent on f and the masses m_{q_H}. For a moderately heavy Higgs ($m_h \sim 200$ GeV), and a mirror mass around $m_{q_H} \sim 350 - 400$ GeV as well as $f \sim 500$ GeV, the production rate can be of the order of 10 pb or more. This is important since other Higgs production channels are reduced in the Littlest Higgs model [50]. The production of two equally charged heavy particles, $q_H^{\pm}q_H^{\pm}$, is possible, yielding striking same-sign lepton signatures but small rates.

In this work we have not considered associated production of heavy quarks with heavy gauge bosons and production of the top quark partners, since pair production of first generation heavy quarks has a substantially larger cross section and thus is more suitable for a first new physics discovery. Nevertheless, a detailed analysis of those processes would be interesting for future work since they could reveal additional information about the model structure.

Because of the small T-violating branching ratios, singly produced T-odd particles are practically non-observable and thus only pair production is phenomenologically relevant.

Finally we have also considered the case of a fermionic lightest T-odd particle. This would lead to still different signatures that will have to be worked out in detail.

2.6 Appendix: T-odd gauge invariant counterterms

The counterterms (2.27) introduced in section 2.3 are not invariant under the global symmetries or gauge transformations because they were constructed to cancel divergencies in particular diagrams. In general, couplings between heavy gauge bosons and SM fermions cannot be written as covariant derivatives in a fermionic kinetic term. Similarly, counterterms involving T-odd gauge bosons as

well as the massive standard model gauge bosons also need to be present; again they do not surface in a symmetric way at first. We note however that the simple counterterms in (2.27) are only required to cancel divergencies affecting broken gauge symmetries and thus no $U(1)_{em}$ breaking counterterms are required.

As is well know in chiral perturbation theory, one can do better and construct directly the required symmetric counterterms, [51]. Also in the present case we can rewrite the counterterms in a form that preserves gauge invariance and furthermore reflect the underlying $SU(5)$ symmetric structure of the models. The point is to insert the non-linear sigma model field Σ into the covariant derivative for the fermions, to define objects with well-defined transformations properties, such as vectorial and axial currents and consider appropriate powers of them. We do not give a systematic exposition here but refer to a future publication. For the purely mesonic WZW term, such a complete analysis was given in [52].

As illustration of the procedure, the counterterms for the diagram in Fig. 2.2 (b) could have contributions from a term

$$c_{ct}\bar{f}Q_W^2(\Sigma^\dagger D_\mu\Sigma - \Sigma D_\mu\Sigma^\dagger)\gamma^\mu P_L f. \tag{2.43}$$

Here $f = (\psi_1, 0, \psi_2)^T$ contains the lefthanded fermion doublets ψ_1 and ψ_2 that yield the lefthanded SM fermions $\psi_{SM} = \frac{1}{\sqrt{2}}(\psi_1 - \psi_2)$ as well as their mirror partners $\psi_H = \frac{1}{\sqrt{2}}(\psi_1 + \psi_2)$. The 5×5 matrix Q_W is defined as $Q_W = Q^+ + Q^-$, where Q^+ and Q^- are the generators of the W^+ and W^- bosons that run in the loop, and c_{ct} is an appropriate coefficient for the counterterm.

This term is gauge invariant. Upon electroweak symmetry breaking it generates counterterms at order v^2/f^2 as required to match the results of Tab. 2.1. The righthanded fermions are gauge singlets, so their counterterms have to be generated differently. A possible term is

$$c_{ct}\bar{f}\gamma^\mu P_R f \,\mathrm{Tr}\left[Q_W^2(\Sigma^\dagger D_\mu\Sigma - \Sigma D_\mu\Sigma^\dagger)\right]. \tag{2.44}$$

Counterterms of this form were introduced in [53] where they are used to regularize the divergencies in the loop induced decay of the neutral pion π^0 into lepton pairs, a process that is similar to the decay of A_H into lepton pairs as discussed in section 2.3.

2.7 Appendix: Feynman rules for the LHT with WZW term

The Feynman rules for the original Littlest Higgs model are listed in Ref. [54]. An almost complete collection (to leading order in $1/f$) of Feynman rules for the Littlest Higgs model with T-parity, including flavor effects, can be found in Ref. [38].

In Tabs. 2.6–2.13 we provide the additional Feynman rules introduced by the WZW term after anomaly cancellation, to leading order in $(1/f)$. The small mixing between A_H and Z_H is neglected since it is numerically less important than other subleading $(1/f)$ corrections.

We use the conventions of Ref. [56] with all momenta incoming. The Feynman rules can be translated to CalcHEP conventions by multiplying each vertex with $(-i)$ and changing $p_i^\mu \to -p_i^\mu$ for all momenta in the vertex. We work in a general covariant gauge. An overall factor $\hat{N} = \frac{N}{48\pi^2}$ has been factored out from all the Feynman rules. Vertices that are zero have been omitted.

Particles			**Vertices**
$A_{H\mu}$	W_ν^+	W_ρ^-	$-\frac{6}{5}\frac{e^3v^2}{c_w s_w^2 f^2}\varepsilon_{\mu\nu\rho\sigma}\left(p_2^\sigma - p_3^\sigma\right)$
$A_{H\mu}$	Z_ν	Z_ρ	$-\frac{6}{5}\frac{e^3v^2}{c_w^3 s_w^2 f^2}\varepsilon_{\mu\nu\rho\sigma}\left(p_2^\sigma - p_3^\sigma\right)$
A_μ	W_ν^+	$W_{H\,\rho}^-$	$\frac{e^3v^2}{s_w^2 f^2}\varepsilon_{\mu\nu\rho\sigma}\left(p_2^\sigma + p_3^\sigma - 2p_1^\sigma\right)$
A_μ	W_ν^-	$W_{H\,\rho}^+$	$\frac{e^3v^2}{s_w^2 f^2}\varepsilon_{\mu\nu\rho\sigma}\left(p_3^\sigma + p_2^\sigma - 2p_1^\sigma\right)$
$A_{H\mu}$	$A_{H\nu}$	$Z_{H\rho}$	$-\frac{4}{5}\frac{e^3v^2}{c_w^2 s_w f^2}\varepsilon_{\mu\nu\rho\sigma}\left(p_1^\sigma - p_2^\sigma\right)$
$A_{H\mu}$	$W_{H\,\nu}^+$	$W_{H\,\rho}^-$	$-\frac{4}{5}\frac{e^3v^2}{c_w s_w^2 f^2}\varepsilon_{\mu\nu\rho\sigma}\left(p_2^\sigma - p_3^\sigma\right)$
$A_{H\mu}$	$Z_{H\nu}$	$Z_{H\rho}$	$\frac{4}{5}\frac{e^3v^2}{c_w s_w^2 f^2}\varepsilon_{\mu\nu\rho\sigma}\left(p_3^\sigma - p_2^\sigma\right)$
W_μ^+	W_ν^-	$Z_{H\rho}$	$-\frac{e^3v^2}{s_w^3 f^2}\varepsilon_{\mu\nu\rho\sigma}\left(p_2^\sigma - p_1^\sigma\right)$
W_μ^+	$W_{H\,\nu}^-$	Z_ρ	$-\frac{e^3v^2}{c_w s_w^3 f^2}\varepsilon_{\mu\nu\rho\sigma}\left((1+s_w^2)p_1^\sigma - 2s_w^2 p_3^\sigma - c_w^2 p_2^\sigma\right)$
W_μ^-	$W_{H\,\nu}^+$	Z_ρ	$\frac{e^3v^2}{c_w s_w^3 f^2}\varepsilon_{\mu\nu\rho\sigma}\left(c_w^2 p_2^\sigma + 2s_w^2 p_3^\sigma - (1+s_w^2)p_1^\sigma\right)$
$W_{H\,\mu}^+$	$W_{H\,\nu}^-$	$Z_{H\rho}$	$\frac{e^3v^2}{s_w^3 f^2}\varepsilon_{\mu\nu\rho\sigma}\left(p_1^\sigma - p_2^\sigma\right)$
Z_μ	Z_ν	$Z_{H\rho}$	$-2\frac{e^3v^2}{c_w^2 s_w^3 f^2}\varepsilon_{\mu\nu\rho\sigma}\left(p_2^\sigma - p_1^\sigma\right)$

Table 2.6: *T-parity violating three gauge boson vertices. The momenta $p_{1,2,3}$ correspond to the particle in the first, second, and third column, respectively.*

Particles				**Vertices**
A_μ	$A_{H\nu}$	W^+_ρ	W^-_σ	$\frac{12}{5}\frac{e^4v^2}{c_w s_w^2 f^2}\varepsilon_{\mu\nu\rho\sigma}$
A_μ	$A_{H\nu}$	$W^+_{H\,\rho}$	$W^-_{H\,\sigma}$	$\frac{8}{5}\frac{e^4v^2}{c_w s_w^2 f^2}\varepsilon_{\mu\nu\rho\sigma}$
A_μ	W^+_ν	W^-_ρ	$Z_{H\sigma}$	$-2\frac{e^4v^2}{s_w^3 f^2}\varepsilon_{\mu\nu\rho\sigma}$
A_μ	W^+_ν	$W^-_{H\,\rho}$	Z_σ	$2\frac{e^4v^2}{c_w s_w^3 f^2}\varepsilon_{\mu\nu\rho\sigma}$
A_μ	W^-_ν	$W^+_{H\,\rho}$	Z_σ	$-2\frac{e^4v^2}{c_w s_w^3 f^2}\varepsilon_{\mu\nu\rho\sigma}$
A_μ	$W^+_{H\,\nu}$	$W^-_{H\,\rho}$	$Z_{H\sigma}$	$-2\frac{e^4v^2}{s_w^3 f^2}\varepsilon_{\mu\nu\rho\sigma}$
$A_{H\mu}$	W^+_ν	W^-_ρ	Z_σ	$-\frac{6}{5}\frac{(3-2s_w^2)e^4v^2}{c_w^2 s_w^3 f^2}\varepsilon_{\mu\nu\rho\sigma}$
$A_{H\mu}$	W^+_ν	$W^-_{H\,\rho}$	$Z_{H\sigma}$	$-\frac{4}{5}\frac{e^4v^2}{c_w s_w^3 f^2}\varepsilon_{\mu\nu\rho\sigma}$
$A_{H\mu}$	W^-_ν	$W^+_{H\,\rho}$	$Z_{H\sigma}$	$\frac{4}{5}\frac{e^4v^2}{c_w s_w^3 f^2}\varepsilon_{\mu\nu\rho\sigma}$
$A_{H\mu}$	$W^+_{H\,\nu}$	$W^-_{H\,\rho}$	Z_σ	$-\frac{4}{5}\frac{(1-2s_w^2)e^4v^2}{c_w^2 s_w^3 f^2}\varepsilon_{\mu\nu\rho\sigma}$
W^+_μ	W^-_ν	Z_ρ	$Z_{H\sigma}$	$-2\frac{(2-s_w^2)e^4v^2}{c_w s_w^4 f^2}\varepsilon_{\mu\nu\rho\sigma}$
$W^+_{H\,\mu}$	$W^-_{H\,\nu}$	Z_ρ	$Z_{H\sigma}$	$-2\frac{c_w e^4v^2}{s_w^4 f^2}\varepsilon_{\mu\nu\rho\sigma}$

Table 2.7: *T-parity violating vertices with four gauge bosons.*

Particles			**Vertices**
W^+_μ	$W^-_{H\,\nu}$	h	$\frac{e^2v}{s_w^2 f^2}\varepsilon_{\mu\nu\rho\sigma}\left(p_2^\rho - p_1^\rho\right)p_3^\sigma$
W^-_μ	$W^+_{H\,\nu}$	h	$\frac{e^2v}{s_w^2 f^2}\varepsilon_{\mu\nu\rho\sigma}\left(p_1^\rho - p_2^\rho\right)p_3^\sigma$

Table 2.8: *T-parity violating vertices with one physical scalar and two gauge bosons. The momenta $p_{1,2,3}$ correspond to the particle in the first, second, and third column, respectively.*

Particles				Vertices
A_μ	W^+_ν	$W^-_{H\,\rho}$	h	$2-\frac{e^3v}{s_w^2f^2}\varepsilon_{\mu\nu\rho\sigma}\big(p_2^\sigma+p_3^\sigma-2p_1^\sigma\big)$
A_μ	W^-_ν	$W^+_{H\,\rho}$	h	$-2\frac{e^3v}{s_w^2f^2}\varepsilon_{\mu\nu\rho\sigma}\big(p_3^\sigma+p_2^\sigma-2p_1^\sigma\big)$
$A_{H\mu}$	$A_{H\nu}$	$Z_{H\,\rho}$	h	$\frac{8}{5}\frac{e^3v}{c_w^2s_wf^2}\varepsilon_{\mu\nu\rho\sigma}\big(p_1^\sigma-p_2^\sigma\big)$
$A_{H\mu}$	W^+_ν	W^-_ρ	h	$\frac{12}{5}\frac{e^3v}{c_ws_w^2f^2}\varepsilon_{\mu\nu\rho\sigma}\big(p_2^\sigma-p_3^\sigma\big)$
$A_{H\mu}$	$W^+_{H\,\nu}$	$W^-_{H\,\rho}$	h	$\frac{8}{5}\frac{e^3v}{c_ws_w^2f^2}\varepsilon_{\mu\nu\rho\sigma}\big(p_2^\sigma-p_3^\sigma\big)$
$A_{H\mu}$	Z_ν	Z_ρ	h	$-\frac{12}{5}\frac{e^3v}{c_w^3s_w^2f^2}\varepsilon_{\mu\nu\rho\sigma}\big(p_3^\sigma-p_2^\sigma\big)$
$A_{H\mu}$	$Z_{H\nu}$	$Z_{H\,\rho}$	h	$\frac{8}{5}\frac{e^3v}{c_ws_w^2f^2}\varepsilon_{\mu\nu\rho\sigma}\big(p_2^\sigma-p_3^\sigma\big)$
W^+_μ	W^-_ν	$Z_{H\,\rho}$	h	$2\frac{e^3v}{s_w^3f^2}\varepsilon_{\mu\nu\rho\sigma}\big(p_2^\sigma-p_1^\sigma\big)$
W^+_μ	$W^-_{H\,\nu}$	Z_ρ	h	$2\frac{e^3v}{c_ws_w^3f^2}\varepsilon_{\mu\nu\rho\sigma}\big((1+s_w^2)p_1^\sigma-2s_w^2p_3^\sigma-c_w^2p_2^\sigma\big)$
W^-_μ	$W^+_{H\,\nu}$	Z_ρ	h	$-2\frac{e^3v}{c_ws_w^3f^2}\varepsilon_{\mu\nu\rho\sigma}\big(c_w^2p_2^\sigma+2s_w^2p_3^\sigma-(1+s_w^2)p_1^\sigma\big)$
$W^+_{H\,\mu}$	$W^-_{H\,\nu}$	$Z_{H\,\rho}$	h	$-2\frac{e^3v}{s_w^3f^2}\varepsilon_{\mu\nu\rho\sigma}\big(p_1^\sigma-p_2^\sigma\big)$
Z_μ	Z_ν	$Z_{H\,\rho}$	h	$4\frac{e^3v}{c_w^2s_w^3f^2}\varepsilon_{\mu\nu\rho\sigma}\big(p_2^\sigma-p_1^\sigma\big)$

Table 2.9: *T-parity violating vertices with one physical scalar and three gauge bosons. The momenta $p_{1,2,3,4}$ correspond to the particle in the first, second, third and fourth column, respectively.*

Particles			Vertices
$A_{H\mu}$	$W^\pm_\nu$	$G^\mp$	$\mp\frac{6}{5}\frac{e^2v}{c_ws_wf^2}\varepsilon_{\mu\nu\rho\sigma}\,p_3^\rho\big(p_1^\sigma-p_2^\sigma\big)$
$A_{H\mu}$	Z_ν	G^0	$-\frac{6}{5}\frac{ie^2v}{c_w^2s_wf^2}\varepsilon_{\mu\nu\rho\sigma}\,p_3^\rho\big(p_1^\sigma-p_2^\sigma\big)$
$W^\pm_{H\mu}$	A_ν	$G^\mp$	$\mp3\frac{e^2v}{s_wf^2}\varepsilon_{\mu\nu\rho\sigma}\,p_3^\rho\big(p_1^\sigma-p_2^\sigma\big)$
$Z_{H\mu}$	$W^\pm_\nu$	$G^\mp$	$\pm\frac{e^2v}{s_w^2f^2}\varepsilon_{\mu\nu\rho\sigma}\,p_3^\rho\big(p_1^\sigma-p_2^\sigma\big)$
$W^\pm_{H\mu}$	Z_ν	$G^\mp$	$\mp\frac{e^2(c_w^2-2s_w^2)v}{c_ws_w^2f^2}\varepsilon_{\mu\nu\rho\sigma}\,p_3^\rho\big(p_1^\sigma-p_2^\sigma\big)$
$W^\pm_{H\mu}$	$W^\pm_\nu$	G^0	$2\frac{ie^2v}{s_w^2f^2}\varepsilon_{\mu\nu\rho\sigma}\,p_3^\rho\big(p_1^\sigma-p_2^\sigma\big)$
$Z_{H\mu}$	Z_ν	G^0	$2\frac{ie^2v}{c_ws_w^2f^2}\varepsilon_{\mu\nu\rho\sigma}\,p_3^\rho\big(p_1^\sigma-p_2^\sigma\big)$

Table 2.10: *T-parity violating vertices with one SM Goldstone and two gauge bosons. The momenta $p_{1,2,3}$ correspond to the particle in the first, second, and third column, respectively.*

Particles				**Vertices**
A_μ	$A_{H\nu}$	Φ^+	Φ^-	$\frac{2}{5}\frac{e^2}{c_w f^2}\varepsilon_{\mu\nu\rho\sigma}\left(p_1^\rho p_4^\sigma - p_2^\rho p_4^\sigma - p_1^\rho p_3^\sigma + p_2^\rho p_3^\sigma - 2p_3^\rho p_4^\sigma\right)$
A_μ	$A_{H\nu}$	Φ^{++}	Φ^{--}	$\frac{4}{5}\frac{e^2}{c_w f^2}\varepsilon_{\mu\nu\rho\sigma}\left(p_1^\rho p_4^\sigma - p_2^\rho p_4^\sigma - p_1^\rho p_3^\sigma + p_2^\rho p_3^\sigma - 2p_3^\rho p_4^\sigma\right)$
A_μ	$W_{H\,\nu}^+$	Φ^+	Φ^{--}	$-2\frac{e^2}{s_w f^2}\varepsilon_{\mu\nu\rho\sigma}\left(p_2^\rho p_4^\sigma - p_1^\rho p_3^\sigma + p_2^\rho p_3^\sigma - p_1^\rho p_4^\sigma\right)$
A_μ	$W_{H\,\nu}^+$	Φ^-	Φ^0	$\frac{e^2\cdot\sqrt{2}}{s_w f^2}\varepsilon_{\mu\nu\rho\sigma}\left(3p_1^\rho p_3^\sigma + p_2^\rho p_4^\sigma - p_1^\rho p_4^\sigma - 3p_2^\rho p_3^\sigma + 4p_3^\rho p_4^\sigma\right)$
A_μ	$W_{H\,\nu}^+$	Φ^-	Φ^p	$\frac{ie^2\cdot\sqrt{2}}{s_w f^2}\varepsilon_{\mu\nu\rho\sigma}\left(3p_1^\rho p_3^\sigma + p_2^\rho p_4^\sigma - p_1^\rho p_4^\sigma - 3p_2^\rho p_3^\sigma + 4p_3^\rho p_4^\sigma\right)$
A_μ	$W_{H\,\nu}^-$	Φ^+	Φ^0	$-\frac{e^2\cdot\sqrt{2}}{s_w f^2}\varepsilon_{\mu\nu\rho\sigma}\left(p_2^\rho p_4^\sigma + 3p_1^\rho p_3^\sigma - 3p_2^\rho p_3^\sigma - p_1^\rho p_4^\sigma + 4p_3^\rho p_4^\sigma\right)$
A_μ	$W_{H\,\nu}^-$	Φ^+	Φ^p	$\frac{ie^2\cdot\sqrt{2}}{s_w f^2}\varepsilon_{\mu\nu\rho\sigma}\left(p_2^\rho p_4^\sigma + 3p_1^\rho p_3^\sigma - 3p_2^\rho p_3^\sigma - p_1^\rho p_4^\sigma + 4p_3^\rho p_4^\sigma\right)$
A_μ	$W_{H\,\nu}^-$	Φ^{++}	Φ^-	$-2\frac{e^2}{s_w f^2}\varepsilon_{\mu\nu\rho\sigma}\left(p_1^\rho p_4^\sigma - p_2^\rho p_3^\sigma + p_1^\rho p_3^\sigma - p_2^\rho p_4^\sigma\right)$
A_μ	$Z_{H\nu}$	Φ^+	Φ^-	$6\frac{e^2}{s_w f^2}\varepsilon_{\mu\nu\rho\sigma}\left(p_1^\rho p_4^\sigma - p_2^\rho p_4^\sigma - p_1^\rho p_3^\sigma + p_2^\rho p_3^\sigma - 2p_3^\rho p_4^\sigma\right)$
A_μ	$Z_{H\nu}$	Φ^{++}	Φ^{--}	$4\frac{e^2}{s_w f^2}\varepsilon_{\mu\nu\rho\sigma}\left(p_1^\rho p_4^\sigma - p_2^\rho p_4^\sigma - p_1^\rho p_3^\sigma + p_2^\rho p_3^\sigma - 2p_3^\rho p_4^\sigma\right)$
$A_{H\mu}$	W_ν^+	Φ^+	Φ^{--}	$\frac{2}{5}\frac{e^2}{c_w s_w f^2}\varepsilon_{\mu\nu\rho\sigma}\left(p_1^\rho p_4^\sigma - p_2^\rho p_4^\sigma + p_2^\rho p_3^\sigma - p_1^\rho p_3^\sigma + 2p_3^\rho p_4^\sigma\right)$
$A_{H\mu}$	W_ν^+	Φ^-	Φ^0	$\frac{1}{5}\frac{e^2\cdot\sqrt{2}}{c_w s_w f^2}\varepsilon_{\mu\nu\rho\sigma}\left(p_1^\rho p_3^\sigma - p_2^\rho p_3^\sigma + p_2^\rho p_4^\sigma - p_1^\rho p_4^\sigma - 2p_3^\rho p_4^\sigma\right)$
$A_{H\mu}$	W_ν^+	Φ^-	Φ^p	$\frac{1}{5}\frac{ie^2\cdot\sqrt{2}}{c_w s_w f^2}\varepsilon_{\mu\nu\rho\sigma}\left(p_1^\rho p_3^\sigma - p_2^\rho p_3^\sigma + p_2^\rho p_4^\sigma - p_1^\rho p_4^\sigma - 2p_3^\rho p_4^\sigma\right)$
$A_{H\mu}$	W_ν^-	Φ^+	Φ^0	$-\frac{1}{5}\frac{e^2\cdot\sqrt{2}}{c_w s_w f^2}\varepsilon_{\mu\nu\rho\sigma}\left(p_2^\rho p_4^\sigma - p_1^\rho p_4^\sigma + p_1^\rho p_3^\sigma - p_2^\rho p_3^\sigma - 2p_3^\rho p_4^\sigma\right)$
$A_{H\mu}$	W_ν^-	Φ^+	Φ^p	$\frac{1}{5}\frac{ie^2\cdot\sqrt{2}}{c_w s_w f^2}\varepsilon_{\mu\nu\rho\sigma}\left(p_2^\rho p_4^\sigma - p_1^\rho p_4^\sigma + p_1^\rho p_3^\sigma - p_2^\rho p_3^\sigma - 2p_3^\rho p_4^\sigma\right)$
$A_{H\mu}$	W_ν^-	Φ^{++}	Φ^-	$-\frac{2}{5}\frac{e^2}{c_w s_w f^2}\varepsilon_{\mu\nu\rho\sigma}\left(p_2^\rho p_4^\sigma - p_1^\rho p_4^\sigma + p_1^\rho p_3^\sigma - p_2^\rho p_3^\sigma - 2p_3^\rho p_4^\sigma\right)$
$A_{H\mu}$	Z_ν	Φ^+	Φ^-	$-\frac{2}{5}\frac{e^2 s_w}{c_w^2 f^2}\varepsilon_{\mu\nu\rho\sigma}\left(p_1^\rho p_4^\sigma - p_2^\rho p_4^\sigma - p_1^\rho p_3^\sigma + p_2^\rho p_3^\sigma + 2p_3^\rho p_4^\sigma\right)$
$A_{H\mu}$	Z_ν	Φ^{++}	Φ^{--}	$\frac{2}{5}\frac{(1-2s_w^2)e^2}{c_w^2 s_w f^2}\varepsilon_{\mu\nu\rho\sigma}\left(p_1^\rho p_4^\sigma - p_2^\rho p_4^\sigma - p_1^\rho p_3^\sigma + p_2^\rho p_3^\sigma + 2p_3^\rho p_4^\sigma\right)$
$A_{H\mu}$	Z_ν	Φ^0	Φ^p	$-\frac{2}{5}\frac{ie^2}{c_w^2 s_w f^2}\varepsilon_{\mu\nu\rho\sigma}\left(p_1^\rho p_3^\sigma - p_2^\rho p_3^\sigma - p_1^\rho p_4^\sigma + p_2^\rho p_4^\sigma - 2p_3^\rho p_4^\sigma\right)$
W_μ^+	$W_{H\,\nu}^+$	Φ^{--}	Φ^0	$-2\frac{e^2\cdot\sqrt{2}}{s_w^2 f^2}\varepsilon_{\mu\nu\rho\sigma}\left(p_1^\rho p_3^\sigma - p_2^\rho p_3^\sigma + p_2^\rho p_4^\sigma - p_1^\rho p_4^\sigma + 2p_3^\rho p_4^\sigma\right)$
W_μ^+	$W_{H\,\nu}^+$	Φ^{--}	Φ^p	$-2\frac{ie^2\cdot\sqrt{2}}{s_w^2 f^2}\varepsilon_{\mu\nu\rho\sigma}\left(p_1^\rho p_3^\sigma - p_2^\rho p_3^\sigma + p_2^\rho p_4^\sigma - p_1^\rho p_4^\sigma + 2p_3^\rho p_4^\sigma\right)$
W_μ^+	$W_{H\,\nu}^-$	h	h	$\frac{e^2}{s_w^2 f^2}\varepsilon_{\mu\nu\rho\sigma}\left(p_2^\rho p_3^\sigma - p_1^\rho p_3^\sigma + p_2^\rho p_4^\sigma - p_1^\rho p_4^\sigma\right)$
W_μ^+	$W_{H\,\nu}^-$	Φ^p	Φ^p	$-2\frac{e^2}{s_w^2 f^2}\varepsilon_{\mu\nu\rho\sigma}\left(p_1^\rho p_3^\sigma - p_2^\rho p_3^\sigma + p_1^\rho p_4^\sigma - p_2^\rho p_4^\sigma\right)$

Table 2.11: *T-parity violating vertices with two scalars and two gauge bosons. The momenta $p_{1,2,3,4}$ correspond to the particle in the first, second, third and fourth column, respectively.* Continued in Tabs. 2.12 and 2.13

Particles				Vertices
W_μ^+	$Z_{H\nu}$	Φ^+	Φ^{--}	$4\frac{e^2}{s_w^2 f^2}\varepsilon_{\mu\nu\rho\sigma}\, p_4^\sigma \left(p_2^\rho - p_1^\rho + p_3^\rho\right)$
W_μ^+	$Z_{H\nu}$	Φ^-	Φ^0	$-2\frac{e^2\cdot\sqrt{2}}{s_w^2 f^2}\varepsilon_{\mu\nu\rho\sigma}\, p_4^\sigma \left(p_1^\rho - p_2^\rho - p_3^\rho\right)$
W_μ^+	$Z_{H\nu}$	Φ^-	Φ^p	$-2\frac{ie^2\cdot\sqrt{2}}{s_w^2 f^2}\varepsilon_{\mu\nu\rho\sigma}\, p_4^\sigma \left(p_1^\rho - p_2^\rho - p_3^\rho\right)$
W_μ^-	$W_{H\nu}^+$	h	h	$\frac{e^2}{s_w^2 f^2}\varepsilon_{\mu\nu\rho\sigma}\left(p_1^\rho p_3^\sigma - p_2^\rho p_3^\sigma + p_1^\rho p_4^\sigma - p_2^\rho p_4^\sigma\right)$
W_μ^-	$W_{H\nu}^+$	Φ^+	Φ^-	$2\frac{e^2}{s_w^2 f^2}\varepsilon_{\mu\nu\rho\sigma}\left(p_1^\rho p_4^\sigma - p_2^\rho p_4^\sigma + p_2^\rho p_3^\sigma - p_1^\rho p_3^\sigma - 2p_3^\rho p_4^\sigma\right)$
W_μ^-	$W_{H\nu}^+$	Φ^{++}	Φ^{--}	$-2\frac{e^2}{s_w^2 f^2}\varepsilon_{\mu\nu\rho\sigma}\left(p_2^\rho p_4^\sigma + 3p_1^\rho p_3^\sigma - 3p_2^\rho p_3^\sigma - p_1^\rho p_4^\sigma + 4p_3^\rho p_4^\sigma\right)$
W_μ^-	$W_{H\nu}^+$	Φ^0	Φ^0	$-2\frac{e^2}{s_w^2 f^2}\varepsilon_{\mu\nu\rho\sigma}\left(p_2^\rho p_3^\sigma - p_1^\rho p_3^\sigma + p_2^\rho p_4^\sigma - p_1^\rho p_4^\sigma\right)$
W_μ^-	$W_{H\nu}^+$	Φ^0	Φ^p	$4\frac{ie^2}{s_w^2 f^2}\varepsilon_{\mu\nu\rho\sigma}\left(p_1^\rho p_3^\sigma - p_1^\rho p_4^\sigma + p_2^\rho p_4^\sigma - p_2^\rho p_3^\sigma + 2p_3^\rho p_4^\sigma\right)$
W_μ^-	$W_{H\nu}^+$	Φ^p	Φ^p	$-2\frac{e^2}{s_w^2 f^2}\varepsilon_{\mu\nu\rho\sigma}\left(p_2^\rho p_3^\sigma - p_1^\rho p_3^\sigma + p_2^\rho p_4^\sigma - p_1^\rho p_4^\sigma\right)$
W_μ^-	$W_{H\nu}^-$	Φ^{++}	Φ^0	$-2\frac{e^2\cdot\sqrt{2}}{s_w^2 f^2}\varepsilon_{\mu\nu\rho\sigma}\left(p_1^\rho p_4^\sigma - p_2^\rho p_4^\sigma + p_2^\rho p_3^\sigma - p_1^\rho p_3^\sigma - 2p_3^\rho p_4^\sigma\right)$
W_μ^-	$W_{H\nu}^-$	Φ^{++}	Φ^p	$2\frac{ie^2\cdot\sqrt{2}}{s_w^2 f^2}\varepsilon_{\mu\nu\rho\sigma}\left(p_1^\rho p_4^\sigma - p_2^\rho p_4^\sigma + p_2^\rho p_3^\sigma - p_1^\rho p_3^\sigma - 2p_3^\rho p_4^\sigma\right)$
W_μ^-	$Z_{H\nu}$	Φ^+	Φ^0	$2\frac{e^2\cdot\sqrt{2}}{s_w^2 f^2}\varepsilon_{\mu\nu\rho\sigma}\, p_4^\sigma \left(p_1^\rho - p_2^\rho - p_3^\rho\right)$
W_μ^-	$Z_{H\nu}$	Φ^+	Φ^p	$-2\frac{ie^2\cdot\sqrt{2}}{s_w^2 f^2}\varepsilon_{\mu\nu\rho\sigma}\, p_4^\sigma \left(p_1^\rho - p_2^\rho - p_3^\rho\right)$
W_μ^-	$Z_{H\nu}$	Φ^{++}	Φ^-	$-4\frac{e^2}{s_w^2 f^2}\varepsilon_{\mu\nu\rho\sigma}\left(p_2^\rho p_3^\sigma - p_1^\rho p_3^\sigma - p_3^\rho p_4^\sigma\right)$
$W_{H\mu}^+$	Z_ν	Φ^+	Φ^{--}	$2\frac{e^2}{c_w s_w^2 f^2}\varepsilon_{\mu\nu\rho\sigma}\big(s_w^2 p_2^\rho p_4^\sigma - s_w^2 p_1^\rho p_4^\sigma + (2-s_w^2) p_1^\rho p_3^\sigma$ $-(2-s_w^2) p_2^\rho p_3^\sigma - 2p_3^\rho p_4^\sigma\big)$
$W_{H\mu}^+$	Z_ν	Φ^-	Φ^0	$-\frac{e^2\cdot\sqrt{2}}{c_w s_w^2 f^2}\varepsilon_{\mu\nu\rho\sigma}\big((2-3s_w^2) p_2^\rho p_3^\sigma - (2-3s_w^2) p_1^\rho p_3^\sigma$ $-s_w^2 p_1^\rho p_4^\sigma + s_w^2 p_2^\rho p_4^\sigma + 2(1-2s_w^2) p_3^\rho p_4^\sigma\big)$
$W_{H\mu}^+$	Z_ν	Φ^-	Φ^p	$-\frac{ie^2\cdot\sqrt{2}}{c_w s_w^2 f^2}\varepsilon_{\mu\nu\rho\sigma}\big((2-3s_w^2) p_2^\rho p_3^\sigma - (2-3s_w^2) p_1^\rho p_3^\sigma$ $-s_w^2 p_1^\rho p_4^\sigma + s_w^2 p_2^\rho p_4^\sigma + 2(1-2s_w^2) p_3^\rho p_4^\sigma\big)$
$W_{H\mu}^-$	Z_ν	Φ^+	Φ^0	$-\frac{e^2\cdot\sqrt{2}}{c_w s_w^2 f^2}\varepsilon_{\mu\nu\rho\sigma}\big(s_w^2 p_1^\rho p_4^\sigma - s_w^2 p_2^\rho p_4^\sigma - (2-3s_w^2) p_2^\rho p_3^\sigma$ $+(2-3s_w^2) p_1^\rho p_3^\sigma - 2(1-2s_w^2) p_3^\rho p_4^\sigma\big)$
$W_{H\mu}^-$	Z_ν	Φ^+	Φ^p	$\frac{ie^2\cdot\sqrt{2}}{c_w s_w^2 f^2}\varepsilon_{\mu\nu\rho\sigma}\big(s_w^2 p_1^\rho p_4^\sigma - s_w^2 p_2^\rho p_4^\sigma - (2-3s_w^2) p_2^\rho p_3^\sigma$ $+(2-3s_w^2) p_1^\rho p_3^\sigma - 2(1-2s_w^2) p_3^\rho p_4^\sigma\big)$
Z_μ	$Z_{H\nu}$	Φ^0	Φ^p	$2\frac{ie^2}{c_w s_w^2 f^2}\varepsilon_{\mu\nu\rho\sigma}\left(p_1^\rho p_3^\sigma - p_2^\rho p_3^\sigma - p_1^\rho p_4^\sigma + p_2^\rho p_4^\sigma + 2p_3^\rho p_4^\sigma\right)$

Table 2.12: (Continuation of Tab. 2.11) *T-parity violating vertices with two scalars and two gauge bosons. The momenta $p_{1,2,3,4}$ correspond to the particle in the first, second, third and fourth column, respectively.* Continued in Tab. 2.13

Particles				**Vertices**
$W_{H\,\mu}^-$	Z_ν	Φ^{++}	Φ^-	$-2\frac{e^2}{c_w s_w^2 f^2}\varepsilon_{\mu\nu\rho\sigma}\big((2-s_w^2)p_1^\rho p_4^\sigma-(2-s_w^2)p_2^\rho p_4^\sigma$ $+s_w^2 p_2^\rho p_3^\sigma-s_w^2 p_1^\rho p_3^\sigma+2p_3^\rho p_4^\sigma\big)$
Z_μ	$Z_{H\nu}$	Φ^+	Φ^-	$6\frac{c_w e^2}{s_w^2 f^2}\varepsilon_{\mu\nu\rho\sigma}\big(p_1^\rho p_4^\sigma-p_2^\rho p_4^\sigma-p_1^\rho p_3^\sigma+p_2^\rho p_3^\sigma-2p_3^\rho p_4^\sigma\big)$
Z_μ	$Z_{H\nu}$	Φ^{++}	Φ^{--}	$2\frac{(1-2s_w^2)e^2}{c_w s_w^2 f^2}\varepsilon_{\mu\nu\rho\sigma}\big(p_1^\rho p_4^\sigma-p_2^\rho p_4^\sigma-p_1^\rho p_3^\sigma+p_2^\rho p_3^\sigma-2p_3^\rho p_4^\sigma\big)$
W_μ^+	$W_{H\nu}^-$	Φ^+	Φ^-	$-2\frac{e^2}{s_w^2 f^2}\varepsilon_{\mu\nu\rho\sigma}\big(p_2^\rho p_4^\sigma-p_1^\rho p_4^\sigma+p_1^\rho p_3^\sigma-p_2^\rho p_3^\sigma+2p_3^\rho p_4^\sigma\big)$
W_μ^+	$W_{H\nu}^-$	Φ^{++}	Φ^{--}	$2\frac{e^2}{s_w^2 f^2}\varepsilon_{\mu\nu\rho\sigma}\big(3p_1^\rho p_4^\sigma+p_2^\rho p_3^\sigma-p_1^\rho p_3^\sigma-3p_2^\rho p_4^\sigma-4p_3^\rho p_4^\sigma\big)$
W_μ^+	$W_{H\nu}^-$	Φ^0	Φ^0	$-2\frac{e^2}{s_w^2 f^2}\varepsilon_{\mu\nu\rho\sigma}\big(p_1^\rho p_3^\sigma-p_2^\rho p_3^\sigma+p_1^\rho p_4^\sigma-p_2^\rho p_4^\sigma\big)$
W_μ^+	$W_{H\nu}^-$	Φ^0	Φ^p	$-4\frac{ie^2}{s_w^2 f^2}\varepsilon_{\mu\nu\rho\sigma}\big(p_2^\rho p_3^\sigma-p_2^\rho p_4^\sigma+p_1^\rho p_4^\sigma-p_1^\rho p_3^\sigma-2p_3^\rho p_4^\sigma\big)$

Table 2.13: (Continuation of Tab. 2.12) *T-parity violating vertices vertices two scalars and two gauge bosons. The momenta $p_{1,2,3,4}$ correspond to the particle in the first, second, third and fourth column, respectively.*

Chapter 3

A Little Higgs Model with Exact Dark Matter Parity

3.1 Introduction

It is often assumed that the new physics entering little Higgs models near the scale of 10 TeV are some strong dynamics similar to technicolor theories[1]. In this case, however, the fundamental theory can induce a Wess-Zumino-Witten (WZW) term [63], which is T-odd [64] if T-parity is implemented as in Ref. [30]. The breaking of T-parity by the WZW term, though suppressed by the large symmetry breaking scale, rules out the lightest T-odd particle as a dark matter candidate, since this particle would decay promptly into gauge bosons, as discussed in the previous section. On the other hand, it was recently shown that a different construction of the parity in moose models leads to a parity-even WZW term [34]. The authors present a simple toy model that shows the relevant features.

In this chapter we adopt the idea of Ref. [34] for the "minimal moose" model [57] in order to construct a fully realistic model which reproduces the Standard Model as a low-energy theory, admits electroweak symmetry breaking (EWSB), is consistent with electroweak precision constraints, and has a viable dark matter candidate. In the following section, the model and the implementation of the new X-parity is described explicitly. In section 3.3 the physical mass spectrum of the model is analyzed, and it is shown that successful electroweak symmetry breaking can be achieved. Finally, section 3.4 discusses electroweak precision constraints and gives a brief overview of the collider phenomenology, before the conclusions are presented in section 3.5.

[1] An alternative approach involving a weakly coupled symmetry breaking sector can be found in Ref. [62].

3.2 The model

The model is based on a large $\mathrm{SU}(3)^8 = [\mathrm{SU}(3)_\mathrm{L} \times \mathrm{SU}(3)_\mathrm{R}]^4$ global symmetry group that is spontaneously broken to the diagonal vector group $\mathrm{SU}(3)^4_\mathrm{V}$ at a scale f, giving rise to four sets of SU(3) valued nonlinear sigma model fields

$$X_i = e^{2ix_i/f}, \qquad i = 1, \ldots, 4. \tag{3.1}$$

Under the global symmetry group they transform as $X_{1,3} \to L_{1,3} X_{1,3} R^\dagger_{1,3}$ and $X_{2,4} \to R_{2,4} X_{2,4} L^\dagger_{2,4}$. The axial components of the global symmetries shift the Goldstone fields, $x_i \to x_i + \epsilon_i$, thereby forbidding any nonderivative couplings for the Goldstone fields. In particular, as long as these symmetries are not explicitly broken, a mass term can't be generated for the Goldstone fields at any loop order.

Adding gauge and Yukawa interactions will in general break some of the global symmetries and therefore generate $\mathcal{O}(f)$ mass terms for the corresponding Goldstone bosons. The idea of collective symmetry breaking is to implement the required interactions in such a way that each interaction respects parts of the global symmetry and therefore keeps the corresponding Goldstone bosons massless. Only the simultaneous presence of different symmetry breaking interactions can then generate a mass for those Goldstone bosons. Since appropriate diagrams only appear at the two-loop level, the generated masses are suppressed by an additional loop factor and can be significantly below the scale f.

Our goal is to have at least one light electroweak doublet that we can identify with the SM Higgs boson. Under the SM gauge interactions, the Goldstone fields x_i decompose as follows

$$x_i = \begin{pmatrix} \phi_i + \eta_i/\sqrt{12} & h_i/2 \\ h_i^\dagger/2 & -\eta_i/\sqrt{3} \end{pmatrix}, \tag{3.2}$$

where $\phi_i = \phi_i^a \sigma^2/2$ are triplets under the SU(2) gauge group, h_i are complex doublets, and η_i are real singlets. We further demand that the physical Higgs boson is even under the dark matter parity that acts as $x_1 \leftrightarrow x_2$ and $x_3 \leftrightarrow x_4$ on the Goldstone fields. This leaves us with two candidates for the SM Higgs doublets,

$$h_a \equiv \tfrac{1}{\sqrt{2}}(h_3 + h_4), \qquad\qquad h_b \equiv \tfrac{1}{\sqrt{2}}(h_1 + h_2). \tag{3.3}$$

The physical Higgs field will later be identified as h_a and is protected by the global symmetries

$$\begin{aligned} \mathrm{SU}(3)_\mathrm{L,a} &= \mathrm{SU}(3)_\mathrm{L,3} \times \mathrm{SU}(3)_\mathrm{L,4}/\mathrm{SU}(3)_\mathrm{DL}\,, \\ \mathrm{SU}(3)_\mathrm{R,a} &= \mathrm{SU}(3)_\mathrm{R,3} \times \mathrm{SU}(3)_\mathrm{R,4}/\mathrm{SU}(3)_\mathrm{DR}\,, \end{aligned}$$

where $\mathrm{SU}(3)_{\mathrm{Di}}$ denotes the diagonal subgroups of these product groups. As long as no single interaction breaks both $\mathrm{SU}(3)_{\mathrm{L,a}}$ and $\mathrm{SU}(3)_{\mathrm{R,a}}$ at the same time, the mass of the Higgs will be sufficiently small.

For models based on the symmetry structure used here, possibilities to introduce interactions that preserve enough global symmetries are discussed in [57]. We found that we could adopt their rules to introduce scalar self-interactions as well as gauge interactions, but that some modifications are required in the Yukawa sector in order to maintain the parity symmetry. In particular partners for the standard model fermions must be introduced so that the dark matter parity can be implemented in a linear way.

3.2.1 Scalar and gauge sector

The global symmetry structure of the model is is depicted in Fig. 3.1. On each site, a $\mathrm{SU}(2) \times \mathrm{U}(1)$ subgroup is gauged, with equal strength for both sites. The gauge group generators are given by

$$Q^a_{\mathrm{L,R}} = \begin{pmatrix} \sigma^a/2 & 0 \\ 0 & 0 \end{pmatrix}, \qquad Y_{\mathrm{L,R}} = \frac{1}{\sqrt{12}} \begin{pmatrix} \mathbb{1} & 0 \\ 0 & -2 \end{pmatrix}, \tag{3.4}$$

written in terms of 2×2 and 1×1 blocks. Here σ^a denote the Pauli matrices. The kinetic term of the sigma fields reads

$$\mathcal{L}_{\mathrm{G}} = \frac{f^2}{4} \sum_{i=1}^{4} \mathrm{Tr}\left[(D_\mu X_i)(D^\mu X_i)^\dagger\right], \tag{3.5}$$

where

$$\begin{aligned} D_\mu X_{1,3} &= \partial_\mu X_{1,3} - i A_{\mathrm{L}\mu} X_{1,3} + i X_{1,3} A_{\mathrm{R}\mu}, \\ D_\mu X_{2,4} &= \partial_\mu X_{2,4} - i A_{\mathrm{R}\mu} X_{2,4} + i X_{2,4} A_{\mathrm{L}\mu}, \\ A_{\mathrm{L}\mu} &\equiv g_{\mathrm{L}} W^a_{\mathrm{L}\mu} Q^a_{\mathrm{L}} + g'_{\mathrm{L}} y_{\mathrm{L}X}\, B_{\mathrm{L}\mu} Y_{\mathrm{L}}, \\ A_{\mathrm{R}\mu} &\equiv g_{\mathrm{R}} W^a_{\mathrm{R}\mu} Q^a_{\mathrm{R}} + g'_{\mathrm{R}} y_{\mathrm{R}X}\, B_{\mathrm{R}\mu} Y_{\mathrm{R}}, \end{aligned}$$

The gauge couplings at the two sites are chosen to be equal, $g_{\mathrm{L}} = g_{\mathrm{R}} = \sqrt{2}g$ and $g'_{\mathrm{L}} = g'_{\mathrm{R}} = \sqrt{2}g'$, and g, g' are the SM gauge couplings. Furthermore, $y_{\mathrm{L}X,\mathrm{R}X}$ denote the U(1) charges of the fields X_i. The choice $y_{\mathrm{L}X} = y_{\mathrm{R}X} = 1/\sqrt{3}$ ensures the correct values for the Higgs doublet hypercharge and Weinberg angle. Note that the definition (3.5) of the covariant derivatives corresponds to assigning opposite directions for the link fields 1,3 and 2,4, which is important for the definition of the X-parity below.

Each gauge interaction separately only break either $\mathrm{SU}(3)_{\mathrm{L,a}}$ or $\mathrm{SU}(3)_{\mathrm{R,a}}$ and therefore respects collective symmetry breaking. Actually since the gauge interactions are either on the left or on the right side of the moose diagram, no large mass is generated for any of the Goldstone fields from these interactions.

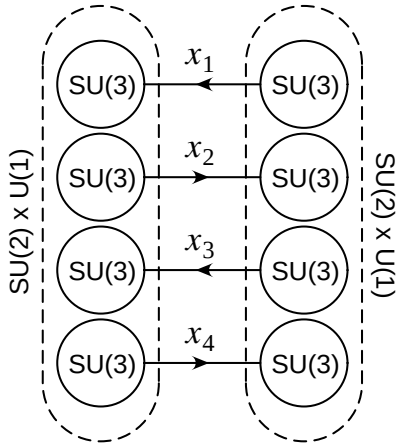

Figure 3.1: *Illustration of the global and gauge symmetry structure of the model.*

The kinetic term (3.5) has a $\mathbb{Z}_2$ symmetry, called X-parity, defined by

$$\text{X-parity:} \qquad A_{\rm L} \leftrightarrow A_{\rm R}\,, \qquad X_1 \leftrightarrow X_2\,, \qquad X_3 \leftrightarrow X_4\,. \tag{3.6}$$

This definition is a straightforward generalization of the parity of the two-link model in Ref. [34]. Under this parity, the WZW terms [63] for the four link fields transform as

$$\begin{aligned} &\Gamma_{\rm WZW}(x_1, A_{\rm L}, A_{\rm R}) \leftrightarrow \Gamma_{\rm WZW}(x_2, A_{\rm R}, A_{\rm L}), \\ &\Gamma_{\rm WZW}(x_3, A_{\rm L}, A_{\rm R}) \leftrightarrow \Gamma_{\rm WZW}(x_4, A_{\rm R}, A_{\rm L}), \end{aligned} \tag{3.7}$$

so that the combined term

$$\begin{aligned} \mathcal{L}_{\rm WZW} =& \Gamma_{\rm WZW}(x_1, A_{\rm L}, A_{\rm R}) + \Gamma_{\rm WZW}(x_2, A_{\rm R}, A_{\rm L}) \\ &+ \Gamma_{\rm WZW}(x_3, A_{\rm L}, A_{\rm R}) + \Gamma_{\rm WZW}(x_4, A_{\rm R}, A_{\rm L}) \end{aligned} \tag{3.8}$$

remains invariant. As a result, X-parity is an exact symmetry of the model and the lightest X-odd particle is stable.

In addition to the X-parity in eq. (3.6) a second $\mathbb{Z}_2$ symmetry, called T-parity, is imposed, under which

$$\text{T-parity:} \qquad A_{\rm L} \leftrightarrow A_{\rm R}\,, \qquad X_i \to \Omega X_i^\dagger \Omega\,, \tag{3.9}$$

where $\Omega \equiv \mathrm{diag}(1, 1, -1)$. Our T-parity is identical to the original version in Ref. [30], and it ensures that the triplet and singlet scalar do not receive any vacuum expectation values. In our implementation, T-parity is respected by the model at the classical level, but broken by $\mathcal{L}_{\rm WZW}$. However, since the stability of the dark matter candidate is already guaranteed by X-parity (3.6), this does not lead to any problems.

In the gauge sector, the X-odd linear combinations of gauge bosons,

$$W_{\rm H}^a = \tfrac{1}{\sqrt{2}}(W_{\rm L}^a - W_{\rm R}^a), \qquad B_{\rm H} = \tfrac{1}{\sqrt{2}}(B_{\rm L} - B_{\rm R}), \tag{3.10}$$

acquire masses of order f from the kinetic term (3.5), while the X-even combinations

$$W^a = \tfrac{1}{\sqrt{2}}(W_{\rm L}^a + W_{\rm R}^a), \qquad B = \tfrac{1}{\sqrt{2}}(B_{\rm L} + B_{\rm R}), \tag{3.11}$$

remain massless before EWSB and are identified with the SM gauge bosons. The scalar fields form the following X-even and X-odd combinations:

$$w = \frac{1}{2}(x_1 - x_2 + x_3 - x_4) \qquad x = \frac{1}{2}(-x_1 + x_2 + x_3 - x_4) \quad \text{(X-odd)}, \tag{3.12}$$

$$y = \frac{1}{2}(-x_1 - x_2 + x_3 + x_4) \quad z = \frac{1}{2}(x_1 + x_2 + x_3 + x_4) \qquad \text{(X-even)}. \tag{3.13}$$

The triplet ϕ_w and the singlet η_w are eaten to form the longitudinal components of $W_{\rm H}^a$ and $B_{\rm H}$.

A large Higgs quartic coupling, required for electroweak symmetry breaking, is generated by the following X-invariant plaquette operator:

$$\mathcal{L}_{\rm P} = \frac{\kappa}{8} f^4 \,{\rm Tr}\,\Big[X_1 X_3^\dagger X_2^\dagger X_4 + X_2 X_4^\dagger X_1^\dagger X_3\Big] + {\rm h.c.} \tag{3.14}$$

This operator contains an explicit $\mathcal{O}(f)$ mass term for the scalar fields in x, but preserves enough global symmetries so it does not generate large masses for any other Goldstone bosons at the one loop level, in particular not for h_a, h_b.

Successful electroweak symmetry also requires the introduction of a second plaquette term [57], which breaks a different subset of the global symmetry:

$$\begin{aligned}\mathcal{L}'_{\rm P} = \frac{\epsilon}{8} f^4 {\rm Tr}\,\Big(&T_8 X_1 X_3^\dagger X_2^\dagger X_4 + T_8 X_2 X_4^\dagger X_1^\dagger X_3 \\ &+ X_1 X_3^\dagger T_8 X_2^\dagger X_4 + X_2 X_4^\dagger T_8 X_1^\dagger X_3\Big) + {\rm h.c.}\end{aligned} \tag{3.15}$$

where $T_8 = {\rm diag}(1,1,-2)/\sqrt{12}$, and ϵ is a complex constant. As explained in Ref. [57], eq. (3.15) can be generated radiatively by two-loop diagrams involving the top quark, and therefore it is natural to assume that $|\epsilon| \sim |\kappa|/10$. We can assume ϵ to be purely imaginary, since the real part only gives small corrections to the scalar potential.

3.2.2 Fermion sector

For the construction of the kinetic and Yukawa terms of the fermions, several conditions need to be considered. First, one has to make sure that these terms do not break too many of the global symmetries, so that the mass of the little Higgs doublet remains protected from quadratic corrections. Secondly, the minimal

construction using only X-even fermions [30] leads to unsuppressed four-fermion operators at one-loop level, thus forcing the scale f be about 10 TeV or larger [66]. The second problem can be solved by introducing "mirror" fermions [66], *i. e.* two sets of fermions that are partners under X-parity. Our implementation closely resembles the setup in the appendix of Ref. [67].

For each SM flavor two doublets of left-handed fermions are introduced, located at the two sites of the moose diagram. With the exception of the top quark, they are embedded into incomplete representations of SU(3) as follows

$$Q_{\rm a} = (d_{\rm a}, u_{\rm a}, 0)^\top, \qquad\qquad Q_{\rm b} = (d_{\rm b}, u_{\rm b}, 0)^\top. \tag{3.16}$$

Under the global $\mathrm{SU}(3)_{\rm L} \times \mathrm{SU}(3)_{\rm R}$ group they transform as $Q_{\rm a} \to L_i Q_{\rm a}$ and $Q_{\rm b} \to R_i Q_{\rm b}$, while X- and T-parity interchange the two fields, $Q_{\rm a} \leftrightarrow Q_{\rm b}$.

Since (3.16) are incomplete multiplets, their interaction terms break the global symmetries that protect the Higgs mass and lead to quadratically divergent contributions from one-loop diagrams involving the Yukawa couplings. For the first two generations this is not a problem since the Yukawa couplings are very small, but for the third generation we need to introduce complete multiplets

$$Q_{3{\rm a}} = (d_{3{\rm a}}, u_{3{\rm a}}, U_{\rm a})^\top, \qquad\qquad Q_{3{\rm b}} = (d_{3{\rm b}}, u_{3{\rm b}}, U_{\rm b})^\top. \tag{3.17}$$

Here the additional singlets $U_{\rm a,b}$ cancel the quadratically divergent Higgs mass contributions induced by the large top Yukawa coupling.

The X- and T-invariant fermion kinetic terms have the standard form

$$\mathcal{L}_{\rm F} = i\overline{Q}_{\rm a}\bar{\sigma}^\mu D^{\rm a}_\mu Q_{\rm a} + i\overline{Q}_{\rm b}\bar{\sigma}^\mu D^{\rm b}_\mu Q_{\rm b}, \tag{3.18}$$

with

$$\begin{aligned} D^{\rm a}_\mu &= \partial_\mu + i g_{\rm L} W^a_{{\rm L}\mu} \, (Q^a_{\rm L})^\top - i g'_{\rm L} \, y_{{\rm L}Q} \, B_{{\rm L}\mu}, \\ D^{\rm b}_\mu &= \partial_\mu + i g_{\rm R} W^a_{{\rm R}\mu} (Q^a_{\rm R})^\top - i g'_{\rm R} y_{{\rm R}Q} \, B_{{\rm R}\mu}, \end{aligned}$$

where $\bar{\sigma}^\mu \equiv (1, -\vec{\sigma})$, and $y_{{\rm L}Q}$ and $y_{{\rm R}Q}$ are diagonal matrices composed of the U(1) charges in Table 3.1. The SM fermions emerge from the X-even linear combination $Q = \frac{1}{\sqrt{2}}(Q_{\rm a} + Q_{\rm b})$. To give mass to the X-odd combination $Q_{\rm H} = \frac{1}{\sqrt{2}}(Q_{\rm a} - Q_{\rm b})$, we need to introduce conjugate Dirac partners

$$Q^c_{\rm c} = (d^c_{\rm c}, u^c_{\rm c}, 0)^\top, \qquad\qquad Q^c_{3{\rm c}} = (d^c_{3{\rm c}}, u^c_{3{\rm c}}, U^c_{\rm c})^\top, \tag{3.19}$$

Under $\mathrm{SU}(3)_{\rm L} \times \mathrm{SU}(3)_{\rm R}$ they transform as $Q^c_{\rm c} \to U_i Q^c_{\rm c}$, where U_i $(i = 1, \ldots, 4)$ belongs to the unbroken diagonal subgroup of $SU(3)_{\rm L} \times SU(3)_{\rm R}$ and is a non-linear function of L_i and R_i. Furthermore, the effect of X- and T-parity is defined as $Q^c_{\rm c} \to -\Omega Q^c_{\rm c}$. Then a X- and T-invariant mass term for the X-odd fermions is given by

$$\mathcal{L}_{\rm M} = -\frac{\lambda_c}{\sqrt{2}} f \left(Q_{\rm a} \xi_1 Q^c_{\rm c} - Q_{\rm b} \Omega \xi_1^\dagger Q^c_{\rm c} - Q_{\rm b} \xi_2 \Omega Q^c_{\rm c} + Q_{\rm a} \Omega \xi_2^\dagger \Omega Q^c_{\rm c} \right) + \text{h.c.}\,, \tag{3.20}$$

where $\xi_i = e^{ix_i/f}$. Under global $SU(3)_\mathrm{L} \times SU(3)_\mathrm{R}$ rotations ξ_i transforms as $\xi_i \to L_i \xi_i U_i^\dagger = U_i \xi_i R_i^\dagger$ for $i = 1, 3$ and analogous for $i = 2, 4$, so that eq. (3.20) is evidently gauge invariant. In general, λ_c is a 3×3 matrix in flavor space. Since it can contribute to flavor-changing neutral currents (FCNCs) at one-loop level, it is constrained by data on heavy-flavor decays and oscillations. Such effects are studied for example in [38] for the case of the littlest Higgs model with T-parity. For the analyses in section 3 and 4 we assume a flavor diagonal λ_c for simplicity.

Since the Q_c^c transform non-linearly, one must make use of the ξ_i fields to construct a gauge- and X- and T-invariant kinetic term. Following the formalism of Callan, Coleman, Wess, and Zumino [68], it can be written as

$$\begin{aligned}\mathcal{L}_\mathrm{c} = i\overline{Q}_\mathrm{c}^c \bar{\sigma}^\mu \Big(\partial_\mu + \frac{1}{4}(\xi_1^\dagger D_\mu \xi_1 + \xi_1 D_\mu \xi_1^\dagger + \xi_2^\dagger D_\mu \xi_2 + \xi_2 D_\mu \xi_2^\dagger) \\ - ig'(y_{Q_\mathrm{c}} + \tfrac{1}{\sqrt{3}} Y_\mathrm{V}) B_\mu \Big) Q_\mathrm{c}^c \,, \end{aligned} \tag{3.21}$$

where

$$\xi_i^\dagger D_\mu \xi_i = \xi_i^\dagger (\partial_\mu + igW^a Q_\mathrm{V}^a + igW_\mathrm{H}^a Q_\mathrm{A}^a + ig' \tfrac{1}{\sqrt{3}} B Y_\mathrm{V} + ig' \tfrac{1}{\sqrt{3}} B_\mathrm{H} Y_\mathrm{A}) \xi_i, \tag{3.22}$$

$$\xi_i D_\mu \xi_i^\dagger = \xi_i (\partial_\mu + igW^a Q_\mathrm{V}^a - igW_\mathrm{H}^a Q_\mathrm{A}^a + ig' \tfrac{1}{\sqrt{3}} B Y_\mathrm{V} - ig' \tfrac{1}{\sqrt{3}} B_\mathrm{H} Y_\mathrm{A}) \xi_i^\dagger, \tag{3.23}$$

and $Q_\mathrm{V}^a, Y_\mathrm{V}$ and $Q_\mathrm{A}^a, Y_\mathrm{A}$ are the unbroken and broken gauge generators, respectively. Both equations (3.20) and (3.21) do not involve the x_3 and x_4 Goldstone fields and therefore do not break the global symmetries that protect the Higgs mass. They do however generate masses for some of the other Goldstone bosons that will be explicitly calculated in section 3.3.2.

Now Yukawa couplings can be constructed for the X-even massless combinations of the fermions. For the up-type quarks of the first two generations they read

$$\mathcal{L}_\mathrm{u} = -\lambda_\mathrm{u} f Q_\mathrm{a} (X_3 + \Omega X_4^\dagger \Omega) \begin{pmatrix} 0 \\ 0 \\ u^c \end{pmatrix} - \lambda_\mathrm{u} f Q_\mathrm{b} (\Omega X_3^\dagger \Omega + X_4) \begin{pmatrix} 0 \\ 0 \\ u^c \end{pmatrix} + \mathrm{h.c.}, \tag{3.24}$$

where u^c is are the right-handed quarks (one for each flavor), which are X- and T-even. As already mentioned above, the presence of incomplete multiplets in the Yukawa couplings leads to quadratically divergent contribution to the Higgs mass. Therefore the top Yukawa coupling has a slightly different form [67],

$$\mathcal{L}_\mathrm{t} = -\lambda f Q_\mathrm{3a} (X_3 + \Omega X_4^\dagger \Omega) \begin{pmatrix} 0 \\ 0 \\ U_\mathrm{b}^c \end{pmatrix} - \lambda f Q_\mathrm{3b} (\Omega X_3^\dagger \Omega + X_4) \begin{pmatrix} 0 \\ 0 \\ U_\mathrm{a}^c \end{pmatrix} + \mathrm{h.c.}. \tag{3.25}$$

Here the two singlets U_a^c and U_b^c transform under X- and T-parity as $U_\mathrm{a}^c \leftrightarrow U_\mathrm{b}^c$. Their X-even combination $U_\mathrm{a}^c + U_\mathrm{b}^c$ emerges in the right-handed top quark, while

the X-odd combination $U_{\rm a}^c - U_{\rm b}^c$ forms the right-handed partner of the X-odd $U_{\rm a} - U_{\rm b}$. In addition there are one more X-even and X-odd fermion in the top sector, which receive masses from eq. (3.20). This will be explained in more detail in section 3.3.1.

The use of complete multiplets $Q_{3{\rm a}}$, $Q_{3{\rm b}}$ in (3.25) makes sure that each term preserves one of the global SU(3) symmetries that protect the Higgs mass.

Finally, the down-type Yukawa couplings are given by

$$\mathcal{L}_{\rm d} = -\lambda_{\rm d} f \widetilde{Q}_{\rm a}(X_3 + \Omega X_4^\dagger \Omega)^* \begin{pmatrix} 0 \\ 0 \\ d^c \end{pmatrix} - \lambda_{\rm d} f \widetilde{Q}_{\rm b}(\Omega X_3^\dagger \Omega + X_4)^* \begin{pmatrix} 0 \\ 0 \\ d^c \end{pmatrix} + {\rm h.c.}, \quad (3.26)$$

where

$$\widetilde{Q}_{\rm a,b} = -2iT_2 Q_{\rm a,b} = (-u_{\rm a,b}, d_{\rm a,b}, 0)^\top, \qquad T_2 = \begin{pmatrix} \sigma^2/2 & 0 \\ 0 & 0 \end{pmatrix}. \quad (3.27)$$

The lepton Yukawa interactions are defined similarly. In contrast to the up-type Yukawa couplings, the all three generations of down-type fermions generate quadratically divergent contributions to the Higgs doublet masses from eq. (3.26), which is permissible since the bottom Yukawa coupling is much smaller than the top Yukawa coupling. The kinetic term for the singlet conjugate fields $\psi^c \equiv u^c, d^c, U_{\rm a}^c, U_{\rm b}^c$ simply reads

$$\mathcal{L}_{\rm R} = i\overline{\psi^c}\sigma^\mu(\partial_\mu - ig' y_{\psi^c} B_\mu)\psi^c = i\overline{\psi^c}\sigma^\mu\big(\partial_\mu - i\sqrt{2}g'(y_{{\rm L}\psi^c} B_{{\rm L}\mu} + y_{{\rm R}\psi^c} B_{{\rm R}\mu})\big)\psi^c, \quad (3.28)$$

where $\sigma^\mu \equiv (1, \vec{\sigma})$ and $y_{\psi^c} = 2y_{{\rm L}\psi^c} = 2y_{{\rm R}\psi^c}$ is the fermion hypercharge.

Table 3.1 summarizes the fermion contained in the model and their transformation properties. Note that the model is non-renormalizable and considered to be a low-energy effective theory of some fundamental dynamics associated with the UV cutoff scale $\Lambda \sim 10\, f \sim 10$ TeV. This UV completion could, but does not need to, consist of some strongly coupled gauge interaction, which breaks the global symmetry through the formation of a fermion condensate, similar to technicolor.

3.3 Mass spectrum

3.3.1 Top quark sector

Expanding the Yukawa couplings (3.20) and (3.25) in the top quark sector in powers of $1/f$ yields

$$\begin{aligned} \mathcal{L}_{\rm t} = &-\sqrt{2}\lambda_c f(u_{3{\rm a}} - u_{3{\rm b}})u_{3{\rm c}}^c - \sqrt{2}\lambda_c f(U_{\rm a} + U_{\rm b})U_c^c - 2\lambda f\,(U_{\rm a}U_{\rm b}^c + U_{\rm b}U_{\rm a}^c) \\ &- \lambda\,(q_{3{\rm a}}(h_y + h_z)U_{\rm b}^c + q_{3{\rm b}}(h_y + h_z)U_{\rm a}^c) \\ &+ \tfrac{1}{2\sqrt{2}}\lambda_c\left[(q_{3a} + q_{3b})(h_y - h_z)U_c^c + (U_a - U_b)(h_y^\dagger - h_z^\dagger)q_c^c\right] + \cdots + {\rm h.c.}\,, \end{aligned} \quad (3.29)$$

	$\mathrm{SU}(2)_\mathrm{L}$	$\mathrm{SU}(2)_\mathrm{R}$	$\mathrm{U}(1)_\mathrm{L}$	$\mathrm{U}(1)_\mathrm{R}$	X	T
q_a	2	1	$\frac{1}{12}$	$\frac{1}{12}$	q_b	q_b
U_a	1	1	$\frac{7}{12}$	$\frac{1}{12}$	U_b	U_b
q_b	1	2	$\frac{1}{12}$	$\frac{1}{12}$	q_a	q_a
U_b	1	1	$\frac{1}{12}$	$\frac{7}{12}$	U_a	U_a
Q_c^c	nonlinear				$-\Omega Q_\mathrm{c}^c$	$-\Omega Q_\mathrm{c}^c$
d^c	1	1	$\frac{1}{6}$	$\frac{1}{6}$	d^c	d^c
u^c	1	1	$-\frac{1}{3}$	$-\frac{1}{3}$	u^c	u^c
U_a^c	1	1	$-\frac{7}{12}$	$-\frac{1}{12}$	U_b^c	U_b^c
U_b^c	1	1	$-\frac{1}{12}$	$-\frac{7}{12}$	U_a^c	U_a^c

Table 3.1: *Quantum numbers of the fermion multiplets under the* $[\mathrm{SU}(2)\times\mathrm{U}(1)]^2$ *gauge symmetry, and their transformation properties under X and T. The physical* $\mathrm{U}(1)_\mathrm{Y}$ *hypercharge is the sum of both* $\mathrm{U}(1)_1+\mathrm{U}(1)_2$ *charges. There is some freedom in the assignment of* $\mathrm{U}(1)_1$ *and* $\mathrm{U}(1)_2$ *charges to* $U_\mathrm{a}^{(c)}$, $U_\mathrm{b}^{(c)}$. *Here the conventions of [67] have been adapted.*

where $q_{3\mathrm{a}}=(d_{3\mathrm{a}},u_{3\mathrm{a}})^\top$, $q_{3\mathrm{b}}=(d_{3\mathrm{b}},u_{3\mathrm{b}})^\top$, and the dots indicate $\mathcal{O}(f^{-1})$ terms and $\mathcal{O}(f^0)$ terms that do not involve Higgs doublets. With suitable phase redefinitions of the fields, both λ and λ_c can be chosen to be real[2]. Introducing the X-even and -odd combinations

$$U_\pm\equiv\frac{1}{\sqrt{2}}(U_\mathrm{a}\pm U_\mathrm{b}),\qquad\qquad U_\pm^c\equiv\frac{1}{\sqrt{2}}(U_\mathrm{a}^c\pm U_\mathrm{b}^c),\tag{3.30}$$

$$q_{3\pm}\equiv\frac{1}{\sqrt{2}}(q_{3\mathrm{a}}\pm q_{3\mathrm{b}}),\qquad\qquad u_{3\pm}\equiv\frac{1}{\sqrt{2}}(u_{3\mathrm{a}}\pm u_{3\mathrm{b}}),\tag{3.31}$$

one obtains

$$\begin{aligned}\mathcal{L}_\mathrm{t}=&-2\lambda_c f u_{3-}u_{3\mathrm{c}}^c-2\lambda_c f U_+U_c^c-2\lambda f\left(U_+U_+^c+U_-U_-^c\right)\\&-\lambda\left(q_{3+}(h_y+h_z)U_+^c+q_{3-}(h_y+h_z)U_-^c\right)+\tfrac{1}{2}\lambda_c q_{3+}(h_y-h_z)U_c^c+\mathrm{h.c.}\end{aligned}\tag{3.32}$$

Neglecting contributions of order v^2/f^2, the X-odd mass eigenstates in the top sector, written in terms of left- and right-handed components, are

$$(T_\mathrm{H},T_\mathrm{H}^c)\equiv(u_{3-},u_{3c}^c),\qquad\qquad(T',T'^c)\equiv(U_-,U_-^c),\tag{3.33}$$

[2]A relative factor i between the second line of (3.29) and (3.25) has been absorbed by this same procedure.

with masses $2\lambda_c f$ and $2\lambda f$, respectively. In the X-even top sector, the following Dirac fermions are formed:

$$(T, T^c) \equiv \left(U_+, \frac{\lambda_c U_c^c + \lambda U_+^c}{\sqrt{\lambda^2 + \lambda_c^2}} \right), \qquad (t, t^c) \equiv \left(u_{3+}, \frac{\lambda_c U_+^c - \lambda U_c^c}{\sqrt{\lambda^2 + \lambda_c^2}} \right). \tag{3.34}$$

The T obtains a mass $m_T = 2\sqrt{\lambda^2 + \lambda_c^2} f$, while the SM-like top quark t remains massless before EWSB and has a Yukawa coupling given by

$$-\lambda_t q_3 h t^c + \text{h.c.}\,, \qquad \lambda_t = \frac{\sqrt{2}\,\lambda\lambda_c}{\sqrt{\lambda^2 + \lambda_c^2}}\,. \tag{3.35}$$

Note that the X-odd top partner T' is responsible for the cancellation of the quadratically divergent contribution to the Higgs mass. Therefore the X-even T as well as the X-odd T_{H} can be given masses of several TeV by increasing λ_c, thus effectively decoupling them from The remaining fermion masses can be found in table 3.2.

Once electroweak symmetry is broken mixing of the top quark with the T quark is reintroduced. The resulting mass matrix can be diagonalized by redefining the t and T quark as follows:

$$t \to c_L t - s_L T, \qquad T \to c_L T + s_L t, \tag{3.36}$$

$$t^c \to c_R t^c - s_R T^c, \qquad T^c \to c_R T^c + s_R t^c, \tag{3.37}$$

where $s_L \equiv \sin\alpha_L$, $c_L \equiv \cos\alpha_L$ are the sine and cosine of the left-handed mixing angle and similarly for s_R, c_R. To leading order in an expansion in (v/f), these mixing angles are given by

$$\sin\alpha_L \approx \alpha_L = \frac{\lambda}{\lambda_c}\frac{m_t}{m_T} + \mathcal{O}\left(\frac{m_t^2}{m_T^2}\right), \tag{3.38}$$

$$\sin\alpha_R \approx \alpha_R = 0 + \mathcal{O}\left(\frac{m_t^2}{m_T^2}\right), \tag{3.39}$$

while the mass eigenvalues remain unperturbed at this order.

3.3.2 Scalar masses

Since the non-linear sigma model breaks the complete symmetry down to its diagonal vector group, the X-odd SU(2) and U(1) gauge bosons, which are associated with the broken generators, become massive by eating the triplet ϕ_w and singlet η_w in the scalar w multiplet, respectively. The other scalars are pseudo-Goldstone bosons that receive masses from all interactions that explicitly break some of the global symmetries. The only tree-level mass terms for the scalars stem from the plaquette operators (3.14) and (3.15), which lead to a mass $M_p^2 = 4\kappa f^2$ for all

fields in the x multiplet, and additional $\mathcal{O}(\epsilon f^2)$ contributions to all doublet fields. However, at one- and two-loop level, scalar mass terms are generated from various other Lagrangian.

One-loop corrections from the mirror fermion mass term (3.20) induce a quadratically divergent mass for the linear combination $x_1 + x_2 = -(y - z)$, of order $\mathcal{O}[\lambda_c^2\Lambda^2/(16\pi^2)] \sim \mathcal{O}(\lambda_c^2 f^2)$. Similarly, the top Yukawa coupling (3.25) generates quadratically divergent one-loop mass terms, of order $\mathcal{O}(\lambda^2 f^2)$ for the doublets in $x_3 - x_4 = x + w$ and singlets in $x_3 + x_4 = y + z$. On the other hand, the kinetic term (3.21) leads to two-loop mass terms that have quartic divergences [30]. As a result, the scalar doublets in $x_1^2 + x_2^2 = \frac{1}{2}(w-x)^2 + \frac{1}{2}(y-z)^2$ pick up masses of order $\mathcal{O}[g^2/(16\pi^2)^2 \times \Lambda^4/f^2] \sim \mathcal{O}(g^2 f^2)$.

The remaining doublet and triplet linear combinations $h_y + h_z$ and $\phi_y + \phi_z$ are protected from quadratically divergent one-loop mass terms. However, all scalar fields obtain logarithmic one-loop contributions and quadratically divergent two-loop contributions from the gauge kinetic terms and the plaquette operator. Furthermore, the doublet $h_y + h_z$ receives a logarithmic one-loop mass term from the top Yukawa coupling. These mass contributions are parametrically of the order of the electroweak scale $v \sim f/(16\pi^2)$. The X-even doublet $h_y + h_z$ will become the dominant component of the light Higgs boson, which is responsible for electroweak symmetry breaking.

Including all the aforementioned contributions, the scalar mass terms are given by

$$
\begin{aligned}
&\mathcal{L}_{\text{mass,scal}} = \\
&-\frac{1}{2}\big[(M_p^2 + m_{g,S}^2 + m_{p,S}^2)\eta_x^2 + (M_t^2 + m_{g,S}^2 + m_{p,S}^2)(\eta_y^2 + \eta_z^2) + M_y^2(\eta_y - \eta_z)^2\big] \\
&-\frac{1}{2}\big[(M_p^2 + m_{g,T}^2 + m_{p,T}^2)|\phi_x|^2 + (m_{g,T}^2 + m_{p,T}^2)(|\phi_y|^2 + |\phi_z|^2) + \tfrac{3}{2}M_y^2|\phi_y - \phi_z|^2\big] \\
&-\frac{1}{2}\big[M_p^2|h_x|^2 + (M_t^2 + m_{g,D}^2 + m_{p,D}^2)(|h_x|^2 + |h_w|^2) + (M_{kin}^2 + M_y^2)|h_w - h_x|^2 \\
&\qquad + (M_{kin}^2 + M_y^2)|h_y - h_z|^2 + m_t^2|h_y + h_z|^2 + (m_{g,D}^2 + m_{p,D}^2)(|h_y|^2 + |h_z|^2) \\
&\qquad + i\, m_\epsilon^2(h_w^\dagger h_x - h_x^\dagger h_w + h_z^\dagger h_y - h_y^\dagger h_z)\big],
\end{aligned}
\tag{3.40}
$$

where the singlet, triplet, and doublet mass terms are shown in the first, second, and remaining lines, respectively. The mass parameters are summarized in the

following list:

$M_p^2 \equiv 4\kappa f^2$	plaquette mass
$m_\epsilon^2 \equiv \frac{\sqrt{3}}{2} f^2 \mathrm{Im}(\epsilon)$	ϵ-plaquette term from (3.15)
$M_{\mathrm{kin}}^2 \equiv c_k g^2 f^2$	2-loop mass from (3.21)
$M_y^2 \equiv c_y \lambda_c^2 f^2$	1-loop mass from (3.20)
$m_{g,X}^2 \equiv c_{g,X}\, g^4 f^2/(4\pi)^2 \log(g^2 f^2/\Lambda^2)$	gauge-loop mass, log part
$M_t^2 \equiv c_T \lambda^2 f^2$	top loop from (3.25), quad. div. part
$m_{t,D}^2 \equiv c_t M_{T'}^2/(4\pi)^2 \log(M_{T'}^2/m_t^2)$	top loop from (3.25), log part
$m_{p,X}^2 \equiv c_{p,X}\, \kappa^2 f^2/(4\pi)^2 \log(\kappa f^2/\Lambda^2)$	plaquette-loop mass, log part

Here the $\mathcal{O}(f)$ terms are written in capital letters, while lower case is used for the lighter mass terms. m_t and $M_{T'}$ denote the top quark mass and the mass of the T' quark. The latter cancels the quadratic divergences in the top loop contribution to the Higgs mass. The c_i are $\mathcal{O}(1)$ coefficients, which, except for c_t, depend on unknown details of the UV completion. However, it is possible to determine the *relative* contributions of the gauge loops to the singlets, doublets, and triplets, which are given by $c_{g,S} = 0$ (since the singlets commute with all gauge generators), $c_{g,T} \sim 1/8$, and $c_{g,D} \sim \frac{3}{64}[1 + (g'/g)^4]$.

The doublet h_w does not get eaten and remains in the physical spectrum. It mixes with the other X-odd doublet h_x to form two mass eigenstates h_{H1} and h_{H2} with $\mathcal{O}(f)$ masses. λ_c can be relatively large, leading to a rather large splitting between the two masses, and to a large mixing. In the limit of large λ_c, the X-odd doublet masses are approximately given by $M_{\mathrm{H1}}^2 \approx M_t^2 + M_p^2/2$ and $M_{\mathrm{H2}}^2 \approx M_{\mathrm{H1}}^2 + 2M_y^2 + 2M_{\mathrm{kin}}^2$.

3.3.3 Electroweak symmetry breaking

The plaquette interactions (3.14) generate quartic couplings for the X-even scalars, which can be written as

$$-\kappa \,\mathrm{Tr}\,[y, z]^2. \tag{3.41}$$

Additional quartic interactions emerge from the second plaquette term (3.15) and from loop corrections but will be neglected at this point.

To further analyse the Higgs potential, it is useful to switch back to the basis (3.3) using

$$h_a = \tfrac{1}{\sqrt{2}}(h_y + h_z), \qquad\qquad h_b = \tfrac{1}{\sqrt{2}}(h_y - h_z). \tag{3.42}$$

In this basis, the quartic potential for the X-even doublets reads

$$V_4 = \frac{\kappa}{8}\left[(h_a^\dagger h_a)(h_b^\dagger h_b) + (h_a^\dagger h_b)(h_b^\dagger h_a) - (h_a^\dagger h_b)^2 - (h_b^\dagger h_a)^2\right], \tag{3.43}$$

while the quadratic potential, taken from eq. (3.40), is given by

$$V_2 = \frac{1}{2}\left[m_a^2|h_a|^2 + m_b^2|h_b|^2 + (m_{ab}^2 h_a^\dagger h_b + \text{h.c.})\right], \tag{3.44}$$

with the mass parameters

$$m_a^2 = 2m_t^2 + m_{g,D}^2 + m_{p,D}^2\,, \tag{3.45}$$
$$m_b^2 = 2M_{kin}^2 + 2M_y^2 + m_{g,D}^2 + m_{p,D}^2\,, \tag{3.46}$$
$$m_{ab}^2 = -im_\epsilon^2\,. \tag{3.47}$$

As evident from these equations, electroweak symmetry breaking is described in this model by an effective Two-Higgs-Doublet model (2HDM). The conditions for successful symmetry breaking are

$$m_{g,D}^2 > -2m_t^2\,, \quad m_\epsilon^4 > (2M_y^2 + 2M_{kin}^2 + m_{g,D}^2 + m_{p,D}^2)(2m_t^2 + m_{g,D}^2 + m_{p,D}^2)\,. \tag{3.48}$$

Since $m_{g,D}^2$ and m_t^2 are of the same order of magnitude and m_t^2 is negative, these conditions can be satisfied naturally. Without the m_ϵ term, the Higgs potential would have an unstabilized flat direction, and electroweak symmetry would not be broken to the SM vacuum.

The potential is then minimized by the vacuum expectation values

$$\langle h_a\rangle = (0, v\cos\beta)^\top \qquad\qquad \langle h_b\rangle = (0, i\,v\sin\beta)^\top\,, \tag{3.49}$$

with

$$\tan^2\beta = m_a^2/m_b^2 = \mathcal{O}(m^2/M^2), \tag{3.50}$$

where M denotes the $\mathcal{O}(f)$ masses in the scalar potential, while m represents any of the suppressed mass terms. We have checked numerically that for reasonable choices of the mass parameters defined above a value for v close to the electroweak scale $v = 246$ GeV can be obtained.

The complex coupling constant ϵ of the second plaquette term (3.15) leads to CP violation in the Higgs sector, as evident by the complex vacuum expectation value of the second Higgs doublet in eq. (3.49). Since it is assumed that $|\epsilon|$ is smaller than $|\kappa|$ by about one order of magnitude, the amount of CP violation is relatively small. Nevertheless, it could lead to potentially important consequences for flavor physics. However, a detailed analysis of CP-violating effects of our model is beyond the scope of this article and is left for future work.

Neglecting the CP-violating contribution from ϵ and m_ϵ^2, the decomposition of the Higgs doublets into physical states is given by

$$h_a = \begin{pmatrix} \sqrt{2}G^+ \\ v + h^0 + iG^0 \end{pmatrix} \qquad\qquad h_b = \begin{pmatrix} \sqrt{2}H^+ \\ H^0 + iA^0 \end{pmatrix}. \tag{3.51}$$

As usual for a 2HDM, one obtains the Goldstone bosons G^0, G^+ and $G^- = (G^+)^\dagger$, which are eaten by the SM gauge bosons, a neutral pseudoscalar A^0, a pair of charged scalars H^+ and $H^- = (H^+)^\dagger$, and two CP-even neutral scalars h^0 and H^0. The pseudoscalar mass is given by $M_A^2 = (m_a^2 + m_b^2)$. The masses of $H^\pm$ and H^0 are very close to M_A, differing only by $\mathcal{O}(m^2/M^2)$ effects.

Including the CP-violating contribution from the m_ϵ^2 parameter would lead to a small mixing between the doublets and between CP eigenstates. However, as mentioned above, these effects will be neglected for the purpose of this work.

The SM-like Higgs boson is h^0, which at tree-level has a very small mass, in conflict with direct search limits[3]. However, loop corrections to the quartic potential yield positive contributions to m_h. For example, loops involving the top quark and its heavy partners generate a correction of the type

$$\Delta m_h^2 \propto \frac{1}{\pi^2} v^2 \lambda_t^4. \tag{3.52}$$

In general, these radiative corrections cannot be computed explicitly in the effective little Higgs theory, since they depend on the UV cutoff Λ. However, they are generally comparable to the electroweak scale and thus could lead to a value of m_h above the current search limit. Since m_h is very sensitive to these loop contributions, we will take it as a free parameters in the following. Note that the loop corrections to the quartic potential have a negligible effect on the masses of the heavy Higgs bosons $A^0, H^\pm, H^0$.

3.4 Phenomenology

In Table 3.2 the particle content of the model beyond the SM gauge bosons and fermions is summarized. Since the model requires a UV completion, additional degrees of freedom are expected at the scale $\Lambda \sim 10$ TeV, but will not be discussed here.

The charge eigenstates of the gauge bosons and scalars are given by

$$W_{\rm H}^0 \equiv W_{\rm H}^3, \qquad W_{\rm H}^\pm \equiv (W_{\rm H}^1 \mp i W_{\rm H}^2)/\sqrt{2}, \tag{3.53}$$

$$\phi_i^0 \equiv \phi_i^3, \qquad \phi_i^\pm \equiv (\phi_i^1 \mp i\phi_i^2)/\sqrt{2}. \tag{3.54}$$

Most new particles have $\mathcal{O}(f) \sim \mathcal{O}(\text{TeV})$ masses. In the table, relative corrections of order $\mathcal{O}(v/f)$ to these mass parameters have been neglected. However, besides the light Higgs boson h^0, an additional scalar triplet ϕ_a with weak-scale mass is predicted. These scalars are odd under T-parity, so that sizable numbers can be produced only in pairs, but since they are even under X-parity, they can

[3]The small tree-level value for m_h is not an artifact of our implementation of X-parity, but would also arise in earlier versions of the minimal moose model in Refs. [30, 57, 58].

Field		X-parity	T-parity	Mass squared
Heavy gauge bosons	$B^0_{\mathrm{H}\mu}$	$-$	$-$	$\frac{4}{3}g'^2f^2$
	$W^0_{\mathrm{H}\mu}, W^\pm_{\mathrm{H}\mu}$	$-$	$-$	$4g^2f^2$
Singlet scalars	η_x	$-$	$-$	$4\kappa f^2$
	$\eta_b \equiv \frac{1}{\sqrt{2}}(\eta_y - \eta_z)$	$+$	$-$	$(2c_y\lambda_c^2 + c_T\lambda^2)f^2$
	$\eta_a \equiv \frac{1}{\sqrt{2}}(\eta_y + \eta_z)$	$+$	$-$	$c_T\lambda^2 f^2$
Triplet scalars	ϕ_x	$-$	$-$	$4\kappa f^2$
	$\phi_b \equiv \frac{1}{\sqrt{2}}(\phi_y - \phi_z)$	$+$	$-$	$3c_y\lambda_c^2 f^2$
	$\phi_a \equiv \frac{1}{\sqrt{2}}(\phi_y + \phi_z)$	$+$	$-$	$m_{g,T}^2 + m_{p,T}^2$
X-odd doublet scalars	$h_{\mathrm{H}1}$	$-$	$+$	$M_{\mathrm{H}1}^2$
	$h_{\mathrm{H}2}$	$-$	$+$	$M_{\mathrm{H}2}^2$
X-even doublet scalars	$H^\pm$	$+$	$+$	M_A^2
	A^0	$+$	$+$	M_A^2
	H^0	$+$	$+$	M_A^2
	h^0	$+$	$+$	m_h^2
Heavy top partners	T_{H}	$-$	$-$	$4\lambda_c^2 f^2$
	T'	$-$	$-$	$4\lambda^2 f^2$
	T	$+$	$+$	$4(\lambda^2 + \lambda_c^2)f^2$
Other heavy quarks	Q_{H}	$-$	$-$	$4\lambda_c^2 f^2$
Heavy leptons	L_{H}	$-$	$-$	$4(\lambda_c^l)^2 f^2$

Table 3.2: *List of particles (besides SM particles) below the strong scale Λ and the dominant contributions to their masses. Mass corrections of order $\mathcal{O}(v/f)$ are neglected.*

decay through the WZW coupling. In principle, the WZW term also permits single ϕ_a production, but at a highly suppressed rate, which is thus completely negligible. For the same reason, all other T-odd particles will decay first to one of the particles in ϕ_a through T-conserving channels instead of directly decaying via the WZW term.

Since X-parity is exactly preserved, the lightest X-odd particle is stable. If all coupling parameters are not much smaller than unity, the lightest X-odd particle is the heavy U(1) gauge boson, $B^0_{\mathrm{H}\mu}$, which is a viable dark matter candidate.

3.4.1 Electroweak precision constraints

X-parity has been shown to largely reduce the constraints on the parameter space in the case of the littlest Higgs model [30,69], since corrections to the electroweak

precision observables arise only at loop level. Here we calculate the corrections to the electroweak S and T parameters [70] in our model to determine the allowed parameter space.

The dominant contribution to S and T from the fermion sector come from gauge boson self energy diagrams with the X-even T quark running in the loop, a contribution that has already been calculated in Ref. [71]. In spite of the different symmetry structure of the model and the modified implementation of the top-Yukawa couplings the results are almost identical to those obtained in the case of the littlest Higgs model [69]. We find

$$\Delta S = \frac{s_L^2}{2\pi}\left[c_L^2\left(\frac{(m_T^2+m_t^2)^2}{(m_T^2-m_t^2)^2}-\frac{8}{3}\right)+\left(\frac{1}{3}+c_L^2\frac{2m_t^4m_T^4(m_t^2-3m_T^2)}{(m_t^2-m_T^2)^3}-c_L^2\right)\log\frac{m_t^2}{m_T^2}\right] \tag{3.55}$$

$$\Delta T = \frac{3}{16\pi}\frac{s_L^2}{c_{\rm W}^2 s_{\rm W}^2}\frac{m_t^2}{m_Z^2}\left[s_L^2\frac{m_T^2}{m_t^2}-1-c_L^2-\frac{2c_L^2}{1-x_t}\log\frac{m_t^2}{m_T^2}\right], \tag{3.56}$$

where s_L, c_L are the mixing angles defined in (3.36) and $s_{\rm W}, c_{\rm W}$ are the sine and cosine of the Weinberg angle, respectively. Inserting the leading order expressions for the mixing angles (3.38) and expanding the expressions in the limit $m_t^2 \ll m_T^2$ one arrives at

$$\Delta S = \frac{1}{2\pi}\frac{\lambda^2}{\lambda_c^2}\frac{m_t^2}{m_T^2}\left(-\frac{5}{3}+\frac{2}{3}\log\frac{m_T^2}{m_t^2}\right), \tag{3.57}$$

$$\Delta T = \frac{3}{16\pi}\frac{1}{s_{\rm W}^2 c_{\rm W}^2}\frac{\lambda^2}{\lambda_c^2}\frac{m_t^4}{m_T^2 m_Z^2}\left(2\log\frac{m_T^2}{m_t^2}-2+\frac{\lambda^2}{\lambda_c^2}\right). \tag{3.58}$$

Another contribution to the T parameter arises from the custodial symmetry violating mass splitting between the neutral and the charged $W_{\rm H}$ gauge bosons. At the one loop level this yields [30, 69]:

$$\Delta T_{W_{\rm H}} = -\frac{9}{16\pi c_{\rm W}^2 s_{\rm W}^2 M_Z^2}\Delta M_{W_{\rm H}}^2 \log\frac{\Lambda^2}{M_{W_{\rm H}}^2}. \tag{3.59}$$

The logarithmic divergence forces one to introduce an appropriate counterterm with an unknown coefficient δ_c of order one [30, 69]. In our model the mass splitting is given by

$$\Delta M_{W_{\rm H}}^2 = \frac{g^2}{16}\frac{v^4}{f^2}\left(3+\sin^2(2\beta)-\cos^2(2\beta)\right) \approx \frac{g^2}{8}\frac{v^4}{f^2} \tag{3.60}$$

Including the counterterm this leads to a contribution to the T parameter of

$$\Delta T_{W_{\rm H}} = -\frac{1}{4\pi s_{\rm W}^2}\frac{v^2}{f^2}\left(\delta_c+\frac{9}{4}\log\frac{4\pi}{g}\right). \tag{3.61}$$

Next we discuss the contributions to electroweak precision observables that arise from the scalar sector. The scalar singlets present in the theory do not contribute to the S and T parameter. Contributions of the scalar triplets to the T parameter are proportional to the mass splitting between the charged and neutral components. This splitting is induced only after electroweak symmetry breaking and is generally small in our model, even for the light X-even triplet.

In the limit of vanishing CP violation in the Higgs sector the contribution of the two X-even Higgs doublets is well approximated by the SM Higgs contribution and the contribution of a heavy Higgs doublet that is given by [72]

$$\Delta T_{\text{2HDM}} = \frac{1}{16\pi s_{\text{W}}^2 c_{\text{W}}^2 m_Z^2} \left[F(M_{H^+}^2, M_{A^0}^2) + F(M_{H^+}^2, M_{H^0}^2) - F(M_{A^0}^2, M_{H^0}^2)) \right], \tag{3.62}$$

where

$$F(m_1^2, m_2^2) = \frac{1}{2}(m_1^2 + m_2^2) - \frac{m_1^2 m_2^2}{m_1^2 - m_2^2} \log \frac{m_1^2}{m_2^2}. \tag{3.63}$$

For small mass differences this contribution is proportional to the mass differences between the charged and neutral heavy Higgs bosons. Since the actual values of $M_{H^\pm}^2 - M_{A^0}^2$ and $M_{H^0}^2 - M_{A^0}^2$ depend on unknown counterterm coefficients and are furthermore sensitive to radiative corrections to the quartic couplings, we take these mass differences as free parameters $\delta_\pm^2$ and δ_0^2 of order $(100\ \text{GeV})^2$. The contribution to the S parameter is small when the mass differences of the heavy scalars are small compared to their masses, so we can neglect it here. Taking into account the CP violation in the Higgs sector only affects the mixing between the Higgs scalars. Since these mixings are small, they do not change the contributions to the S and T parameter significantly.

The X-odd doublets lead to a contribution of similar size, which depends on the incalculable $\mathcal{O}(v^2)$ mass splittings in the h_w and h_x doublets. For simplicity, we do not include these terms explicitly, since the overall magnitude of the Higgs corrections can be estimated sufficiently well from equation (3.62).

Other one loop contributions to the T parameter arise from mass splittings in the mirror fermion doublets. The magnitude of such corrections has been estimated in Ref. [69] and it was found that they are suppressed compared to the contributions discussed above.

Apart from the loop-induced contributions to the T parameter the custodial symmetry violating kinetic term of the Goldstone bosons (3.5) contributes at the tree level through operators of the form[4]

$$\frac{c}{f^2} \left| h_{a,b}^\dagger D_\mu h_{a,b} \right|^2, \tag{3.64}$$

[4]We thank Ian Low for pointing out the relevance of this operator to us.

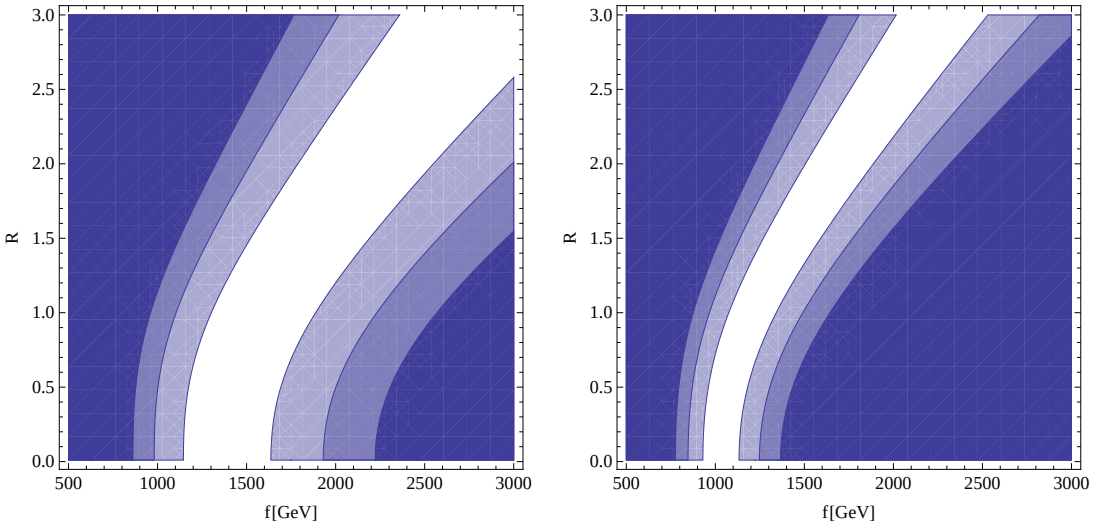

Figure 3.2: *Allowed regions in the f-R parameter space for fixed values of δ_c, $\delta_\pm$ and δ_0. From lightest to darkest the shaded regions indicate a deviation of the T parameter from the experimental value by more than one, two and three sigma, respectively. Both plots use $\delta_c = 5$. The mass splittings are $\delta_\pm^2 = 0.1f^2$ and $\delta_0^2 = 0.2f^2$ in the left plot and $\delta_\pm^2 = -0.15f^2$ and $\delta_0^2 = -0.3f^2$ in the right plot.*

where $h_{a,b}$ are the X-even Higgs doublets. In our model this leads to a sizable contribution to the T parameter of

$$\Delta T \approx 0.5 \frac{\text{TeV}}{f^2}\,. \tag{3.65}$$

This contribution seems to disfavor values of f below about 2 TeV. However, it will be shown below that values of f around 1 TeV can be in agreement with experimental data due to cancellations between different contributions to the T parameter[5].

The experimental values for the S and T parameters are [73]

$$S = -0.04 \pm 0.09 \tag{3.66}$$

$$T = 0.02 \pm 0.09 \tag{3.67}$$

for a Higgs mass of $m_h = 117$ GeV and fixing the U parameter to $U = 0$. The contributions to the S parameter from the top sector are small for all reasonable choices of parameters, and in particular do not lead to additional constraints on regions that give a satisfactory T parameter.

[5]Note that a larger custodial symmetry violating contribution from heavy gauge boson exchange in the model of Ref. [58] is forbidden by X- and T-parity.

For values of $f > 1$ TeV the contributions of the top sector and the gauge boson sector each stay within the experimental limit of T for most choices of the parameters R and δ_c respectively. The contribution (3.65), taken separately, would push this value towards $f \gtrsim 2$ TeV. The contribution of the Higgs doublets does not directly constrain the scale f but essentially depends on the mass splitting $\delta_\pm$ and δ_0. When the mass splittings are such that one neutral Higgs is lighter and one heavier than the charged Higgs boson, this contribution is negative and can partially cancel the contribution (3.65), thus allowing lower values of f. In figure 3.2 we show that for reasonable choices of the mass splitting parameters and of δ_c these cancellations take place, allowing for values of f at the 1 TeV scale, and even slightly below.

The left plot shows an example where the H^0 is the heaviest Higgs boson and $H^\pm$ is heavier than A^0, while the right plot shows an example with the hierarchy inverted. For both plots the splittings have been chosen proportional to the mass scale f. This causes some regions in the f-R plane to be excluded also for large values of f, since there the contributions from the Higgs loops become dominant.

A moderate amount of fine tuning is involved to cancel the contribution of eq. (3.65) for smaller values of f. At this point it is worth mentioning that this contribution is absent in models where the Higgs sector has a custodial symmetry, which can be achieved by enlarging the global symmetry group. A concrete realization of this idea, based on a $SO(5) \times SO(5)$ group structure, has been constructed *e. g.* in Ref. [61]. It is certainly possible to extend the present model in a similar way in order to enlarge the allowed parameter space at low scales, however for the sake of simplicity we decided against discussing this here. Furthermore, while this model allows a straightforward ultraviolet completion with QCD-like dynamics, such a construction is less obvious for models that implement a custodial symmetry using orthogonal groups.

3.4.2 Decays of heavy particles

For concreteness, we assume the plaquette parameter to be close to unity, $\kappa \approx 1$. Furthermore, the UV-sensitive coefficients c_i, introduced below eq. (3.40), are also assumed to be of order $\mathcal{O}(1)$. As pointed out above, the Yukawa coupling λ_c of the mirror fermions can be chosen relatively large, $\lambda_c \gg 1$, since these fermions do not play any role in compensating the quadratic divergences in the Higgs mass. In this case also the X-even top partner T will be heavy. As examples, two scenarios will be considered, one with mirror fermion masses near the breaking scale f, and one with very heavy mirror quarks:

$$\text{“Light mirror fermion” scenario:} \qquad \lambda_c \approx \lambda \approx 1/\sqrt{2}, \qquad R \approx 1, \tag{3.68}$$

$$\text{“Heavy mirror fermion” scenario:} \qquad \lambda_c \approx 4, \;\; \lambda \approx 1/2, \qquad R \approx 1/8. \tag{3.69}$$

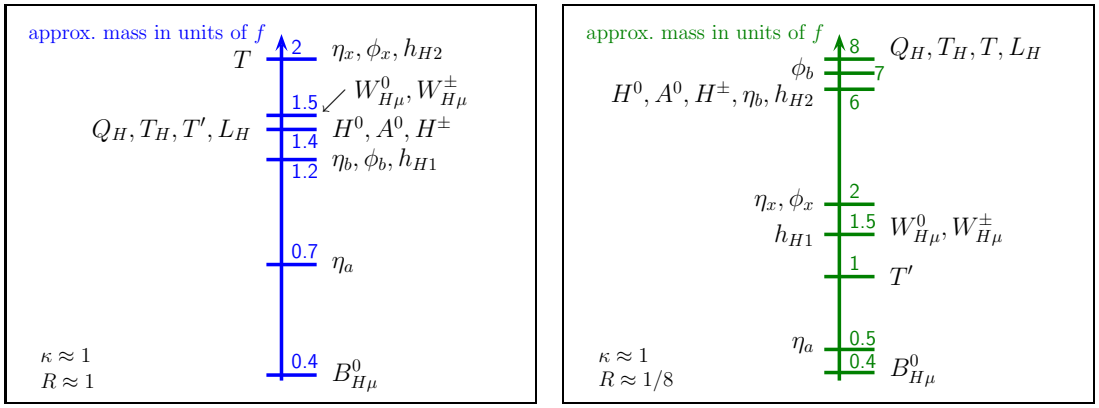

Figure 3.3: *Approximate patterns of two typical spectra of $\mathcal{O}(f)$ particle masses. In both cases, the non-calculable coefficients are assumed to be of order unity, $c_i \approx 1$.*

Note that λ_c, λ and $R = \lambda/\lambda_c$ are related through the top Yukawa coupling (3.35), which must be $\lambda_t \approx 1/\sqrt{2}$ to reproduce the experimental value for the top-quark mass. The mass hierarchy of the two scenarios is sketched in Fig. 3.3.

The mass pattern and the conservation of X- and T-parity and gauge symmetries strongly constrain the possible decay channels of the heavy particles. The gauge symmetries, however, are violated by electroweak symmetry breaking, leading to a small mixing between the heavy gauge bosons $W^0_{\rm H}$ and $B^0_{\rm H}$, with the mixing angle given by

$$\sin\theta_{\rm H} = \frac{3gg'}{16(3g^2 - g'^2)}\,\frac{v^2}{f^2}. \tag{3.70}$$

While this mixing is suppressed by two powers of v/f, it nevertheless can be relevant for decays of some particles that do not have any other possible decay modes.

The dominant decay channels are summarized in Table 3.3, for the two scenarios introduced above. Not included in the table are weakly interacting particles with masses larger than about $2f$ and strongly interacting particles with masses larger than about $5f$, since they are expected to be beyond the reach of the LHC (assuming $f \gtrsim 500$ GeV). As mentioned above, the lightest T-odd particle decays through the WZW term, but the WZW contribution is negligible compared to T-conserving interactions for all decays of heavier T-odd particles.

Independent of other parameters, the lightest T-odd particle will be one of the scalars in the triplet ϕ_a, since they do not receive any $\mathcal{O}(f)$ mass terms. At leading order in $1/f$ the WZW term induces decays of into pairs of SM gauge bosons [63]. The masses of the three scalars $\phi_a^{0,\pm}$ are almost degenerate, with a small splitting between the neutral ϕ_a^0 and the charged $\phi_a^\pm$ incurred from EWSB and the gauge boson loop contribution $m_{g,T}$ in eq. (3.40) only at order $\mathcal{O}[g^4 f^2/(4\pi^2)] \sim \mathcal{O}[g^4 v^2]$. At this order, higher-order operators from the UV completion could yield

"Light mirror fermions" $\kappa \approx 1, R \approx 1$	"Heavy mirror fermions" $\kappa \approx 1, R \approx 0.09$
$Q_{\rm H} \to q\, B^0_{\rm H}$; $\quad L_{\rm H} \to l\, B^0_{\rm H}$ $T' \to t\, B^0_{\rm H}$ $T \to t\, h^0,\ t\, H^0,\ t\, A^0,\ b\, H^+,\ T'\, B^0_{\rm H}$	$T' \to t\, B^0_{\rm H}$
$W^0_{\rm H} \to \bar{f}\, F_{\rm H},\ f\, \overline{F}_{\rm H}$ $W^\pm_{\rm H} \to \bar{f}'\, F_{\rm H},\ f'\, \overline{F}_{\rm H}$	$W^0_{\rm H} \to h^0\, B^0_{\rm H}$ $W^\pm_{\rm H} \to W^\pm B^0_{\rm H}$
$H^0 \to t\bar{t}$ $A^0 \to t\bar{t}$; $\quad H^+ \to t\bar{b}$	
$h^{0,\pm}_{\rm H1} \to t\bar{t}\, \phi^{0,\pm}_a\, B^0_{\rm H}$	$h^{0,\pm}_{\rm H1} \to t\, \overline{T}'\, \phi^{0,\pm}_a,\ \bar{t}\, T'\, \phi^{0,\pm}_a$
$\eta_a \to h^0\, \phi^0_a$ $\phi^0_a \to W^+W^-,\ Z^0Z^0,\ Z^0\gamma,\ \gamma\gamma$ $\phi^\pm_a \to (W^\pm)^* \phi^0_a,\ W^\pm Z,\ W^\pm\gamma$	$\eta_a \to h^0\, \phi^0_a$ $\phi^0_a \to W^+W^-,\ Z^0Z^0,\ Z^0\gamma,\ \gamma\gamma$ $\phi^\pm_a \to (W^\pm)^* \phi^0_a,\ W^\pm Z,\ W^\pm\gamma$
$\eta_b \to (A^0)^*\, \phi^0_a,\ (H^\pm)^*\, \phi^\mp_a,\ (A^0)^*\, \eta_a$ $\phi^0_b \to (A^0)^*\, \phi^0_a,\ (H^\pm)^*\, \phi^\mp_a,\ (A^0)^*\, n_a$ $\phi^\pm_b \to h^0\, \phi^\pm_a$	

Table 3.3: *Dominant decay modes for heavy particles expected to be observable at the LHC, for the two qualitative spectra in Fig. 3.3. Weakly interacting particles with masses $M \gtrsim 2f$ and strongly interacting particles with masses $M \gtrsim 5f$ are not listed, since they are assumed to be beyond the reach of the LHC. $(X)^*$ indicates an off-shell particle.*

additional contributions to the mass splitting, so that it cannot be calculated reliably from the effective little Higgs model. For concreteness, we will therefore assume that the $\phi^\pm_a$ are slightly heavier than ϕ^0_a, opening up the decay $\phi^\pm_a \to (W^\pm)^*\phi^0_a$ through a virtual W boson. Depending on the magnitude of the mass splitting, this decay could dominate over the direct decays into $W^\pm\gamma$ and $W^\pm Z$ that are mediated by the WZW term.

In the "light mirror fermion" scenario, since the SU(2) gauge bosons $W^{0,\pm}_{\rm H}$ are relatively heavy, they can decay into a mirror fermion plus the corresponding SM partner fermion. Decays of $W^{0,\pm}_{\rm H}$ directly to the lightest X-odd particle $B^0_{\rm H}$ via emission of SM gauge bosons or Higgs bosons are suppressed by $\mathcal{O}(v^2/f^2)$. Therefore, these channels have a branching ratio of at most a few per-cent. Similarly, to leading order in v/f, the other two top partners T and T' are SU(2) singlets and thus only interact through Yukawa or U(1) couplings. Consequently, the do not contribute significantly to heavy SU(2) gauge boson decays.

The X-odd fermions can only decay to the heavy hypercharge boson $B^0_{\rm H}$. Although the mirror fermions are not charged under the heavy hypercharge group

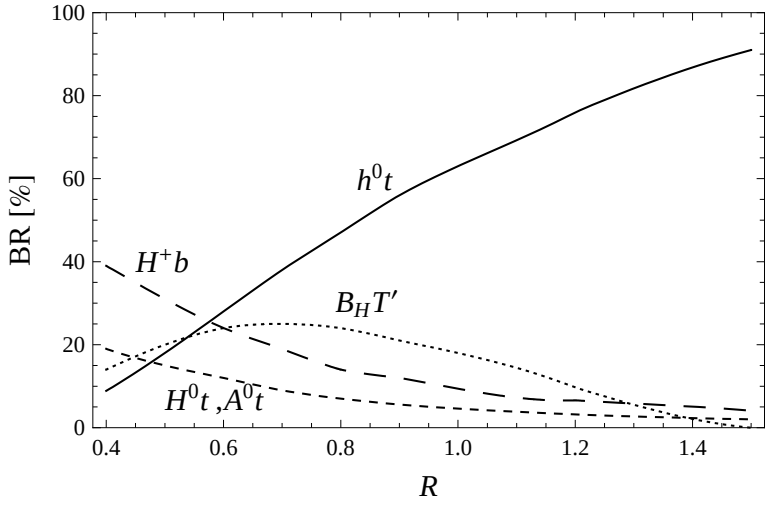

Figure 3.4: *Branching fractions for the dominant decay modes of the X-even T quark, as a function of $R = \lambda/\lambda_c$, and for $f = 1$ TeV.*

(see Table 3.1), this decay is enabled through the mixing between $W_{\rm H}^0$ and $B_{\rm H}^0$.

The situation is different for the X-even T quark, which has sizable couplings to the Higgs bosons from the top Yukawa term (3.32) and to the $B_{\rm H}^0$ boson via its hypercharge quantum number. Figure 3.4 shows the branching fractions for the dominant decay modes as a function of the Yukawa coupling ratio R. For the purpose of this plot, the Higgs boson masses have been calculated using the loop-induced mass terms from section 3.3.2 with $c_i = 1$. The branching ratios depend only mildly on f. As evident from the plot, the decay $T \to h^0 t$ is dominant in most of the parameter space, but decays into the heavier Higgs boson can become sizable.

In the second scenario, the mirror fermions and many scalar particles are too heavy to be observables at the LHC. In this case, the gauge bosons $W_{\rm H}^{0,\pm}$ decay to the $B_{\rm H}^0$ via emission of a SM gauge boson or the little Higgs boson. As mentioned above, the T' top partner, which is always lighter than the heavy SU(2) gauge bosons, is a SU(2) singlet. As a result, the decay $W_{\rm H}^+ \to T'\bar{b}$ is forbidden, while the channel $W_{\rm H}^0 \to T'\bar{t}, \overline{T}'t$ can only proceed through the small mixing of the $W_{\rm H}^0$ with the $B_{\rm H}^0$. Therefore this leads to an additional suppression compared to the decay $W_{\rm H}^0 \to h^0\, B_{\rm H}^0$:

$$\Gamma[W_{\rm H}^0 \to T'\bar{t}, \overline{T}'t] \propto \cos^2\theta_{\rm H} \approx 10^{-3} \times v^4/f^4, \qquad \Gamma[W_{\rm H}^0 \to h^0\, B_{\rm H}^0] \ \propto v^2/f^2. \tag{3.71}$$

Consequently, the decay of the heavy SU(2) gauge bosons into the top partner T' can be neglected.

The X-even Higgs bosons H^0, A^0, and $H^\pm$ decay predominantly into third-generation SM fermions through the Yukawa couplings eqs. (3.20),(3.25). On the other hand, their coupling to the SM gauge bosons is suppressed by the small

mixing angle β, see eq. 3.50, rendering these decay channels negligible.

Of the X-odd doublet scalars, one doublet is typically very heavy. The lighter doublet h_{H1} contains one CP-even and one CP-odd neutral scalar and two charged states. Their decays are strongly constrained by their charges under X- and T-parity. If the T' is light enough, three-body decay channels are open, otherwise the scalars in h_{H1} can only decay into a four-body final state.

For the singlet scalars the plaquette operator (3.14) is the only interaction term in the model. At tree-level, the η_b singlet can decay into $A^0\,\phi_a^0$, $H^\pm\,\phi_a^\mp$, and $A^0\,\eta_a$, which all have partial widths of the roughly the same order. As the masses of η_b, A^0 and $H^\pm$ are close to each other, the doublet Higgs bosons must be slightly off-shell in these decays. In the same way one obtains the decay modes of $\phi_b^{0,\pm}$.

3.4.3 Collider phenomenology

For values of f near 1 TeV, several of the new particles predicted by the minimal moose model with exact X-parity are within reach of the LHC. We have calculated cross sections using the program CompHEP 4.4 [74], using a model file generated with the help of the LanHEP package [75].

The production of heavy gauge bosons ($W_{\mathrm{H}}^{0,\pm}$) and mirror quarks (Q_{H}) proceeds in the same way as for the littlest Higgs model with T-parity, since all relevant interactions are constrained by gauge invariance. The reader is referred to the literature on the littlest Higgs model for more details on production channels and cross sections [76]. However, compared to the littlest Higgs model, the X-odd gauge bosons are heavier in the minimal moose model (as a function of f). As a result, production cross section for these heavy gauge bosons are relatively small throughout the allowed parameter range.

A special feature of our model are the light triplet scalars $\phi_a^{0,\pm}$. Since they are odd under T-parity, the single production cross section is negligible, but pair production can lead to sizable rates. The lightest T-odd scalar, assumed to be the ϕ_a^0, decays through the WZW interaction into two SM gauge bosons. In particular, the decay into two photons is allowed, leading to striking signatures with one charged lepton or jet and up to four photons in the final state.

The main production mode for ϕ_a pairs at the LHC are the Drell-Yan processes with the Feynman diagrams shown at the left of Fig. 3.5. The tree-level cross sections are also shown in Fig. 3.5. The production of ϕ_a pairs from gluon fusion through s-channel Higgs boson exchange is suppressed by several powers of v/f. We have checked explicitly that this channel is negligible compared to the leading Drell-Yan mode. $W^\pm + 3\gamma$ and $W^\pm + 4\gamma$ are the most exciting final states that result from ϕ_a pair production.

For all other exotic scalars in the model the productions cross sections are small, $\mathcal{O}$(fb) or below, since those particles are relatively heavy and have only

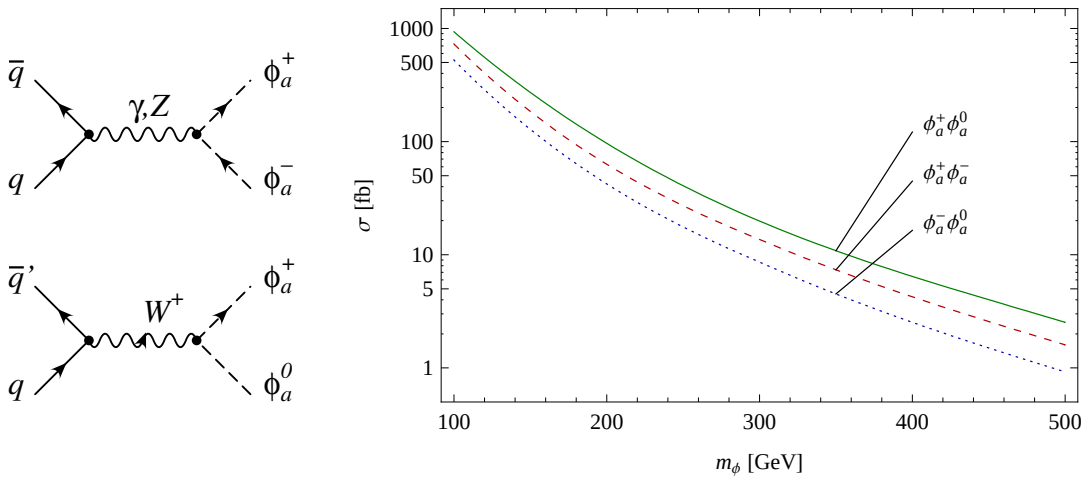

Figure 3.5: *Pair production diagrams and LHC cross sections for the particles in the lightest scalar triplet, as a function of their mass. The factorization scale has been set to m_ϕ, and the center-of-mass energy is $\sqrt{s} = 14$ TeV.*

couplings of weak interaction strength. Therefore the observation of any of these scalars from direct production at the LHC would be very challenging.

On the other hand, colored particles have relatively large cross sections at the LHC, in particular the top-quark partners T, which can be produced singly, and T', which is predicted to be relatively light to cancel the quadratic divergences to the Higgs mass parameter.

Single T production, $pp \to T\bar{b} + X$, $\bar{T}b + X$ proceeds dominantly through the partonic processes $b\bar{q} \to T\bar{q}'$ and $\bar{b}q \to \overline{T}q'$, where q, q' are SM quarks of the first two generations. The initial-state bottom quarks can be thought of originating from gluon splitting, $g \to b\bar{b}$, but for the purpose of this analysis we use the alternative formulation where the bottom quarks are included in the parton distribution functions, see for example Ref. [77]. T quarks can also be produced in pairs through the partonic processes $gg \to T\overline{T}$ and $q\bar{q} \to T\overline{T}$. The LHC production cross sections are shown in Fig. 3.6 (a).

Single T production is mediated mainly by t-channel exchange of W bosons, which couple only to the small top-quark admixture in T, see eq. (3.38). As a result, the single T cross section strongly depends on the mixing parameters, and thus on $R = \lambda/\lambda_c$. In contrast, the pair production process is mainly governed by QCD gluon exchange and thus insensitive to mixing. In spite of the coupling suppression of the single T contribution this process is dominant for $M_T \gtrsim 1$ TeV, owing to the smaller mass of the final state system (see Fig. 3.6 (a)).

For relatively low values of M_T, the production rates can reach several tens of fb. The dominant decay mode $T \to h^0 t$ leads to the signature $4b + W$ in the single T mode if the little Higgs is light, $m_{h^0} \lesssim 130$ GeV, and thus mainly decays via $h^0 \to b\bar{b}$. The separation of this signal from the SM background is challenging

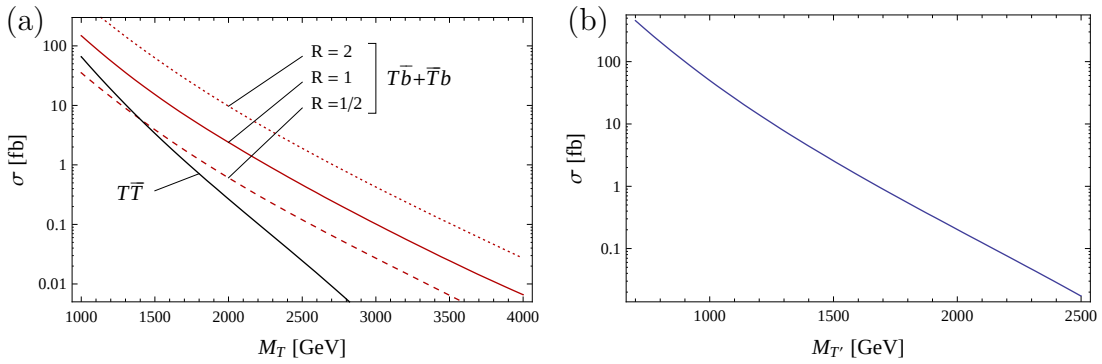

Figure 3.6: **(a)** *LHC cross sections for single T and $T\overline{T}$ production, as a function of the T quark mass, and for different values of $R \equiv \lambda/\lambda_c$.* **(b)** *LHC cross section for $T'\overline{T}'$ production, as a function of the T' mass. In each plot, the QCD and factorization scales have been set to $M_{T^{(\prime)}}$, and the center-of-mass energy is $\sqrt{s} = 14$ TeV.*

and requires a dedicated analysis.

Figure 3.6 (b) shows the pair production cross section for T' quarks. Since it is quite possible that the $M_{T'} < 1$ TeV, the cross section can amount to several 100 fb. However, the decay $T'\overline{T}' \to t\bar{t}\, B_{\rm H}^0\, B_{\rm H}^0$ leads to a signature that is very similar to SM $t\bar{t}$ production and requires a careful analysis to disentangle from this background [76, 78].

Besides new particle production, SM processes can be modified by the effect of virtual heavy particle contributions. In particular, the production rate of the SM-like light Higgs boson h^0 via gluon fusion can receive sizable corrections from loop diagrams involving the heavy top partners. However, this effect is not unique to our implementation of X-parity, but it is completely analogous to the littlest Higgs model, described in detail in Ref. [79].

3.5 Summary

In this chapter we present a little Higgs model where a new X-parity is implemented such that it is not broken by operators that are typically introduced in strongly coupled ultraviolet completions. This symmetry can therefore be exact up to very high scales and in particular reestablishes the lightest X-odd particle as a viable Dark Matter candidate for little Higgs models.

Our construction is based on the Minimal Moose little Higgs model. Following [34] we introduce X-parity as an exchange symmetry between the link fields in the model. The gauge transformation properties of the link fields are chosen such that the gauged WZW term is even under X-parity while ensuring that the additional heavy gauge bosons present in the model remain X-odd. An additional approximate $\mathbb{Z}_2$ symmetry further restricts the interactions in the scalar

sector and removes potentially dangerous operators. In the fermion sector a set of mirror-fermions is introduced in order to implement X-parity without generating large four fermion operators. An additional pair of top quark partners is introduced to avoid large breaking of the global symmetry that protects the Higgs mass. Mass terms for the mirror fermions and the additional top quark are introduced in a X-invariant way while preserving enough global symmetries to not generate a large mass for the Higgs fields.

Below the symmetry breaking scale f, a light X-even Higgs boson and a scalar triplet ϕ_a remains in the spectrum of the model. In addition, the masses of the B_H gauge boson and of the scalar singlet η_a are parametrically smaller than f. For all reasonable choices of parameters the B_H is the lightest X-odd particle and therefore the Dark Matter candidate, similar to the original little Higgs models with X-parity. The Higgs sector has the structure of a two-Higgs doublet model with one heavy doublet. Successful electroweak symmetry breaking is achieved with moderate fine tuning of parameters and yields a light physical Higgs boson. The model includes a number of additional scalars, which do not acquire vacuum expectation values since they are odd under one of the two parities. Most of these scalars obtain large $\mathcal{O}(f)$ masses, except for the aforementioned ϕ_a, which has a mass of order the electroweak scale.

The contributions to the electroweak S and T parameters from our model are moderate, allowing for new physics scales as low as $f \sim 1$ TeV. This opens the possibility for the model to be detectable at the LHC within the first years of running. In addition to the usual decay signatures of little Higgs models, the light scalar triplet can be pair-produced copiously at hadron colliders and yields a peculiar signature from its main decay channels into photons or W and Z boson pairs. Probing the top quark sector of the model is more challenging since most signatures suffer from a large standard model background. It would be interesting to study the phenomenological signatures of this model in more detail, in particular whether it can be distinguished from other little Higgs models. Also the question whether the B_H can account for the observed dark matter density in the universe remains to be answered.

Our model is a realistic realization of the little Higgs mechanism with dark matter. More elaborate constructions can be envisaged where the parameter space is less constrained by low energy bounds.

Chapter 4

Multi-Photon Signals from Composite Models at LHC

4.1 Introduction

New physics models that involve new strong dynamics often manifest themselves at low energies through new scalar or pseudoscalar fields. Examples of such models are Technicolour theories as well as composite Higgs and little Higgs models. Recently another class of models that are not directly involved in electroweak symmetry breaking has emerged, going by the name of vectorlike confinement [22].

The lowest order effective Lagrangians that describe these models often have an additional symmetry that forbids the decay of the lightest pseudoscalar at the tree level. The most prominent example for such a behaviour is the low energy effective theory of QCD, where the decay of the neutral pion is only understood after including a higher order term, the Wess Zumino Witten (WZW) term, into the effective action. The same happens in little Higgs models, where T-parity is only broken after the WZW term is added, as discussed in chapter 2. More general, when the fermions that condense to form the pseudoscalars come in vectorlike representations of all gauge interactions, the most important decay channel for the lightest scalar arises from the WZW term.

The nonvanishing three point interactions in the WZW term contain at least two gauge bosons, therefore the pseudoscalar will decay dominantly into the lightest available gauge bosons which are usually those of the standard model. Depending on the quantum numbers of the scalars, the decays can be into photons pairs or into $V\gamma$, VV', where V and V' can be any standard model gauge bosons, including gluons [24].

In this work, we focus on the signature of pseudoscalar electroweak triplets that are pair produced at hadron colliders. These scalars have significant branching fractions into photon pairs, giving rise to signals with three or four photons

in the final state.

Signals with more than two hard photons provide a promising signature at hadron colliders. One reason is that the standard model backgrounds for these processes are relatively low, so a signal can be found early even if the production cross section is at the femtobarn level, which is quite common for uncolored new states in BSM scenarios. Furthermore the energy resolution is good, therefore the mass of the decaying particles can be determined with a good accuracy without requiring high statistics. Finally some information about the spin of the particle can be obtained right away.

The work in this chapter is organized as follows: In the following section a brief overview is given about models that predict triplet scalars and their width and branching fractions are discussed. In section 4.3 signals and backgrounds are calculated for the 7 TeV and the 14 TeV LHC. In section 4.4 we determine how precise the mass and spin of the particle can be measured, before we summarize in section 4.5.

4.2 Pseudoscalar Triplets in Extensions of the Standard Model

Our main objects of interest are pseudoscalar electroweak triplets $\phi = (\phi^+, \phi^0, \phi^-)$ that transform as $(3, 0)$ under the electroweak $\mathrm{SU}(2)\times\mathrm{U}(1)$ gauge symmetry. The leading interactions with the standard model are contained in the kinetic term

$$\mathcal{L}_{\mathrm{kin}} = \mathrm{Tr}\,\left(D^\mu\phi D_\mu\phi^\dagger\right) + \mathcal{O}(\phi^4)\,. \tag{4.1}$$

When ϕ is part of a larger multiplet that is involved with electroweak symmetry breaking, the above interactions will receive corrections of order $(v/f)^2$, where v is the Higgs vacuum expectation value and f is the global symmetry breaking scale at which the Goldstone bosons emerge. The scale f typically lies around the TeV scale so we expect these corrections to be at most 10%. Also the higher point interactions contained in 4.1 are not of interest here.

We are in particular interested in cases where the $\phi^{\pm,0}$ are the lightest particles that are odd under an approximate parity symmetry. In the little Higgs model presented in chapter 3 this happens due to the symmetry structure of the coset spaces, and is a remnant of the original T-parity in these models [30]. To make contact with the previous chapter we will refer to the scalar triplet as ϕ_a for the rest of this chapter.

While it is often assumed that little Higgs models originate from a theory that becomes strongly coupled around the 10 TeV scale, this UV completion is usually not specified. In contrast in models of vectorlike confinement [22, 23] the full theory at the high scale is given. The benchmark model discussed in [23] contains a pseudoscalar triplet with the required quantum numbers. In that case

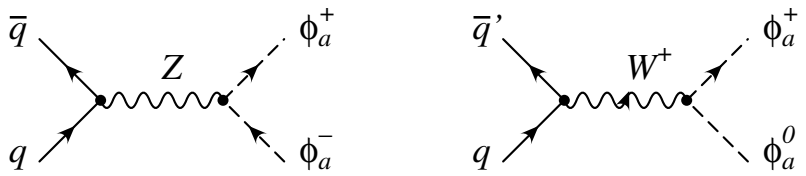

Figure 4.1: Pair production diagrams for the scalar triplets at hadron colliders. The charge conjugate of the second diagram is not shown.

the accidental parity symmetry appears because the fermions that condense to yield the Goldstone bosons transform in vectorlike representations of the standard model gauge group. Similar models that also contain a pseudoscalar triplet were presented in [24, 25].

To a large extent the properties of the triplets are fixed by gauge invariance and by the parity symmetry, so they can be studied independently of the model they belong to. Masses for the triplet are generated through radiative corrections. The little Higgs model with X-parity [2] predicts that mass to be of order of the electroweak scale. The same mass range is assumed in [23]. For the present analysis, we will assume

$$100 \text{ GeV} < m_{\phi_a} < 600 \text{ GeV} . \tag{4.2}$$

Due to the approximate parity symmetry, the triplets are mostly produced in pairs through an intermediate $W^\pm$ or Z boson, through interactions contained in the kinetic term (4.1). The relevant Feynman diagrams for production at hadron colliders are shown in figure 4.1. Note that there is no direct $\phi_a^0\phi_a^0$ production.

Additional contributions to ϕ_a pair production from BSM particles are possible. For example, the model in [23] contains an additional vector boson that is produced in the s-channel and decays into ϕ_a pairs. The cross sections obtained from the diagrams in figure 4.1 can nevertheless be used as lower bounds on the pair production rates.

Since the lowest order Lagrangian is symmetric under pseudoscalar parity decays are only mediated through the fourth order WZW term:

$$\Gamma_{\text{WZW}} = \frac{N}{16\pi^2 f} \int d^4x \epsilon_{\mu\nu\rho\sigma} \text{Tr} \, (\phi_a F_{\mu\nu} F_{\rho\sigma}) + \dots , \tag{4.3}$$

where the dots denote terms that do not contribute to ϕ decays at leading order and the gauge couplings have been absorbed into the definition of the field strength tensor. Note that unlike the case of vector boson decays that were discussed in chapter 2, here the neutral ϕ_a^0 can decay into two photons. On the other hand the decay $\phi_0 \to W^+W^-$ is not possible since the corresponding anomaly coefficient vanishes.

The relative branching fractions between ϕ_a^0 decay modes are completely fixed by this expression - the nontrivial dependence on m_{ϕ_a} that is displayed in figure

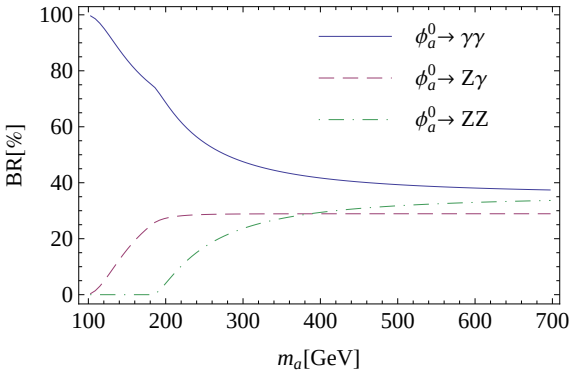

Figure 4.2: Branching fractions of ϕ_a^0 depending on the mass m_a.

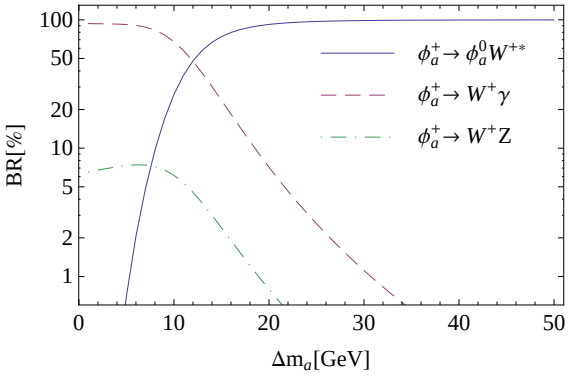

Figure 4.3: Branching fractions of ϕ_a^+ as a function of the mass splitting Δm_a, for $m_a = 300$ GeV.

4.2 is purely from kinematic suppression. The total widths in addition depends on the integer N and on the scale f, and typically lie in the keV range.

After electroweak symmetry breaking, radiative corrections introduce an additional splitting between the neutral and the charged components of the multiplet. For purely electromagnetic interactions, and in the limit $m_a \gg m_W$, it was found in [26] that

$$\Delta m_a = m_{\phi_a^+} - m_{\phi_a^0} \approx 170 \text{ MeV} . \tag{4.4}$$

Since there are additional contributions to this mass splitting in models with extended gauge and scalar sectors, we treat Δm_a as a free parameter. The decay $\phi_a^\pm \to \phi_a^0 W^{\pm,*}$ becomes relevant around $\delta m_a = 5$ GeV and dominant for larger splittings, as shown in figure 4.3. This behaviour is mostly independent of the absolute mass scale m_{ϕ_a}. For small mass splitting the dominant decay mode for the charged triplet is $\phi^\pm \to \gamma W^\pm$ with a branching fraction decreasing from almost 100% at $m_{\phi_a} = 100$ GeV to around 80% at $m_{\phi_a} = 700$ GeV.

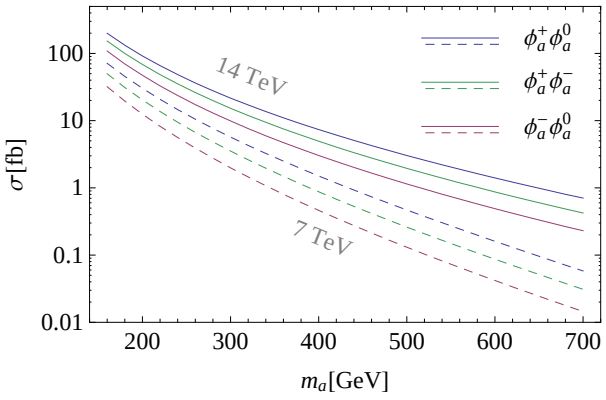

Figure 4.4: Production of $\phi_a\phi_a$ pairs at the 7 TeV LHC (dashed lines) and the 14 TeV LHC (solid lines).

4.3 Signals and Backgrounds

4.3.1 The signal

The cross sections for $\phi^\pm\phi^0$ and $\phi^+\phi^-$ production are shown in figure 4.4 for the LHC running at 7 TeV and 14 TeV center of mass energy. With 14 TeV the production cross sections are sizeable up to $m_{\phi_a} = 700$ GeV, while the reach of the current LHC run with $\sqrt{s} = 7$ TeV and 1 fb^{-1} of target luminosity is clearly limited.

In the case of a small mass splitting, $\Delta m_a \ll 5$ GeV, the most interesting signal arises from $\phi^\pm\phi^0$ decaying into $3\gamma + W^\pm$. On the other hand, if the splitting is larger than about 5 GeV all production channels contribute to a $4\gamma + X$ signal.

Our analysis will focus on the inclusive 3γ signal, i.e. on the case of a small mass splitting. To be definite we will consider three scenarios with $m_{\phi_a} = 200$ GeV, 400 GeV and 600 GeV. We use CompHEP [74] with CTEQ6L1 parton distributions to simulate the processes

$$pp \longrightarrow \phi^\pm\phi^0 \longrightarrow \gamma\gamma\gamma W^\pm \tag{4.5}$$

at $\sqrt{s} = 7$ TeV and 14 TeV. The resulting events are passed to PYTHIA 6.4 [80] for hadronization and W boson decay and through PGS4 [81] with the CMS parameter set to account for detector efficiencies and energy smearing. The cuts used for event generation are summarized in table 4.1 and the resulting cross sections for the 7 TeV and the 14 TeV LHC are given in table 4.2.

The standard model background to three photon production is almost of order of the signal, and will be discussed in the next sections. The backgrounds for 4γ signals are suppressed by an additional power of α and thus negligible. We will comment on the 4γ signal at the end of section 4.3.4.

p_T all photons	> 40GeV
$\|\eta\|$ all photons	< 2.5
ΔR all photons	> 0.3

Table 4.1: Cuts used to generate $pp \longrightarrow \phi^{\pm}\phi^{0} \longrightarrow \gamma\gamma\gamma W^{\pm}$ events. We also require all photons to be separated from the $W^{\pm}$ by more than 0.3 rad.

LHC Energy \ Mass	**200 GeV**	**400 GeV**	**600 GeV**
7 TeV	17.3	-	-
14 TeV	43.5	2.69	0.13

Table 4.2: Detector level cross sections in fb for the $3\gamma + X$ signal for the benchmark masses. The cuts imposed on the photons are given in table 4.1. Detector efficiencies are estimated using PGS4. The 7 TeV run does not give a detectable signal for the heavier scenarios.

Before turning to the backgrounds, let us briefly discuss the experimental bounds on the 3γ signal and on the mass m_{ϕ_a}. The D0 experiment analyzed for $3\gamma + X$ events in the search for fermiophobic Higgs bosons [82] in a sample corresponding to 0.83 fb^{-1} of collected data. The absence of an excess of events in the sample translates into an upper bound on the production cross section of fermiophobic Higgs bosons $\sigma \leq 25.3$ fb. For our model this is satisfied provided that $m_{\phi_a} \geq 150$ GeV.

Another possibility for the model to show up at the Tevatron experiments is through a bump in the di-photon invariant mass spectrum. The most recent searches [83,84] for graviton resonances in that channel with 5.4 fb^{-1} of integrated luminosity however do not impose further constraints on m_{ϕ_a}.

4.3.2 Real Backgrounds

There are two types of standard model backgrounds for the $3\gamma + X$ signal: real backgrounds with three or more photons in the final state, and fake backgrounds where one or more photons are actually jets that were misidentified in the detector. At the tree level pure photon final states are only produced from quark anti-quark initial states. Only at the NLO level the gluon gluon channels become available through a quark loop. This leads to large K factors, in particular at the LHC where gluons are abundant.

The main source of real backgrounds is direct three photon production accompanied with any number of jets. This background has been generated using MadGraph/MadEvent [85] with the same cuts as for the signal and then processed through PYTHIA and PGS4 for initial and final state radiation and to model detector effects. To account for uncertainties from NLO corrections and for processes where additional jets are present, we multiply these background by

process	7 TeV:	MG/ME	PGS4	14 TeV:	MG/ME	PGS4
$3\gamma + n$ jets		2.51	2.01		5.44	4.54
$3\gamma + W^{\pm}$		0.0051	0.0036		0.014	0.009
$2\gamma + n$ jets		7190	5.9		13700	8.9

Table 4.3: Real and fake backgrounds for inclusive 3γ searches with $p_{T,\gamma} > 40$ GeV at LHC with $E_{\rm cm} = 7$ TeV and 14 TeV. The first column gives the partonic cross sections obtained with MadGraph/MadEvent, while the second column gives the fraction of events that are reconstructed as $3\gamma + X$ events in PGS4. Note that for the fake backgrounds the first column shows the cross section for $2\gamma + n$ jet processes with $p_{T,\gamma} > 40$ GeV. Backgrounds are multiplied by two to account for NLO k-factors and uncertainties from matching. All cross sections in femtobarn.

two.

The production of three photons together with a W boson has a tiny cross section in the standard model and can be neglected. The background rates for the 7 TeV and 14 TeV LHC are given in table 4.3.

4.3.3 Fake Backgrounds

The most important source of fake backgrounds are the processes $pp \to \gamma\gamma + n$ jets where one of the jets is misidentified as a photon.

We use MLM type matching with the k_T jet algorithm to match events with $\gamma\gamma + 0, 1, 2$ jets between MadEvent and PYTHIA with a matching scale of 30 GeV. The matched sample is then run through PGS4 to model detector effects and in particular to get an estimate for the fake jet rate and for the magnitude of the fake backgrounds. The resulting background after application of the cuts in table 4.1 and multiplication by 2 to account for the cross section uncertainty due to leading order matching and NLO corrections are given in table 4.3.

A few comments are in order. The matched sample can contain additional photons from initial and final state radiation. Imposing the cut of $p_T > 40$ GeV on all photons in the sample effectively removes most of this contribution.

Additional hard photons that remain in the sample are therefore due to jets that were reconstructed as photons in PGS4. Tests with a pure two jet sample with $p_T > 40$ GeV show that the fake rate in PGS4 lies at the per mille level. This should be compared with the fake rates obtained by CMS [86] using a full detector simulation. A fake photon candidate in the electromagnetic calorimeter is produced by about 1 in 200 jets. Using additional isolation cuts they obtain an additional rejection factor of 100 while keeping a reasonable photon efficiency (80%), i.e. they obtain a rejection factor of 20000 corresponding to a fake rate of

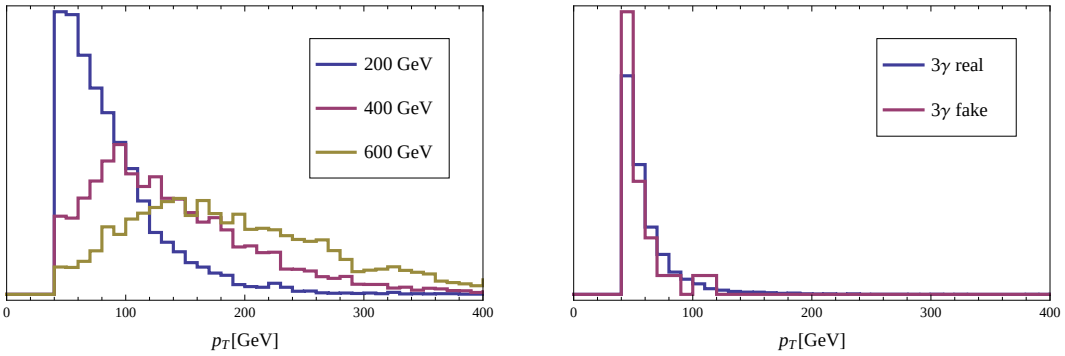

Figure 4.5: Transverse momentum distribution of the third hardest photon for signal events (left) and for background events (right) at the 14 TeV LHC. All distributions normalized to unity.

0.005%.[1] This is about one order of magnitude better than the PGS4 estimate, at the expense of a reduced photon efficiency compared to PGS4 ($> 90\%$).

Since PGS4 does not implement the dedicated isolation cuts that were proposed in [86] its performance is acceptable, and in particular it is sufficient for the present work. Improving this performance would still be desireable, in particular since the fake backgrounds are larger than the real backgrounds.

4.3.4 LHC Sensitivity

For masses m_a above 400 GeV the backgrounds become comparable to the signal. It is therefore necessary to look for possibilities to increase the signal to background ratio without loosing too many signal events.

An immediate possibility to do so is to impose stronger cuts on the transverse momentum of the photons. Since the signal photons come from the decay of heavy particles their p_T spectrum is relatively flat up to $p_T = m_a/2$ while the backgrounds fall off rather quickly with increasing p_T. The best results are obtained with a uniform p_T cut on all photons. The p_T distribution of the third hardest photon for signal and background events is displayed in figure 4.5. With a p_T cut of 60 GeV (80 GeV) we obtain a background suppression of 66% (86%) while loosing at most 30% (54%) of the signal in the light scenario, and much less for the heavier cases.

In signal events the three photons effectively recoil against a W-boson which can carry away a significant amount of transverse momentum. On the other hand most background events will be balanced in transverse momentum except for those cases where an additional hard jet is present.

[1] ATLAS [87] gives a rejection rate of 7000 for $p_T > 40$ GeV independent of the luminosity.

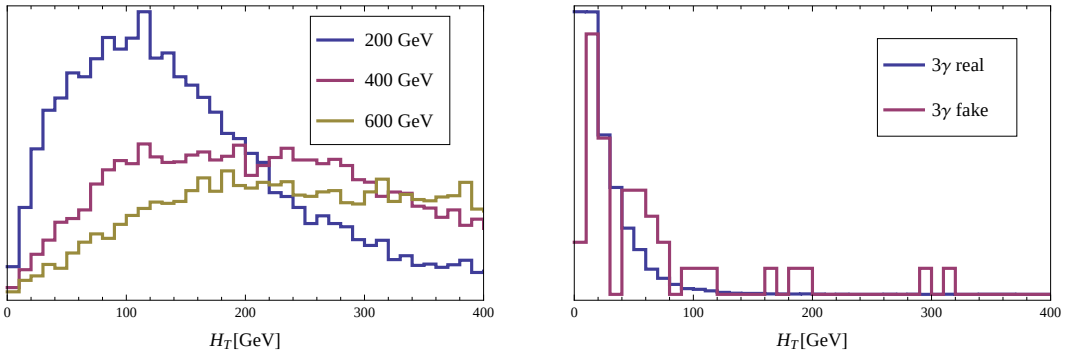

Figure 4.6: H_T distributions for signal (left plot) and background (right plot) events at the LHC with $E_{\text{cm}} = 14$ TeV. The unsteady shape of the fake background distribution is due to the smallness of the fake sample. The results were cross checked against the H_T distribution of two photons plus one jet and found to agree.

	$p_T > 80$ GeV	$H_T > 80$ GeV	**combined**	**Events**
200 GeV	46.4%	75.3%	36.0%	470
400 GeV	80.8%	90.3%	72.7%	59
600 GeV	93.2%	94.1%	87.7%	3.4
real BG	13.6%	3.2%	1.3%	1.8
fake BG	10.7%	20.5%	3.5%	9.3

Table 4.4: Cut efficiencies on signal and background events. Shown are the fraction of events that pass the indicated cuts. The last column shows the expected number of Events at the LHC with 30 fb^{-1} after the cuts have been applied.

We define

$$H_T \equiv \sqrt{\left(\sum_{i=1}^{3} p_x^i\right)^2 + \left(\sum_{i=1}^{3} p_y^i\right)^2} \tag{4.6}$$

as a measure of the p_T imbalance of the three photon system. The H_T distributions for signal and backgrounds are displayed in figure 4.6. It is easy to see that a moderate cut on H_T can reduce the backgrounds by up to an order of magnitude without loosing too many signal events even in the low mass scenario.

As final cuts for the analysis we choose $p_{T,\gamma} > 80$ GeV for the three hardest photons in the event and $H_T > 80$ GeV. The effects of these cuts on the signal and backgrounds are summarized in table 4.4. They improve the signal to background ratio by more than an order of magnitude.

Also shown in table 4.4 are the expected signal and background events at the

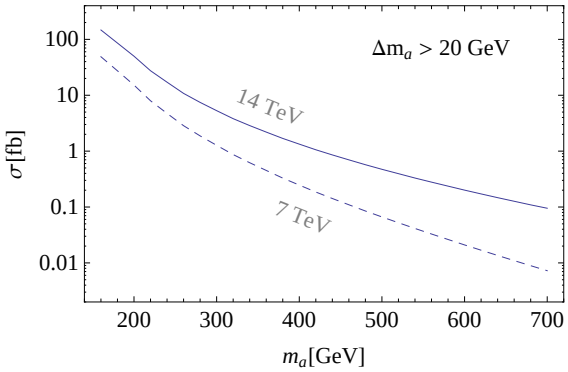

Figure 4.7: Cross sections for the $4\gamma + X$ signal for a large mass splitting, $\Delta m_a > 20$ GeV. Cross sections estimated as discussed in the text.

LHC for a luminosity of 30 fb^{-1}. This is enough for a 5 sigma discovery for both the 200 GeV and the 400 GeV scenario, and the 5 sigma reach roughly extends up to $m_{\phi_a} = 500$ GeV.

For the heavy scenario clearly the full design luminosity of the LHC is needed, and the backgrounds need to be reduced further. This is possible by imposing even stronger cuts on the photon transverse momentum, but even more important is a better photon identification to reduce the fake background. In this context it is also worth looking at the di-photon invariant mass spectrum to find peaks above the smooth background.

The LHC is currently running at a center of mass energy of 7 TeV and is supposed to collect at least 1 fb^{-1} before the shutdown in 2011. It is therefore reasonable to ask whether this is enough to detect a signal at least in the light scenario. From table 4.2 we expect 17 signal events. The backgrounds are smaller than for the 14 TeV case and have an even steeper p_T spectrum. Imposing a p_T cut of 60 GeV on all photons we expect 11.4 signal events and 2.0 background events with 1 fb^{-1} so a discovery at the 5σ level is possible.

Finally let us comment on the case of a large mass splitting between $\phi_a^\pm$ and ϕ_a^0, where the dominant signal is from a $4\gamma + X$ final state. Radiating an additional photon in any of the discussed background events costs an additional factor of $\alpha = 1/128$, while requiring an additional fake photon reduces the cross section even further. It is therefore safe to say that the 4γ signal with the cuts listed in table 4.1 is essentially background free. In addition to the $\phi_a^\pm \phi_a^0$ channel now also the $\phi_a^+ \phi_a^-$ channel contributes to the $4\gamma + X$ final states.

We estimate the cross sections for the $4\gamma + X$ signal in the large splitting case as follows. We assume $\Delta m_a > 20$ GeV which implies $B(\phi_a^\pm \to \phi_a^0 W^\pm) > 95\%$. The ϕ_a pair production rates are taken from figure 4.4 and multiplied by the corresponding $\phi_a^0 \to \gamma\gamma$ branching fractions. We further multiply the results by 0.5 to account for losses through cuts and detector effects. The results are shown

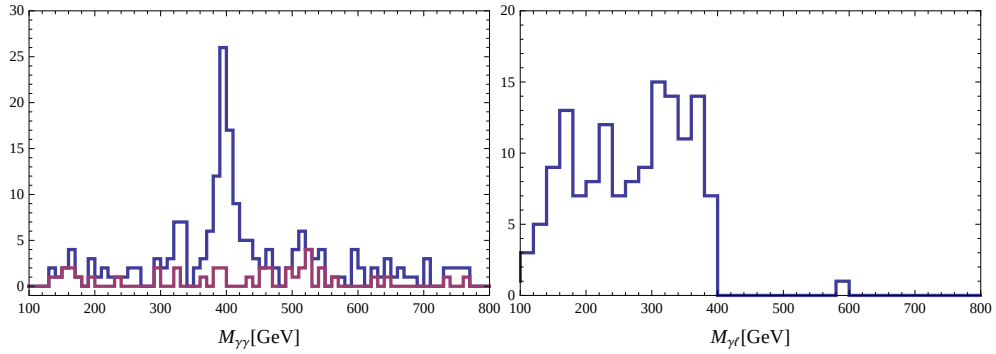

Figure 4.8: Left plot: Invariant mass distribution of photon pairs in signal plus background events (blue) and backgrounds only (red), for 30 fb^{-1}. Note that each event gives three entries, one for each possible pairing of photons. Right plot: Lepton photon invariant mass plot, with events corresponding to 300 fb^{-1} of collected data at LHC.

in figure 4.7. Since the backgrounds are negligible, we require a minimum of 5 signal events for a discovery. This gives a discovery range for the current LHC run up to $m_{\phi_a} = 250$ GeV, while the LHC with $\sqrt{s} = 14$ TeV will be able to probe and exclude the full parameter range with about 30 fb^{-1}.

4.4 Measuring Particle Properties

4.4.1 Mass Measurements

The mass of the neutral ϕ_a^0 can directly be determined from the invariant mass distribution of photon pairs in the three photon samples. Since the width of ϕ_a^0 is small and the photons don't loose much energy while propagating to the electromagnetic calorimeters, the quality of the measurement is entirely determined by the energy resolution of the detector.

The left plot in figure 4.8 shows the invariant mass distribution of photon pairs from signal and background events for $m_{\phi_a} = 400$ GeV and a luminosity of 30 fb^{-1}, corresponding to 59 signal and 11 background events. The peak around $m_{\gamma\gamma} = 400$ GeV is clearly visible on top of the combinatoric background from signal and background events, and the mass can be determined with an uncertainty of less than 20 GeV.

Measuring the mass of the charged $\phi_a^\pm$ is more difficult since it decays into $\gamma W^\pm$. Leptonic decays of the W boson occur in 32% of all cases and lead to a $3\gamma + \ell$ signal that is essentially free of backgrounds. A fraction of the W boson momentum is carried away by the neutrino. Since the neutrino as well as the photon and the lepton are essentially massless, the invariant mass of the visible

lepton-photon system, $m_{\gamma\ell}$, is bounded by

$$(m_{\gamma\ell}^{\max})^2 = m_{\phi_a^+}^2 - m_W^2. \tag{4.7}$$

It is then possible to obtain the mass from the end point of the $m_{\gamma\ell}$ distribution. To this end we identify the photon that does not come from the ϕ_a^0 decay and combine it with the lepton that we require to have $p_{T,\ell} > 20$ GeV. If it is unclear which photon pair reconstructs the ϕ_a^0 the event is thrown away.

The resulting invariant mass distribution is shown in figure 4.8. For this analysis we use a sample with 600 signal events corresponding to 300 fb^{-1} of data and that contain a total of 190 events with one lepton that satisfies our cuts. The kinematic endpoint at $\sqrt{m_{\phi_a}^2 - m_W^2}$ is clearly visible between 380 GeV and 400 GeV.

4.4.2 Spin and CP Properties

Most information about the spin of the resonance can readily be extracted from the nature of the final state. A two body decay into photon pairs is only possible for spin zero or spin two resonances due to angular momentum conservation.

It is then interesting to ask whether spin zero and spin two resonances can be distinguished using just information contained in the three photon final states. In [88] an analysis was performed for the production of a graviton in association with a photon with the graviton decaying into a photon pair. They find that the spin can be determined from the angular distribution of one of the photons in the rest frame of the decaying graviton. An analysis of this distribution for the case of a scalar or pseudoscalar resonance is currently being performed. In this context also the $\phi_a^0 \to \gamma Z$ channel with a leptonic decay of the Z boson is being investigated.

It would also be interesting to measure the CP properties of the scalar resonance. Since this information is contained in the polarization of the photons that is not measured by the LHC experiments, it is not possible to determine the parity of the neutral scalar from the photon photon final state. Full information about the particle properties can be obtained from the so called golden channel decay

$$\phi_a^0 \longrightarrow ZZ^{(*)} \longrightarrow \ell\bar{\ell}\ell\bar{\ell}\,, \tag{4.8}$$

where ℓ denotes charged leptons, in particular electrons and muons. Detailed studies on how to extract spin information using these channels have been recently performed in [89,90]. According to them, a small number of events, 20-30, is enough to obtain a 3σ discrimination between different spin and parity hypotheses. Due to the small branching fraction of the Z boson into leptons this channel can only be used for spin determination if the ϕ_a are light, below $m_{\phi_a} = 350$ GeV, and after the LHC has delivered its full design luminosity.

4.4.3 Extracting Model Information

The peculiar feature of the underlying new physics models that we assume here is that the branching fractions of ϕ_a^0 and $\phi_a^\pm$ are completely fixed by the global symmetry structure. Clearly if these particles are found in the multi-photon channel one can start looking for the possible decays of ϕ_a^0 into $Z\gamma$ and ZZ pairs as well as for the $ZW^\pm$ decay mode of the $\phi_a^\pm$. The branching fractions will then unambiguously determine whether the decays are mediated by the WZW term and thus reveal information about the symmetry structure of the model.

If the mass splitting between the charged and neutral components can be measured, for example indirectly by observing the $4\gamma + X$ decay modes, more information can be obtained. Since the splitting is purely due to radiative corrections a mass splitting larger than the one generated by standard model gauge interactions hints towards the existence of additional global symmetry breaking operators, e.g. additional gauge bosons or new fermions, as is the case of little Higgs models.

4.5 Conclusions

In this chapter we discuss multi photon signals from pseudoscalar electroweak triplets and the prospects for the LHC to detect them. These triplet fields do not only appear in certain little Higgs models but also in a more general class of composite extensions of the standard model where parts of the fermion sector transforms vectorlike under the electroweak SU(2) gauge symmetry. The multi photon signal is therefore an important channel for detection or exclusion of these models.

Since the leading order effective Lagrangian for the pseudoscalars is parity symmetric, the decays of the triplets are only induced at next to leading order through the WZW term, and the decay channels and branching fractions are fully determined by the global symmetry structure. In particular we find that the neutral component has a large branching fraction into photon pairs even for masses well above the ZZ threshold. Due to the parity symmetry, at the LHC the triplets are mostly produced in pairs, with a sizable cross section for masses up to $m_{\phi_a} \sim 600$ GeV.

There are two important sources of backgrounds for 3γ signals at the LHC. In addition to direct three photon production, there are important contributions from $2\gamma + n$ jet production where one of the jets is misidentified as a photon. We use MadGraph/MadEvent to simulate the background processes at the parton level. The events are then passed to PYTHIA where the matching for the $2\gamma + n$ jet signal is performed. The fast detector simulation PGS4 is used to obtain an estimate of the photon fake rate and to account for detector efficiencies and energy smearing. We perform a number of cuts to reduce the background and

find that with these cuts a 5σ discovery is possible at the 14 TeV LHC with 30 fb^{-1} over a large range of parameter space. For the current 7 TeV run of the LHC a discovery is only possible if the ϕ_a are lighter than 250 GeV.

Due to the cleanness of the photon signal in the detector, the mass of the neutral ϕ_a^0 can be measured with a high accuracy with only a small number of events. The mass of the charged component can be determined from the kinematic endpoint of the invariant mass of the lepton photon system from the decay chain $\phi_a^\pm \to \gamma W^\pm \to \gamma \ell^\pm \nu_\ell$, but it requires a larger number of events due to the small branching fraction of $W^\pm$ into leptons and the loss of information from the undetected neutrino. The spin of the neutral component is partially determined by the two photon final state, which is possible only for spin zero or spin two particles. The possibility to distinguish these two cases using angular correlations in the three photon signal is currently being studied.

Other decay modes of the triplets, in particular into ZZ or $Z\gamma$ final states, offer additional possibilities to obtain information about the nature of the observed particles. The fully leptonic decay of both Z bosons can be used to measure not only the spin but also the parity of the ϕ_a^0, while the branching fractions for the different channels yield information about the global symmetry structure of the model.

Finally it is interesting to note that the current limit for the $3\gamma + X$ signal from the D0 experiment at the Tevatron was obtained with only 0.83 fb^{-1} of collected data, and translates into a bound of $m_{\phi_a} > 150$ GeV for our model. This bound could easily be improved using the $6 - 8$ fb^{-1} that are now available there.

Part II

Leptogenesis

Chapter 5

Finite Number Density Corrections to Leptogenesis

5.1 Introduction

In the light of the present knowledge of elementary particle physics phenomenology, leptogenesis appears as one of the most plausible explanations for the dynamical emergence of the baryon asymmetry of the Universe [91, 92]. Leptogenesis in turn is a variant of baryogenesis from out-of-equilibrium decays of heavy particles during the expansion and cooling of the early Universe [93, 94]. The deviation from equilibrium provides the breaking of time reversal invariance which is a necessary condition for baryogenesis [95] as a consequence of the CPT theorem.

The most common approach for making quantitative predictions is to formulate and solve a network of Boltzmann equations that describes the evolution of the number densities of the particle species relevant to baryogenesis. In simple scenarios for leptogenesis, a setup that leads to meaningful results is to compute the distribution function of a heavy right-handed Majorana neutrino N_1 and of the charge density of a lepton doublet ℓ, while one may assume that the remaining species are in thermal equilibrium. More realistic models typically take account of the presence of the several generations. The Boltzmann equations are usually written in a form, where on the left hand side there is a kinetic term that traces the particle number distributions, while on the right hand side there is a collision term. The collision term accounts for elastic and inelastic (particle number violating) scatterings. It arises from weighting reaction rates, computed in vacuum scattering theory (in-out formalism), with the distribution functions of the species involved.

When setting up the Boltzmann equations, one encounters the following issue: Let $\Gamma_{Ni\to\ell\phi}$, the rate for the decay process $N_i \to \ell\phi$, be proportional to $1+\varepsilon$, where ε parametrises the CP asymmetry of the decay. Then, by complex conjugation of the involved coupling constants, it follows that $\Gamma_{Ni\to\bar{\ell}\phi^*} \propto 1-\varepsilon$. Application

of the CPT theorem then implies that the inverse decay rates $\Gamma_{\ell\phi\to Ni} \propto 1-\varepsilon$ and $\Gamma_{\bar{\ell}\phi^*\to Ni} \propto 1+\varepsilon$. If these were the only contributions that are accounted for in the collision term, one might conclude that the two-by-two rate $\ell\phi \to \bar{\ell}\phi^*$ is proportional to $1-2\varepsilon$, while the rate of $\bar{\ell}\phi^* \to \ell\phi$ is proportional to $1+2\varepsilon$. An asymmetry even in equilibrium would result, in apparent contradiction with CPT invariance. But of course, there is no contradiction, since the heavy neutrinos are unstable and therefore do not belong to the Hilbert space of asymptotic states of a unitary S-matrix. The total lepton number violating two-by-two rates are therefore not given by the above naive multiplication of the rates for decay and inverse decay. Yet, it is crucial that one tracks the neutrino densities in the Boltzmann equations. The issue is fixed when realising that the resonant parts of the two-by-two scatterings, where the intermediate neutrino is on-shell, contribute to the Boltzmann equations at the same order in coupling constants as the decay and inverse decay processes. Technically, one adds the full two-by-two rates and subtracts from these the on-shell contribution, since this is already accounted for in the decays and inverse decays [94]. This procedure is known as the subtraction of real intermediate states (RIS).

One expects that the RIS subtraction is naturally realised within a first principle approach that is less heuristic than the Boltzmann ansatz. This first principle approach is given by applying the Schwinger-Keldysh Closed Time Path (CTP) formalism [96, 97] to field theory [98, 99]. In this paper, we derive and solve the Kadanoff-Baym equations for leptogenesis that result from the CTP formalism. We pay particular attention to demonstrating that no lepton asymmetry is generated in equilibrium, or more generally in situations that are time-reversal invariant. For models with fermionic leptons this result has been reported earlier in works based on the CTP formalism [100–102], though no detailed derivation has been given. (The main focus of Refs. [101,102] is the study of memory effects.) For the case of scalar leptons, the vanishing of the asymmetry in equilibrium has been demonstrated recently in Refs. [103, 104].

In addition to offering the framework for a first-principle derivation of equations that describe leptogenesis, the CTP formalism also provides finite density corrections that do not straightforwardly follow in the Boltzmann approach. These corrections take the form of an integral over terms linear in the Higgs boson and lepton distribution functions. Historically, it has been proposed to compute the CP asymmetry from the discontinuity of the correlation functions in the Matsubara (imaginary time) formalism. In the CTP (real time) approach, this corresponds to the imaginary part of the time-ordered correlation functions [105, 106]. It is characteristic of these Green functions, that they feature not only terms that are linear in the lepton and Higgs boson distribution functions, but also a product term of these distributions. In contrast, it appears to be the consensus among the more recent papers [101–104] that the CP asymmetry does not receive corrections from a product term of Higgs boson and lepton distribution functions. This has been shown in detail for the model with scalar leptons in Refs. [103,104].

Here we find the same property in the model with fermionic leptons: The CP asymmetry results from terms that can be written as the difference of Wightman type correlators (no explicit time-ordering of the field operators).

After deriving the kinetic equation for the lepton asymmetry in the CTP formalism we solve it numerically in various situations. We find that the effect of the new quantum statistical corrections is small when the bulk of the lepton asymmetry is produced at temperatures $T \ll M_1$, where M_1 is the mass of the neutrino that decays out of equilibrium. The reason is that the distribution functions are strongly suppressed for momenta much larger than T. This situation corresponds to the strong-washout scenario, which is of particular interest, since the resulting asymmetry is independent of both the initial abundance of heavy neutrinos and a possible primordial lepton asymmetry. On the other hand, when the bulk of the asymmetry is produced for $T \sim M_1$ or larger, corresponding to weak washout, the impact is more sizable. For a vanishing initial lepton asymmetry and thermal initial conditions of N_1 we find an enhancement of the asymmetry, as apparently the Bose enhancement from the Higgs particle distribution function dominates over the Fermi suppression from the lepton distribution. This qualitatively confirms what has been reported for scalar leptons [103,104]. In this context, we note that in [107,108] finite density effects were considered in the quantum statistical factors in the initial and final states, but not in the loop corrections. However, the quantum statistical factors in the loop corrections appear within the CTP approach on the same footing and with the same size as the external state factors, which is why they cannot be neglected consistently.

The remainder of this chapter is organised as follows: In Section 5.2, we specify the model, introduce the free CTP propagators and provide the one-loop self energies. These ingredients are used in Section 5.3 to derive the Kadanoff-Baym equations that correspond to the tree-level Boltzmann equations with quantum statistical factors. The wave-function correction that leads to a CP asymmetry arises from a two-loop diagram in the CTP formalism, which we discuss in Section 5.4. We explicitly show that no asymmetry is produced in equilibrium and we relate this fact to the usual procedure of RIS subtraction. Similarly, we discuss the vertex correction in Section 5.5. In Section 5.6, we numerically evaluate the effective CP-violating parameter and solve the Boltzmann equations for different strengths of washout, which demonstrates that finite density corrections are important for weak washout, but may be neglected in the strong-washout domain. We conclude in Section 5.7.

5.2 CTP Approach to Leptogenesis

In the simplest scenario of leptogenesis, there are two right handed neutrinos N_i ($i = 1, 2$) with lepton-number violating Majorana masses M_i, one scalar SU(2) Higgs doublet ϕ and an active left-handed lepton doublet ℓ. The Lagrangian of the model is

$$\mathcal{L} = \frac{1}{2}\bar{\psi}_{Ni}(\mathrm{i}\partial\!\!\!/ - M_i)\psi_{Ni} + \bar{\psi}_\ell \mathrm{i}\partial\!\!\!/\psi_\ell + (\partial^\mu\phi^\dagger)(\partial_\mu\phi) - Y_i^*\bar{\psi}_\ell\phi^\dagger P_\mathrm{R}\psi_{Ni} - Y_i\bar{\psi}_{Ni}P_\mathrm{L}\phi\psi_\ell\,, \tag{5.1}$$

where a summation over $i = 1, 2$ is understood and $P_{\mathrm{L/R}} = (1 \mp \gamma_5)/2$. Besides, it is implicitly assumed that the SU(2) indices are contracted in a gauge-invariant way, that is $\phi\psi_\ell = -\phi_A\epsilon_{AB}\psi_{\ell B}$ and $\bar{\psi}_\ell\phi^\dagger = (\bar{\psi}_\ell)_A\epsilon_{AB}(\phi^\dagger)_B$, where ϵ_{AB} denotes the antisymmetric 2×2 matrix with $\epsilon_{12} = 1$. Upon the four-component spinor ψ_{Ni}, we impose the Majorana constraint

$$\psi_{Ni}^c = C\bar{\psi}_{Ni}^T = \psi_{Ni}\,, \tag{5.2}$$

with C the charge conjugation matrix.

5.2.1 Propagators

For the CTP formalism we follow closely the notational conventions of Refs. [109–111] and define the CTP propagators for the leptons by

$$\mathrm{i}S^{+-}_{\ell\alpha\beta}(u,v) = \mathrm{i}S^{<}_{\ell\alpha\beta}(u,v) = -\langle\bar{\psi}_{\ell\beta}(v)\psi_{\ell\alpha}(u)\rangle\,, \tag{5.3a}$$

$$\mathrm{i}S^{-+}_{\ell\alpha\beta}(u,v) = \mathrm{i}S^{>}_{\ell\alpha\beta}(u,v) = \langle\psi_{\ell\alpha}(u)\bar{\psi}_{\ell\beta}(v)\rangle\,, \tag{5.3b}$$

$$\mathrm{i}S^{++}_{\ell\alpha\beta}(u,v) = \mathrm{i}S^{T}_{\ell\alpha\beta}(u,v) = \langle T(\psi_{\ell\alpha}(u)\bar{\psi}_{\ell\beta}(v))\rangle\,, \tag{5.3c}$$

$$\mathrm{i}S^{--}_{\ell\alpha\beta}(u,v) = \mathrm{i}S^{\bar{T}}_{\ell\alpha\beta}(u,v) = \langle \bar{T}(\psi_{\ell\alpha}(u)\bar{\psi}_{\ell\beta}(v))\rangle\,. \tag{5.3d}$$

We perform a perturbation and gradient expansion of the full Kadanoff-Baym equations that uses the tree-level propagators and vertices as elementary building blocks. The tree-level propagators are therefore given by the vacuum propagators plus a finite-density contribution proportional to the spectral function of the free theory. When there are no correlations between modes of different momentum and spin, we can characterize the state by particle number distribution functions. In case there is also no preferred direction for the spin, the usual averaging procedure applies. These assumptions lead to the explicit expressions

$$\mathrm{i}S^{<}_\ell(p) = -2\pi\delta(p^2)P_\mathrm{L}p\!\!\!/P_\mathrm{R}\left[\vartheta(p_0)f_\ell(\mathbf{p}) - \vartheta(-p_0)(1-\bar{f}_\ell(-\mathbf{p}))\right]\,, \tag{5.4a}$$

$$\mathrm{i}S^{>}_\ell(p) = -2\pi\delta(p^2)P_\mathrm{L}p\!\!\!/P_\mathrm{R}\left[-\vartheta(p_0)(1-f_\ell(\mathbf{p})) + \vartheta(-p_0)\bar{f}_\ell(-\mathbf{p})\right]\,, \tag{5.4b}$$

$$\mathrm{i}S^{T}_\ell(p) = P_\mathrm{L}\frac{\mathrm{i}p\!\!\!/}{p^2+\mathrm{i}\varepsilon}P_\mathrm{R} - 2\pi\delta(p^2)P_\mathrm{L}p\!\!\!/P_\mathrm{R}\left[\vartheta(p_0)f_\ell(\mathbf{p}) + \vartheta(-p_0)\bar{f}_\ell(-\mathbf{p})\right]\,, \tag{5.4c}$$

$$\mathrm{i}S^{\bar{T}}_\ell(p) = -P_\mathrm{L}\frac{\mathrm{i}p\!\!\!/}{p^2-\mathrm{i}\varepsilon}P_\mathrm{R} - 2\pi\delta(p^2)P_\mathrm{L}p\!\!\!/P_\mathrm{R}\left[\vartheta(p_0)f_\ell(\mathbf{p}) + \vartheta(-p_0)\bar{f}_\ell(-\mathbf{p})\right]\,, \tag{5.4d}$$

for the lepton propagators, where $f_\ell(\mathbf{k})$ denotes the distribution function of leptons and $\bar{f}_\ell(\mathbf{k})$ of anti-leptons. The leptons ℓ occur within an SU(2) doublet, but since this symmetry is unbroken at the time of leptogenesis, we assume that the lepton densities are SU(2)-symmetric and hence diagonal. In particular, the lepton propagators defined here are the diagonal components of a diagonal propagator with additional SU(2) indices:

$$S^{\mathrm{SU}(2)}_{\ell AB}(u,v) = \delta_{AB} S_\ell(u,v) \quad A,B = 1,2\,. \tag{5.5}$$

Similarly, for the Majorana-fermion propagators we find

$$\mathrm{i}S^<_{Ni}(p) = -2\pi\delta(p^2 - M_i^2)(\not{p} + M_i)\left[\vartheta(p_0) f_{Ni}(\mathbf{p}) - \vartheta(-p_0)(1 - f_{Ni}(-\mathbf{p}))\right]\,, \tag{5.6a}$$

$$\mathrm{i}S^>_{Ni}(p) = -2\pi\delta(p^2 - M_i^2)(\not{p} + M_i)\left[-\vartheta(p_0)(1 - f_{Ni}(\mathbf{p})) + \vartheta(-p_0) f_{Ni}(-\mathbf{p})\right]\,, \tag{5.6b}$$

$$\mathrm{i}S^T_{Ni}(p) = \frac{\mathrm{i}(\not{p} + M_i)}{p^2 - M_i^2 + \mathrm{i}\varepsilon} - 2\pi\delta(p^2 - M_i^2)(\not{p} + M_i)\left[\vartheta(p_0) f_{Ni}(\mathbf{p}) + \vartheta(-p_0) f_{Ni}(-\mathbf{p})\right]\,, \tag{5.6c}$$

$$\mathrm{i}S^{\bar{T}}_{Ni}(p) = \frac{-\mathrm{i}(\not{p} + M_i)}{p^2 - M_i^2 - \mathrm{i}\varepsilon} - 2\pi\delta(p^2 - M_i^2)(\not{p} + M_i)\left[\vartheta(p_0) f_{Ni}(\mathbf{p}) + \vartheta(-p_0) f_{Ni}(-\mathbf{p})\right]\,. \tag{5.6d}$$

As a consequence of the Majorana condition (5.2), the distribution functions for neutrinos and anti-neutrinos are identical, and the propagators inherit the property

$$S_{Ni}(u,v) = C S^t_{Ni}(v,u) C^\dagger\,, \tag{5.7}$$

where the transposition acts here on both the CTP and the Dirac indices. Finally the scalar propagators take the form

$$\mathrm{i}\Delta^<_\phi(p) = 2\pi\delta(p^2)\left[\vartheta(p_0) f_\phi(\mathbf{p}) + \vartheta(-p_0)(1 + \bar{f}_\phi(-\mathbf{p}))\right]\,, \tag{5.8a}$$

$$\mathrm{i}\Delta^>_\phi(p) = 2\pi\delta(p^2)\left[\vartheta(p_0)(1 + f_\phi(\mathbf{p})) + \vartheta(-p_0)\bar{f}_\phi(-\mathbf{p})\right]\,, \tag{5.8b}$$

$$\mathrm{i}\Delta^T_\phi(p) = \frac{\mathrm{i}}{p^2 + \mathrm{i}\varepsilon} + 2\pi\delta(p^2)\left[\vartheta(p_0) f_\phi(\mathbf{p}) + \vartheta(-p_0)\bar{f}_\phi(-\mathbf{p})\right]\,, \tag{5.8c}$$

$$\mathrm{i}\Delta^{\bar{T}}_\phi(p) = -\frac{\mathrm{i}}{p^2 - \mathrm{i}\varepsilon} + 2\pi\delta(p^2)\left[\vartheta(p_0) f_\phi(\mathbf{p}) + \vartheta(-p_0)\bar{f}_\phi(-\mathbf{p})\right]\,. \tag{5.8d}$$

As for the leptons, it is understood that

$$\Delta^{\mathrm{SU}(2)}_{\phi AB}(u,v) = \delta_{AB}\Delta_\phi(u,v) \quad A,B = 1,2\,. \tag{5.9}$$

In the following, an occasional multiplicity factor $g_w = 2$ arises from performing SU(2) traces such as

$$\mathrm{tr}_{\mathrm{SU}(2)}[\Delta_\phi^{\mathrm{SU}(2)}\epsilon^\dagger S_\ell^{\mathrm{SU}(2)}\epsilon] = \Delta_\phi S_\ell\,\mathrm{tr}_{\mathrm{SU}(2)}[\epsilon^\dagger\epsilon] = g_w\Delta_\phi S_\ell\,. \tag{5.10}$$

In thermal equilibrium the distribution functions assume the usual Fermi-Dirac and Bose-Einstein forms, respectively:

$$\begin{aligned} f_\ell(\mathbf{p}) = \bar{f}_\ell(\mathbf{p}) = f_\ell^{\mathrm{eq}}(\mathbf{p}) &= \frac{1}{e^{\beta|\mathbf{p}|}+1}\,, \\ f_{Ni}(\mathbf{p}) = f_{Ni}^{\mathrm{eq}}(\mathbf{p}) &= \frac{1}{e^{\beta\sqrt{\mathbf{p}^2+M_i^2}}+1}\,, \\ f_\phi(\mathbf{p}) = \bar{f}_\phi(\mathbf{p}) = f_\phi^{\mathrm{eq}}(\mathbf{p}) &= \frac{1}{e^{\beta|\mathbf{p}|}-1}\,. \end{aligned} \tag{5.11}$$

Furthermore the equilibrium Green functions satisfy the Kubo-Martin-Schwinger (KMS) relation,

$$\mathrm{i}S_\ell^>(p) = -\mathrm{e}^{\beta p_0}\,\mathrm{i}S_\ell^<(p)\,, \quad \mathrm{i}S_{Ni}^>(p) = -\mathrm{e}^{\beta p_0}\,\mathrm{i}S_{Ni}^<(p)\,, \quad \mathrm{i}\Delta_\phi^>(p) = \mathrm{e}^{\beta p_0}\,\mathrm{i}\Delta_\phi^<(p)\,, \tag{5.12}$$

an extremely useful property that we employ exhaustively throughout this paper.

5.2.2 One-loop self-energies

The one-loop neutrino self-energy in the CTP formalism is given by (*cf.* the vacuum expression in Ref. [112])

$$\begin{aligned} \mathrm{i}\not{\Sigma}_{Nij}^{ab}(k) = {} & g_w\int\frac{d^4k'}{(2\pi)^4}\frac{d^4k''}{(2\pi)^4}(2\pi)^4\delta^{(4)}(k-k'-k'') \\ & \times\Big\{Y_iY_j^*P_{\mathrm{L}}\mathrm{i}S_\ell^{ab}(k')P_{\mathrm{R}}\mathrm{i}\Delta_\phi^{ab}(k'') + Y_i^*Y_jC\left[P_{\mathrm{L}}\mathrm{i}S_\ell^{ba}(-k')P_{\mathrm{R}}\right]^T C^\dagger\mathrm{i}\Delta_\phi^{ba}(-k'')\Big\}\,, \end{aligned} \tag{5.13}$$

where $a, b = \pm$ denote the CTP indices, see Eqs. (5.3a)–(5.3d). Our definition for the self-energies is such that $-i\Sigma$ corresponds to the sum of all one-particle irreducible diagrams. The one-loop lepton self-energy reads

$$\mathrm{i}\not{\Sigma}_\ell^{ab}(k) = |Y_i|^2\int\frac{d^4k'}{(2\pi)^4}\frac{d^4k''}{(2\pi)^4}(2\pi)^4\delta^{(4)}(k-k'-k'')P_{\mathrm{R}}\mathrm{i}S_{Ni}^{ab}(k')P_{\mathrm{L}}\mathrm{i}\Delta_\phi^{ba}(-k'')\,, \tag{5.14}$$

where we sum over the neutrino flavours i. In thermal equilibrium these self-energies inherit the KMS property

$$\not{\Sigma}_{Ni,\ell}^>(p) = -\mathrm{e}^{\beta p_0}\not{\Sigma}_{Ni,\ell}^<(p) \tag{5.15}$$

from the constituent CTP Green functions. At the one-loop order it is easy to verify this explicitly by inserting the tree-level propagators (5.4), (5.6), (5.8) into the self-energies (5.13), (5.14). One of the main objectives of this paper is to show explicitly how KMS also remains valid when considering the next-to-leading order contributions to $\not{\Sigma}^{<,>}_{Ni,\ell}$. It turns out that this encompasses the subtraction of RIS as it is performed in the conventional approach to baryo- and leptogenesis.

5.3 Tree-Level Contributions to the Kinetic Equations

The theoretical description of leptogenesis is concerned with the time evolution of non-equilibrium densities of active leptons and of right-handed neutrinos. This is described by the Kadanoff-Baym equations (see *e.g.* [109–111]). We perform the standard Wigner transformation and gradient expansion. Since we are interested in finite-density effects from loops in the CTP formalism, we restrict ourselves to the leading term in the gradient expansion. We regard this as a self-consistent leading-order approximation to the full Kadanoff-Baym equations, relative to which corrections from higher gradients and loops may eventually be considered. Thus, the kinetic equations take the form

$$\frac{d}{dt}\gamma_0 \mathrm{i}S^{<,>}_{\ell}(k) = -\left[\mathrm{i}\not{\Sigma}^{>}_{\ell}(k)P_{\mathrm{L}}\mathrm{i}S^{<}_{\ell}(k) - \mathrm{i}\not{\Sigma}^{<}_{\ell}(k)P_{\mathrm{L}}\mathrm{i}S^{>}_{\ell}(k)\right] , \tag{5.16a}$$

$$\frac{d}{dt}\gamma_0 \mathrm{i}S^{<,>}_{Ni}(k) = -\left[\mathrm{i}\not{\Sigma}^{>}_{Nii}(k)\mathrm{i}S^{<}_{Ni}(k) - \mathrm{i}\not{\Sigma}^{<}_{Nii}(k)\mathrm{i}S^{>}_{Ni}(k)\right] , \tag{5.16b}$$

where we recognize the familiar expression for the collision term in the CTP formalism on the right-hand side. Here and in the following we assume spatial isotropy, which means that there is no angular dependence in the distribution functions and we may identify $f_{\ell,\phi,Ni}(\mathbf{k}) \equiv f_{\ell,\phi,Ni}(|\mathbf{k}|)$. In particular, we repeatedly use $f_{\ell,\phi,Ni}(-\mathbf{k}) = f_{\ell,\phi,Ni}(\mathbf{k})$ to simplify the arguments of distribution functions. When performing the Wigner transformation and gradient expansion in a slowly varying background, all time dependence in the propagators (5.4), (5.6), (5.8) is isolated in the distribution functions $f_{\ell,\phi,Ni}$, where we suppress an explicit time argument. The equation for the lepton density can be simplified when taking the Dirac trace of Eq. (5.16a), multiplying by minus one and integrating over k_0. Inserting Eq. (5.4), we obtain

$$\frac{d}{dt}\left(f_{\ell}(\mathbf{k}) - \bar{f}_{\ell}(\mathbf{k})\right) = \mathcal{C}_{\ell}(\mathbf{k}) = \int \frac{dk_0}{2\pi}\mathrm{tr}\left[\mathrm{i}\not{\Sigma}^{>}_{\ell}(k)P_{\mathrm{L}}\mathrm{i}S^{<}_{\ell}(k) - \mathrm{i}\not{\Sigma}^{<}_{\ell}(k)P_{\mathrm{L}}\mathrm{i}S^{>}_{\ell}(k)\right] , \tag{5.17}$$

which defines $\mathcal{C}_\ell(\mathbf{k})$. In a similar way we obtain the equation for the time dependence of the Majorana neutrino distribution function

$$\frac{d}{dt}f_{Ni}(\mathbf{k}) = \mathcal{C}_{Ni}(\mathbf{k}) = \frac{1}{4}\int\frac{dk_0}{2\pi}\mathrm{sign}(k_0)\mathrm{tr}\left[\mathrm{i}\not{\Sigma}^{>}_{Nii}(k)\mathrm{i}S^{<}_{Ni}(k) - \mathrm{i}\not{\Sigma}^{<}_{Nii}(k)\mathrm{i}S^{>}_{Ni}(k)\right]. \tag{5.18}$$

5.3.1 Tree-level collision terms

The tree-level collision term for the leptons can be straightforwardly evaluated by inserting the tree-level propagators into Eq. (5.17) and the expression (5.14) for the self-energy. Since we are interested only in the lepton number density

$$n_\ell = \int\frac{d^3k}{(2\pi)^3}\,f_\ell(\mathbf{k}), \tag{5.19}$$

we integrate $\mathcal{C}_\ell(\mathbf{k})$ over $\mathbf{k}$ and find

$$\begin{aligned}\int\frac{d^3k}{(2\pi)^3}\,\mathcal{C}_\ell(\mathbf{k}) = -|Y_i|^2\int\frac{d^3k}{(2\pi)^3 2|\mathbf{k}^2|}\frac{d^3k'}{(2\pi)^3 2\sqrt{\mathbf{k}'^2+M_i^2}}\frac{d^3k''}{(2\pi)^3 2|\mathbf{k}''|} \\ \times(2\pi)^4\delta^4(k'-k-k'')\,2k'\cdot k\Big\{(1-f_{Ni}(\mathbf{k}'))\times[f_\ell(\mathbf{k})f_\phi(\mathbf{k}'') - \bar{f}_\ell(\mathbf{k})\bar{f}_\phi(\mathbf{k}'')] \\ - f_{Ni}(\mathbf{k}')\times[(1-f_\ell(\mathbf{k}))(1+f_\phi(\mathbf{k}'')) - (1-\bar{f}_\ell(\mathbf{k}))(1+\bar{f}_\phi(\mathbf{k}''))]\Big\}.\end{aligned} \tag{5.20}$$

Due to the fast violation of Higgs number, we can assume that $f_\phi = \bar{f}_\phi \equiv f^{\mathrm{eq}}_\phi$. For the leptons we may assume $f_\ell - f^{\mathrm{eq}}_\ell = -(\bar{f}_\ell - f^{\mathrm{eq}}_\ell)$, as justified by fast pair-annihilating and -creating interactions among the leptons. Expanding to linear order in the deviations from equilibrium, the lepton collision term simplifies to

$$\begin{aligned}\int\frac{d^3k}{(2\pi)^3}\,\mathcal{C}_\ell(\mathbf{k}) = -|Y_i|^2\int\frac{d^3k}{(2\pi)^3 2|\mathbf{k}|}\frac{d^3k'}{(2\pi)^3 2\sqrt{\mathbf{k}'^2+M_i^2}}\frac{d^3k''}{(2\pi)^3 2|\mathbf{k}''|} \\ \times(2\pi)^4\delta^4(k'-k-k'')\,2k'\cdot k\,\left[f^{\mathrm{eq}}_\phi(\mathbf{k}'') + f_{Ni}(\mathbf{k}')\right]\times\left[f_\ell(\mathbf{k}) - \bar{f}_\ell(\mathbf{k})\right].\end{aligned} \tag{5.21}$$

This term describes the washout of a lepton asymmetry through inverse decays. In a similar way we obtain the tree-level collision terms for the neutrinos by inserting the tree-level propagators into Eq. (5.18) and the expression (5.14) for the self-energy. For the neutrinos, we shall need the phase-space distributions, so we need the unintegrated collision term, for which we find

$$\begin{aligned}\mathcal{C}_{Ni}(\mathbf{k}) = \frac{1}{4}g_w|Y_i|^2\frac{1}{2\sqrt{\mathbf{k}^2+M_i^2}}\int\frac{d^3k'}{(2\pi)^3 2|\mathbf{k}'|}\frac{d^3k''}{(2\pi)^3 2|\mathbf{k}''|}\,(2\pi)^4\delta^4(k-k'-k'') \\ \times\mathrm{tr}\Big[\not{k}'(\not{k}+M_i)\left\{-f_{Ni}(\mathbf{k})[1-f_\ell(\mathbf{k}')][1+f_\phi(\mathbf{k}'')] + [1-f_{Ni}(\mathbf{k})]f_\ell(\mathbf{k}')f_\phi(\mathbf{k}'')\right\} \\ +\not{k}'(\not{k}+M_i)\left\{-f_{Ni}(\mathbf{k})[1-\bar{f}_\ell(\mathbf{k}')][1+\bar{f}_\phi(\mathbf{k}'')] + [1-f_{Ni}(\mathbf{k})]\bar{f}_\ell(\mathbf{k}')\bar{f}_\phi(\mathbf{k}'')\right\}\Big].\end{aligned} \tag{5.22}$$

It is useful to check that when setting the Higgs and lepton distribution functions to zero, this reproduces the negative total decay rate of N_i,

$$\mathcal{C}_{Ni}^{f,\bar{f}_{\ell,\phi}=0}(\mathbf{k}) = -\frac{g_w}{16\pi}|Y_i^2|\frac{M_i^2}{\sqrt{\mathbf{k}^2+M_i^2}}f_{Ni}(\mathbf{k})\,. \tag{5.23}$$

Next, introducing

$$\delta f_{Ni} = f_{Ni} - f_{Ni}^{\rm eq}, \tag{5.24}$$

and using the same approximations on f_ℓ, $\bar{f}_\ell$, f_ϕ and $\bar{f}_\phi$ as above, the Majorana collision term simplifies to

$$\mathcal{C}_{Ni}(\mathbf{k}) = -\,g_w|Y_i|^2\frac{1}{2\sqrt{\mathbf{k}^2+M_i^2}}\int\frac{d^3k'}{(2\pi)^3 2|\mathbf{k}'|}\frac{d^3k''}{(2\pi)^3 2|\mathbf{k}''|}(2\pi)^4\delta^4(k-k'-k'') \tag{5.25}$$

$$\times\, 2k\cdot k'\,\delta f_{Ni}(\mathbf{k})[1-f_\ell^{\rm eq}(\mathbf{k}')+f_\phi^{\rm eq}(\mathbf{k}'')]\,.$$

Note that δf_{Ni} is not necessarily small in some realistic scenarios for leptogenesis, *e.g.* for weak washout. Above equation is accurate for arbitrary δf_{Ni} and up to linear order in $f_\ell - f_\ell^{\rm eq} = -(\bar{f}_\ell - f_\ell^{\rm eq})$.

It is easy to see from Eqs (5.21), (5.25) that in thermal equilibrium the collision terms vanish. Alternatively, one may either directly use the KMS relations (5.12), (5.15) in Eqs. (5.17), (5.18) or explicitly insert the equilibrium distributions into Eqs. (5.20), (5.22). This means that the equilibrium state is a static (time-independent) solution to the Kadanoff-Baym equations.

5.3.2 Expansion of the Universe

Before proceeding we comment on how the effects of particle dilution due to the expansion of the Universe can be systematically incorporated into our equations. So far we have formulated the Kadanoff-Baym equation on the Minkowski background. Neglecting Planck-scale suppressed corrections the only effect of replacing the Minkowski background by the Friedmann-Robertson-Walker one is that the particle modes are red-shifted.

This can be conveniently implemented by adopting conformal coordinates, which are defined by the metric

$$g_{\mu\nu} = a^2(\eta)\,\mathrm{diag}(1,-1,-1,-1)\,,$$

where $\eta = x^0$ denotes the conformal time and $a(\eta)$ the scale factor. Then the Lagrangian (5.1) describes the dynamics in the expanding background, provided that we have redefined the fields such that their kinetic terms are canonically normalized, that we replace $M_i \to aM_i$ and that we assume that the Higgs field has no coupling to the scalar curvature R. Consequently all expressions given

earlier in this Section and in Sections 5.4 and 5.5 below remain valid in the expanding Universe if momenta $\mathbf{k}$ are understood as comoving momenta $\mathbf{k}_{\rm com}$, temperature T (and $\beta = 1/T$) as comoving temperature $T_{\rm com}$ (and $\beta_{\rm com}$), time t as conformal time η, $f(\mathbf{k}_{\rm com})$ and n as comoving phase-space distributions and particle number densities, respectively, and if finally masses M_i are replaced by aM_i, wherever they appear.

For the scale factor in the radiation-dominated Universe we use the relation

$$a(\eta) = a_{\rm R}\eta\,. \tag{5.26}$$

Using the Friedmann equation and the free energy, we can relate this to the temperature as

$$T = \frac{T_{\rm com}}{a(\eta)} = \frac{1}{a(\eta)}\sqrt{\frac{a_{\rm R} m_{\rm Pl}}{2}}\left(\frac{45}{g_*\pi^3}\right)^{1/4}\,, \tag{5.27}$$

where g_* denotes the number of relativistic degrees of freedom and $m_{\rm Pl} = 1/\sqrt{G_N} = 1.22\cdot 10^{19}\,\text{GeV}$ the Planck mass. The variable $z = M_1/T$ that will be used in Section 5.6 is therefore related to η by a constant proportionality factor.

Kinetic equations are often formulated in terms of physical momenta and physical time. In order to make contact, we can replace in our equations the comoving momenta by physical momenta $k_{\rm ph} = k_{\rm com}/a$ and the comoving temperature by the physical temperature $T_{\rm ph} = T_{\rm com}/a$. Doing so and dividing by a factor of a for convenience, the right-hand sides (*i.e.* the collision terms), simply take the same form as given earlier in this Section, where now all momenta are to be understood as physical. The left-hand sides change according to

$$\begin{aligned}\frac{1}{a(\eta)}\frac{d}{d\eta}f(\mathbf{k}_{\rm com}) &= \frac{\partial}{\partial t}f(\mathbf{k}_{\rm ph}) + \left(\frac{\partial}{\partial|\mathbf{k}_{\rm ph}|}f(\mathbf{k}_{\rm ph})\right)\frac{\partial|\mathbf{k}_{\rm ph}|}{\partial t} \\ &= \frac{\partial}{\partial t}f(\mathbf{k}_{\rm ph}) - H|\mathbf{k}_{\rm ph}|\frac{\partial}{\partial|\mathbf{k}_{\rm ph}|}f(\mathbf{k}_{\rm ph})\,,\end{aligned} \tag{5.28}$$

where f may stand for f_N or $f_\ell - \bar{f}_\ell$. This formula applies to the treatment of the densities of right-handed neutrinos, that do not necessarily maintain kinetic equilibrium during leptogenesis, implying that one cannot substitute for f_{Ni} a Fermi-Dirac distribution with a (pseudo-)chemical potential. For the lepton charge, it is suitable to consider the integrated version

$$\frac{1}{a(\eta)}\int\frac{d^3k_{\rm ph}}{(2\pi)^3}\frac{d}{d\eta}f(\mathbf{k}_{\rm com}) = \frac{\partial}{\partial t}n_{\rm ph} + 3Hn_{\rm ph} \tag{5.29}$$

of the above equation. This is just the familiar cosmological dilution law, where $n_{\rm ph}$ denotes a physical number density and H the Hubble parameter with respect to time t. However, in Section 5.6 we will solve the kinetic equations directly in conformal coordinates.

5.3.3 Boltzmann equations

We now write down explicitly the Boltzmann equations that describe the time evolution of the distribution function f_{N1} and of the lepton asymmetry in conformal coordinates:

$$\frac{d}{d\eta} f_{N1}(\mathbf{k}_{\rm com}) = D(\mathbf{k}_{\rm com})\,, \tag{5.30}$$

$$\frac{d}{d\eta}(n_\ell - \bar{n}_\ell) = W + S\,. \tag{5.31}$$

Here $D(\mathbf{k}_{\rm com})$ denotes the contributions (5.25) from decays and inverse decays of N_1, while W denotes the washout term (5.21). $S = S^{\rm wf} + S^{\rm v}$ is the source term for the lepton asymmetry, which we decompose into a wave-function contribution $S^{\rm wf}$ and a vertex contribution $S^{\rm v}$. Note that here and below, unless indicated otherwise, n_ℓ refers to the comoving particle number density.

Performing the substitution of variables pertinent to conformal coordinates as discussed above in Eq. (5.22) and summing contributions from particles and antiparticles, we obtain:

$$\begin{aligned} D(\mathbf{k}_{\rm com}) =& 2g_w|Y_1|^2 \frac{1}{2\sqrt{\mathbf{k}_{\rm com}^2 + a^2(\eta)M_1^2}} \int \frac{d^3k'_{\rm com}}{(2\pi)^3 2|\mathbf{k}'_{\rm com}|} \frac{d^3k''_{\rm com}}{(2\pi)^3 2|\mathbf{k}''_{\rm com}|} \\ & \times (2\pi)^4\delta^4(k_{\rm com} - k'_{\rm com} - k''_{\rm com}) k_{\rm com}\cdot k'_{\rm com} \\ & \times \Big[- f_{N1}(\mathbf{k}_{\rm com}) \left(1 - f_\ell^{\rm eq}(\mathbf{k}_{\rm com}) + f_\phi^{\rm eq}(\mathbf{k}''_{\rm com})\right) + f_\ell^{\rm eq}(\mathbf{k}'_{\rm com})\, f_\phi^{\rm eq}(\mathbf{k}''_{\rm com}) \Big]\,. \end{aligned} \tag{5.32}$$

In the evaluation of the tree-level collision term we have set f_ℓ, $\bar{f}_\ell$, f_ϕ and $\bar{f}_\phi$ equal to the equilibrium distributions given in Eq. (5.11) (but expressed in terms of comoving momentum and temperature), which allows us to evaluate the phase-space integrals. It proves useful to define the quantity

$$\Sigma_N^\mu(k) = g_w \int \frac{d^3p}{(2\pi)^3 2|\mathbf{p}|} \frac{d^3q}{(2\pi)^3 2|\mathbf{q}|} (2\pi)^4\delta^4(k-p-q)\, p^\mu \left(1 - f_\ell^{\rm eq}(\mathbf{p}) + f_\phi^{\rm eq}(\mathbf{q})\right)\,, \tag{5.33}$$

which we will calculate analytically in Section 5.6. In terms of this we find for the decay and inverse decay term

$$D(\mathbf{k}_{\rm com}) = -2|Y_1|^2 \frac{k_{\rm com\,\mu}}{2k_{\rm com\,0}} \Sigma_N^\mu(k_{\rm com}) \left[f_{N1}(\mathbf{k}_{\rm com}) - f_{N1}^{\rm eq}(\mathbf{k}_{\rm com}) \right], \tag{5.34}$$

where $k_{\rm com\,0} = \sqrt{\mathbf{k}_{\rm com}^2 + a_{\rm R}^2\eta^2 M_1^2}$ and

$$f_{N1}^{\rm eq}(\mathbf{k}_{\rm com}) = \frac{1}{{\rm e}^{k_{\rm com0}/T_{\rm com}} + 1}\,. \tag{5.35}$$

To calculate the washout term (5.21) we approximate f_{Ni} by the equilibrium distribution $f_{Ni}^{\rm eq}$ and assume that the leptons are in kinetic equilibrium so that f_ℓ can be parameterized in terms of a chemical potential. Expanding to linear order in the chemical potential, the latter assumption yields the relation

$$f_\ell(\mathbf{k}) - \bar{f}_\ell(\mathbf{k}) = (n_\ell - \bar{n}_\ell) \times \frac{12\beta^3 e^{\beta|\mathbf{k}|}}{\left(e^{\beta|\mathbf{k}|}+1\right)^2}\,. \tag{5.36}$$

We then obtain for the wash-out term

$$\begin{aligned} W &= \int \frac{d^3k}{(2\pi)^3}\, \mathcal{C}_\ell(\mathbf{k}) \\ &= -\frac{3|Y_1|^2}{8\pi^3}\frac{a^2M_1^2}{T_{\rm com}}\,(n_\ell - \bar{n}_\ell)\int\limits_0^\infty dx\,\frac{\mathrm{e}^x}{(\mathrm{e}^x+1)^2}\ln\left(\frac{\mathrm{e}^{\frac{a^2M_1^2}{4T_{\rm com}^2 x}+x}+1}{\mathrm{e}^{\frac{a^2M_1^2}{4T_{\rm com}^2 x}+x}-\mathrm{e}^x}\right)\,. \end{aligned} \tag{5.37}$$

The substitution $f_{Ni} \to f_{Ni}^{\rm eq}$, which was made to take analytical integrations further, is strictly speaking only a correct approximation when $\delta f_{Ni} \ll f_{Ni}^{\rm eq}$. As in scenarios of strong washout or in the transition region from weak to strong washout most of the asymmetry is eventually produced when N_1 is close to equilibrium, the error from assuming an equilibrium abundance of N_1 in the washout term at all times should be small in the final result. (In fact, when assuming Maxwell statistics [92,106,113] the absence of Pauli blocking factors in Eq. (5.20) implies an even more drastic approximation, since then $f_{Ni}(\mathbf{k}') \to 0$ in Eq. (5.21).) We have checked this explicitly by evaluating W with the non-equilibrium neutrino distribution which amounts to replacing the logarithm in Eq. (5.37) by a numerical integral according to

$$\ln\left(\frac{\mathrm{e}^{\frac{a^2M_1^2}{4T_{\rm com}^2 x}+x}+1}{\mathrm{e}^{\frac{a^2M_1^2}{4T_{\rm com}^2 x}+x}-\mathrm{e}^x}\right) \;\to\; \int_b^\infty dy\left(f_{N1}(|\mathbf{k}|) + \frac{1}{e^{y-x}-1}\right) \tag{5.38}$$

with $|\mathbf{k}| = \sqrt{(y\,T_{\rm com})^2 - a^2M_1^2}$ and $b = x + a^2M_1^2/(4T_{\rm com}^2 x)$. We find that the numerical results for the lepton asymmetry presented in Section 5.6 change by about 10% in the weak-washout scenario ($Y_1 = 10^{-2}$) and less in the cases of larger washout. Hence we will use the simpler expression in Eq. (5.37) in the following.

As is well known, the source term S for the lepton asymmetry in Eq. (5.31) only arises in fourth order in the couplings Y_i. Deriving this source term including all quantum statistical factors is the subject of the following two sections.

5.4 Self-Energy Contribution to the CP Asymmetry

A key ingredient to baryogenesis calculations in the conventional framework is the subtraction of RIS. If this were omitted, a baryon asymmetry would result in thermal equilibrium in contradiction with the CPT theorem and the unitarity of scattering matrices. In this Section we show how the RIS subtraction arises within the CTP framework for leptogenesis and derive the CP asymmetry from the wave-function correction in the presence of finite number densities.

5.4.1 Wave-Function Correction to $\mathcal{C}_\ell$

The aim is the calculation of the wave-function correction to the lepton collision term (5.17),

$$\mathcal{C}_\ell^{\rm wf}(\mathbf{k}) = \int \frac{dk_0}{2\pi} {\rm tr}\left[{\rm i}\not{\Sigma}_\ell^{\rm wf>}(k) P_{\rm L} {\rm i}S_\ell^<(k) - {\rm i}\not{\Sigma}_\ell^{\rm wf<}(k) P_{\rm L} {\rm i}S_\ell^>(k)\right] , \tag{5.39}$$

where the correction to the lepton self-energy is

$${\rm i}\not{\Sigma}_\ell^{\rm wf<,>}(k) = \int \frac{d^4k'}{(2\pi)^4}\frac{d^4k''}{(2\pi)^4}(2\pi)^4\delta^4(k-k'-k'') Y_i^* Y_j P_{\rm R} {\rm i}S_{Nij}^{\rm wf<,>}(k') P_{\rm L} {\rm i}\Delta_\phi^{>,<}(-k'') . \tag{5.40}$$

In contrast to Eq. (5.20) the propagator ${\rm i}S_{Nij}^{\rm wf<,>}$ in this expression is not the tree propagator, but the propagator including a one-loop self-energy correction. Hence, we must also allow for off-diagonal terms and obtain for the wave-function corrections to the neutrino Wightman functions:

$$-{\rm i}S_{Nij}^{\rm wf>}(k') = {\rm i}S_{Ni}^> {\rm i}\not{\Sigma}_{Nij}^T {\rm i}S_{Nj}^T - {\rm i}S_{Ni}^{\bar T} {\rm i}\not{\Sigma}_{Nij}^> {\rm i}S_{Nj}^T - {\rm i}S_{Ni}^> {\rm i}\not{\Sigma}_{Nij}^< {\rm i}S_{Nj}^> + {\rm i}S_{Ni}^{\bar T} {\rm i}\not{\Sigma}_{Nij}^{\bar T} {\rm i}S_{Nj}^> \Big|_{k'} , \tag{5.41a}$$

$$-{\rm i}S_{Nij}^{\rm wf<}(k') = {\rm i}S_{Ni}^< {\rm i}\not{\Sigma}_{Nij}^{\bar T} {\rm i}S_{Nj}^{\bar T} - {\rm i}S_{Ni}^T {\rm i}\not{\Sigma}_{Nij}^< {\rm i}S_{Nj}^{\bar T} - {\rm i}S_{Ni}^< {\rm i}\not{\Sigma}_{Nij}^> {\rm i}S_{Nj}^< + {\rm i}S_{Ni}^T {\rm i}\not{\Sigma}_{Nij}^T {\rm i}S_{Nj}^< \Big|_{k'} , \tag{5.41b}$$

The different signs are a consequence of the Feynman rules on the CTP, and all functions on the right-hand side carry momentum argument k' as indicated after the bar.

In order to reduce the number of terms that we need to write, we assume that $M_2 \gg M_1$, such that the density of N_2 can be neglected at the time of

leptogenesis. In that case, the off-diagonal components reduce to

$$-\mathrm{i}S^{\mathrm{wf}>}_{N12} = \mathrm{i}S^{>}_{N1}\mathrm{i}\not{\Sigma}^{T}_{N12}\mathrm{i}S^{T}_{N2} - \mathrm{i}S^{\bar{T}}_{N1}\mathrm{i}\not{\Sigma}^{>}_{N12}\mathrm{i}S^{T}_{N2}\,, \tag{5.42a}$$

$$-\mathrm{i}S^{\mathrm{wf}<}_{N12} = \mathrm{i}S^{<}_{N1}\mathrm{i}\not{\Sigma}^{\bar{T}}_{N12}\mathrm{i}S^{\bar{T}}_{N2} - \mathrm{i}S^{T}_{N1}\mathrm{i}\not{\Sigma}^{<}_{N12}\mathrm{i}S^{\bar{T}}_{N2}\,, \tag{5.42b}$$

$$-\mathrm{i}S^{\mathrm{wf}>}_{N21} = -\mathrm{i}S^{\bar{T}}_{N2}\mathrm{i}\not{\Sigma}^{>}_{N21}\mathrm{i}S^{T}_{N1} + \mathrm{i}S^{\bar{T}}_{N2}\mathrm{i}\not{\Sigma}^{\bar{T}}_{N21}\mathrm{i}S^{>}_{N1}\,, \tag{5.42c}$$

$$-\mathrm{i}S^{\mathrm{wf}<}_{N21} = -\mathrm{i}S^{T}_{N2}\mathrm{i}\not{\Sigma}^{<}_{N21}\mathrm{i}S^{\bar{T}}_{N1} + \mathrm{i}S^{T}_{N2}\mathrm{i}\not{\Sigma}^{T}_{N21}\mathrm{i}S^{<}_{N1}\,. \tag{5.42d}$$

As long as $|M_2 - M_1| \gg \Gamma_{N1}, \Gamma_{N2}$, where Γ_{Ni} are the total decay rates of N_i, we can straightforwardly extend the present analysis to situations where $M_2 \gg M_1$ does not hold by simply adding the corresponding contributions that arise from a non-vanishing density of N_2, i.e. the asymmetry produced in N_2 decays. The reason for this is that not both of the neutrinos in the wave-function diagram can be on-shell simultaneously, provided their mass terms are not degenerate. Because of this we do not further simplify $\mathrm{i}S^{T,\bar{T}}_{N2}$ to $-\mathrm{i}/M_2$ at this point.

5.4.2 KMS and Real Intermediate State Subtraction

It follows from Eq. (5.39) that $\mathcal{C}^{\mathrm{wf}}_{\ell}$ vanishes provided both $\not{\Sigma}^{\mathrm{wf}<,>}_{\ell}$ and $S^{<,>}_{\ell}$ satisfy the KMS relation. The correction $\not{\Sigma}^{\mathrm{wf}<,>}_{\ell}$ in turn satisfies KMS provided it also holds for $\mathrm{i}S^{\mathrm{wf}<,>}_{Nij}$, see Eq. (5.40). It is instructive to show this property,

$$\mathrm{i}S^{\mathrm{wf}>}_{Nij}(k) = -\mathrm{e}^{\beta k_0}\mathrm{i}S^{\mathrm{wf}<}_{Nij}(k) \tag{5.43}$$

explicitly, because it illustrates how the RIS subtraction is realised within the CTP framework.

To show the validity of the KMS relation for the wave-function correction (5.43) explicitly, we define

$$\mathcal{K}_{ij} = \mathrm{i}S^{\mathrm{wf}>}_{Nij}(k) + e^{\beta k_0}\mathrm{i}S^{\mathrm{wf}<}_{Nij}(k). \tag{5.44}$$

The claim is $\mathcal{K}_{ij} = 0$ when substituting equilibrium distributions. We show this on the example $\mathcal{K}_{12}$, from which it will be clear how to generalize to all components of $\mathcal{K}_{ij}$. Applying KMS to $\not{\Sigma}^{<,>}_{N12}$ and $S^{<,>}_{N1}$, we find

$$\mathcal{K}_{12} = -\mathrm{i}S^{>}_{N1}\mathrm{i}\left(\not{\Sigma}^{T}_{N12} + \not{\Sigma}^{\bar{T}}_{N12}\right)\mathrm{i}S^{T}_{N2} + \mathrm{i}S^{T}_{N1}\mathrm{i}\not{\Sigma}^{>}_{N12}\mathrm{i}S^{T}_{N2} + \mathrm{i}S^{\bar{T}}_{N1}\mathrm{i}\not{\Sigma}^{>}_{N12}\mathrm{i}S^{T}_{N2}\,. \tag{5.45}$$

In addition, we have used that S_{N2} is evaluated here only when N_2 is off-shell, such that we can set $S^{\bar{T}}_{N2} = -S^{T}_{N2}$. To further simplify this expression, we make use of the following identities:

$$S^{T}_{N\mathrm{i}} + S^{\bar{T}}_{N\mathrm{i}} = S^{>}_{N\mathrm{i}} + S^{<}_{N\mathrm{i}}\,, \tag{5.46}$$

$$\not{\Sigma}^{T}_{Nij} + \not{\Sigma}^{\bar{T}}_{Nij} = \not{\Sigma}^{>}_{Nij} + \not{\Sigma}^{<}_{Nij}\,. \tag{5.47}$$

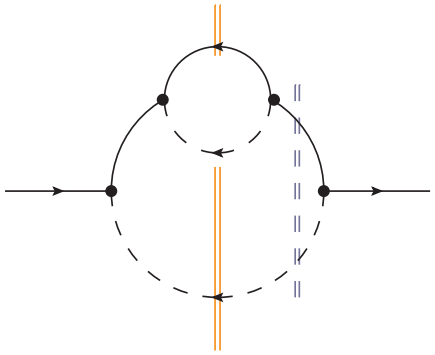

Figure 5.1: Diagrammatic representation of the lepton-number violating contribution to $\not{\Sigma}_\ell^{\mathrm{wf}<,>}$. The solid lines with arrows represent the lepton ℓ, the solid lines without arrows the neutrinos $N_{1,2}$ and the dashed lines with arrows the Higgs boson ϕ. The solid (light grey/orange) double line represents the cut that corresponds to the subtracted real intermediate states when finite density corrections to CP violation are neglected. The dashed (dark-grey/blue) double line represents the cut that corresponds to decays and inverse decays when finite density corrections are neglected.

Note that the first identity, applied to the heavy neutrino N_2, recovers the property $S^T_{N2} = -S^{\bar{T}}_{N2}$, when evaluated for off-shell momenta. It follows that

$$\mathcal{K}_{12} = -\mathrm{i}S^{>}_{N1}\mathrm{i}\left(\not{\Sigma}^{<}_{N12} + \not{\Sigma}^{>}_{N12}\right)\mathrm{i}S^{T}_{N2} + \mathrm{i}(S^{<}_{N1} + \mathrm{i}S^{>}_{N1})\mathrm{i}\not{\Sigma}^{>}_{N12}\mathrm{i}S^{T}_{N2} = 0\,, \tag{5.48}$$

where we have once more applied the KMS relation to obtain the last equality. An immediate consequence of this result is that no asymmetry is produced in thermal equilibrium, as required.

Besides verifying the KMS relation for $S^{<,>}_{Nij}$ and consequently also for $\not{\Sigma}^{<,>}_{Nij}$ and $\not{\Sigma}^{<,>}_{\ell}$, the above calculation shows how the RIS subtraction emerges in the CTP framework. To see this, we neglect the finite density corrections in $\not{\Sigma}^{<,>}_{\ell}$ implying that we set $f_\ell = \bar{f}_\ell = f_\phi = \bar{f}_\phi \equiv 0$ in the propagators of the T and $\bar{T}$ type. Then, in order to see which process a certain contribution in the collision term corresponds to, we cut through the propagators of the $<,>$ type, while leaving the propagators of the $T, \bar{T}$ type intact. We can then identify the terms in Eqs. (5.41) and (5.45) that involve $\not{\Sigma}^{T,\bar{T}}_{Nij}$ and $S^{<,>}_{N1}$ with decays and inverse decays. In the Feynman diagram representation of $\not{\Sigma}_\ell$, that is given in Figure 5.1, this corresponds to the cut indicated by the dashed double line, which gives the interference term between the tree-level decay amplitudes and the wave-function corrections to the decay amplitudes. The terms in Eqs. (5.41) and (5.45) that involve $\not{\Sigma}^{<,>}_{Nij}$ and $S^{T,\bar{T}}_{N1}$ correspond to scatterings. Since S^T_{N1} and $S^{\bar{T}}_{N1}$ are added together in Eq. (5.45) and within Eq. (5.39) (provided that we

substitute the equilibrium propagators for S_ℓ and Δ_ϕ, which is consistent within the present approximations), precisely the pole contribution, when N_1 is on-shell, is isolated from the scatterings, which takes the effect of RIS subtraction. In the Feynman diagram in Figure 5.1 this corresponds to the cut indicated by the solid double lines. It represents the squared amplitudes of the scatterings of leptons and Higgs bosons through N_1 and N_2 as well as the interference terms between these, which are crucial for the cancellation of CP-violating effects in equilibrium. Within the full CTP framework, $\not{\Sigma}_{Nij}^{T,\bar{T}}$ and the $T, \bar{T}$-type propagators also acquire contributions from real particles in the plasma, such that the clear separation in decay and scattering processes through the cuts in Figure 5.1 no longer persists.

Note that Equations (5.41a) and (5.41b) also contain terms with purely $<,>$-type propagators that appear to describe processes with six external particles that should clearly be absent at this order in the perturbative expansion. When inserting these particular contributions into the lepton-collision term, one notices a cancellation under the exchange $< \leftrightarrow >$. One may think of this as a representation of a decay process immediately followed by an inverse decay, which does not contribute to the evolution of the lepton charge distribution. Alternatively, one may note that the chronological and anti-chronological propagators can be rewritten in terms of retarded and advanced propagators that are defined by

$$G^{R,A} = G^{T} - G^{<,>} = G^{>,<} - G^{\bar{T}}\,, \tag{5.49}$$

and which do not depend on the particle distribution functions at zeroth order. Inserting this definition in Eqs. (5.41), it is easily seen that each term contains at least one retarded or advanced propagator that corresponds to an internal (virtual) particle exchange.

In order to see the role of the violation of time reversal symmetry, we note that for the vanishing of $\mathcal{K}_{ij}$, we make use of the KMS relation in the form of

$$\mathrm{i}S_{Ni}^{>}(k)\mathrm{i}S_{\ell}^{<}(k')\mathrm{i}\Delta_{\phi}^{<}(k'') = \mathrm{i}S_{Ni}^{<}(k)\mathrm{i}S_{\ell}^{>}(k')\mathrm{i}\Delta_{\phi}^{>}(k'') \tag{5.50}$$

for momenta satisfying $k = k' + k''$. This equation is valid not only in thermal equilibrium, but it is also another way of expressing that the process $N_i \to \ell\phi$ and its inverse $\ell\phi \to N_i$ occur at the same rate, and that the same holds true for $N_i \to \bar{\ell}\phi^*$ and $\bar{\ell}\phi^* \to N_i$. Hence, the above discussion does not only show that no CP asymmetry is generated in equilibrium, but more generally that no asymmetry is generated in situations that are symmetric with respect to time reversal, as it is of course expected by the CPT theorem.

5.4.3 CP Source

We now derive the CP-violating source within the lepton collision term, that arises due to deviations of N_1 from equilibrium and a violation of the KMS

relations. First, we note that because of Eq. (5.6) we can identify

$$\mathrm{i}\delta S^{>}_{N1} = \mathrm{i}\delta S^{<}_{N1} = \mathrm{i}\delta S^{T}_{N1} = \mathrm{i}\delta S^{\bar{T}}_{N1} \equiv \mathrm{i}\delta S_{N1}\,, \tag{5.51}$$

where $\mathrm{i}\delta S^{>,<,T,\bar{T}}_{N1}$ denotes the difference between the non-equilibrium neutrino propagators and their equilibrium versions. Using this the CP-source collision term (5.39) reads

$$\begin{aligned}
\mathcal{C}^{\mathrm{wf}}_{\ell}(\mathbf{k}) = \int \frac{dk_0}{2\pi}\frac{d^4k'}{(2\pi)^4}\frac{d^4k''}{(2\pi)^4}(2\pi)^4\delta^4(k-k'-k'')\times \qquad (5.52)\\
(-1)\Bigg\{ \Big[Y_1^* Y_2 \mathrm{i}\delta S_{N1}\mathrm{i}\left(\not{\Sigma}^{T}_{N12} - \not{\Sigma}^{>}_{N12}\right)\mathrm{i}S^{T}_{N2} - Y_1 Y_2^* \mathrm{i}S^{T}_{N2}\left(\not{\Sigma}^{\bar{T}}_{N21} - \not{\Sigma}^{>}_{N21}\right)\mathrm{i}\delta S_{N1}\Big]_{k'}\\
\times\ \mathrm{i}\Delta^{<}_{\phi}(-k'')\mathrm{i}S^{<}_{\ell}(k)\\
+\ \Big[Y_1^* Y_2 \mathrm{i}\delta S_{N1}\mathrm{i}\left(\not{\Sigma}^{\bar{T}}_{N12} - \not{\Sigma}^{<}_{N12}\right)\mathrm{i}S^{T}_{N2} - Y_1 Y_2^* \mathrm{i}S^{T}_{N2}\left(\not{\Sigma}^{T}_{N21} - \not{\Sigma}^{<}_{N21}\right)\mathrm{i}\delta S_{N1}\Big]_{k'}\\
\times\ \mathrm{i}\Delta^{>}_{\phi}(-k'')\mathrm{i}S^{>}_{\ell}(k)\Bigg\}\,.
\end{aligned}$$

In this expression, the terms involving the dispersive parts $\not{\Sigma}^{\mathrm{disp}T,\bar{T}}_{Nij}$ of $\not{\Sigma}^{T,\bar{T}}_{Nij}$ cancel. To see this, first note that $\mathrm{i}\not{\Sigma}^{\mathrm{disp}T}_{Nij} = -\mathrm{i}\not{\Sigma}^{\mathrm{disp}\bar{T}}_{Nij}$. Then, since $\delta S_{N1}(k_0,\mathbf{k}) = \delta S_{N1}(-k_0,\mathbf{k})$ and since for equilibrium distributions $\mathrm{i}\Delta^{<}_{\phi}(k_0',\mathbf{k}')\mathrm{i}S^{<}_{\ell}(k_0',\mathbf{k}') = \mathrm{i}\Delta^{>}_{\phi}(-k_0',\mathbf{k}')\mathrm{i}S^{>}_{\ell}(-k_0',\mathbf{k}')$, the cancellation occurs when performing the integrals. We can therefore make the replacements

$$\not{\Sigma}^{T,\bar{T}}_{ij} - \not{\Sigma}^{>}_{ij} \to \frac{1}{2}\left(\not{\Sigma}^{<}_{ij} - \not{\Sigma}^{>}_{ij}\right)\,, \quad \not{\Sigma}^{T,\bar{T}}_{ij} - \not{\Sigma}^{<}_{ij} \to -\frac{1}{2}\left(\not{\Sigma}^{<}_{ij} - \not{\Sigma}^{>}_{ij}\right)\,, \tag{5.53}$$

and write the wave-function correction to the lepton collision integral as

$$\begin{aligned}
\int \frac{d^3k}{(2\pi)^3}\mathcal{C}^{\mathrm{wf}}_{\ell}(\mathbf{k}) = \int \frac{d^4k}{(2\pi)^4}\frac{d^4k'}{(2\pi)^4}\frac{d^4k''}{(2\pi)^4}\,(2\pi)^4\delta^4(k-k'-k'')\times \qquad (5.54)\\
\mathrm{tr}\Bigg[\left(-Y_1^* Y_2 \mathrm{i}\delta S_{N1}\frac{\mathrm{i}}{2}\left(\not{\Sigma}^{<}_{N12} - \not{\Sigma}^{>}_{N12}\right)\mathrm{i}S^{T}_{N2} + Y_1 Y_2^* \mathrm{i}S^{T}_{N2}\frac{\mathrm{i}}{2}\left(\not{\Sigma}^{<}_{N21} - \not{\Sigma}^{>}_{N21}\right)\mathrm{i}\delta S_{N1}\right)_{k'}\\
\times\left(\mathrm{i}\Delta^{<}_{\phi}(-k'')\mathrm{i}S^{<}_{\ell}(k) - \mathrm{i}\Delta^{>}_{\phi}(-k'')\mathrm{i}S^{>}_{\ell}(k)\right)\Bigg]\,.
\end{aligned}$$

The spectral self-energy is

$$\begin{aligned}
\mathrm{i}\not{\Sigma}^{<}_{Nij}(k) - \mathrm{i}\not{\Sigma}^{>}_{Nij}(k) = -\int \frac{d^3k'}{(2\pi)^3 2|\mathbf{k}'|^2}\frac{d^3k''}{(2\pi)^3 2|\mathbf{k}''|^2}(2\pi)^4\delta^4(k-k'-k'') \qquad (5.55)\\
\times\,\mathrm{sign}(k_0)\left[Y_i Y_j^* \not{k}' P_{\mathrm{R}} + Y_i^* Y_j \not{k}' P_{\mathrm{L}}\right]\times\left[1 - f^{\mathrm{eq}}_{\ell}(\mathbf{k}') + f^{\mathrm{eq}}_{\phi}(\mathbf{k}'')\right]\,.
\end{aligned}$$

In further simplifying $\mathcal{C}_\ell^{\rm wf}$, we obtain another factor of sign(k_0) from

$$\begin{aligned}&\mathrm{i}\Delta_\phi^<(-k'')\mathrm{i}S_\ell^<(k) - \mathrm{i}\Delta_\phi^>(-k'')\mathrm{i}S_\ell^>(k)\big|_{\mathrm{sign}(k_0)=-\mathrm{sign}(k_0'')} \\ &= -P_{\rm L}\not{k}P_{\rm R}\,(2\pi)^2\delta(k^2)\delta(k''^2)\mathrm{sign}(k_0)\left(1 - f_\ell^{\rm eq}(\mathbf{k}) + f_\phi^{\rm eq}(\mathbf{k}'')\right)\,.\end{aligned} \tag{5.56}$$

Using this result in Eq. (5.54), the tree-level propagators, and substituting after performing the Dirac trace the definition (5.33), we obtain our final result for the CP-violating wave-function correction to the lepton collision term:

$$\begin{aligned}S^{\rm wf} &= \int \frac{d^3k}{(2\pi)^3}\mathcal{C}_\ell^{\rm wf}(\mathbf{k}) \\ &= \int \frac{d^3k}{(2\pi)^3 2|\mathbf{k}|}\frac{d^3k'}{(2\pi)^3 2\sqrt{\mathbf{k}'^2+M_1^2}}\frac{d^3k''}{(2\pi)^3 2|\mathbf{k}''|}(2\pi)^4\delta^4(k'-k-k'') \\ &\quad\times\frac{M_1M_2}{k'^2-M_2^2}2\mathrm{Im}[Y_1^2Y_2^{*2}]2k_\mu\Sigma_N^\mu(k')\delta f_N(\mathbf{k}')\left(1-f_\ell^{\rm eq}(\mathbf{k})+f_\phi^{\rm eq}(\mathbf{k}'')\right) \\ &= 4\,\mathrm{Im}[Y_1^2Y_2^{*2}]\,\frac{M_1M_2}{M_1^2-M_2^2}\int\frac{d^3k'}{(2\pi)^3 2\sqrt{\mathbf{k}'^2+M_1^2}}\,\delta f_N(\mathbf{k}')\,\frac{\Sigma_{N\mu}(\mathbf{k}')\Sigma_N^\mu(\mathbf{k}')}{g_w}\,.\end{aligned} \tag{5.57}$$

Note that at zero temperature, we find

$$\Sigma_N^\mu(k)\Big|_{T=0} = g_w\frac{k^\mu}{16\pi}. \tag{5.58}$$

Then, by comparison with the tree-level lepton collision term (5.20), we reproduce the zero-temperature result for the decay asymmetry

$$\varepsilon_{T=0}^{\rm wf} = \frac{\Gamma_{N1\to\ell H}-\Gamma_{N1\to\bar\ell H^\dagger}}{\Gamma_{N1\to\ell H}+\Gamma_{N1\to\bar\ell H^\dagger}} = \frac{1}{8\pi}\frac{\mathrm{Im}[Y_1^2Y_2^{*2}]}{|Y_1|^2}\frac{M_1M_2}{M_1^2-M_2^2}\,, \tag{5.59}$$

where Γ denotes the decay rate of the process indicated in the subscript. On the other hand, if finite-density effects are kept for the initial and final states but not in the self-energy loop, then in the final expression of Eq. (5.57) one substitutes

$$\frac{\Sigma_{N\mu}(\mathbf{k}')\Sigma_N^\mu(\mathbf{k}')}{g_w} \to \frac{k'^\mu\Sigma_{N\mu}(\mathbf{k}')}{16\pi}\,. \tag{5.60}$$

5.5 Vertex Contribution to the CP Asymmetry

5.5.1 Vertex Correction to $\mathcal{C}_\ell$

The vertex correction contribution to the CP asymmetry arises from the two-loop self-energy diagram for the lepton propagator (see Figure 5.2):

$$\begin{aligned}\mathrm{i}\not{\Sigma}_\ell^{vab}(k) = &-cd\,Y_i^{*2}Y_j^{\,2}\int\frac{d^4p}{(2\pi)^4}\frac{d^4q}{(2\pi)^4}\,P_{\rm R}\mathrm{i}S_{Ni}^{ac}(-p)C\left[P_{\rm L}\mathrm{i}S_\ell^{dc}(p+k+q)P_{\rm R}\right]^t C^\dagger \\ &\times\mathrm{i}S_{Nj}^{db}(-q)P_{\rm L}\mathrm{i}\Delta_\phi^{da}(-p-k)\mathrm{i}\Delta_\phi^{bc}(-q-k)\,.\end{aligned} \tag{5.61}$$

Here, the transposition t acts on the Dirac indices, and i, j and the CTP indices $c, d = \pm$ are summed over. The charge conjugation arises as a consequence of lepton number violation and the reversed flow of the internal lepton in the self-energy diagram.

We again consider the case where $M_2 \gg M_1$ in order to reduce the number of terms to be considered by one half. Furthermore, we neglect the diagonal ($i = j$) contributions to the self-energy since they do not contribute to the CP asymmetry. This can be easily verified along the lines of the calculation presented in this Section. With these simplifications, we obtain

$$\begin{aligned}
\mathrm{i}\not{\Sigma}_\ell^{\mathrm{v}>}(k) = &- \int \frac{d^4p}{(2\pi)^4}\frac{d^4q}{(2\pi)^4} \qquad (5.62)\\
\times &\Big\{ {Y_1^*}^2 {Y_2}^2 \Big[\mathrm{i}S^{>}_{N1}(-p) C \left[P_\mathrm{L} \mathrm{i}S^T_\ell(Q) P_\mathrm{R}\right]^t C^\dagger \mathrm{i}S^T_{N2}(-q) \mathrm{i}\Delta^<_\phi(-p-k) \mathrm{i}\Delta^T_\phi(-q-k)\\
&\quad - \mathrm{i}S^{\bar{T}}_{N1}(-p) C \left[P_\mathrm{L} \mathrm{i}S^<_\ell(Q) P_\mathrm{R}\right]^t C^\dagger \mathrm{i}S^T_{N2}(-q) \mathrm{i}\Delta^<_\phi(-p-k) \mathrm{i}\Delta^<_\phi(-q-k) \Big]\\
+ {Y_1}^2 {Y_2^*}^2 &\Big[- \mathrm{i}S^{\bar{T}}_{N2}(-p) C \left[P_\mathrm{L} \mathrm{i}S^<_\ell(Q) P_\mathrm{R}\right]^t C^\dagger \mathrm{i}S^T_{N1}(-q) \mathrm{i}\Delta^<_\phi(-p-k) \mathrm{i}\Delta^<_\phi(-q-k)\\
&\quad + \mathrm{i}S^{\bar{T}}_{N2}(-p) C \left[P_\mathrm{L} \mathrm{i}S^{\bar{T}}_\ell(Q) P_\mathrm{R}\right]^t C^\dagger \mathrm{i}S^>_{N1}(-q) \mathrm{i}\Delta^{\bar{T}}_\phi(-p-k) \mathrm{i}\Delta^<_\phi(-q-k) \Big] \Big\},
\end{aligned}$$

where $Q = p + k + q$ for notational simplicity. The expression for $\mathrm{i}\not{\Sigma}_\ell^{\mathrm{v}<}(k)$ is obtained through interchange of the CTP indices $T \leftrightarrow \bar{T}$ and $< \leftrightarrow >$.

5.5.2 KMS and Real Intermediate State Subtraction

Before proceeding with the calculation of the CP source, we again show that this contribution leads to a vanishing asymmetry in equilibrium, which in particular means that the KMS relation, $\mathrm{i}\not{\Sigma}_\ell^{\mathrm{v}>}(k) + \mathrm{e}^{\beta k_0}\mathrm{i}\not{\Sigma}_\ell^{\mathrm{v}<}(k) = 0$, must hold when equilibrium distributions are inserted. To see explicitly how this arises, we consider the contributions $\propto {Y_1^*}^2 {Y_2}^2$. First, we define

$$\mathrm{i}\not{\Sigma}_\ell^{\mathrm{v}>}(k) + \mathrm{e}^{\beta k_0}\mathrm{i}\not{\Sigma}_\ell^{\mathrm{v}<}(k) = \int \frac{d^4p}{(2\pi)^4}\frac{d^4q}{(2\pi)^4} \mathcal{J}(k,p,q) \qquad (5.63)$$

and note that by virtue of the KMS relation

$$\begin{aligned}
&\mathcal{J}(k,p,q) = \\
&\quad {Y_1^*}^2 {Y_2}^2 \left[\mathrm{i}S^T_{N1}(-p) + \mathrm{i}S^{\bar{T}}_{N1}(-p)\right] C \left[P_\mathrm{L} \mathrm{i}S^<_\ell(p+k+q) P_\mathrm{R}\right]^t C^\dagger \mathrm{i}S^T_{N2}(-q)\\
&\quad \times \mathrm{i}\Delta^<_\phi(-p-k) \mathrm{i}\Delta^<_\phi(-q-k)\\
&\quad - {Y_1^*}^2 {Y_2}^2 \mathrm{i}S^>_{N1}(-p) C \Big[P_\mathrm{L} \mathrm{i}S^T_\ell(p+k+q) P_\mathrm{R} \Delta^T_\phi(-q-k)\\
&\quad + P_\mathrm{L} \mathrm{i}S^{\bar{T}}_\ell(p+k+q) P_\mathrm{R} \Delta^{\bar{T}}_\phi(-q-k)\Big]^t C^\dagger \mathrm{i}S^T_{N2}(-q) \mathrm{i}\Delta^<_\phi(-p-k)\,. \qquad (5.64)
\end{aligned}$$

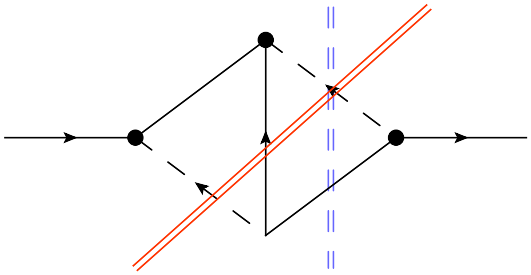

Figure 5.2: Diagrammatic representation of $\not{\Sigma}_\ell^{\mathrm{v}<,>}$. The solid lines with arrows represent the lepton ℓ, the solid lines without arrows the neutrinos $N_{1,2}$ and the dashed lines with arrows the Higgs boson ϕ. The solid (light-grey/orange) double line represents the cut that corresponds to the subtracted real intermediate states when finite density corrections to CP violation are neglected. The dashed (dark-grey/blue) double line represents the cut that corresponds to decays and inverse decays when finite density corrections are neglected.

Further simplification is achieved when deriving from the explicit expressions (5.4) and (5.8) that for $\mathrm{sign}(r_0) = \mathrm{sign}(s_0)$,

$$\mathrm{i}S_\ell^T(r)\mathrm{i}\Delta_\phi^T(s) + \mathrm{i}S_\ell^{\bar{T}}(r)\mathrm{i}\Delta_\phi^{\bar{T}}(s) = \mathrm{i}S_\ell^<(r)\mathrm{i}\Delta_\phi^<(s) + \mathrm{i}S_\ell^>(r)\mathrm{i}\Delta_\phi^>(s)\,. \tag{5.65}$$

We find

$$\begin{aligned}\mathcal{J}(k,p,q) = {} & Y_1^{*2}Y_2{}^2\left[\mathrm{i}S_{N1}^<(-p) + \mathrm{i}S_{N1}^>(-p)\right] C\left[P_\mathrm{L}\mathrm{i}S_\ell^<(p+k+q)P_\mathrm{R}\right]^t C^\dagger \mathrm{i}S_{N2}^T(-q) \\ & \times \mathrm{i}\Delta_\phi^<(-p-k)\mathrm{i}\Delta_\phi^<(-q-k) \\ & - Y_1^{*2}Y_2{}^2\mathrm{i}S_{N1}^>(-p)C\Big[P_\mathrm{L}\mathrm{i}S_\ell^<(p+k+q)P_\mathrm{R}\Delta_\phi^<(-q-k) \\ & + P_\mathrm{L}\mathrm{i}S_\ell^>(p+k+q)P_\mathrm{R}\Delta_\phi^>(-q-k)\Big]^t C^\dagger \mathrm{i}S_{N2}^T(-q)\mathrm{i}\Delta_\phi^<(-p-k) \\ & = 0\,,\end{aligned} \tag{5.66}$$

where for the last equality, we have again used the KMS relation. Likewise, one can show the vanishing of the terms $\propto Y_1{}^2Y_2^{*2}$ in equilibrium.

Again, we can relate this verification of the KMS relation to the standard procedure of RIS subtraction. As in the wave-function contribution, at zero temperature the $<,>$ type Green functions correspond to cut propagators. The terms in (5.62) involving $S_{N1}^{<,>}$ and $\Delta_\phi^{<,>}$ thus correspond to the cut indicated by the dashed double line in Figure 5.2 that represents the interference between the tree-level and one-loop contribution to the N_1 decay amplitude. The terms involving $S_{N1}^{T,\bar{T}}$ on the other hand correspond to N_1 mediated scatterings, as indicated by the solid cut line in Figure 5.2. Note that here the cut corresponds to the interference between s-channel and t-channel diagrams, while the central

cuts through the wave-function correction yield the squares of the s-channel and t-channel contributions to the scatterings. This complementarity is crucial for the separate cancellation of the asymmetries from the wave function and the vertex correction in equilibrium.

5.5.3 CP Source

We now extract the CP source in the lepton collision term using the same simplifications as in the calculation of the wave-function correction. In particular, the deviation of N_1 from equilibrium is parametrised again by δS_{N1}. We obtain

$$
\begin{aligned}
\mathcal{C}^{\mathrm{v}}_\ell(\mathbf{k}) &= \int \frac{dk_0}{2\pi} \mathrm{tr}\left[\mathrm{i}\not{\Sigma}^{\mathrm{v}>}_\ell(k)\mathrm{i}S^<_\ell(k) - \mathrm{i}\not{\Sigma}^{\mathrm{v}<}_\ell(k)\mathrm{i}S^>_\ell(k)\right] \qquad (5.67)\\
&= \int \frac{dk_0}{2\pi}\frac{d^4p}{(2\pi)^4}\frac{d^4q}{(2\pi)^4} \times \mathrm{tr}\Big[\Big\{ - {Y_1}^{*2}{Y_2}^2 \mathrm{i}\delta S_{N1}(-p) C\big[\mathrm{i}S^T_\ell(p+k+q)\mathrm{i}\Delta^T_\phi(-q-k)\\
&\qquad -\mathrm{i}S^<_\ell(p+k+q)\mathrm{i}\Delta^<_\phi(-q-k)\big]^t C^\dagger \mathrm{i}S^T_{N2}(-q)\mathrm{i}\Delta^<_\phi(-p-k)\\
&\quad + {Y_1}^2{Y_2}^{*2}\mathrm{i}S^T_{N2}(-p)C\big[\mathrm{i}S^{\bar T}_\ell(p+k+q)\mathrm{i}\Delta^{\bar T}_\phi(-q-k)\\
&\qquad -\mathrm{i}S^<_\ell(p+k+q)\mathrm{i}\Delta^<_\phi(-q-k)\big]^t C^\dagger \mathrm{i}\delta S^T_{N1}(-q)\mathrm{i}\Delta^<_\phi(-p-k)\Big\}\mathrm{i}S^<_\ell(k)\\
&\quad - \Big\{ - {Y_1}^2{Y_2}^{*2}\mathrm{i}S^T_{N2}(-p)C\big[\mathrm{i}S^T_\ell(p+k+q)\mathrm{i}\Delta^T_\phi(-q-k)\\
&\qquad -\mathrm{i}S^>_\ell(p+k+q)\mathrm{i}\Delta^>_\phi(-q-k)\big]^t C^\dagger \mathrm{i}\delta S^T_{N1}(-q)\mathrm{i}\Delta^>_\phi(-p-k)\\
&\quad + {Y_1}^{*2}{Y_2}^2\mathrm{i}\delta S_{N1}(-p)C\big[\mathrm{i}S^{\bar T}_\ell(p+k+q)\mathrm{i}\Delta^{\bar T}_\phi(-q-k)\\
&\qquad -\mathrm{i}S^>_\ell(p+k+q)\mathrm{i}\Delta^>_\phi(-q-k)\big]^t C^\dagger \mathrm{i}S^T_{N2}(-q)\mathrm{i}\Delta^>_\phi(-p-k)\Big\}\mathrm{i}S^>_\ell(k)\Big]\,,
\end{aligned}
$$

where $\mathrm{i}S^{\bar T}_{N2} = -\mathrm{i}S^T_{N2}$ for off-shell neutrinos N_2 has been used. Inspection of the Dirac structure reveals that $S_{N1,2}$ only contribute through terms proportional to $M_{1,2}$, which is familiar from the standard calculation of the decay asymmetry [91]. Finally, similar to the replacement (5.53) we can substitute here

$$
\begin{aligned}
S^{T,\bar T}_\ell \Delta^{T,\bar T}_\phi - S^>_\ell \Delta^>_\phi &\to +\frac{1}{2}\left(S^<_\ell\Delta^<_\phi - S^>_\ell\Delta^>_\phi\right)\,, \qquad (5.68)\\
S^{T,\bar T}_\ell \Delta^{T,\bar T}_\phi - S^<_\ell \Delta^<_\phi &\to -\frac{1}{2}\left(S^<_\ell\Delta^<_\phi - S^>_\ell\Delta^>_\phi\right)
\end{aligned}
$$

under the integrals.

The expression (5.67) closely resembles the result for the wave-function contribution, except that $\mathrm{i}S^T_{N2}$ now depends on the loop momentum q. In the limit where $M_2 \gg M_1$, the N_2 propagator can be expanded in powers of $\tilde k^2/M_2^2$ where $\tilde k = (p,k)$, showing that in this limit the vertex correction is just one half of the self-energy contribution, where the factor one half arises since there is no summation over SU(2) indices within the loop.

Inserting the explicit expressions for the lepton and Higgs boson Green functions, we obtain our final result for the vertex correction to the CP asymmetry. To this end we introduce

$$\Gamma_\mu(k,p'',M_2) = \int \frac{d^3k'}{(2\pi)^3 2|\mathbf{k}'|}\frac{d^3k''}{(2\pi)^3 2|\mathbf{k}''|}(2\pi)^4\delta^4(k-k'-k'')\,k'_\mu\,\frac{M_1M_2}{(k'-p'')^2-M_2^2} \times [1-f_\ell(\mathbf{k}')+f_\phi(\mathbf{k}'')]\;. \tag{5.69}$$

This has to be integrated over the initial and final state phase space in the collision term, such that we additionally define

$$V(k,M_2) = \int \frac{d^3p'}{(2\pi)^3 2|\mathbf{p}'|}\frac{d^3p''}{(2\pi)^3 2|\mathbf{p}''|}(2\pi)^4\delta^4(k-p'-p'')\,p'^\mu\,\Gamma_\mu(k,p'',M_2) \times [1-f_\ell(\mathbf{p}')+f_\phi(\mathbf{p}'')]\;. \tag{5.70}$$

In terms of these quantities, the lepton collision term can be expressed as

$$S^{\rm v} = \int \frac{d^3p'}{(2\pi)^3}\,\mathcal{C}^{\rm v}_\ell(\mathbf{p}') = 4\,\mathrm{Im}[Y_1^2Y_2^{*2}]\int \frac{d^3k}{(2\pi)^3 2\sqrt{\mathbf{k}^2+M_1^2}}\,\delta f_{N1}(\mathbf{k})\,V(k,M_2)\,. \tag{5.71}$$

5.5.4 Source term in the strongly hierarchical limit

For the strongly hierarchical case, $M_2 \gg M_1$, which we will focus on for the numerical analysis, the vertex contribution is simply one half of the self energy contribution. To see this, we note that in the limit $M_2 \gg M_1$,

$$\frac{M_1M_2}{(k'-p'')^2-M_2^2} \to -\frac{M_1}{M_2} \tag{5.72}$$

in Eq. (5.69), which implies

$$\Gamma_\mu(k,p'',M_2) = -\frac{M_1}{M_2}\,\frac{\Sigma_\mu(k)}{g_W} \qquad \text{and} \qquad V(k,M_2) = -\frac{M_1}{M_2}\frac{\Sigma_{N\mu}(\mathbf{k}')\Sigma_N^\mu(\mathbf{k}')}{g_w^2}. \tag{5.73}$$

Inserting this into Eq. (5.71) and adding the wave-function contribution (5.57) the source term for the lepton asymmetry in Eq. (5.31) is given by

$$S_{M_2\gg M_1} = \frac{3}{2}\times\,4\,\mathrm{Im}[Y_1^2Y_2^{*2}]\left(-\frac{M_1}{M_2}\right)\int \frac{d^3k'}{(2\pi)^3 2\sqrt{\mathbf{k}'^2+M_1^2}}\,\delta f_N(\mathbf{k}')\,\frac{\Sigma_{N\mu}(\mathbf{k}')\Sigma_N^\mu(\mathbf{k}')}{g_w}\,, \tag{5.74}$$

with $\Sigma_{N\mu}(\mathbf{k}')$ given in Eq. (5.33).

5.6 Numerical Estimates of Finite Density Effects

In this Section we solve the kinetic equation for the final lepton asymmetry with CP-violating collision terms derived in Sections 5.3 – 5.5. We compare our results with all finite density effects included to the case where these effects are included in the initial and final state phase-space distributions, but not in the quantum corrections.

5.6.1 Effective CP-violating parameter

To begin with, however, we present a rough estimate for the total magnitude of CP violation in the lepton collision term. This estimate is provided through an effective CP-violating parameter, which we define as:

$$\varepsilon_{\rm eff} \equiv -\frac{\frac{d}{d\eta}(n_\ell - \bar{n}_\ell) - W}{\frac{d}{d\eta} n_{N1}}\,, \tag{5.75}$$

where $n_{\ell,N1} = \int \frac{d^3k}{(2\pi)^3} f_{\ell,N1}(\mathbf{k})$ are the comoving number densities of lepton and neutrino. The tree-level (washout) contribution W, see Eq. (5.37), is subtracted from this definition, so that the numerator involves only the CP source, which is comprised of self-energy and vertex type corrections to the lepton collision term, given by Eqs. (5.57) and (5.71). The CP-violating parameter thus also breaks into the corresponding two parts. For the self-energy part we get by using Eqs. (5.34), (5.57):

$$\varepsilon^{\rm wf}_{\rm eff} = \varepsilon^{\rm wf}_{T=0} \frac{16\pi}{g_w} \frac{\int d|\mathbf{k}| \frac{|\mathbf{k}|^2}{k_0} \Sigma^\mu_{N1}(k) \Sigma_{N1\,\mu}(k)\, \delta f_{N1}(\mathbf{k})}{\int d|\mathbf{k}| \frac{|\mathbf{k}|^2}{k_0} k_\mu \Sigma^\mu_{N1}(k)\, \delta f_{N1}(\mathbf{k})}\,, \tag{5.76}$$

where $\varepsilon^{\rm wf}_{T=0}$ is the CP-violating parameter in the vacuum, given by Eq. (5.59). We see right away, that Eq. (5.76) indeed reduces to $\varepsilon^{\rm wf}_{T=0}$ in the limit where the finite density effects in the loop are neglected in which case one factor of $\Sigma^\mu_N(k)$ in the numerator is replaced by $g_w k^\mu/(16\pi)$. We will not compute the vertex correction part here in full generality, but we note that in the strongly hierarchical case, where $M_2 \gg M_1$, the vertex CP-source reduces to one-half of the self energy CP-source, as shown in the previous Section. The same is then obviously true for the corresponding CP-violating parameter $\varepsilon^{\rm v}_{\rm eff}$, so that the ratio $\varepsilon_{\rm eff}/\varepsilon_{T=0}$ is the same for the total and the wave-function contribution alone.

To compute $\varepsilon^{\rm wf}_{\rm eff}$ requires the knowledge of the neutrino distribution function $f_{N1}(\mathbf{k})$ for each instant of time (or temperature in the expanding Universe), which is obtained by solving the tree-level Boltzmann equation (5.34). Before doing this we make an estimate for $\varepsilon^{\rm wf}_{\rm eff}$ by factoring out the nontrivial time-dependence in

Eq. (5.76). This can be achieved by assuming that the decaying heavy neutrino N_1 remains in kinetic equilibrium and making an ansatz with a pseudo-chemical potential μ_{N1}:

$$f_{N1}(\mathbf{k}) = \frac{1}{\exp[\beta(\sqrt{\mathbf{k}^2 + M_1^2} - \mu_{N1})] + 1}\,. \tag{5.77}$$

For small deviations from thermal equilibrium, this can be expanded in linear order of μ_{N1} as

$$\delta f_{N1}(\mathbf{k}) = f_{N1}^{\mathrm{eq}}(\mathbf{k})\,(1 - f_{N1}^{\mathrm{eq}}(\mathbf{k}))\,\frac{\mu_{N1}}{T}\,. \tag{5.78}$$

Using this ansatz the pseudo-chemical potential μ_{N1} involving the time dependence cancels out in the ratio in Eq. (5.76), and we get

$$\varepsilon_{\mathrm{eff}}^{\mathrm{wf}} = \varepsilon_{T=0}^{\mathrm{wf}}\frac{16\pi}{g_w}\frac{\int d|\mathbf{k}|\frac{|\mathbf{k}|^2}{k_0}\,\Sigma_{N1}^{\mu}(k)\Sigma_{N1\,\mu}(k)\,f_{N1}^{\mathrm{eq}}(\mathbf{k})\,(1 - f_{N1}^{\mathrm{eq}}(\mathbf{k}))}{\int d|\mathbf{k}|\frac{|\mathbf{k}|^2}{k_0}\,k_\mu\Sigma_{N1}^{\mu}(k)\,f_{N1}^{\mathrm{eq}}(\mathbf{k})\,(1 - f_{N1}^{\mathrm{eq}}(\mathbf{k}))}\,. \tag{5.79}$$

To evaluate this expression, we see that the phase space integrals in $\Sigma_{N1}^{\mu}(k)$, Eq. (5.33), can be computed to give

$$\Sigma_N^0(k) = \frac{g_w T^2}{8\pi|\mathbf{k}|}\,I_1\left(\frac{k_0}{T}, \frac{|\mathbf{k}|}{T}\right)\,, \tag{5.80a}$$

$$\Sigma_N^i(k) = \frac{g_w T^2}{8\pi|\mathbf{k}|}\left(\frac{k_0}{|\mathbf{k}|}\,I_1\left(\frac{k_0}{T}, \frac{|\mathbf{k}|}{T}\right) - \frac{M_1^2}{2|\mathbf{k}|T}\,I_0\left(\frac{k_0}{T}, \frac{|\mathbf{k}|}{T}\right)\right)\frac{k^i}{|\mathbf{k}|}\,, \tag{5.80b}$$

with

$$I_n(y_0, y) \equiv \int\limits_{\frac{1}{2}(y_0 - y)}^{\frac{1}{2}(y_0 + y)} dx\; x^n\left(1 - \frac{1}{\mathrm{e}^x + 1} + \frac{1}{\mathrm{e}^{y_0 - x} - 1}\right)\,, \tag{5.81}$$

which have analytical expressions

$$I_0(y_0, y) = \ln\left(\frac{e^{y_0 + y} - 1}{e^{y_0 - y} - 1}\right) - y\,, \tag{5.82}$$

$$\begin{aligned} I_1(y_0, y) =& \frac{1}{2}(y_0 + y)\ln\left(\frac{1 + e^{\frac{y_0 + y}{2}}}{1 - e^{\frac{-y_0 + y}{2}}}\right) - \frac{1}{2}(y_0 - y)\ln\left(\frac{1 + e^{\frac{y_0 - y}{2}}}{1 - e^{\frac{-y_0 - y}{2}}}\right) \\ &+ \mathrm{Li}_2\left(-e^{\frac{y_0 + y}{2}}\right) + \mathrm{Li}_2\left(e^{\frac{-y_0 - y}{2}}\right) - \mathrm{Li}_2\left(-e^{\frac{y_0 - y}{2}}\right) - \mathrm{Li}_2\left(e^{\frac{-y_0 + y}{2}}\right)\,, \end{aligned} \tag{5.83}$$

where Li_2 denotes dilogarithm. The remaining one-dimensional momentum integrations in Eq. (5.79) can then easily be computed numerically. We plot the resulting ratio $\varepsilon_{\mathrm{eff}}^{\mathrm{wf}}/\varepsilon_{T=0}^{\mathrm{wf}}$ (equal to $\varepsilon_{\mathrm{eff}}/\varepsilon_{T=0}$ in the strongly hierarchical limit) as a function of $z = M_1/T$ in Figure 5.3. We find that the medium effects tend to enhance the effective asymmetry, in particular, the Bose enhancement of the Higgs particle dominates over the Fermi suppression of the lepton.

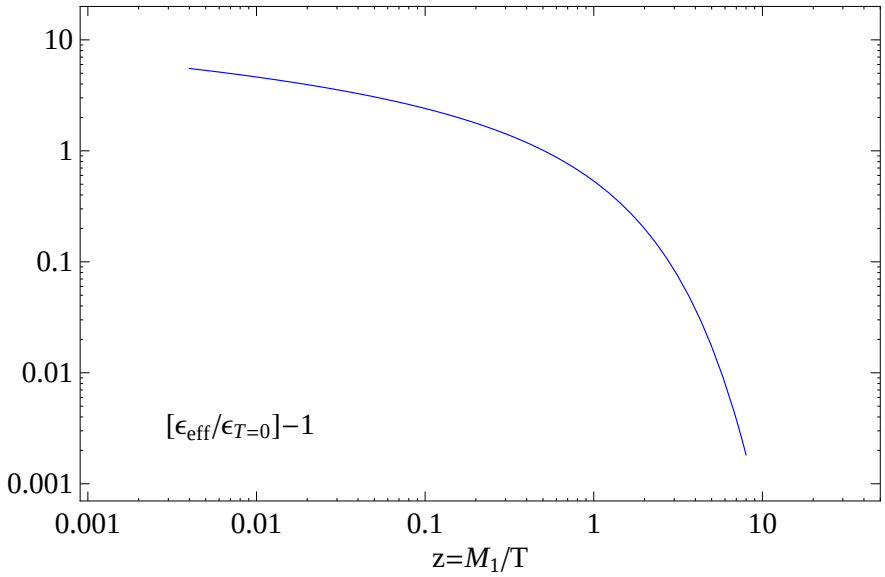

Figure 5.3: The ratio of the CP-violating parameter when taking effects of finite density in the loop into account over the CP-violating parameter at $T = 0$.

5.6.2 Numerical solution of the Boltzmann equations

We now scrutinise how the enhancement of the asymmetry is reflected in the solution of the Boltzmann equations (5.30), (5.31). Note that the former is an equation for the distribution function of right-handed neutrinos, while the latter is an equation for the number density of left-handed leptons. For our numerical analysis we consider the asymmetries in the limit of strong hierarchy: $M_2 \gg M_1$, when the total CP source in Eq. (5.31) is given by Eq. (5.74). The vector Σ_N^μ can be evaluated according to Eqs. (5.80) when substituting for T the "comoving" temperature $T_{\rm com} = a(\eta)T$. The washout term on the right-hand side of Eq. (5.31) has been given in Eq. (5.37).

In the parametric region of strong washout, the neutrino density and also the lepton asymmetry will eventually become independent of the initial conditions, while this is not the case in the weak-washout domain. When dropping the assumption that the right-handed neutrinos are in equilibrium [107, 108], we can integrate the equations for the comoving modes $\mathbf{k}_{\rm com}$ of the neutrino number distribution separately, which is the method that we pursue here. Thus, to solve the time-evolution equation for the lepton asymmetry, we first calculate the out-of-equilibrium neutrino distribution by solving Eq. (5.30) with the decay and inverse decay term $D(\mathbf{k}_{\rm com})$ given by Eq. (5.34). This solution is then inserted into the source term. The expression (5.34) carries dependence on conformal time η through the dependence on $k_{\rm com\,0} = \sqrt{\mathbf{k}_{\rm com}^2 + a_{\rm R}^2\eta^2 M_1^2}$, and the dependence of

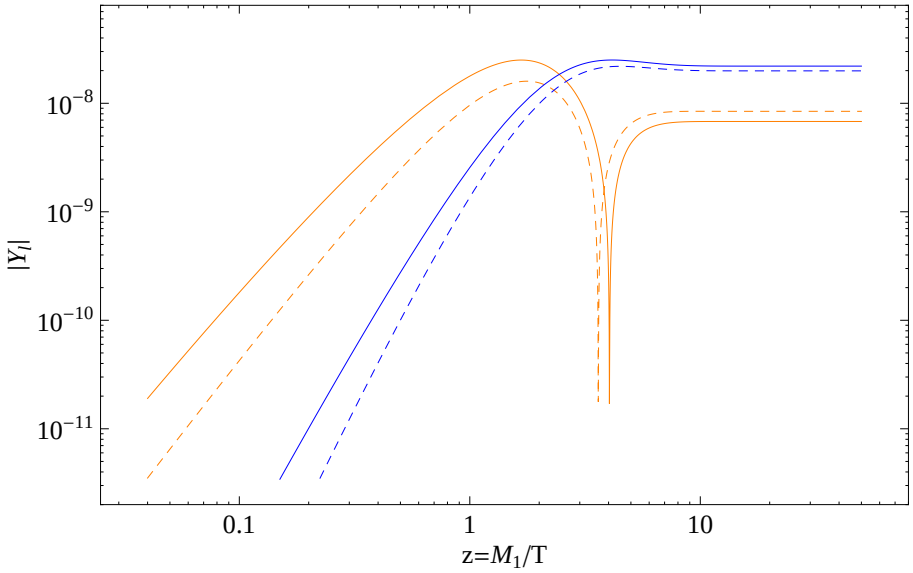

Figure 5.4: The absolute value of lepton-to-entropy ratio Y_ℓ over $z = M_1/T$. The parameters are $M_1 = 10^{13}\,\mathrm{GeV}$, $M_2 = 10^{15}\,\mathrm{GeV}$, $Y_1 = 2 \times 10^{-2}$, $Y_2 = 10^{-1}$ and a maximal CP phase. Both, thermal initial conditions (dark grey/blue) and vanishing initial conditions (light grey/red) for N_1 are chosen. The solid lines correspond to solutions where finite density corrections in the loop are taken into account, the dotted lines to solutions where these are omitted.

$\Sigma_N^\mu(k_{\mathrm{com}})$ and $f_{N1}^{\mathrm{eq}}(\mathbf{k}_{\mathrm{com}})$ on $k_{\mathrm{com}\,0}$. Thus a numerical solution of Eq. (5.30) for the out-of-equilibrium neutrino distribution is necessary.

In Figure 5.4, we show solutions to the Boltzmann equations in the intermediate regime between weak and strong washout. What is shown is the asymmetry summed over spin and SU(2) degrees of freedom and normalized to the entropy density,

$$Y_\ell = 2g_w \frac{n_{\mathrm{ph},\ell} - \bar{n}_{\mathrm{ph},\ell}}{s} = 2g_w \frac{n_{\mathrm{com},\ell} - \bar{n}_{\mathrm{com},\ell}}{\frac{2\pi^2}{45} g_\star T_{\mathrm{com}}^3}, \tag{5.84}$$

where the last form is convenient since we calculate directly the comoving particle densities. We assume an effective number of relativistic degrees of freedom according to the Standard Model ($g_\star = 106.75$). In the Figure, we provide results both with (solid lines) and without (dashed lines) the additional finite density enhancement in the loops. We choose the parameters $M_1 = 10^{13}\,\mathrm{GeV}$, $M_2 = 10^{15}\,\mathrm{GeV}$, $|Y_1| = 2 \times 10^{-2}$, $|Y_2| = 10^{-1}$ and a maximal CP phase such that $\mathrm{Im}[Y_1^2 Y_2^{*2}]$ is purely imaginary. Besides, we consider two different initial conditions, namely vanishing (light grey/red lines) and thermal (dark grey/blue lines) initial distributions for N_1. Recall also that the parameter $z = M_1/T$ is proportional to η. We observe from the Figure that there is a sizable effect of

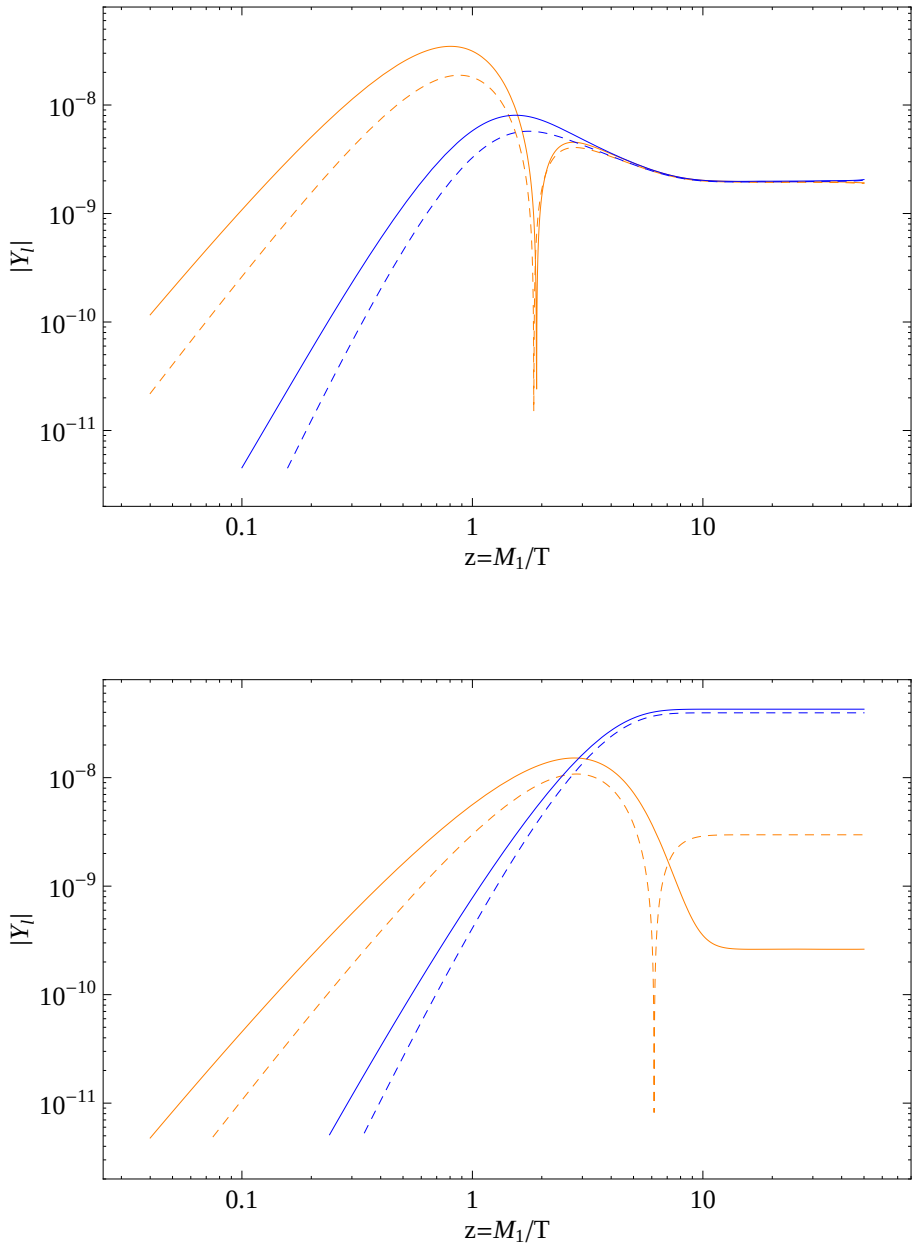

Figure 5.5: The absolute value of lepton-to-entropy ratio Y_ℓ over $z = M_1/T$. The parameters are $M_1 = 10^{13}\,\mathrm{GeV}$, $M_2 = 10^{15}\,\mathrm{GeV}$, $Y_1 = 5 \times 10^{-2}$, $Y_2 = 10^{-1}$ and a maximal CP phase in the upper panel (strong washout) and $Y_1 = 10^{-2}$, $Y_2 = 10^{-1}$ in the lower panel (weak washout). Both, thermal initial conditions (dark grey/blue) and vanishing initial conditions (light grey/red) for N_1 are chosen. The solid lines correspond to solutions where finite density corrections in the loop are taken into account, the dotted lines to solutions where these are omitted.

order $(10-20)\%$ from the finite density terms in the loops surviving at late times, since the asymmetry is partly produced at early times, when M_1 is not much larger than T and quantum statistical corrections are of importance. This situation no longer persists at larger coupling, $Y_1 = 5 \times 10^{-2}$, corresponding to strong washout. We display the result in the upper panel of Figure 5.5. Here the final asymmetry is determined at late times when $M_1 \gg T$, such that quantum statistical factors have no sizable impact.

Finally, we consider a scenario of weak washout (here we choose $Y_1 = 10^{-2}$). The resulting asymmetries are displayed in the lower panel of Figure 5.5. In the case of vanishing initial conditions for N_1, we find the impact of the finite-density effects in the loop in this scenario quite drastic: When they are taken into account, the asymmetry produced at early times when the N_1-abundance is below its equilibrium value becomes larger, due to the Bose enhancement of the Higgs particles. This "wrong-sign" asymmetry is then too large to be cancelled by the "right-sign" asymmetry produced at later times, when the N_1-abundance is above its equilibrium value. Not only the temperature dependence of the washout, but also the temperature-dependence of the effective CP-violating parameter is crucial for determining the final lepton asymmetry. This feature does not occur when the loop enhancement is neglected, since in that case, the effective CP asymmetry is temperature independent and the resulting asymmetry is always of the"right-sign". Therefore, neglecting the finite density effects in the loop in weak washout scenarios is in general not justifiable and may under certain circumstances even lead to an error in the predicted sign of the asymmetry.

5.7 Conclusions

We presented a full derivation and numerical solution of the kinetic equations describing leptogenesis in the CTP framework. The results extend existing approaches since all quantum statistical factors are accounted for systematically for the first time in a realistic model of leptogenesis. We have put particular emphasis on establishing a connection to the conventional Boltzmann approach and elucidated how RIS subtraction is realised in the CTP formalism. The numerical analysis shows that finite density corrections do not play a significant role in the strong-washout regime, while they may have a sizable impact in weak-washout scenarios.

The detailed analysis of the simple model of leptogenesis presented in this work should be seen as a first step toward applications of the CTP formalism to situations where the Boltzmann framework needs to be modified. One may think of flavour effects [114–117], the inclusion of additional thermal effects [106] or resonant leptogenesis [112, 115, 118, 119] in the limit of degenerate right-handed neutrino masses. Examples of approaches to these more advanced problems using the CTP formalism may already be found in the literature [101, 102, 120].

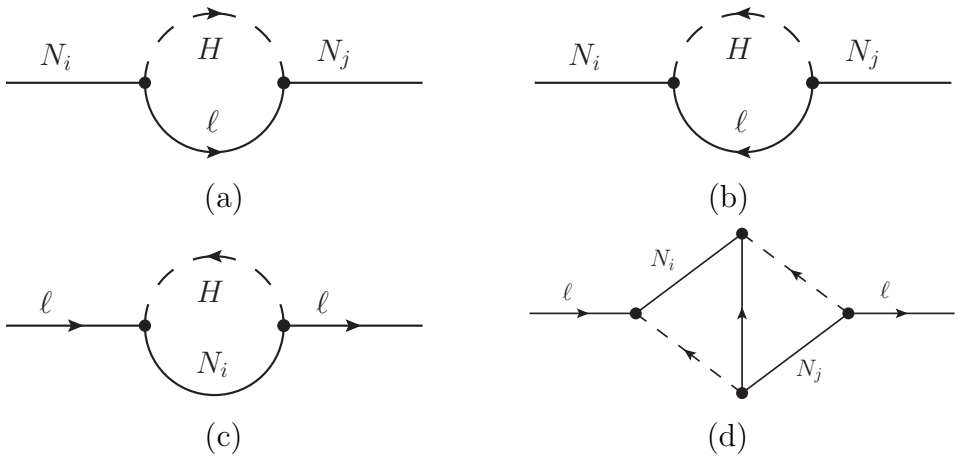

Figure 5.6: Diagrammatic representation of the one-loop contributions to the neutrino self energies, Figures (a) and (b), and the one loop (c) and two loop (d) contribution to the lepton self energy. The two loop wave-function correction in Figure 5.1 results from inserting (b) for the propagator of N_i in (c).

However, so far there has been no complete derivation and solution of the equations describing the standard scenario of leptogenesis within the CTP framework. The present work may be viewed as a self-consistent leading-order approximation in this framework, which serves as a starting point for investigating further corrections and variations.

5.8 Appendix: Calculation of the Self Energies

In this section we sketch the derivation of the neutrino one-loop self energy (5.13) and the one- and two-loop self energies for the leptons, (5.14) and (5.61).

The Feynman diagrams contributing to these self energies are shown in Figure 5.6(a)-(d). The required CTP components Σ^{ab} are obtained by assigning the positions a and b to the vertices connected to external legs, while all internal vertices have to be summed over the possible positions on the upper and lower branch of the CTP contour.

For the propagators we use the following set of Feynman rules:

$$= iS^{ab}_{N_i}(k) \tag{5.85}$$

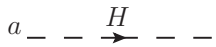

$$= i\Delta^{ab}_{\phi}(k) \tag{5.86}$$

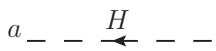

$$= i\Delta^{ba}_{\phi}(-k) = i\Delta^{ab}_{\phi^c}(k) \tag{5.87}$$

$$= iS^{ab}_{\ell}(k) \tag{5.88}$$

$$= C\left(iS^{ba}_{\ell}(-k)\right)^t C^\dagger = iS^{ab}_{\ell^c}(k) \tag{5.89}$$

where the arrow indicates the positive (negative) charge flow in the boson (fermion) propagator line and the transposition t acts on the Dirac indices, and the momentum flows from left to right. The CTP indices define an ordering that makes the distinction between particle and anti-particle propagators necessary. Furthermore, the Dirac structure imposes a unique "fermion flow" (cf. Ref. [122]) that uniquely specifies how S^{ab}_{Ni} has to be inserted in a particular diagram.

The vertices are obtained from the Lagrangian (5.1). In addition to the vacuum Feynman rules [122] a factor of $a = \pm 1$ appears for each internal vertex. For vertices connected to an external leg this factor is compensated by an additional factor of a on the external leg. An easy way to see this is to notice that the self energies can also be derived from the 2PI effective action through differentiation,

$$\mathrm{i}\not{\Sigma}^{ab}_{\psi} = ab\frac{\delta\Gamma_2}{\delta G^{ba}_{\psi}} \tag{5.90}$$

where ψ denotes an arbitrary boson or fermion field. Using these rules it is straightforward to obtain the expressions (5.13), (5.14) and (5.61).

We obtain the wave function correction from the lepton self energy by inserting the leading correction into the neutrino propagator in (5.14) i.e. by expanding

$$S^{ab}_{Nij} = S^{ab}_{Ni}\delta_{ij} + S^{\mathrm{wf},ab}_{Nij} + \mathcal{O}(Y^4_{i,j})\,, \tag{5.91}$$

where S^{ab}_{Ni} denotes the diagonal tree-level propagator. Inserting this expansion into the Dyson-Schwinger equation $\mathrm{i}S = \mathrm{i}S^0 - \mathrm{i}S^0\mathrm{i}\not{\Sigma}\mathrm{i}S$ and expanding in orders of $Y_{i,j}$ one obtains Eqs. (5.41) for $S^{\mathrm{wf}<,>}_{Nij}$. A more complete treatment would be to resum the self-energy corrections to the neutrino propagator, including finite width effects. This is required for an analysis of the resonant leptogenesis scenario which lies beyond the scope of this work.

Chapter 6

Closed Time Path Approach to Flavor Effects in Leptogenesis

6.1 Introduction

The discussion of Leptogenesis in the previous chapter is for a single flavor of Standard Model leptons ℓ, which is appropriate in those situations where the different Standard Model Yukawa couplings of these flavours are negligible because an asymmetry is only produced for one particular linear combination of the lepton flavours. However, at smaller temperatures, when the lepton Yukawa couplings h of the Standard Model approach equilibrium, the flavour degeneracy is broken and effects of flavour have to be taken into account [114–117]. The derivation of a set of kinetic equations from non-equilibrium quantum field theory which covers both the unflavoured and fully flavoured regimes, and which is valid in between, is the subject of this chapter.

A simple model that encompasses the salient features of flavoured leptogenesis and which we consider in the present work is specified by the Lagrangian

$$\begin{aligned}\mathcal{L} =& \frac{1}{2}\bar{\psi}_{Ni}(\mathrm{i}\partial\!\!\!/ - M_i)\psi_{Ni} + \bar{\psi}_{\ell a}\mathrm{i}\partial\!\!\!/\psi_{\ell a} + \bar{\psi}_{\mathrm{R}b}\mathrm{i}\partial\!\!\!/\psi_{\mathrm{R}b} + (\partial^\mu\phi^\dagger)(\partial_\mu\phi) \\ & - Y^*_{ia}\bar{\psi}_{\ell a}\tilde{\phi}\psi_{Ni} - Y_{ia}\bar{\psi}_{Ni}\tilde{\phi}^\dagger\psi_{\ell a} - h_{ab}\phi^\dagger\bar{\psi}_{\mathrm{R}a}P_{\mathrm{L}}\psi_{\ell b} - h^*_{ab}\phi\bar{\psi}_{\ell b}P_{\mathrm{R}}\psi_{\mathrm{R}a}\,,\end{aligned} \tag{6.1}$$

where ψ_{Ni} is the four-component Majorana spinor representing the right handed singlet neutrino N_i, $\psi_{\ell a}$ is the spinor for the $\mathrm{SU}(2)_{\mathrm{L}}$ doublet of left handed Standard Model leptons ℓ_a, where a is the flavour index, and $\psi_{\mathrm{R}a}$ are the corresponding charged right handed leptons. The $\mathrm{SU}(2)_{\mathrm{L}}$ doublet of Higgs fields is represented by ϕ, and we define $\tilde{\phi} = (\epsilon\phi)^\dagger$ with ϵ the antisymmetric 2 matrix in the $\mathrm{SU}(2)_{\mathrm{L}}$ indices with $\epsilon_{12} = 1$. For simplicity, we assume $i = 1, 2$. The generalisation to more than two right handed neutrinos N_i is straightforward.

Single-flavour calculations for leptogenesis can be easily generalised to the multi-flavour situation, provided there is a flavour basis in which one can express

the lepton-number densities of the several flavours and at the same time neglect possible correlations between the different flavours. When the lepton Yukawa couplings are fully in equilibrium, the appropriate flavour basis is where these couplings h are diagonal. In contrast, in the unflavoured regime the appropriate basis is determined by the linear combination, in which the lepton asymmetry is produced.

These considerations raise the following questions: First, is there a kinetic equation that is manifestly covariant under the choice of the flavour basis? And second, can such an equation also deal with the intermediate regime where the couplings h are not yet in full equilibrium but are non-negligible at the same time? The latter point is of particular importance since leptogenesis is a process that takes a finite amount of time while temperature is decreasing, such that the flavour-sensitive interactions may be out of equilibrium initially, but equilibrate at later times. Clearly, in order to address this question, one has to promote the set of lepton number distributions within a certain flavour basis to a matrix, that also allows for off-diagonal flavour correlations. In a heuristic approach, by appealing to the Hamiltonian evolution of a density matrix, such a set of equations has been proposed [116], and numerical solutions to these equations have been obtained [123].

On the other hand, it is clear that the Green functions within the CTP formalism allow for the possibility of off-diagonal correlations in a straightforward way. Indeed, once the appropriate Kadanoff-Baym equations for unflavoured leptogenesis are known [3], the multi-flavour generalisation is easily written down. However, the Kadanoff-Baym equations are a coupled set of integro-differential equations that needs to be subjected to some analytic approximations before solving it numerically. Key simplifications are first the gradient expansion, which effectively is an expansion in terms of time derivatives, in deviations of the distribution functions from equilibrium, and in the small coupling constants. Second, one makes use of a separation of time scales between the interactions induced by the small Yukawa couplings Y and h and the faster gauge interactions, that maintain kinetic equilibrium and induce lepton-antilepton pair creation and annihilation processes. This allows to describe the distribution functions by generalised chemical potentials.

The application of these strategies of simplification to the multi-flavour case constitutes the main body of the present work. In Section 6.2, we set up the multi-flavour Kadanoff-Baym equations and show that the flavour-dependent dispersion relations for the leptons, that are induced by the right handed neutrino and Yukawa couplings Y and h, respectively, give rise to commutator terms in the kinetic equations which are also characteristic of flavour oscillations in the presence of tree-level mass terms. In Section 6.3, we make use of the short time scale for kinetic equilibration in order to express the lepton densities in terms of a generalised chemical potential. We show that the gauge interactions in addition to enforcing kinetic equilibrium damp the flavour oscillations and that paramet-

rically, flavoured leptogenesis is in the overdamped regime. The processes that turn out to dominate the decay of the off-diagonal flavour correlations are the flavour-sensitive three-body scatterings through the couplings h.

Let $q_{\ell ab}$ denote the Hermitian matrix of lepton charge densities, including flavour off-diagonal correlations, which is defined more precisely below. The main result of the present work is the kinetic evolution equation

$$\frac{\partial q_{\ell ab}}{\partial \eta} = \sum_c \left[q_{\ell ac}\Xi_{cb} - \Xi_{ac}q_{\ell cb} - W_{ac}q_{\ell cb} - q_{\ell ac}W_{cb}\right] + 2S_{ab} - \Gamma^{\rm fl}_{\ell ab}\,. \tag{6.2}$$

In this equation, η denotes the conformal time, which is related to the physical comoving time through $dt = a(\eta)d\eta$, where $a(\eta)$ is the scale factor of the expanding Universe. The matrices W, S and $\Gamma^{\rm fl}_\ell$ are all Hermitian. Lepton number and CP-violating source terms are represented by S, W encompasses the washout rates for the various lepton flavours, and $\Gamma^{\rm fl}_\ell$ is the matrix of flavour-sensitive damping rates. In case we impose that $q_{\ell ab}$ is evaluated in the basis of mass eigenstates of leptonic quasi-particles, the anti-Hermitian matrix Ξ compensates for possible time-dependent flavour rotations. Numerical solutions to this equation are presented in Section 6.4, and it is shown that it indeed interpolates between the fully flavoured and the unflavoured regimes. We conclude in Section 6.5. Appendix 6.6 contains a discussion of the constraint and mass-shell equations including finite width effects.

6.2 Flavoured Leptons

The usual strategy for deriving kinetic equations is to decompose the Schwinger-Dyson equations on the CTP into equations for the retarded and advanced propagators and the Kadanoff-Baym equations. In the weak coupling limit, one can solve the latter when approximating the particle densities as purely on-shell. This corresponds to taking the particle width to zero.

In this Section, we reiterate these arguments for the left-handed leptons. As an extension of earlier approaches [120, 125, 126], where mass terms are introduced at tree-level, we describe here the dynamics that arises from thermal one-loop corrections to the dispersion relations, which are mediated by flavour-blind gauge interactions as well as flavour-sensitive Yukawa interactions.

6.2.1 Schwinger-Dyson Equations

We employ here the notations and conventions for the CTP formalism and the gradient expansion that are explained in more detail within Ref. [3,109,110]. The Schwinger-Dyson equation for the flavoured left-handed lepton propagator is

$$\mathrm{i}\partial\!\!\!/_u S^{fg}_{\ell ab}(u,v) = f\delta^{fg}\delta_{ab}\delta^4(u-v)P_{\rm R} + \sum_h \int d^4w \Sigma^{fh}_{\ell ac}(u,w)S^{hg}_{\ell cb}(w,v)\,, \tag{6.3}$$

which can be more compactly written as [109, 110]

$$\mathrm{i}\not{\partial} S_\ell^{fg} = f\delta^{fg}\delta P_\mathrm{R} + \sum_h \not{\Sigma}_\ell^{fh} \odot S_\ell^{hg}\,, \tag{6.4}$$

where the symbol $\odot$ denotes a convolution and δ the delta function, $f, g, h = \pm$ are the CTP indices and a, b, c flavour indices. The CTP structure can be decomposed into equations for the retarded and advanced propagators and a Kadanoff-Baym equation,

$$\mathrm{i}\not{\partial} S_\ell^{A,R} = \delta P_\mathrm{R} + \Sigma_\ell^H \odot S_\ell^{A,R} \pm \mathrm{i}\not{\Sigma}_\ell^{\mathcal{A}} \odot S_\ell^{A,R}\,, \tag{6.5a}$$

$$\mathrm{i}\not{\partial} S_\ell^{<,>} = \not{\Sigma}_\ell^H \odot S_\ell^{<,>} + \not{\Sigma}_\ell^{<,>} \odot S_\ell^H + \frac{1}{2}\left(\Sigma_\ell^> \odot S_\ell^< - \Sigma_\ell^< \odot S_\ell^>\right)\,. \tag{6.5b}$$

Here and in what follows, we make use of the definitions

$$G^< = G^{+-}\,, \quad G^> = G^{-+}\,, \quad G^T = G^{++}\,, \quad G^{\bar{T}} = G^{--} \tag{6.6}$$

and the combinations

$$\begin{aligned} G^A &= G^T - G^> = G^< - G^{\bar{T}} \quad \text{(advanced)}\,, \\ G^R &= G^T - G^< = G^> - G^{\bar{T}} \quad \text{(retarded)}\,, \\ G^H &= \frac{1}{2}(G^R + G^A) \quad \text{(Hermitian)}\,, \\ G^{\mathcal{A}} &= \frac{1}{2\mathrm{i}}(G^A - G^R) = \frac{\mathrm{i}}{2}(G^> - G^<) \quad \text{(anti-Hermitian, spectral)}\,, \end{aligned} \tag{6.7}$$

where G may stand for any two-point function on the CTP, in particular the propagators and self-energies.

The Wigner transformation is defined as a Fourier transformation of a two-point function with respect to the relative coordinate, while keeping the average coordinate fixed:

$$G(k,x) = \int d^4 r\, \mathrm{e}^{\mathrm{i}k\cdot r} G(u,v)\,, \quad \text{where } \; r = u - v \;\text{ and }\; x = \frac{u+v}{2}\,. \tag{6.8}$$

It provides a separation between the typical energy scale (which is the temperature T in the present case) and the small macroscopic inverse time-scale, that governs the evolution of state parameters (particle number and charge distributions in the present case). The ratio of these two time scales is then used to define the gradient expansion. In Wigner space, Eqs. (6.5) take the form

$$\mathrm{e}^{-\mathrm{i}\diamond}\left\{\not{k} - \not{\Sigma}_\ell^H \mp \not{\Sigma}_\ell^{\mathcal{A}}\right\}\left\{S_\ell^{A,R}\right\} = P_\mathrm{R}\,, \tag{6.9a}$$

$$\mathrm{e}^{-\mathrm{i}\diamond}\left\{\not{k} - \not{\Sigma}_\ell^H\right\}\left\{S_\ell^{<,>}\right\} - \mathrm{e}^{-\mathrm{i}\diamond}\left\{\not{\Sigma}_\ell^{<,>}\right\}\left\{S_\ell^H\right\} = \frac{1}{2}\mathrm{e}^{-\mathrm{i}\diamond}\left(\left\{\not{\Sigma}_\ell^>\right\}\left\{S_\ell^<\right\} - \left\{\not{\Sigma}_\ell^<\right\}\left\{S_\ell^>\right\}\right)\,, \tag{6.9b}$$

where

$$\diamond\{A(k,x)\}\{B(k,x)\} = \frac{1}{2}\left([\partial^{\mu}_{(x)}A(k,x)]\,\partial_{(k)\mu}B(k,x) - [\partial_{(k)\mu}A(k,x)]\,\partial^{\mu}_{(x)}B(k,x)\right) . \tag{6.10}$$

Eqs. (6.9) correspond to an infinite tower of integro-differential equations. Approximate solutions can be obtained within the scheme of gradient expansion [99]. In the context of leptogenesis, gradients occur due to the deviation of particle number distributions from equilibrium, which is induced by the Hubble expansion of the Universe. At the same time, for a sizeable lepton asymmetry to occur, it is crucial, that during leptogenesis, the rate $|Y_{1a}|^2T$ is not very different from expansion rate H. Similarly, within this chapter we are particularly interested in the parametric region where the τ-lepton Yukawa coupling h_τ relates to H as $h_\tau^2 T \sim H$, since otherwise we are either in the fully flavoured or in the unflavoured regime, which can be described by conventional approaches. In the present context, gradient expansion is therefore understood not only as an expansion in time-derivatives, but also as a perturbative expansion in Y and h.

Performing the expansion of Eqs. (6.9) up to first order in gradients, we obtain

$$\left(\not{k} - \not{\Sigma}^{H}_{\ell} \mp \not{\Sigma}^{\mathcal{A}}_{\ell}\right) S^{A,R}_{\ell} = P_{\rm R}\,, \tag{6.11a}$$

$$\frac{\mathrm{i}}{2}\not{\partial} S^{<,>}_{\ell} + (\not{k} - \not{\Sigma}^{H}_{\ell}) S^{<,>}_{\ell} - \not{\Sigma}^{<,>}_{\ell} S^{H}_{\ell} = \frac{1}{2}\left(\not{\Sigma}^{>}_{\ell} S^{<}_{\ell} - \not{\Sigma}^{<}_{\ell} S^{>}_{\ell}\right) . \tag{6.11b}$$

The derivative term $\frac{\mathrm{i}}{2}\not{\partial} S^{A,R}_{\ell}$ would contribute to Eq. (6.11a) only at second order in gradients, since the retarded and advanced propagators do not depend on the particle distribution functions at tree level. Damping occurs explicitly through the collision term on the right hand side of Eq. (6.11b) (for a detailed discussion, see Ref. [111]). At the same time, damping is contained in the $\not{\Sigma}^{\mathcal{A}}_{\ell}$ term in Eq. (6.11a), as it is well known from linear response theory.

The dilution of particles due to the expansion of the universe is taken into account as explained in the previous chapter. We first observe that after appropriate field redefinitions and the rescaling $M_i \to a(\eta)M_i$, the Lagrangian (6.1) describes the fields in the background of a flat Friedmann-Robertson-Walker Universe in conformal coordinates defined by the metric

$$g_{\mu\nu} = a^2(\eta)\,\mathrm{diag}(1,-1,-1,-1)\,.$$

We then take all explicit momentum variables within the equations for the Wigner transformed quantities as conformal. The relation to a physical momentum is given by $k_{\rm ph} = k/a(\eta)$ and the time coordinate is understood as the conformal time η. Likewise, T denotes a comoving temperature that is related to the physical temperature as $T_{\rm ph} = T/a(\eta)$, and $\beta = 1/T$. The masses of the right-handed neutrinos M_i are the physical masses. When they occur explicitly in the Wigner

transformed equations, they are accompanied by the scale factor $a(\eta)$ to give the conformally rescaled mass $a(\eta)M_i$.

The Hermitian and anti-Hermitian parts of the Kadanoff-Baym equations (6.11b) lead us to the constraint and the kinetic equations

$$2k^0\mathrm{i}\gamma^0 S_\ell^{<,>} - \left\{\mathbf{k}\cdot\boldsymbol{\gamma}\gamma^0 + \not{\Sigma}_\ell^H\gamma^0, \mathrm{i}\gamma^0 S_\ell^{<,>}\right\} - \left\{\mathrm{i}\not{\Sigma}_\ell^{<,>}\gamma^0, \gamma^0 S_\ell^H\right\} = -\frac{1}{2}\left(\mathrm{i}\mathcal{C}_\ell - \mathrm{i}\mathcal{C}_\ell^\dagger\right), \tag{6.12a}$$

$$\mathrm{i}\partial_\eta\mathrm{i}\gamma^0 S_\ell^{<,>} - \left[\mathbf{k}\cdot\boldsymbol{\gamma}\gamma^0 + \not{\Sigma}_\ell^H\gamma^0, \mathrm{i}\gamma^0 S_\ell^{<,>}\right] - \left[\mathrm{i}\not{\Sigma}_\ell^{<,>}\gamma^0, \gamma^0 S_\ell^H\right] = -\frac{1}{2}\left(\mathrm{i}\mathcal{C}_\ell + \mathrm{i}\mathcal{C}_\ell^\dagger\right), \tag{6.12b}$$

with the collision term

$$\mathcal{C}_\ell = \mathrm{i}\not{\Sigma}_\ell^{>}\mathrm{i}S_\ell^{<} - \mathrm{i}\not{\Sigma}_\ell^{<}\mathrm{i}S_\ell^{>}\,. \tag{6.13}$$

6.2.2 Thermal Self Energies

We now specify the form of the Hermitian self energy $\not{\Sigma}_\ell^H$, which determines the thermal corrections to the dispersion relation. For the purpose of this discussion, we assume that the deviation of the right handed neutrino distribution from thermal equilibrium is small, so that the self energy, being proportional to coupling constants, can be evaluated with thermal propagators to first order in the gradient expansion. The self energy receives contributions from the interactions specified in Eq. (6.1), but also from $\mathrm{SU(2)_L}\times\mathrm{U(1)}_Y$ gauge interactions. We parametrise this as

$$\not{\Sigma}_\ell^H = P_\mathrm{R}\left[\gamma^0(\bar{\varsigma}^\mathrm{bl} + \bar{\varsigma}^\mathrm{fl}) + \frac{\mathbf{k}\cdot\boldsymbol{\gamma}}{|\mathbf{k}|}\left(\varsigma^\mathrm{bl} + \varsigma^\mathrm{fl} - \mathrm{sign}(k^0)\,[\bar{\varsigma}^\mathrm{bl} + \bar{\varsigma}^\mathrm{fl}]\right)\right]P_\mathrm{L}\,, \tag{6.14}$$

where we have decomposed the contributions to the self energy into a flavour blind part that originates from $\mathrm{SU(2)_L}\times\mathrm{U(1)}_Y$ gauge interactions

$$\bar{\varsigma}^\mathrm{bl}_{ab}(k^0,\mathbf{k}) = \delta_{ab}\bar{\varsigma}^\mathrm{bl}(k^0,\mathbf{k})\,, \qquad \varsigma^\mathrm{bl}_{ab}(k^0,\mathbf{k}) = \delta_{ab}\varsigma^\mathrm{bl}(k^0,\mathbf{k})\,, \tag{6.15}$$

and a flavour dependent part that receives contributions from the charged lepton and the singlet neutrino Yukawa couplings. To one loop order, these can be parametrised as

$$\bar{\varsigma}^\mathrm{fl}_{ab}(k^0,\mathbf{k}) = h^\dagger_{ac}h_{cb}\bar{\varsigma}^{\mathrm{fl},h}(k^0,\mathbf{k}) + \sum_i Y^*_{ia}Y_{ib}\bar{\varsigma}^{\mathrm{fl},Y}_i(k^0,\mathbf{k})\,, \tag{6.16}$$

$$\varsigma^\mathrm{fl}_{ab}(k^0,\mathbf{k}) = h^\dagger_{ac}h_{cb}\varsigma^{\mathrm{fl},h}(k^0,\mathbf{k}) + \sum_i Y^*_{ia}Y_{ib}\varsigma^{\mathrm{fl},Y}_i(k^0,\mathbf{k})\,.$$

In the hierarchical mass limit ($M_1 \ll M_2$), which we assume within this chapter, we may restrict the sum to $i = 1$. Note that $\gamma^0\not{\Sigma}_\ell^H$ is Hermitian, such that ς^fl and $\bar{\varsigma}^\mathrm{fl}$ are Hermitian matrices in flavour space.

The fact that two independent functions $\varsigma(k^0, \mathbf{k})$ and $\bar{\varsigma}(k^0, \mathbf{k})$ occur is because the self energy $\not{\Sigma}^H_\ell$ acquires contributions that are proportional to $\not{k}$ and $\not{u}$, where $u^\mu = (1, 0, 0, 0)^T$ is the plasma vector [133]. The relation between $\varsigma(k^0, \mathbf{k})$, $\bar{\varsigma}(k^0, \mathbf{k})$ and the terms proportional to $\not{k}$ and $\not{u}$ can be easily established. The motivation for our parametrisation is that it corresponds to a decomposition into a correction ς for the dispersion relation and a correction $\bar{\varsigma}$ that leaves the dispersion relation unaltered [see Eqs. (6.26) and (6.105) below]. Besides, ς and $\bar{\varsigma}$ exhibit useful symmetry properties under the exchange $k^0 \to -k^0$ [see Eq. (6.35) below].

The matrix ς^{fl} can be diagonalised through a unitary transformation U and we define

$$\varsigma^{\mathrm{fl}}_{\mathrm{D}} = U^\dagger \varsigma^{\mathrm{fl}} U \,. \tag{6.17}$$

Note that in general, U is momentum- and time-dependent. At temperatures $M_{2,3} \gg T/a(\eta) \gg M_1$ and momenta $|\mathbf{k}| \sim T$, both $\varsigma^{\mathrm{fl},h}$ and $\varsigma^{\mathrm{fl},Y}$ are approximately proportional to $T^2/|\mathbf{k}|$, such that the diagonalisation matrix U is constant in time. When the temperature $T/a(\eta)$ drops below M_1, the distribution of N_1 becomes Maxwell suppressed. The function $\varsigma_i^{\mathrm{fl,Y}}$ then falls toward zero as $\sim [T/(aM_1)]^4$, and U may generically undergo a change. Afterwards, at temperatures $T/a(\eta) \ll M_1$, U becomes constant again and the matrix $U^\dagger h^\dagger h U$ is diagonal.

All quantities that carry left-handed flavour indices transform under the basis transformation defined by U. We denote matrices evaluated in the flavour-diagonal basis by a subscript D. For example,

$$\not{\Sigma}^H_{\ell\mathrm{D}} = U^\dagger \not{\Sigma}^H_\ell U \,, \tag{6.18a}$$

$$\mathrm{i}S^{fg}_{\ell\mathrm{D}} = U^\dagger \mathrm{i}S^{fg}_\ell U \,. \tag{6.18b}$$

Note that unlike $\varsigma^{\mathrm{fl}}_{\mathrm{D}}$, these matrices are in general not diagonal in flavour-space.

Inserting the definitions (6.18a) and (6.18b) into (6.12b) and multiplying with $U^\dagger$ from the left and with U from the right, we obtain the kinetic equation in the lepton thermal mass basis[1]

$$\mathrm{i}\partial_\eta \mathrm{i}\gamma^0 S^{<,>}_{\ell\mathrm{D}} + \mathrm{i}\left[\Xi, \mathrm{i}\gamma^0 S^{<,>}_{\ell\mathrm{D}}\right] - \left[\not{\Sigma}^H_{\ell\mathrm{D}}\gamma^0, \mathrm{i}\gamma^0 S^{<,>}_{\ell\mathrm{D}}\right] = \frac{1}{2}\left(\mathrm{i}\mathcal{C}_{\ell\mathrm{D}} + \mathrm{i}\mathcal{C}^\dagger_{\ell\mathrm{D}}\right) \,, \tag{6.19}$$

where $\mathcal{C}_{\ell\mathrm{D}} = U^\dagger \mathcal{C}_\ell U$ and

$$\Xi = U^\dagger \partial_\eta U \tag{6.20}$$

is the compensation matrix for time-dependent flavour rotations. At first order in gradients, the only consequence of a time dependent U is the additional term involving Ξ. Therefore, we switch to the diagonal basis and drop the subscript D from all subsequent expressions.

[1] The terms $\boldsymbol{\gamma}\gamma^0$ and $\gamma^0 S^{<,>}_\ell$ commute when using the ansatz (6.21) below.

6.2.3 Kinetic and Constraint Equations

The Weyl fermion propagator can be parametrised through the vector and pseudovector functions

$$\mathrm{i}\gamma^0 S_\ell^{<,>} = \frac{1}{2}\sum_{h=\pm}\left[g_{h0}^{<,>}\left(\mathbb{1} + h\hat{\mathbf{k}}\cdot\gamma^5\gamma^0\boldsymbol{\gamma}\right) + g_{h3}^{<,>}\left(\gamma^5 + h\hat{\mathbf{k}}\cdot\gamma^0\boldsymbol{\gamma}\right)\right], \tag{6.21}$$

where $\hat{\mathbf{k}} = \mathbf{k}/|\mathbf{k}|$. When compared to the case of a Dirac fermion, there are no scalar and pseudoscalar contributions. This is because gauge symmetry prevents the dynamical generation of scalar, pseudoscalar and tensor densities, provided the gauge symmetry is neither broken spontaneously nor through initial conditions, as we assume here. Thus, Eq. (6.21) is the most general form of the lepton propagator compatible with isotropy and chiral symmetry. Besides, from the fact that the leptons ℓ are left-handed, we immediately obtain

$$g_{h0}^{<,>} = g_{h3}^{<,>} \equiv g_h^{<,>}\,. \tag{6.22}$$

We furthermore see that $\mathbf{k}\cdot\boldsymbol{\gamma}\gamma^0$ and $\mathrm{i}\gamma^0 S_\ell^{<,>}$ commute, such that the constraint and kinetic Eqs. (6.12) simplify to

$$2(k^0 - \mathbf{k}\cdot\boldsymbol{\gamma}\gamma^0)\mathrm{i}\gamma^0 S_\ell^{<,>} - \left\{\not{\Sigma}_\ell^H\gamma^0, \mathrm{i}\gamma^0 S_\ell^{<,>}\right\} - \left\{\mathrm{i}\not{\Sigma}_\ell^{<,>}\gamma^0, \gamma^0 S_\ell^H\right\} = -\frac{1}{2}\left(\mathrm{i}\mathcal{C}_\ell - \mathrm{i}\mathcal{C}_\ell^\dagger\right), \tag{6.23a}$$

$$\mathrm{i}\partial_\eta\mathrm{i}\gamma^0 S_\ell^{<,>} - \left[\not{\Sigma}_\ell^H\gamma^0, \mathrm{i}\gamma^0 S_\ell^{<,>}\right] - \left[\mathrm{i}\not{\Sigma}_\ell^{<,>}\gamma^0, \gamma^0 S_\ell^H\right] = -\frac{1}{2}\left(\mathrm{i}\mathcal{C}_\ell + \mathrm{i}\mathcal{C}_\ell^\dagger\right). \tag{6.23b}$$

To zeroth order, the constraint equation (6.12a) reduces to the simple form

$$\left\{\not{k}, \mathrm{i}S_\ell^{<,>}\right\} = 0\,. \tag{6.24}$$

Substituting the ansatz (6.21) leads us to

$$g_{h0}^{<,>}k^0 + h|\mathbf{k}|g_{h3}^{<,>} = 0\,, \tag{6.25a}$$

$$g_{h3}^{<,>}k^0 + h|\mathbf{k}|g_{h0}^{<,>} = 0\,. \tag{6.25b}$$

The constraint (6.22) then implies that $g_h^{<,>}(k^0, \mathbf{k})$ is non-vanishing only when $k^0 = -h|\mathbf{k}|$, which corresponds to the singular zero-mass shell. In particular $h = -\mathrm{sign}(k^0)$, that is for leptons ($k^0 > 0$) the helicity $h = -1$ is negative, while for anti-leptons ($k^0 < 0$) the helicity $h = 1$ is positive, as expected. This relation is weakly broken for momenta $|\mathbf{k}| \sim T$ when including thermal corrections, because hole modes exhibit an opposite connection between frequency and helicity. For momenta $|\mathbf{k}| \ll T$, the hole modes couple to the plasma at a similar strength as the particle modes. However, this region only corresponds to a small portion of the available phase space, such that we may neglect it here.

Substituting the parametrisations (6.14), (6.21) and the constraint (6.22) into the kinetic equations (6.23b) and taking the trace leads us to

$$\mathrm{i}\partial_\eta g_h^{<,>} + \mathrm{i}\left[\Xi, g_h^{<,>}\right] + h\left[\varsigma^{\mathrm{fl}}, g_h^{<,>}\right] = -\frac{1}{4}\mathrm{tr}\left(\mathrm{i}\mathcal{C}_\ell + \mathrm{i}\mathcal{C}_\ell^\dagger\right), \tag{6.26}$$

where the trace is taken only in Dirac space, and ς^{fl} and all other objects are evaluated in the mass-diagonal basis. As explained above, the helicity is determined from the zeroth order constraint equation by the relation $h = -\mathrm{sign}(k^0)$. Eq. (6.26) is accurate up to first order in gradients, because ς^{fl} itself is of first order. We note that the term $\left[\mathrm{i}\not{\Sigma}_\ell^{<,>}\gamma^0, \gamma^0 S_\ell^H\right]$ in Eq. (6.23b) does not contribute to Eq. (6.26) at first order, since first, S_ℓ^H can be evaluated at zeroth order, where is it independent of the particle distribution functions and therefore proportional to the unit matrix in flavour space; and second, in Dirac space the commutator reads

$$\left[\mathrm{i}\not{\Sigma}_\ell^{<,>}\gamma^0, \gamma^0 S_\ell^H\right] \propto -\mathrm{i}\left[P_{\mathrm{R}}\,(a^{<,>}\not{k} + b^{<,>}\gamma^0)P_{\mathrm{L}}\gamma^0, \gamma^0 P_{\mathrm{L}}\not{k}P_{\mathrm{R}}\right] = 0\,. \tag{6.27}$$

Since we work in the flavour-diagonal basis, where ς^{fl} is diagonal, the commutator involving ς^{fl} in Eq. (6.26) can be explicitly evaluated, which yields

$$\mathrm{i}\partial_\eta g_{hab}^{<,>} + \mathrm{i}\left[\Xi, g_h^{<,>}\right]_{ab} + h(\varsigma_{aa}^{\mathrm{fl}} - \varsigma_{bb}^{\mathrm{fl}})g_{hab}^{<,>} = -\frac{1}{4}\left(\mathrm{tr}\left[\mathrm{i}\mathcal{C}_\ell + \mathrm{i}\mathcal{C}_\ell^\dagger\right]\right)_{ab}. \tag{6.28}$$

Hence, the thermal dispersion relations have the same impact on the equation of motion for the lepton density as explicit Dirac masses would [120, 125, 126].

An important feature of Eq. (6.26) is the sign change of the commutator term involving the thermal dispersion relation through ς^{fl} when $h \to -h$ or, alternatively, $k^0 \to -k^0$. We now show that at the one-loop level, the elements of $h\varsigma^{\mathrm{fl}} = -\mathrm{sign}(k^0)\,\varsigma^{\mathrm{fl}}(k^0, \mathbf{k})$ are indeed odd functions in k^0. We define charge and parity conjugation through

$$\psi^C(x) = C\bar{\psi}^T(x)\,, \tag{6.29}$$

$$\psi^P(x) = P\psi(\bar{x})\,, \tag{6.30}$$

where $\bar{u} \equiv (u_0, -\mathbf{u})$ and where in the Weyl representation, the conjugation matrices are given by $C = i\gamma^0\gamma^2$ and $P = \gamma^0$. Thereby, we fix possible CP phases that can arise in the definition of these conjugations to zero. The charge and parity conjugate propagators are

$$\mathrm{i}S_{\ell ab}^{C,fg}(u,v) = \langle\psi_{\ell a}^C(u^f)\bar{\psi}_{\ell b}^C(v^g)\rangle = C\left[\mathrm{i}S_{\ell ba}^{gf}(v,u)\right]^T C^\dagger\,, \tag{6.31a}$$

$$\mathrm{i}S_{\ell ab}^{P,fg}(u,v) = \langle\psi_{\ell a}^P(u^f)\bar{\psi}_{\ell b}^P(v^g)\rangle = P\mathrm{i}S_{\ell ab}^{fg}(\bar{u},\bar{v})P^\dagger\,. \tag{6.31b}$$

The transposition acts here only on the Dirac indices, which in contrast to the flavour and CTP indices are not written explicitly. The CP conjugate of the

Hermitian self energy is then given by (we suppress the average coordinate in the argument of ς and $\bar{\varsigma}$)

$$\begin{aligned}\not{\Sigma}^{CP,H}_{\ell ab}(k,x) &= CP\left[\not{\Sigma}^{H}_{\ell ba}(-\bar{k},\bar{x})\right]^{T}(CP)^{\dagger} \\ &= P_{\mathrm{R}}\Big[-\gamma^{0}(\bar{\varsigma}^{\mathrm{bl}}_{ba}(-\bar{k})+\bar{\varsigma}^{\mathrm{fl}}_{ba}(-\bar{k}))+\hat{\mathbf{k}}\cdot\boldsymbol{\gamma}(\varsigma^{\mathrm{bl}}_{ba}(-\bar{k})+\varsigma^{\mathrm{fl}}_{ba}(-\bar{k}) \\ &\qquad +\mathrm{sign}(k^{0})[\bar{\varsigma}^{\mathrm{bl}}_{ba}(-\bar{k})+\bar{\varsigma}^{\mathrm{fl}}_{ba}(-\bar{k})])\Big]P_{\mathrm{L}}\,.\end{aligned} \tag{6.32}$$

On the other hand, we may calculate this self energy from the CP-conjugate Lagrangian, within which the coupling constants are complex conjugated, as

$$\not{\Sigma}^{CP,H}_{\ell ab}(k,x) = \not{\Sigma}^{H}_{\ell ab}(k,x)\Big|_{\substack{Y\to Y^{*}\\ h\to h^{*}}}\,, \tag{6.33}$$

provided the initial conditions preserve CP symmetry (no primordial asymmetry). To the one-loop order, the coupling constants appear as the prefactors $h^{\dagger}h$ and $Y^{\dagger}Y$ within $\not{\Sigma}^{H}_{\ell}$, *cf.* Eq. (6.16). The effect of CP conjugation therefore amounts to the replacements $[h^{\dagger}h]_{ab}\to[h^{\dagger}h]^{*}_{ab}=[h^{\dagger}h]_{ba}$ and $[Y^{\dagger}Y]_{ab}\to[Y^{\dagger}Y]^{*}_{ab}=[Y^{\dagger}Y]_{ba}$, and it follows that to one-loop order

$$\not{\Sigma}^{CP,H}_{\ell ab}(k,x) = \not{\Sigma}^{H}_{\ell ba}(k,x)\,. \tag{6.34}$$

Comparing this to the relation (6.32) and substituting Eq. (6.14), we find that

$$\bar{\varsigma}^{\mathrm{fl}}_{ab}(-k^{0},\mathbf{k}) = -\bar{\varsigma}^{\mathrm{fl}}_{ab}(k^{0},\mathbf{k}) \qquad \text{and} \qquad \varsigma^{\mathrm{fl}}_{ab}(-k^{0},\mathbf{k}) = \varsigma^{\mathrm{fl}}_{ab}(k^{0},\mathbf{k})\,, \tag{6.35}$$

and accordingly for $\bar{\varsigma}^{\mathrm{bl}}$ and ς^{bl}, which implies the result to be shown for the elements of ς^{fl}. These symmetry properties with respect to k^{0} are in accordance with the equilibrium results from Ref. [133]. The present argument shows moreover that they also hold under out-of-equilibrium conditions.

For calculating the momentum integrals in the collision terms, we use on-shell conditions that we obtain from the constraint equations. In order to achieve accuracy to first order in gradients, it again suffices to solve the constraint equations to zeroth order, since the collision term is suppressed by higher orders in the coupling constants. A similar approximation is applied in Ref. [120], where in contrast to the present work, within the constraint equations, small tree-level mass differences rather than differences between one-loop dispersion relations and finite widths are neglected. A general solution to the zeroth-order constraint equation (6.24) is given by the Kadanoff-Baym ansatz

$$\mathrm{i}S^{<}_{\ell ab} = -2S^{\mathcal{A}}_{\ell}\left[\vartheta(k^{0})f^{+}_{\ell ab}(\mathbf{k})-\vartheta(-k^{0})(\mathbb{1}_{ab}-f^{-}_{\ell ab}(-\mathbf{k}))\right]\,, \tag{6.36a}$$

$$\mathrm{i}S^{>}_{\ell ab} = -2S^{\mathcal{A}}_{\ell}\left[-\vartheta(k^{0})(\mathbb{1}_{ab}-f^{+}_{\ell ab}(\mathbf{k}))+\vartheta(-k^{0})f^{-}_{\ell ab}(-\mathbf{k})\right]\,. \tag{6.36b}$$

where

$$S^{\mathcal{A}}_{\ell} = \pi P_{\mathrm{L}}\not{k}P_{\mathrm{R}}\delta\big(k^{2}\big)\,, \tag{6.37}$$

and $f^{\pm}_{\ell ab}$ are the distribution function matrices of leptons and anti-leptons. Comparing Eqs. (6.36) to Eq. (6.21) we identify

$$\begin{aligned} g^{<}_{-} &= -2\pi\delta(k^2)\vartheta(k^0)|\mathbf{k}|f^{+}_{\ell}(\mathbf{k})\,, \\ g^{>}_{-} &= 2\pi\delta(k^2)\vartheta(k^0)|\mathbf{k}|(\mathbb{1}-f^{+}_{\ell}(\mathbf{k}))\,, \\ g^{<}_{+} &= -2\pi\delta(k^2)\vartheta(-k^0)|\mathbf{k}|(\mathbb{1}-f^{-}_{\ell}(-\mathbf{k}))\,, \\ g^{>}_{+} &= 2\pi\delta(k^2)\vartheta(-k^0)|\mathbf{k}|f^{-}_{\ell}(-\mathbf{k})\,, \end{aligned} \tag{6.38}$$

which is consistent with $h = -\mathrm{sign}(k^0)$ and $k^0 = \pm|\mathbf{k}|$. While for the present work, these zeroth-order solutions to the constraint equations are sufficient, we show in Appendix 6.6 how to extend them to first order in consistency with the equations for the retarded and the advanced propagators (6.11a).

Note that if we identify $f^{\pm}_{\ell ab}$ with expectation values of number density operators then it follows from Eqs. (6.36) and the operator definition of $\mathrm{i}S^{<,>}_{\ell ab}$ that $f^{+}_{\ell ab} \sim \langle a^{\dagger}_b a_a\rangle$ corresponds to the lepton density matrix, while $f^{-}_{\ell ab} \sim \langle b^{\dagger}_a b_b\rangle$ corresponds to the *transpose* of the anti-lepton densities. This may also be seen when relating the CP conjugate to the original propagator as

$$\begin{aligned} \mathrm{i}S^{CP,fg}_{\ell ab}(k,x) &= CP\left[\mathrm{i}S^{gf}_{\ell ba}(-\bar{k},\bar{x})\right]^{T}(CP)^{\dagger} \\ &= -\frac{1}{2}\sum_{h=\pm} g^{gf}_{hba}(-k)\left[(1-\gamma^5)\gamma^0 - (1-\gamma^5)h\hat{\mathbf{k}}\cdot\boldsymbol{\gamma}\right] = -\mathrm{i}S^{gf}_{\ell ba}(-k,x)\,, \end{aligned} \tag{6.39}$$

where we have used the ansatz (6.21) and have assumed spatial homogeneity, $g^{gf}_{h}(k) = g^{gf}_{h}(\bar{k})$. Therefore, a sign flip in k yields the negative of the flavour- and CTP-transposed CP conjugate propagator. The use of $S^{<,>}_{\ell}(k,x)$ with $k^0 < 0$ rather than $S^{CP,<,>}_{\ell}(k,x)$ with $k^0 > 0$ to describe the anti-lepton densities has the advantage that the resulting kinetic equations are flavour covariant. This is because the former propagator has the same flavour transformation properties as $S^{<,>}_{\ell}(k,x)$ with $k^0 > 0$, while the latter transforms in the complex conjugate representation. This property has been described and used before in the context of electroweak baryogenesis [125, 126].

6.3 Kinetic Equations for Lepton Number Densities

In this Section, we perform simplifications of the kinetic equations (6.28), such that they attain a form which can be solved numerically. The key simplification arises from the separation of the time scales of kinetic equilibration and flavour-sensitive interactions. Because the former is much faster, the distribution functions are driven to kinetic equilibrium, such that they can be approximated by the Bose-Einstein or Fermi-Dirac form, parametrised through a matrix of

chemical potentials. An integration over the momentum then allows to express the kinetic equations in terms of charge densities. We shall often use spatial homogeneity to set $f^{\pm}_{\ell ab}(-\mathbf{k}) = f^{\pm}_{\ell ab}(\mathbf{k})$.

6.3.1 Matrices for Lepton Number Densities

The lepton number density matrices are defined as

$$n^{+}_{\ell ab} = \int \frac{d^3k}{(2\pi)^3} f^{+}_{\ell ab}(\mathbf{k}) = -\int \frac{d^3k}{(2\pi)^3} \int_0^{\infty} \frac{dk^0}{2\pi} \mathrm{tr}\left[\mathrm{i}\gamma^0 S^{<}_{\ell ab}\right] , \tag{6.40a}$$

$$n^{-}_{\ell ab} = \int \frac{d^3k}{(2\pi)^3} f^{-}_{\ell ab}(\mathbf{k}) = \int \frac{d^3k}{(2\pi)^3} \int_{-\infty}^{0} \frac{dk^0}{2\pi} \mathrm{tr}\left[\mathrm{i}\gamma^0 S^{>}_{\ell ab}\right] . \tag{6.40b}$$

Due to the presence of the fast gauge interactions, we may assume kinetic equilibrium for the leptons, and denote $\delta n^{\pm}_{\ell ab} = n^{\pm}_{\ell ab} - n^{\pm \mathrm{eq}}_{\ell ab}$ and $\delta f^{\pm}_{\ell ab} = f^{\pm}_{\ell ab} - f^{\pm \mathrm{eq}}_{\ell ab}$. Then, we can introduce a matrix of generalised chemical potentials $\mu^{\pm}_{ab}$ for particles and antiparticles, and write

$$f^{\pm}_{\ell ab}(\mathbf{k}) = \left(\frac{1}{\mathrm{e}^{\beta|\mathbf{k}| - \beta\mu^{\pm}} + 1}\right)_{ab} , \tag{6.41}$$

such that the number density matrices are, to first order in the chemical potentials,

$$\delta n^{\pm}_{\ell ab} = \mu^{\pm}_{ab} \frac{T^2}{12} . \tag{6.42}$$

This allows to relate the lepton number densities to the distribution functions:

$$\delta f^{\pm}_{\ell ab}(\mathbf{k}) = 12 \delta n^{\pm}_{\ell ab} \frac{\beta^3 \mathrm{e}^{\beta|\mathbf{k}|}}{(\mathrm{e}^{\beta|\mathbf{k}|} + 1)^2} . \tag{6.43}$$

We also introduce the deviation of the $<, >$ propagators from equilibrium,

$$\mathrm{i}\delta S_{\ell ab} = -2 S^{\mathcal{A}}_{\ell} \left[\vartheta(k^0) \delta f^{+}_{ab}(\mathbf{k}) + \vartheta(-k^0) \delta f^{-}_{ab}(-\mathbf{k})\right] . \tag{6.44}$$

Besides, we use corresponding approximations and expressions for the right-handed leptons of the Standard Model by replacing $\ell \to \mathrm{R}$.

The ansatz (6.41) is valid provided the interactions that establish kinetic equilibrium, which are the pair creation and annihilation processes and scatterings with gauge bosons, are faster than processes that distinguish between the particle flavours, in particular flavour oscillations and flavour-sensitive damping rates. Provided these assumptions hold, which is verified in Section 6.3.3, the time scales for kinetic equilibration and for flavour effects separate. Since $\mu^{\pm}$ is Hermitian, it is always possible to bring Eq. (6.41) to diagonal form by a flavour rotation.

Due to the separation of time scales, kinetic equilibrium in this diagonal basis is then attained at a rate that is faster than the flavour effects that may change the flavour orientation of μ_{ab}.

Using the ansatz (6.36) and the spectral function (6.37) together with the decomposition (6.21) and the constraint (6.22) gives the relations

$$f_\ell^\pm(\mathbf{k}) = \mp 2 \int\limits_{0,-\infty}^{\infty,0} \frac{dk^0}{2\pi} g_\mp^{<,>}(k^0,\mathbf{k})\,. \tag{6.45}$$

Performing a k^0-integration of Eq. (6.28) and using Eqs. (6.40) then yields

$$\partial_\eta f_{\ell ab}^\pm(\mathbf{k}) = [\Xi, f_\ell^\pm(\mathbf{k})]_{ab} \mp \mathrm{i}(\varsigma_{aa}^{\mathrm{fl}} - \varsigma_{bb}^{\mathrm{fl}}) f_{\ell ab}^\pm(\mathbf{k}) \pm \frac{1}{2}\,\mathrm{tr} \int\limits_{0,-\infty}^{\infty,0} \frac{dk^0}{2\pi} (\mathcal{C}_{\ell ab} + \mathcal{C}_{\ell ab}^\dagger)\,. \tag{6.46}$$

Integrating over three momenta and applying the expansions explained above, we find

$$\partial_\eta \delta n_{\ell ab}^\pm = [\Xi^{\mathrm{eff}}, \delta n_\ell^\pm]_{ab} \mp \mathrm{i}\Delta\omega_{\ell ab}^{\mathrm{eff}} \delta n_{\ell ab}^\pm \pm \frac{1}{2}\,\mathrm{tr} \int\limits_{0,-\infty}^{\infty,0} \frac{dk_0}{2\pi} \int \frac{d^3k}{(2\pi)^3} (\mathcal{C}_{\ell ab} + \mathcal{C}_{\ell ab}^\dagger)\,, \tag{6.47}$$

where we have used that the equilibrium distributions are diagonal in flavour, $n_{\ell ab}^{\pm\mathrm{eq}} = \delta_{ab} n_{\ell aa}^{\pm\mathrm{eq}}$. We have defined here the thermally averaged frequencies of flavour oscillations and the compensation matrix as

$$\Delta\omega_{\ell ab}^{\mathrm{eff}}(\eta) = \int \frac{d^3k}{(2\pi)^3} \frac{12\beta^3 \mathrm{e}^{\beta|\mathbf{k}|}}{(\mathrm{e}^{\beta|\mathbf{k}|}+1)^2} \left(\varsigma_{aa}^{\mathrm{fl}}(|\mathbf{k}|,\mathbf{k},\eta) - \varsigma_{bb}^{\mathrm{fl}}(|\mathbf{k}|,\mathbf{k},\eta)\right), \tag{6.48a}$$

$$\Xi^{\mathrm{eff}}(\eta) = \int \frac{d^3k}{(2\pi)^3} \frac{12\beta^3 \mathrm{e}^{\beta|\mathbf{k}|}}{(\mathrm{e}^{\beta|\mathbf{k}|}+1)^2} \Xi(|\mathbf{k}|,\mathbf{k},\eta)\,, \tag{6.48b}$$

and used that ς^{fl} and Σ are symmetric in their first argument, *cf.* (6.35). The dominant contributions to the phase space integrals originate from regions where $|\mathbf{k}| \sim T$, where $\varsigma_{ab}^{\mathrm{fl}}$ can be approximated by [133]

$$\varsigma_{ab}^{\mathrm{fl}}(k^0,\mathbf{k}) = \frac{h_{ac}^\dagger h_{cb} T^2}{16|\mathbf{k}|} + \sum_i Y_{ia}^* Y_{ib} \varsigma_i^{\mathrm{fl},Y}(k^0,\mathbf{k})\,. \tag{6.49}$$

While the form of $Y^\dagger Y \varsigma_i^{\mathrm{fl},Y}$ is more complicated in general, it is of the same order or smaller than $h^\dagger h\, \varsigma^{\mathrm{fl},h}$ when flavour effects are important. We can therefore estimate

$$\Delta\omega_{\ell ab}^{\mathrm{eff}} = \mathcal{O}\left(h_\tau^2 T\right)\,, \tag{6.50}$$

where h_τ is the τ-lepton Yukawa coupling.

We decompose the collision term[2] as

$$\mathcal{C}_\ell = \mathcal{C}_\ell^Y + \mathcal{C}_\ell^{\rm fl} + \mathcal{C}_\ell^{\rm bl} \,. \tag{6.51}$$

The term $\mathcal{C}_\ell^Y$ describes decays and inverse decays of N_1 and hence the washout and the CP-asymmetric source of the lepton densities. Flavour sensitive interactions mediated by the Standard Model Yukawa couplings are encompassed in $\mathcal{C}_\ell^{\rm fl}$, while flavour-blind interactions mediated by gauge couplings are taken account of within $\mathcal{C}_\ell^{\rm bl}$. In the following, we show that these particular contributions can be cast into the form

$$\begin{aligned}\frac{\partial \delta n^\pm_{\ell ab}}{\partial \eta} &= \Xi^{\rm eff}_{ac}\delta n^\pm_{\ell cb} - \delta n^\pm_{\ell ac}\Xi^{\rm eff}_{cb} \mp {\rm i}\Delta\omega^{\rm eff}_{\ell ab}\delta n^\pm_{\ell ab} \\ &\quad - \sum_c [W_{ac}\delta n^\pm_{\ell cb} + \delta n^{\pm *}_{\ell ca} W^*_{bc}] \pm S_{ab} - \Gamma^{\rm bl}(\delta n^+_{\ell ab} + \delta n^-_{\ell ab}) - \Gamma^{\pm {\rm fl}}_{\ell ab} \,.\end{aligned} \tag{6.52}$$

6.3.2 Source and Washout Term

The washout term for $\delta n^+_{\ell ab}$ is given by

$$\begin{aligned}-\sum_c W_{ac}\delta n^+_{\ell cb} &= \frac{1}{2}\,{\rm tr}\int\frac{d^3k}{(2\pi)^3}\int_0^\infty\frac{dk_0}{2\pi}\,\mathcal{C}^Y_{\ell ab} \\ &= \sum_c\int\frac{d^3k}{(2\pi)^3}\int_0^\infty\frac{dk_0}{2\pi}\,\frac{1}{2}{\rm tr}\,\left[{\rm i}\not{\Sigma}^>_{\ell ac}(k){\rm i}S^<_{\ell cb}(k) - {\rm i}\not{\Sigma}^<_{\ell ac}(k){\rm i}S^>_{\ell cb}(k)\right] \,,\end{aligned} \tag{6.53}$$

evaluated to order Y^2_{ia} (certain higher order terms are accounted for by the source term). Close to equilibrium, we can write

$${\rm i}\not{\Sigma}^>_{\ell ac}(k){\rm i}S^<_{\ell cb}(k) - {\rm i}\not{\Sigma}^<_{\ell ac}(k){\rm i}S^>_{\ell cb}(k) = -{\rm i}\left(\not{\Sigma}^<_{\ell ac}(k) - \not{\Sigma}^>_{\ell ac}(k)\right){\rm i}\delta S_{\ell cb}(k) \,, \tag{6.54}$$

and we note that

$$\begin{aligned}{\rm i}\not{\Sigma}^<_{\ell ac}(k) - {\rm i}\not{\Sigma}^>_{\ell ac}(k) = & \\ &- Y^*_{1a}Y_{1c}\int\frac{d^3k'}{(2\pi)^3 2\sqrt{\mathbf{k'}^2 + (a(\eta)M_1)^2}}\frac{d^3k''}{(2\pi)^3 2|\mathbf{k}''|}\,(2\pi)^4\delta^4(k'-k-k'') \\ &\times {\rm sign}(k_0)P_{\rm R}(\not{k}' + a(\eta)M_1)P_{\rm L}\left(f_{Ni}(\mathbf{k}') + f_\phi(\mathbf{k}'')\right) \,.\end{aligned} \tag{6.55}$$

Substituting Eqs. (6.43) and (6.44), we can identify

$$\begin{aligned}W_{ac} = &\frac{1}{2}\,Y^*_{1a}Y_{1c}\int\frac{d^3k}{(2\pi)^3 2|\mathbf{k}|}\frac{d^3k'}{(2\pi)^3 2\sqrt{\mathbf{k'}^2 + (a(\eta)M_1)^2}}\frac{d^3k''}{(2\pi)^3 2|\mathbf{k}''|}(2\pi)^4\delta^4(k'-k-k'') \\ &\times 2k\cdot k'\left(f_{N1}(\mathbf{k}') + f_\phi(\mathbf{k}'')\right)\frac{12\beta^3\,{\rm e}^{\beta|\mathbf{k}|}}{({\rm e}^{\beta|\mathbf{k}|}+1)^2} \,.\end{aligned} \tag{6.56}$$

[2]The definition of the collision terms $\mathcal{C}$ in the previous chapter differs from the present ones by an additional integration $\int dk^0/(2\pi)$.

The washout term for $\delta n^-_{\ell ab}$ follows correspondingly.

In straightforward generalisation of the single flavour case, the CP-violating source term for $\delta n^+_{\ell ab}$ is

$$S_{ab} = \frac{3}{2}\,\mathrm{i}\sum_c \left[Y^*_{1a}Y^*_{1c}Y_{2c}Y_{2b} - Y^*_{2a}Y^*_{2c}Y_{1c}Y_{1b}\right] \times \left(-\frac{M_1}{M_2}\right)\int \frac{d^3k'}{(2\pi)^3 2\sqrt{\mathbf{k}'^2 + (a(\eta)M_1)^2}}\frac{\Sigma_{N\mu}(\mathbf{k}')\Sigma^\mu_N(\mathbf{k}')}{g_w}\delta f_{N1}(\mathbf{k}')\,, \tag{6.57}$$

where (see previous chapter)

$$\Sigma^\mu_N(k) = g_w\int \frac{d^3p}{(2\pi)^3 2|\mathbf{p}|}\frac{d^3q}{(2\pi)^3 2|\mathbf{q}|}(2\pi)^4\delta^4(k-p-q)\,p^\mu\left(1 - f^{\mathrm{eq}}_\ell(\mathbf{p}) + f^{\mathrm{eq}}_\phi(\mathbf{q})\right)\,, \tag{6.58}$$

with $g_w = 2$, and where the source for the anti-leptons $\delta n^-_{\ell ab}$ is $-S_{ab}$. The deviation of the distribution function of the right-handed neutrinos from equilibrium is denoted by $\delta f_{N1}(\mathbf{k}) = f_{N1}(\mathbf{k}) - f^{\mathrm{eq}}_{N1}(\mathbf{k})$. This source term is understood to include both, wave-function and vertex contributions in the hierarchical limit, $M_1 \ll M_2$. Note that there is an additional wave-function contribution that violates lepton flavour but conserves total lepton number [114, 117]. Within flavoured models of leptogenesis, this may contribute to the final lepton asymmetry. Compared to the total lepton-number violating contributions, it is however suppressed by a factor M_1/M_2 since one picks up the $\not{k} \sim M_1$ rather than the M_2 term from the numerator of the intermediate neutrino propagator in the wave-function diagram. Hence, we do not account for this term here.

6.3.3 Flavour Blind Interactions

The flavour-blind contribution to the lepton self-energy that is mediated by gauge interactions can be expressed as

$$\mathrm{i}\not{\Sigma}^{\mathrm{bl}\,fg}_{\ell ab} = g^2\int\frac{d^4k'}{(2\pi)^4}\frac{d^4k''}{(2\pi)^4}(2\pi)^4\delta^4(k-k'-k'')\gamma^\nu\mathrm{i}S^{fg}_{\ell ab}(k')\gamma^\mu\mathrm{i}\Delta^{fg}_{A\mu\nu}(k'')\,, \tag{6.59}$$

where $\mathrm{i}\Delta^{fg}_{A\mu\nu}$ is the gauge boson propagator on the CTP. The corresponding collision term is then

$$\begin{aligned}\mathcal{C}^{\mathrm{bl}}_{\ell ab}(k) &= \mathrm{i}\not{\Sigma}^{\mathrm{bl}>}_{\ell ac}(k)\mathrm{i}S^<_{\ell cb}(k) - \mathrm{i}\not{\Sigma}^{\mathrm{bl}<}_{\ell ac}(k)\mathrm{i}S^>_{\ell cb}(k) \\ &= g^2\int\frac{d^4k'}{(2\pi)^4}\frac{d^4k''}{(2\pi)^4}(2\pi)^4\delta^4(k-k'-k'')\Big[\gamma^\nu\mathrm{i}S^>_{\ell ac}(k')\gamma^\mu\mathrm{i}\Delta^>_{A\mu\nu}(k'')\mathrm{i}S^<_{\ell cb}(k) \\ &\quad - \gamma^\nu\mathrm{i}S^<_{\ell ac}(k')\gamma^\mu\mathrm{i}\Delta^<_{A\mu\nu}(k'')\mathrm{i}S^>_{\ell cb}(k)\Big]\,.\end{aligned} \tag{6.60}$$

To check the consistency of the generalised chemical potential ansatz (6.41), we now verify that the collision term (6.60) vanishes provided the leptons and anti-leptons have opposite chemical potentials, $\mu^-_{ab} = -\mu^+_{ab}$. To see this, we first note that $\mu^-_{ab} = -\mu^+_{ab} \equiv -\mu_{ab}$ implies the generalised KMS relation $S^>_{\ell ab}(k) = -\left(e^{\beta k_0 - \beta\mu}\right)_{ac} S^<_{\ell cb}(k)$. Using this and the fact that the gauge bosons are in thermal equilibrium, which implies $\Delta^>_{A\mu\nu}(k) = e^{\beta k_0}\Delta^<_{A\mu\nu}(k)$, in Eq. (6.59) yields the analogous relation $\not{\Sigma}^{\rm bl>}_{\ell ab} = -\left(e^{\beta k_0 - \beta\mu}\right)_{ac} \not{\Sigma}^{\rm bl<}_{\ell cb}$ for the lepton self energy. This allows us to write

$$\mathcal{C}^{\rm bl}_\ell(k) = \left[\mathrm{i}\not{\Sigma}^{\rm bl<}_\ell(k), e^{\beta k_0 - \beta\mu}\right] \mathrm{i}S^<_\ell(k) \tag{6.61}$$

Inserting Eq. (6.59) leaves the commutator $\left[\mathrm{i}S^{\rm bl<}_\ell(k), e^{\beta k_0 - \beta\mu}\right]$ in flavour space, which is easily seen to vanish upon use of the ansatz (6.36) together with Eq. (6.41) and $\mu^-_{ab} = -\mu^+_{ab}$. The vanishing of the collision term under the conditions $\mu^-_{ab} = -\mu^+_{ab}$ means that the kinetic equilibrium distribution (6.41) with opposite chemical potentials is indeed a stationary solution of the kinetic equation in the limit when only the fast flavour-blind gauge interactions are present.

Furthermore, when the gauge bosons are in equilibrium and the equilibrium deviation of the leptons is small and parametrised as in Eq. (6.43), we can approximate the collision term (6.60) as

$$\begin{aligned}
\mathcal{C}^{\rm bl}_{\ell ab}(k) \;\approx\; & g^2 \int \frac{d^4k'}{(2\pi)^4}\frac{d^4k''}{(2\pi)^4}(2\pi)^4\delta^4(k-k'-k'') \\
& \times \Big\{\gamma^\nu \mathrm{i}\delta S_{\ell ab}(k')\gamma^\mu \left[\mathrm{i}\Delta^>_{A\mu\nu}(k'')\mathrm{i}S^<_{\ell bb}(k) - \mathrm{i}\Delta^<_{A\mu\nu}(k'')\mathrm{i}S^>_{\ell bb}(k)\right] \\
& \quad + \left[\gamma^\nu \mathrm{i}S^>_{\ell aa}(k')\gamma^\mu \mathrm{i}\Delta^>_{A\mu\nu}(k'') - \gamma^\nu \mathrm{i}S^<_{\ell aa}(k')\gamma^\mu \mathrm{i}\Delta^<_{A\mu\nu}(k'')\right] \mathrm{i}\delta S_{\ell ab}(k)\Big\}\,.
\end{aligned} \tag{6.62}$$

For this expression, we note that the terms in square brackets are odd under a change of sign of the momenta, since to leading order in deviations from equilibrium, we may substitute the equilibrium distributions and make use of the fact that $\mathrm{i}\Delta^{\rm eq>}_{A\mu\nu}(k) = \mathrm{i}\Delta^{\rm eq<}_{A\mu\nu}(-k)$ and $\mathrm{i}S^{\rm eq>}_{\ell aa}(k) = \mathrm{i}S^{\rm eq<}_{\ell aa}(-k)$. Hence, after performing the k^0 integration of the collision term, the same sign contributions to the equations (6.47) and (6.52) for δn^+_ℓ and δn^-_ℓ occur due to a cancellation of the relative sign in Eq. (6.47).

However, if we substituted tree-level propagators in Eq. (6.62), this collision term would vanish, since all the three particles involved are massless. It is therefore necessary to account for thermal masses and for finite width effects, that relax the zero-temperature on-shell conditions. When employing finite width propagators, analytical simplifications of the collision integral due to on-shell δ-functions no longer apply. In the present work, we therefore do not perform collision integrals that vanish for zero-temperature propagators explicitly. Rather, we discuss their general form and give estimates, while relegating more precise numerical evaluations to future studies.

Of particular interest within the collision term (6.62) are contributions for which $\mathrm{sign}(k'^0) = -\mathrm{sign}(k'^0) = \mathrm{sign}(k^0)$. These are allowed when we account for the finite width in the spectral functions (for both, ℓ and the gauge fields A) and they correspond to lepton anti-lepton pair creation and annihilation processes. After performing the integrations and the Dirac trace, lepton- and antilepton contributions are identical. Therefore, we may parametrise the flavour blind contribution to the collision term in Eq. (6.47) by

$$\pm\frac{1}{2}\,\mathrm{tr}\int\limits_{0,-\infty}^{\infty,0}\frac{dk_0}{2\pi}\int\frac{d^3k}{(2\pi)^3}(\mathcal{C}^{\mathrm{bl}}_{\ell ab}+\mathcal{C}^{\mathrm{bl}\,\dagger}_{\ell ab}) = -\Gamma^{\mathrm{bl}}\left(\delta n^{+}_{\ell ab}+\delta n^{-}_{\ell ab}\right), \tag{6.63}$$

which leads to the corresponding term in Eq. (6.52). Here $\delta n^{\pm}_{\ell ab}$ has been factored out by substituting Eqs. (6.43) and (6.44). Note that by use of Eqs. (6.43) and (6.44) this defines Γ^{bl}, which therefore may readily be evaluated within a more detailed numerical study. For the purposes of the present work, we estimate $\Gamma^{\mathrm{bl}} \sim g_2^4 T$, where g_2 is the $\mathrm{SU(2)_L}$ gauge coupling and where the additional factor of g_2^2 compared to the tree-level matrix element arises from the finite-width effects [111].

The fact that the flavour-blind collision terms for δn^{+}_{ℓ} and δn^{-}_{ℓ} are of the same sign also implies that in the absence of additional flavour-sensitive effects, $\delta n^{+}_{\ell} - \delta n^{-}_{\ell}$ is conserved, as it is required for the ansatz of generalised chemical potentials (6.41) to be valid.

6.3.4 Flavour Sensitive Interactions

We now turn to the active lepton Yukawa couplings. These contribute to the self-energy of the left-handed leptons as

$$\mathrm{i}\not{\Sigma}^{\mathrm{fl}\,fg}_{\ell ab}(k) = h^{\dagger}_{ac}h_{db}\int\frac{d^4k'}{(2\pi)^4}\frac{d^4k''}{(2\pi)^4}(2\pi)^4\delta^4(k-k'-k'')\,\mathrm{i}S^{fg}_{\mathrm{R}cd}(k')\mathrm{i}\Delta^{fg}_{\phi}(k'')\,. \tag{6.64}$$

To linear order in deviations from equilibrium, the collision term is

$$\begin{aligned}
\mathcal{C}^{\mathrm{fl}}_{\ell ab}(k) &= \mathrm{i}\not{\Sigma}^{\mathrm{fl}>}_{\ell ac}(k)\mathrm{i}S^{<}_{\ell cb}(k) - \mathrm{i}\not{\Sigma}^{\mathrm{fl}<}_{\ell ac}(k)\mathrm{i}S^{>}_{\ell cb}(k) \approx \int\frac{d^4k'}{(2\pi)^4}\frac{d^4k''}{(2\pi)^4}(2\pi)^4\delta^4(k-k'-k'')\\
&\quad\times\Big\{h^{\dagger}_{ac}h_{de}\mathrm{i}\delta S_{\mathrm{R}cd}(k')\left[\mathrm{i}\Delta^{>}_{\phi}(k'')\mathrm{i}S^{<}_{\ell eb}(k) - \mathrm{i}\Delta^{<}_{\phi}(k'')\mathrm{i}S^{>}_{\ell eb}(k)\right]\\
&\qquad + h^{\dagger}_{ac}h_{de}\left[\mathrm{i}S^{>}_{\mathrm{R}cd}(k')\mathrm{i}\Delta^{>}_{\phi}(k'') - \mathrm{i}S^{<}_{\mathrm{R}cd}(k')\mathrm{i}\Delta^{<}_{\phi}(k'')\right]\mathrm{i}\delta S_{\ell eb}(k)\Big\}\\
&= \int\frac{d^4k'}{(2\pi)^4}\frac{d^4k''}{(2\pi)^4}(2\pi)^4\delta^4(k-k'-k'')\\
&\quad\times\Big\{h^{\dagger}_{ac}h_{db}\mathrm{i}\delta S_{\mathrm{R}cd}(k')\left[\mathrm{i}\Delta^{>}_{\phi}(k'')\mathrm{i}S^{\mathrm{eq}<}_{\ell}(k) - \mathrm{i}\Delta^{<}_{\phi}(k'')\mathrm{i}S^{\mathrm{eq}>}_{\ell}(k)\right]\\
&\qquad + h^{\dagger}_{ac}h_{ce}\left[\mathrm{i}S^{\mathrm{eq}>}_{\mathrm{R}}(k')\mathrm{i}\Delta^{>}_{\phi}(k'') - \mathrm{i}S^{\mathrm{eq}<}_{\mathrm{R}}(k')\mathrm{i}\Delta^{<}_{\phi}(k'')\right]\mathrm{i}\delta S_{\ell eb}(k)\Big\}\,.
\end{aligned} \tag{6.65}$$

Again, the leading thermal corrections to the propagators should be employed, since at tree-level, this integral is vanishing for kinematic reasons. We have to distinguish two relevant kinematic situations: First, when $\mathrm{sign}(k^0) = -\mathrm{sign}(k'^0)$, the collision term corresponds to pair creation or annihilation of a left- and a right-handed Standard Model lepton. Second, when $\mathrm{sign}(k^0) = \mathrm{sign}(k'^0)$ the left- and right-handed leptons scatter from a Higgs boson. Again, both configurations are only possible due to the finite width of the spectral functions of ℓ, R and ϕ. We summarise both contributions to Eq. (6.47) by writing

$$\begin{aligned}\Gamma^{\pm\mathrm{fl}}_{\ell ab} = &\pm \frac{1}{2}\mathrm{tr}\int\limits_{0,-\infty}^{\infty,0}\frac{dk^0}{2\pi}\int\frac{d^3k}{(2\pi)^3}\left(\mathcal{C}^{\mathrm{fl}}_{\ell ab}(k) + \mathcal{C}^{\mathrm{fl}\dagger}_{\ell ab}(k)\right) \\ =&\Gamma^{\mathrm{an}}\left([h^\dagger h]_{ac}\delta n^{\pm}_{\ell cb} + \delta n^{\pm\dagger}_{\ell ac}[h^\dagger h]_{cb} + h^\dagger_{ac}\delta n^{\mp}_{\mathrm{R}cd}h_{db} + h^\dagger_{ad}\delta n^{\mp\dagger}_{\mathrm{R}dc}h_{cb}\right) \\ &+\Gamma^{\mathrm{sc}}\left([h^\dagger h]_{ac}\delta n^{\pm}_{\ell cb} + \delta n^{\pm\dagger}_{\ell ac}[h^\dagger h]_{cb} - h^\dagger_{ac}\delta n^{\pm}_{\mathrm{R}cd}h_{db} - h^\dagger_{ad}\delta n^{\pm\dagger}_{\mathrm{R}dc}h_{cb}\right) .\end{aligned} \tag{6.66}$$

For later use we note that for the right handed leptons, we have the corresponding flavour sensitive scattering rate

$$\begin{aligned}\Gamma^{\pm\mathrm{fl}}_{\mathrm{R}ab} =&\Gamma^{\mathrm{an}}\left([hh^\dagger]_{ac}\delta n^{\pm}_{\mathrm{R}cb} + \delta n^{\pm\dagger}_{\mathrm{R}ac}[hh^\dagger]_{cb} + h_{ac}\delta n^{\mp}_{\ell cd}h^\dagger_{db} + h_{ad}\delta n^{\mp\dagger}_{\ell dc}h^\dagger_{cb}\right) \\ &+\Gamma^{\mathrm{sc}}\left([hh^\dagger]_{ac}\delta n^{\pm}_{\mathrm{R}cb} + \delta n^{\pm\dagger}_{\mathrm{R}ac}[hh^\dagger]_{cb} - h_{ac}\delta n^{\pm}_{\ell cd}h^\dagger_{db} - h_{ad}\delta n^{\pm\dagger}_{\ell dc}h^\dagger_{cb}\right) .\end{aligned} \tag{6.67}$$

We estimate the factors Γ^{an} and Γ^{sc} as $\sim g_2^2 T$, which is again due to the finite width of ℓ and ϕ at finite temperature. (The $\mathrm{U}(1)_Y$ contribution is smaller because of the smaller gauge coupling and the smaller number of gauge bosons). We recall that within these expressions, $\delta n^{\pm}_{\ell}$ and the second index of the coupling h transform under left-handed flavour rotations, while $\delta n^{\pm}_{\mathrm{R}}$ and the first index of h remain without change. By a unitary transformation of the right-handed flavour basis, we may choose the matrix $hh^\dagger$ to be diagonal, which is what we assume here.

This concludes the derivation of the kinetic equation (6.52) for the number densities. An analogous equation (without washout and source terms) holds for the right-handed Standard Model leptons.

6.3.5 Suppression of Flavour Oscillations

The largest collision term within the kinetic equations (6.52) is $\Gamma^{\mathrm{bl}} = O(g_2^4 T)$. Close to equilibrium, it imposes the constraint

$$\delta n^{+}_{ab} = -\delta n^{-}_{ab} . \tag{6.68}$$

This is expected, since in the flavour-blind limit where $h_{ab} \to 0$, this condition is manifestly invariant with respect to flavour rotations and it reduces to the

assumption that the lepton charge density of leptons is the same as the lepton charge density of anti-leptons. Therefore, this condition is implicitly employed in the previous chapter as well as in many other kinetic-theory approaches to various problems. Now, due to the $\pm$ in the first term on the right hand side of the kinetic equations (6.52), a large $\Gamma^{\rm bl}$ effectively inhibits flavour oscillations, which would be present in the absence of collisions. To see this in more detail, consider the toy system of differential equations

$$\frac{d}{dt}\delta g^+(t) = -\mathrm{i}\Delta\omega\delta g^+(t) - \Gamma[\delta g^+(t) + \delta g^-(t)]\,, \tag{6.69a}$$

$$\frac{d}{dt}\delta g^-(t) = +\mathrm{i}\Delta\omega\delta g^-(t) - \Gamma[\delta g^-(t) + \delta g^+(t)]\,. \tag{6.69b}$$

The relevant parameters for flavoured leptogenesis can be estimated as

$$\Gamma = \Gamma^{\rm bl} \sim g_2^4 T\,, \quad \Delta\omega \sim h_\tau^2 T \ll \Gamma\,, \tag{6.70}$$

where h_τ denotes the τ-lepton Yukawa coupling. Since $g_2^4 \gg h_\tau^2$, the solutions are linear combinations of two eigenmodes with short $\tau_{\rm s} = 1/(\Gamma + \sqrt{\Gamma^2 - \Delta\omega^2}) \approx 1/(2\Gamma)$ and long $\tau_{\rm l} = 1/(\Gamma - \sqrt{\Gamma^2 - \Delta\omega^2}) \approx 2\Gamma/\Delta\omega^2$ decay times, respectively. The corresponding eigenvectors are given by

$$\delta g_{\rm s,l} = \delta g^+ + \frac{-\mathrm{i}\Delta\omega \pm \sqrt{\Gamma^2 - \Delta\omega^2}}{\Gamma}\delta g^- \approx \delta g^+ \pm \left(1 \mp \mathrm{i}\frac{\Delta\omega}{\Gamma}\right)\delta g^-\,, \tag{6.71}$$

with

$$\delta g_{\rm s,l} = (\delta g_{\rm s,l})_0\, \mathrm{e}^{-t/\tau_{\rm s,l}}\,. \tag{6.72}$$

The short mode $\delta g_{\rm s} \approx \delta g^+ + \delta g^-$ is thus damped to zero very rapidly by pair annihilations, implying an effective constraint

$$\delta g^+ \sim -\left(1 - \mathrm{i}\frac{\Delta\omega}{\Gamma}\right)\delta g^-\,. \tag{6.73}$$

Note that the different sign of $\Delta\omega$ terms in Eq. (6.69) is decisive, since it implies that the driving term for oscillations in

$$\frac{d}{dt}\left(\delta g^+(t) - \delta g^-(t)\right) = -\mathrm{i}\Delta\omega\left(\delta g^+(t) + \delta g^-(t)\right) \tag{6.74}$$

is damped away, while in the case of same sign $\delta g^+ - \delta g^-$, could have freely oscillated. As explained in Section 6.2.3 the opposite sign of the $\Delta\omega$ term in Eq. (6.52) is a consequence of CP invariance at leading order.

Within the gradient expansion, the first order correction to Eq. (6.68) therefore is of order $\Delta\omega^{\rm eff}/\Gamma^{\rm bl}$. Since the source terms for the off-diagonal correlations

are already of first order in gradients, it is justified to use the zeroth order constraint Eq. (6.68) within our approximations. The long-lived mode describes the damping of flavour coherence in the lepton charge density matrix due to flavour-blind interactions. It is much slower compared to the damping rate due to flavour sensitive interactions, $\Delta\omega^{\mathrm{eff}\,2}/\Gamma^{\mathrm{bl}} \sim h_\tau^4 g_2^{-4} T \ll \Gamma^{\mathrm{fl}} \sim g_2^2 h_\tau^2 T$ since $h_\tau \ll g_2^3$. Therefore, we may neglect the damping due to flavour-blind interactions, while we keep the direct damping due to flavour sensitive processes. While in the case of leptogenesis, we conclude that because of $\Delta\omega \ll \Gamma$, flavour oscillations are overdamped and effectively frozen, we note that for $\Delta\omega > \Gamma$, there are damped flavour oscillations. It is interesting to note that even though we assume flavour blind interactions, the off-diagonal flavour coherence functions are decaying. Such a behaviour, in particular in the oscillatory regime, has been observed numerically in Ref. [120].

We emphasise that the conclusion that the oscillations induced by $\Delta\omega$ are overdamped for $\Gamma \gg \Delta\omega$ does not depend on the choice of the flavour basis. To see this, we extend $g^\pm$ to a vector of functions and consider the system of matrix equations

$$\frac{d}{dt}\delta g^+(t) = -\mathrm{i}[\omega, \delta g^+(t)] - \Gamma[\delta g^+(t) + \delta g^-(t)]\,, \tag{6.75a}$$

$$\frac{d}{dt}\delta g^-(t) = +\mathrm{i}[\omega, \delta g^-(t)] - \Gamma[\delta g^-(t) + \delta g^+(t)]\,. \tag{6.75b}$$

Here, Γ is proportional to the unit matrix and $\omega = \omega^{\mathrm{fl}} + \omega^{\mathrm{bl}}$, where ω^{bl} is proportional to the unit matrix and $\omega^{\mathrm{fl}}_{ab} \ll \Gamma_{cc}$ for all a, b, c. It then follows that $[\omega, \delta g^\pm(t)] = [\omega^{\mathrm{fl}}, \delta g^\pm(t)]$. By taking the sum of Eqs. (6.75), we again conclude that $\delta g^+(t) + \delta g^-(t) \sim \mathrm{e}^{-2\Gamma t}$. Consequently, the difference of Eqs. (6.75) yields

$$\frac{d}{dt}\left[\delta g^+(t) - \delta g^-(t)\right] = 0 + \left[\delta g^+(t) - \delta g^-(t)\right] \times \mathcal{O}\left(\frac{\omega_{ab}^2}{\Gamma_{cc}}\right)\,, \tag{6.76}$$

where the right hand side is estimated as the eigenvalues of a matrix with large diagonal and small off-diagonal elements. Alternatively, this can be seen by substituting in the right hand side of the difference of Eqs. (6.75)

$$\left[\omega, \delta g^+(t) + \delta g^-(t)\right] = \left(\delta g^+(t) - \delta g^-(t)\right) \times \mathcal{O}\left(\omega^2/\Gamma\right)\,, \tag{6.77}$$

where an estimate according to Eq. (6.73) is made. This confirms the suppression of the effect of ς^{fl} by Γ^{bl} in a general flavour-basis.

We can also generalise this discussion to the case of a time-dependent mass basis. In order to model this situation, consider the system

$$\frac{d}{dt}\delta g^+_{ab}(t) = -\mathrm{i}\Delta\omega_{ab}\delta g^+_{ab}(t) + \Xi_{ac}\delta g^+_{cb} - \delta g^+_{ac}\Xi_{cb} - \Gamma[\delta g^+_{ab}(t) + \delta g^-_{ab}(t)]\,, \tag{6.78a}$$

$$\frac{d}{dt}\delta g^-_{ab}(t) = +\mathrm{i}\Delta\omega_{ab}\delta g^-_{ab}(t) + \Xi_{ac}\delta g^-_{cb} - \delta g^-_{ac}\Xi_{cb} - \Gamma[\delta g^-_{ab}(t) + \delta g^+_{ab}(t)]\,. \tag{6.78b}$$

In the limit $\Gamma \gg \Delta\omega_{ab}$, we may find an approximate solution by imposing $\delta g^+ = -\delta g^-$. This leads to

$$\frac{d}{dt}\left(\delta g^+_{ab}(t) - \delta g^-_{ab}(t)\right) = \left[\delta g^+_{ab}(t) - \delta g^-_{ab}(t), \Xi\right] , \tag{6.79}$$

which is solved by the unitary evolution

$$\delta g^+_{ab}(t) - \delta g^-_{ab}(t) = \left(T\mathrm{e}^{-\Xi t}\right)\left(\delta g^+_{ab}(t=0) - \delta g^-_{ab}(t=0)\right)\left(\bar{T}\mathrm{e}^{\Xi t}\right) , \tag{6.80}$$

where T implies the time-ordered exponential. Therefore, the freezing of flavour oscillations also persists when we account for the time dependence of the mass basis. From above equation, we recover Eq. (6.76) by undoing the flavour rotation, that is by left multiplication by U and right multiplication by $U^\dagger$.

6.3.6 Kinetic Equations for Left and Right Handed Number Densities

We now define the charge number density matrix as

$$q_{\ell ab} = \delta n^+_{\ell ab} - \delta n^-_{\ell ab} . \tag{6.81}$$

Imposing that fast (compared to the interactions accounted for in W_{ab} and S_{ab}) pair creating and annihilating interactions enforce the constraint

$$\delta n^+_{\ell ab} = -\delta n^-_{\ell ab} , \tag{6.82}$$

we can take the linear combinations from Eq. (6.52) that solve for the charge density matrix (6.81). For the flavour-sensitive interactions, define

$$\begin{aligned}\Gamma^{\mathrm{fl}}_{\ell ab} =& \Gamma^{\mathrm{an}}\left([h^\dagger h]_{ac} q_{\ell cb} + q^\dagger_{\ell ac}[h^\dagger h]_{cb} - h^\dagger_{ac} q_{\mathrm{R}cd} h_{db} - h^\dagger_{ad} q^\dagger_{\mathrm{R}dc} h_{cb}\right) \\ &+ \Gamma^{\mathrm{sc}}\left([h^\dagger h]_{ac} q_{\ell cb} + q^\dagger_{\ell ac}[h^\dagger h]_{cb} - h^\dagger_{ac} q_{\mathrm{R}cd} h_{db} - h^\dagger_{ad} q^\dagger_{\mathrm{R}dc} h_{cb}\right) .\end{aligned} \tag{6.83}$$

Using this and the results of the previous sections, we obtain the kinetic equations (6.2) which we repeat here for completeness:

$$\frac{\partial q_{\ell ab}}{\partial \eta} = \sum_c \left[q_{\ell ac}\Xi_{cb} - \Xi_{ac} q_{\ell cb} - W_{ac} q_{\ell cb} - q_{\ell ac} W_{cb}\right] + 2S_{ab} - \Gamma^{\mathrm{fl}}_{\ell ab} . \tag{6.84}$$

Note that similar to the toy system of equations the flavour-blind term drops out in the equation for $q_{\ell ab}$, while it is consistent to neglect the $\Delta\omega^{\mathrm{eff}}_{ab}$ term, which would multiply $\delta n^+_{\ell ab} + \delta n^-_{\ell ab}$ in this equation, which is strongly damped. This holds in an arbitrary, time-independent basis in flavour space, where the Ξ terms are absent. In a time-dependent basis such as the basis where ς_{ab} is diagonal, the Ξ terms are introduced to account for the time-dependent basis rotation.

For the right-handed leptons, there is the analogous equation

$$\frac{\partial q_{\mathrm{R}ab}}{\partial \eta} = -\Gamma^{\mathrm{fl}}_{\mathrm{R}ab} \tag{6.85}$$

with

$$\begin{aligned}\Gamma^{\mathrm{fl}}_{\mathrm{R}ab} =& \Gamma^{\mathrm{an}} \left([hh^\dagger]_{ac} q_{\mathrm{R}cb} + q^\dagger_{\mathrm{R}ac} [hh^\dagger]_{cb} - h_{ac} q_{\ell cd} h^\dagger_{db} - h_{ad} q^\dagger_{\ell dc} h^\dagger_{cb} \right) \\ &+ \Gamma^{\mathrm{sc}} \left([hh^\dagger]_{ac} q_{\mathrm{R}cb} + q^\dagger_{\mathrm{R}ac} [hh^\dagger]_{cb} - h_{ac} q_{\ell cd} h^\dagger_{db} - h_{ad} q^\dagger_{\ell dc} h^\dagger_{cb} \right) .\end{aligned} \tag{6.86}$$

Similar results have been obtained earlier within an approach that makes use of the density matrix in an occupation number basis. In its details, the equation for the difference between lepton and anti-lepton densities in Ref. [116] exhibits however differences to our kinetic equation (6.84). It is not clear whether the lepton charge densities in Ref. [116] should correspond to our $q_{\ell ab}$ (which is the difference of the lepton density and the transpose of the anti-lepton density) or to the difference of the lepton density and the anti-lepton density. In the former case, the flavour oscillations frequencies in Ref. [116] should have opposite signs for particle and transposed antiparticle modes, if they were to agree with our result obtained within the CTP formalism. This is apparently not the situation within the equation for the lepton charge density in Ref. [116]. In the latter case, as it follows from Eq. (6.39) and the discussion at the end of Section 6.2.3, within the CTP formalism the washout and source matrices for the lepton and anti-lepton densities are transposed (or complex conjugated, as these matrices are Hermitian) with respect to each other, which is apparently not the case in Ref. [116]. Furthermore, the same conclusions on damping of coherence would result from our equations if the charge density matrix were defined as $\delta n^+_{\ell ab} - \delta n^-_{\ell ba}$. Hence, with either interpretation, there is a difference between the occupation number formalism result that is derived in Ref. [116] and the kinetic equation (6.2) derived within the CTP formalism. The phenomenological consequence of this can be seen when comparing the present work with Ref. [123], where the kinetic equations from Ref. [116] are solved numerically. While in the present work, we conclude that flavour oscillations effectively freeze out due to fast pair creation and annihilation processes, the results in Refs. [116, 123] imply that the flavour oscillations are important and in particular faster than the flavour-sensitive damping processes.

6.4 Solutions to the Flavoured Kinetic Equations

We are considering a scenario with two lepton flavours and assume that there is one dominant Standard Model Yukawa coupling h_τ. In the basis where the

lepton Yukawa coupling matrix is diagonal, the matrix h is therefore simply

$$h = \begin{pmatrix} h_\tau & 0 \\ 0 & 0 \end{pmatrix} . \tag{6.87}$$

Provided the μ and e Yukawa-couplings are negligible $h^2_{\mu,e} T/a(\eta) \ll H$, the realistic case with three lepton flavours can be reduced to the present case by separating out a linear combination of lepton flavours, for which no asymmetry is produced. This corresponds to an unflavoured approximation for the e and μ flavours, *cf.* the discussion of the unflavoured limit below. We note that Eq. (6.2) is manifestly invariant under flavour rotations induced by U, while Eqs. (6.46) and (6.47) are not, because the term that describes flavour oscillations is given in the diagonal basis. In our approximation, we can drop this term, because we have shown in Section 6.3 that due to the constraints from kinetic equilibrium, the time scale for flavour oscillations is suppressed when compared to the time scale of decoherence from flavour-sensitive scatterings. We use this freedom of choice of a lepton flavour basis and perform the discussion in this section within the time-independent basis of charged lepton flavours, which is more transparent than the time-dependent basis of the leptonic quasi-particles, that is determined by the diagonalisation of $\varsigma^{\rm fl}$. Likewise, we present all numerical results in the basis of charged lepton flavours.[3]

In the charged lepton basis, the flavour-sensitive collision terms read

$$\Gamma^{\rm fl}_\ell = (\Gamma^{\rm an} + \Gamma^{\rm sc})\, h_\tau^2 \left[\begin{pmatrix} 1 & 0 \\ 0 & 0 \end{pmatrix} q_\ell + q_\ell \begin{pmatrix} 1 & 0 \\ 0 & 0 \end{pmatrix} - 2 \begin{pmatrix} q_{\rm R11} & 0 \\ 0 & 0 \end{pmatrix} \right] , \tag{6.88a}$$

$$\Gamma^{\rm fl}_{\rm R} = (\Gamma^{\rm an} + \Gamma^{\rm sc})\, h_\tau^2 \left[\begin{pmatrix} 1 & 0 \\ 0 & 0 \end{pmatrix} q_{\rm R} + q_{\rm R} \begin{pmatrix} 1 & 0 \\ 0 & 0 \end{pmatrix} - 2 \begin{pmatrix} q_{\ell 11} & 0 \\ 0 & 0 \end{pmatrix} \right] . \tag{6.88b}$$

In the fully flavoured limit, which we define by the requirement $(\Gamma^{\rm an} + \Gamma^{\rm fl}) h_\tau^2 \gg H$ (note that for the present purposes, "fully flavoured" refers to the situation where h_μ and h_e are still assumed to be out-of-equilibrium), we see that within this setup, the flavour sensitive collision terms enforce

$$q_{\ell 11} - q_{\rm R11} = 0 , \qquad q_{\ell 12} = q_{\ell 21} = q_{\rm R12} = q_{\rm R21} = 0 . \tag{6.89}$$

This agrees with the expectation that when Standard Model Yukawa couplings are in equilibrium, the lepton asymmetries are projected onto the charged lepton basis.

The processes $\ell + \bar{\rm R} \leftrightarrow \phi^*$ (annihilation) and $\ell + \phi \leftrightarrow {\rm R}$ (scattering) are kinematically forbidden when all the three particles involved are massless. At finite temperature, this holds no longer true due to effects that at leading order can be either thought of as thermal masses and finite widths or as radiation of

[3] Yet, we have used the requirement that computations in both bases must yield the same results as a consistency check on the numerical results.

gauge bosons. The latter point of view is taken in Ref. [127] to calculate $\Gamma^{\rm sc}$. However, important t-channel diagrams are not included there and a calculation of $\Gamma^{\rm an}$ is not provided. A systematic calculation of these rates may be performed along the lines of Ref. [124], which is however beyond the scope of the current work. Motivated by the partial result of Ref. [127], we take here for numerical definiteness the estimate

$$\Gamma^{\rm an} + \Gamma^{\rm sc} \approx 0.7\alpha_{\rm W} T/a(\eta) = 1.75 \times 10^{-2}\, T/a(\eta)\,, \tag{6.90}$$

which should be accurate up to a factor of order unity. Besides, we take here $\alpha_{\rm W} = 1/40$ as the weak coupling constant at the scale of about $10^{12}\,\mathrm{GeV}$. The precise value depends on the particular extension of the Standard Model.

To obtain numerical solutions, we first solve the kinetic equations for the distribution of the right-handed neutrinos N_1. They are given in the previous chapter, and the generalisation from the single flavour to the two-flavour case follows by the straightforward replacement $|Y_1|^2 \to \sum_a |Y_{1a}|^2$. We employ this distribution to calculate the washout and the source terms within Eq. (6.2). To be specific, we choose thermal initial conditions for N_1. For the singlet neutrino masses, we choose $M_1 = 10^{12}\,\mathrm{GeV}$ and $M_2 = 10^{14}\,\mathrm{GeV}$. For the Yukawa couplings of the right handed neutrinos, we consider two scenarios

$$Y = \begin{pmatrix} 1.4 \times 10^{-2} & 1 \times 10^{-2} \\ \mathrm{i} \times 10^{-1} & 10^{-1} \end{pmatrix}, \qquad \text{Scenario (A)}\,, \tag{6.91}$$

$$Y = \begin{pmatrix} 1.4 \times 10^{-2} & 3 \times 10^{-3} \\ \mathrm{i} \times 10^{-1} & 10^{-1} \end{pmatrix}, \qquad \text{Scenario (B)}\,.$$

We vary the Yukawa coupling h_τ, since this will directly exhibit the dependence of the results on the flavour effects, while of course, for a phenomenological study, it would be more pertinent to vary the unknown parameters Y and $M_{1,2}$.

In Figure 6.1 we show the interaction rates $\Gamma^{\rm fl} = h_\tau^2(\Gamma^{\rm an} + \Gamma^{\rm sc})$ for different values of h_τ and compare them to the expansion rate of the universe H and to the inverse decay rate for the individual flavours a, $\Gamma^a_{\rm ID} = 2W_{aa}$ as a function of the ratio of M_1 to the physical temperature, $z = a(\eta)M_1/T$. Scenario (A) exhibits moderate to strong washout in both flavours, where the dominant contributions to the lepton asymmetry are generated between $z \approx 3$ and the point when the lepton asymmetry freezes out, $\Gamma_{ID} \approx H$. We expect flavour effects to be negligible when $\Gamma^{\rm fl} \lesssim H \approx \Gamma^a_{\rm ID}$ during these times before freeze out [128], i.e. for h_τ significantly smaller than 4×10^{-3} by inspection of Figure 6.1. On the other hand a fully flavoured description should be applicable when $\Gamma^{\rm fl} \gtrsim \Gamma^a_{\rm ID}$ during the times when the quantitatively relevant contributions to the lepton asymmetry are produced, i.e. for h_τ significantly larger than 7×10^{-3}. The numerical solutions to the kinetic equations for Scenario (A) are displayed in Figure 6.2. Shown are the absolute values of the entropy normalised asymmetries

$$Y_{\ell ab} = 2g_w \frac{q_{\ell ab}}{\frac{2\pi^2}{45} g_\star T^3}\,, \tag{6.92}$$

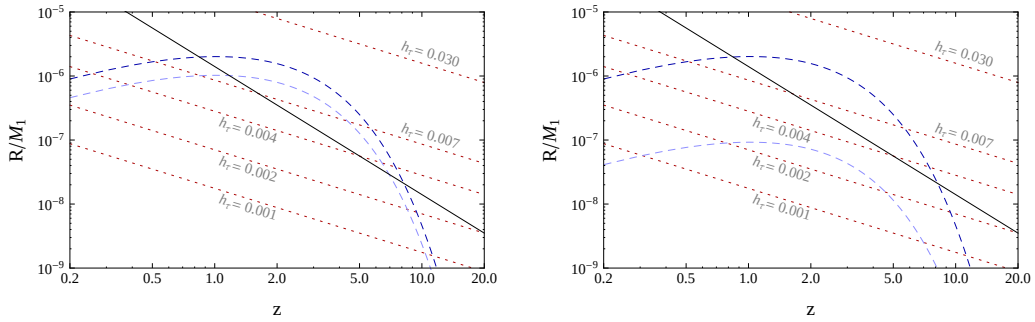

Figure 6.1: Comparison of the relevant rates $R = \Gamma^a_{\rm ID}$, H, $h_\tau^2(\Gamma^{\rm an} + \Gamma^{\rm sc})$ for Scenarios (A) and (B). The colour key is H (solid, black), $\Gamma^1_{\rm ID}$ (dashed, dark blue), $\Gamma^2_{\rm ID}$ (dashed, light blue), $h_\tau^2(\Gamma^{\rm an}+\Gamma^{\rm sc})$ with $h_\tau = 3\times10^{-2},\ 7\times10^{-3},\ 4\times10^{-3},\ 2\times10^{-3},\ 10^{-3}$ (from top right to bottom left, dotted, red).

where we use $g_\star = 106.75$. Since Y_ℓ is Hermitian, we plot the real and imaginary parts of $Y_{\ell 12}$. The results confirm our expectations about the validity of the fully flavoured and the unflavoured descriptions of leptogenesis. For $h_\tau \lesssim 2\times10^{-3}$ the total lepton asymmetry $\mathrm{tr}[Y_\ell] = Y_{\ell 11} + Y_{\ell 22}$ is almost independent of h_τ, and the off diagonal densities decay away after freeze out ($z \approx 10$) only. (Only the initial stages of this decay are visible in the plots for $h_\tau = 2\times10^{-3}$, 10^{-2} in Figure 6.2 due to the cut off at $z = 20$. For $h_\tau = 0$, the off-diagonal densities do not decay.) On the other hand in the fully flavoured regime, for $h_\tau \gtrsim 3\times10^{-2}$, the off diagonal densities are strongly suppressed before freeze-out. This confirms that neglecting the off-diagonal densities, an approximation that is commonly used in the fully flavoured regime, is indeed justified in this regime. In the intermediate regime, where neither of these approximations is valid, the correct lepton asymmetry is obtained by solving the full kinetic equation (6.2).

Scenario (B) is a situation with strong washout due to Y_{11} and weak washout for Y_{12}. The numerical solutions are displayed in Figure 6.3. Since $\Gamma^2_{\rm ID}$ is now significantly smaller, it takes also smaller values of h_τ before the unflavoured description may be expected to be valid, *cf.* Figure 6.1. In the fully flavoured regime, we observe that one of the lepton flavours suffers from strong washout while the other one is only weakly washed out. On the other hand, in the basis where the source term is diagonal, the flavours apparently mix in such a way that both lepton flavours are strongly washed out when flavour effects are turned off. This importance of flavour effects for washout is well known [115–117], and it can be easily understood when we recall how the fully flavoured and the unflavoured regimes are described.

First, in the fully flavoured case, densities that are off-diagonal in the flavour basis undergo fast damping through flavour-sensitive interactions. As a result,

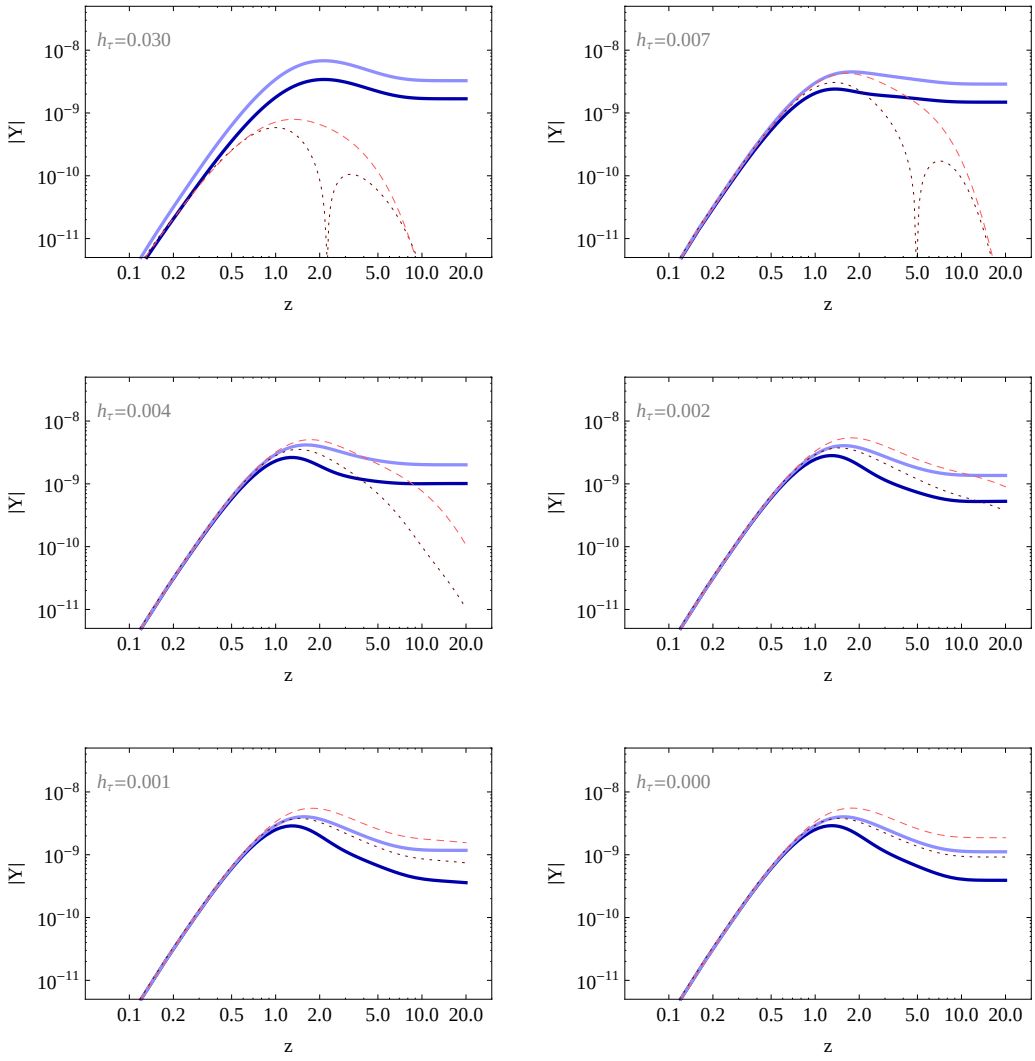

Figure 6.2: Results for Scenario (A) with $h_\tau = 3 \times 10^{-2},\ 7 \times 10^{-3},\ 4 \times 10^{-3},\ 2 \times 10^{-3}\ , 10^{-3},\ 0$, from top left to bottom right. The key is $Y_{\ell 11}$ (dark blue, solid), $Y_{\ell 22}$ (light blue, solid), Re$[Y_{\ell 12}]$ (dark red, dotted), Im$[Y_{\ell 12}]$ (light red, dashed). The densities are evaluated in the flavour eigenbasis, which means that the larger the flavour effects are (the larger h_τ is), the smaller are the off-diagonal densities.

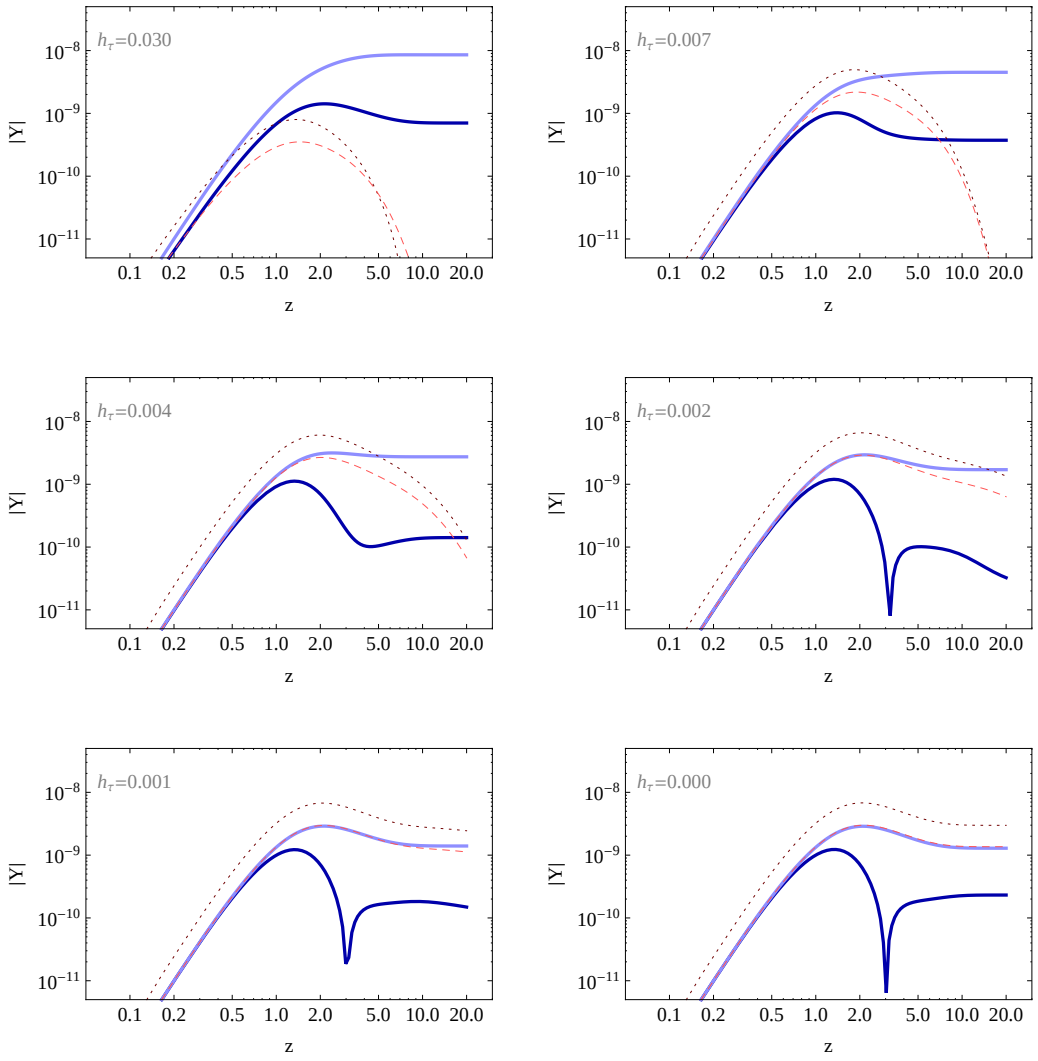

Figure 6.3: Results for Scenario (B) with $h_\tau = 3 \times 10^{-2},\ 7 \times 10^{-3},\ 4 \times 10^{-3},\ 2 \times 10^{-3}\ , 10^{-3},\ 0$ from top left to bottom right. The key is $Y_{\ell 11}$ (dark blue, solid), $Y_{\ell 22}$ (light blue, solid), Re$[Y_{\ell 12}]$ (dark red, dotted), Im$[Y_{\ell 12}]$ (light red, dashed).

there are two washout rates that are proportional to $|Y_{11}^2|$ and $|Y_{12}^2|$, respectively. Second, in the unflavoured regime, it is convenient to bring Y to a triangular form through

$$Y_{ia}^{\Delta} = Y_{ib} V_{ba} \,, \tag{6.93}$$

where

$$V = \frac{1}{\sqrt{|Y_{21}|^2 + |Y_{22}|^2}} \begin{pmatrix} Y_{22} & Y_{21}^* \\ -Y_{21} & Y_{22}^* \end{pmatrix} . \tag{6.94}$$

In the triangular basis, a lepton asymmetry is only produced for the linear combination

$$\frac{1}{\sqrt{|Y_{21}|^2 + |Y_{22}|^2}} \left(Y_{21} \ell_1 + Y_{22} \ell_2 \right) . \tag{6.95}$$

The washout rate for this linear combination is proportional to

$$|Y_{12}^{\Delta}|^2 = \frac{1}{|Y_{21}|^2 + |Y_{22}|^2} \left(|Y_{11}|^2 |Y_{21}|^2 + |Y_{12}|^2 |Y_{22}|^2 + 2\mathrm{Re}\left[Y_{11} Y_{21}^* Y_{12}^* Y_{22} \right] \right) . \tag{6.96}$$

The change of the effective flavour basis in the transition from the unflavoured to the flavoured regime therefore explains the apparent change in the washout rates for the individual flavours for Scenario (B), that are visible in Figure 6.3.

To obtain an estimate of the extent of the intermediate regime in terms of the parameter M_1, we now fix the τ-Yukawa coupling to $h_\tau = 0.007$, close to its physical value, and vary $M_1 \to \alpha M_1$ instead. To keep the effect of the washout term and the source term constant, we also scale $Y_{11} \to \sqrt{\alpha}\, Y_{11}$ and $Y_{12} \to \sqrt{\alpha}\, Y_{12}$ as well as $M_2 \to \alpha M_2$. This scaling behaviour can be seen when recasting Eq. (6.2) into the form

$$zH \frac{\partial q_{\ell ab}}{\partial z} = \frac{1}{a} \left\{ \sum_c \left[q_{\ell ac} \Xi_{cb} - \Xi_{ac} q_{\ell cb} - W_{ac} q_{\ell cb} - q_{ac} W_{cb} \right] + 2 S_{ab} - \Gamma_{\ell ab}^{\mathrm{fl}} \right\} . \tag{6.97}$$

The terms on the right hand side now correspond to the physical instead of conformal interaction rates per unit volume. Since at fixed z, $T/a(\eta) \to \alpha T/a(\eta)$, $H \to \alpha^2 H$ and $q_\ell \to \alpha^3 q_\ell$, both sides scale as α^5, except for the term $1/a \times \Gamma_\ell^{\mathrm{fl}}$, which scales as α^4. Therefore, all the scale-dependence is isolated within the flavour-dependent damping rate.

We solve the kinetic equations for $10^{10}\,\mathrm{GeV} < M_1 < 2 \times 10^{14}\,\mathrm{GeV}$. Parametrically this brings us from a regime where flavour effects are maximal to the unflavoured regime [128]. For comparison we also calculate the lepton asymmetry over this parameter range using first the unflavoured approximation ($h_\tau = 0$)

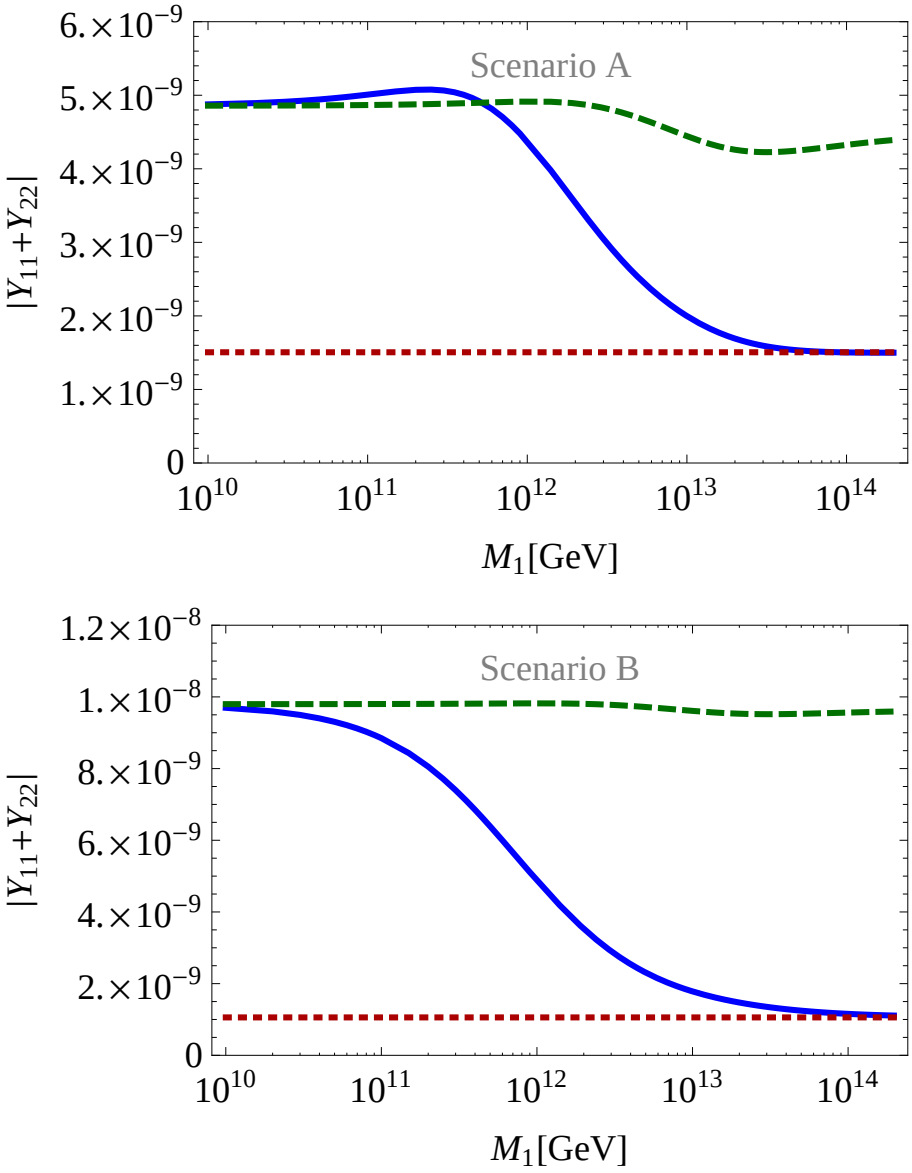

Figure 6.4: Shown is the total lepton asymmetry $\mathrm{tr}[Y_\ell] = Y_{\ell 11} + Y_{\ell 22}$ as a function of the righthanded neutrino mass M_1, for parameters corresponding to Scenarios (A) and (B). The result of the full kinetic equations including flavour effects (solid blue line) is compared to the results of the unflavoured approximation $h_\tau = 0$ (red, dotted) and to the results from a fully flavoured approximation that neglects off-diagonal flavour excitations (green, dashed).

and then using the fully flavoured approximation, where the off-diagonal number densities are set to zero throughout the calculation.

The results are shown in Figure 6.4. We find that both the fully flavoured approximation and the unflavoured approach lead to accurate predictions of the total lepton asymmetry within their expected ranges of validity. The intermediate regime where the full kinetic equation needs to be solved ranges from around $5 \times 10^{11}\,\mathrm{GeV} - 10^{13}\,\mathrm{GeV}$ for Scenario (A) and even further for Scenario (B) where the unflavoured behaviour is only recovered for $M_1 \gtrsim 10^{14}\,\mathrm{GeV}$. This is because the condition for the unflavoured description to be valid, $\Gamma^a_{\mathrm{ID}} \gtrsim h_\tau^2(\Gamma^{\mathrm{an}} + \Gamma^{\mathrm{sc}})$ for $a = 1, 2$ is only fulfilled for larger values of M_1 within Scenario (B). Besides, within the flavoured approximation of Scenario (B), the flavour $a = 2$ is only weakly washed out. Therefore, quantitatively relevant contributions to the lepton asymmetry arise at earlier times, where $\Gamma^a_{\mathrm{ID}}/[h_\tau^2(\Gamma^{\mathrm{an}} + \Gamma^{\mathrm{sc}})]$ is enhanced compared to this ratio close to freeze-out. As a consequence, the fully flavoured description of Scenario (B) requires smaller values for M_1 when compared to Scenario (A). Note that the absolute limits for the validity of the unflavoured or fully flavoured description may vary by up to order one factors due to the uncertainty in the overall prefactor of Γ^{fl}. We identify this also as a probable source of the numerical difference between the present work and Ref. [128], where it was found using $\Gamma^{\mathrm{an}} + \Gamma^{\mathrm{sc}} \approx 5 \times 10^{-3}\, T/a(\eta)$ that the unflavoured description is valid already for $M_1 \geq 5 \times 10^{11}$ GeV.

6.5 Conclusions

Using the CTP formalism, we have derived and solved kinetic equations that describe flavoured leptogenesis. Our results allow for systematic calculations of the lepton asymmetry within the intermediate regime, that is neither fully flavoured nor unflavoured, and where off-diagonal correlations between the lepton densities are of importance. The CTP framework proves particularly suitable for this problem, since off-diagonal densities are straightforwardly implemented within the two-point Green functions.

So far, kinetic equations that describe flavoured leptogenesis within the intermediate regime have only been available as extrapolations from a toy model description of number density matrices in the occupation number formalism [116]. The importance of a more systematic derivation of these equations has been emphasised for example in Ref. [128]. Our main result, Eq. (6.2), that is derived within the CTP framework with the Lagrangian (6.1) as the starting point, turns out to resemble the corresponding equation of Ref. [116] in many details of its flavour structure, but it also exhibits qualitative differences. The main improvements provided with the present work may be summarised as follows:

- We derive the impact of the thermal dispersion relations on the kinetic equations for the left-handed leptons. This confirms the expectation that

the effects of these dispersion relations share some qualitative features with flavour oscillations induced by tree-level mass terms and allows for quantitative predictions. Our results might also be useful for describing the dynamics of neutrino flavours in interacting backgrounds.

- We find that fast pair creation and annihilation processes through gauge interactions effectively overdamp flavour oscillations. This is a qualitatively distinct feature from the results of Refs. [116, 123].

- The washout, source and damping terms in the kinetic equations are derived from first principles. They correspond to collision terms which we explicitly present in the form of integrals. Some of these integrals crucially depend on finite width effects, which make their evaluation difficult. For the purpose of our numerical examples, we make only estimates for those collision terms that strongly depend on finite-width effects. Yet, these collision terms are well-defined, and their quantitatively accurate evaluation may be the subject of future work, possibly using the methods of Ref. [124].

For a more accurate prediction of the lepton asymmetry, the present analysis has to be supplemented by a number of improvements, which vary in how detailed they have been discussed in the literature yet and in how straightforwardly the present work can be generalised to include them.

First, there are the so-called spectator processes [129, 130], which are transitions induced by Yukawa couplings and by strong and weak sphalerons and which transfer charges between the ℓ_a and ϕ to other particles of the Standard Model. Note that also the scatterings induced by h, that transfer charges to the charged right-handed leptons belong to this category. Depending on whether the additional interactions are fully equilibrated, out-of equilibrium or in an intermediate regime, the kinetic equations have either to be supplemented by algebraic constraints for the various charges, or the network of equations has to be extended in a way that is similar to how we account for the charged right-handed leptons.

Conceptually more interesting and challenging is the systematic inclusion of thermal effects. In the present work, we have noted that the finite width and thermal mass effects allow for certain three-body processes that are kinematically forbidden in the vacuum. Again, the CTP formalism bears the potential to account for thermal effects more systematically and may hence serve to confirm or to extend earlier results on these effects [106]. Therefore, important improvements remain to be incorporated in order to calculate the lepton asymmetry of the Universe to a good accuracy and with a quantifyable account of the theoretical uncertainty. In order to achieve this goal, the systematic computation of the flavour effects from first principles as presented in this work may serve as a building block.

6.6 Appendix: Pole-Mass Equation and Finite Width Propagators

In this Appendix, we show how close to equilibrium, the constraint equation (6.12a) and the equations for the retarded and advanced propagators (6.11a) can be solved consistently to first order in gradients. The first order corrections account for modified dispersion relations and for finite widths.

In thermal equilibrium, the collision term is vanishing on the right-hand side of the constraint equation (6.12a). Since the collision term is already first order in gradients, we may therefore neglect it within the constraint equations when being close to equilibrium. Furthermore, the propagators and self-energies are approximately flavour-diagonal, such that we can express the constraint equation (6.12a) in the simple form

$$\left\{ \not{k} - \not{\Sigma}^{H}_{\ell}, \mathrm{i}S^{<,>}_{\ell} \right\} - \left\{ \not{\Sigma}^{<,>}_{\ell}, \mathrm{i}S^{H}_{\ell} \right\} = 0 \,. \tag{6.98}$$

The spectral function $S^{\mathcal{A}}_{\ell}$ is defined through Eq. (6.7). In order to solve the pole-mass equation (6.11a), it is useful to introduce

$$\tilde{\not{\Sigma}}_{\ell} = \begin{pmatrix} 0 & \Sigma_{\ell} \cdot \sigma \\ \Sigma_{\ell} \cdot \bar{\sigma} & 0 \end{pmatrix} , \tag{6.99}$$

where $\Sigma^{\mu}_{\ell} = \frac{1}{2}\mathrm{tr}\gamma^{\mu}\not{\Sigma}_{\ell}$. This facilitates the inversion of propagators within the four component formalism in analogy with the doubling of degrees of freedom within the Weyl-fermion propagators that is familiar from the in-out framework [122]. We obtain (*cf.* [111])

$$S^{\mathcal{A}}_{\ell} = P_{\mathrm{L}} \frac{2\left(\not{k} - \tilde{\not{\Sigma}}^{H}_{\ell}\right)\Sigma^{\mathcal{A}}_{\ell} \cdot (k - \Sigma^{H}_{\ell}) - \tilde{\not{\Sigma}}^{\mathcal{A}}_{\ell}\left(\not{k} - \tilde{\not{\Sigma}}^{H}_{\ell}\right)^{2} + \tilde{\not{\Sigma}}^{\mathcal{A}\,3}_{\ell}}{\left[\left(\not{k} - \tilde{\not{\Sigma}}^{H}_{\ell}\right)^{2} - \tilde{\not{\Sigma}}^{\mathcal{A}\,2}_{\ell}\right]^{2} + 4\left[\Sigma^{\mathcal{A}}_{\ell} \cdot (k - \Sigma^{H}_{\ell})\right]^{2}} P_{\mathrm{R}} \,. \tag{6.100}$$

Note again that we have used simplifications due to the flavour-diagonal structure in equilibrium. Similarly, we find the Hermitian propagator

$$S^{H}_{\ell} = P_{\mathrm{L}} \frac{\left(\not{k} - \tilde{\not{\Sigma}}^{H}_{\ell}\right)\left[\left(\not{k} - \tilde{\not{\Sigma}}^{H}_{\ell}\right)^{2} - \tilde{\not{\Sigma}}^{\mathcal{A}\,2}_{\ell}\right] + 2\tilde{\not{\Sigma}}^{\mathcal{A}}_{\ell}\Sigma^{\mathcal{A}}_{\ell} \cdot (k - \Sigma^{H}_{\ell})}{\left[\left(\not{k} - \tilde{\not{\Sigma}}^{H}_{\ell}\right)^{2} - \tilde{\not{\Sigma}}^{\mathcal{A}\,2}_{\ell}\right]^{2} + 4\left[\Sigma^{\mathcal{A}}_{\ell} \cdot (k - \Sigma^{H}_{\ell})\right]^{2}} P_{\mathrm{R}} \,. \tag{6.101}$$

Now, if we use that in equilibrium

$$\vartheta(k^0) f^{\mathrm{eq}+}_{\ell ab}(\mathbf{k}) - \vartheta(-k^0)(\mathbb{1}_{ab} - f^{\mathrm{eq}-}_{\ell ab}(\mathbf{k})) = \delta_{ab} \frac{1}{\mathrm{e}^{\beta k^0} + 1} \tag{6.102}$$

and the KMS relation to substitute

$$\tilde{\not{\Sigma}}_\ell^{\mathcal{A}} = -\frac{\mathrm{i}}{2}(\mathrm{e}^{\beta k^0}+1)\tilde{\not{\Sigma}}_\ell^{<}\,, \tag{6.103}$$

we find that Eq. (6.36a) with $S_\ell^{\mathcal{A}}$ given by Eq. (6.100) indeed solves the constraint equation (6.98) in equilibrium. In a similar way, the same observation holds for Eq. (6.36b). A related discussion can be found in Ref. [109]. Note that relation (6.103) establishes the connection between the finite width and the collision term (6.13), that controls how fast a small perturbation in the lepton density relaxes to its equilibrium value. The zero-width approximation (6.37) follows from the result (6.100) in the limit $\Sigma_\ell^{\mathcal{A}} \cdot (k - \Sigma_\ell^H) \to 0$.

Close to the poles, where $(\not{k} - \tilde{\not{\Sigma}}_{\ell aa}^H)^2 = 0$, the Hermitian propagator S_ℓ^H is suppressed compared to the spectral function $S_\ell^{\mathcal{A}}$ by an additional factor $O(\Sigma^{\mathcal{A}}/k)$. To first order in the gradient expansion and in the narrow width limit, where $\Sigma_\ell^{\mathcal{A}} \cdot (k - \Sigma_\ell^H) \ll {k^0}^2$, we can therefore neglect the terms involving S_ℓ^H in Eqs. (6.12).

Plugging the ansatz (6.21) into the constraint equation (6.98) and neglecting the term $\{\tilde{\not{\Sigma}}_\ell^{<,>}, \mathrm{i}S_\ell^H\}$ leads us to

$$g_{h0}^{<,>}k^0 + h|\mathbf{k}|g_{h3}^{<,>} - \frac{1}{2}\left\{\bar{\varsigma}^{\mathrm{bl}} + \bar{\varsigma}^{\mathrm{fl}}, g_{h0}^{<,>}\right\} - \frac{h}{2}\left\{\mathrm{sign}(k^0)(\bar{\varsigma}^{\mathrm{bl}} + \bar{\varsigma}^{\mathrm{fl}}) - \varsigma^{\mathrm{bl}} - \varsigma^{\mathrm{fl}}, g_{h3}^{<,>}\right\} = 0\,, \tag{6.104a}$$

$$g_{h3}^{<,>}k^0 + h|\mathbf{k}|g_{h0}^{<,>} - \frac{1}{2}\left\{\bar{\varsigma}^{\mathrm{bl}} + \bar{\varsigma}^{\mathrm{fl}}, g_{h3}^{<,>}\right\} - \frac{h}{2}\left\{\mathrm{sign}(k^0)(\bar{\varsigma}^{\mathrm{bl}} + \bar{\varsigma}^{\mathrm{fl}}) - \varsigma^{\mathrm{bl}} - \varsigma^{\mathrm{fl}}, g_{h0}^{<,>}\right\} = 0\,. \tag{6.104b}$$

When neglecting the hole modes, for leptons ($k^0 > 0$) the helicity $h = -1$ is negative, while for anti-leptons ($k^0 < 0$) the helicity $h = 1$ is positive. In conjunction with the constraint (6.22), this implies within the flavour-diagonal basis the dispersion relations

$$k^0 = \pm\left[|\mathbf{k}| + \varsigma^{\mathrm{bl}} + \frac{1}{2}(\varsigma_{aa}^{\mathrm{fl}} + \varsigma_{bb}^{\mathrm{fl}})\right] \tag{6.105}$$

for $g_{hab}^{<,>}$. Note that in the present case, $\varsigma^{\mathrm{bl}} \sim g_2^2$, while $\varsigma_{aa}^{\mathrm{fl}} \sim [h^\dagger h]_{aa}$. Since $g_2^2 \gg [h^\dagger h]_{aa}$, the expressions for the dispersion relations (6.105), that are accurate to order g_2^2, are not reliable to order $[h^\dagger h]_{aa}$ in case $g_2^4 \gtrsim [h^\dagger h]_{aa}$. However, since the flavour-blind terms are universal, the differences between the dispersion relations for different i, j are nonetheless accurate to order $[h^\dagger h]_{aa}$.

Appendix A

Nonequilibrium Quantum Field Theory

A.1 Fermions

A.1.1 Definition of Greens functions

The basic objects of interest are the two-point Greens functions that we define as

$$i\Delta_{ij}(u,v) = \langle T_{\mathcal{C}}\phi_i(u)\phi_j^\dagger(v)\rangle\,, \tag{A.1}$$
$$iS_{ij,\alpha\beta}(u,v) = \langle T_{\mathcal{C}}\psi_{i,\alpha}(u)\bar{\psi}_{j,\beta}(v)\rangle\,, \tag{A.2}$$

for scalars and fermion fields respectively. Here $T_{\mathcal{C}}$ denotes time ordering along the closed time path $\mathcal{C}$. Splitting the contour into a positive and a negative branch and indicating by $a = \pm$ the branch on which the variable lies, we obtain four Greens functions:

$$iS^{++}_{ij,\alpha\beta}(u,v) \equiv iS^{t}_{ij,\alpha\beta}(u,v) = \langle T\psi_{i,\alpha}(u)\bar{\psi}_{j,\beta}(v)\rangle\,, \tag{A.3}$$
$$iS^{--}_{ij,\alpha\beta}(u,v) \equiv iS^{\bar{t}}_{ij,\alpha\beta}(u,v) = \langle \bar{T}\psi_{i,\alpha}(u)\bar{\psi}_{j,\beta}(v)\rangle\,, \tag{A.4}$$
$$iS^{+-}_{ij,\alpha\beta}(u,v) \equiv iS^{<}_{ij,\alpha\beta}(u,v) = -\langle \bar{\psi}_{j,\beta}(v)\psi_{i,\alpha}(u)\rangle\,, \tag{A.5}$$
$$iS^{-+}_{ij,\alpha\beta}(u,v) \equiv iS^{>}_{ij,\alpha\beta}(u,v) = \langle \psi_{i,\alpha}(u)\bar{\psi}_{j,\beta}(v)\rangle\,. \tag{A.6}$$

These four functions are not independent. In particular, we have that

$$S^t + S^{\bar{t}} = S^> + S^<\,. \tag{A.7}$$

It is further useful to define retarded and advanced Greens functions as follows:

$$S^r = S^t - S^< = S^> - S^{\bar{t}} \tag{A.8}$$
$$S^a = S^t - S^> = G^< - S^{\bar{t}} \tag{A.9}$$

where the last equalities follow from (A.7). From the above definitions it is easy to work out the following hermiticity properties of the Greens functions:

$$(i\gamma^0 S^{<,>}(u,v))^\dagger = i\gamma^0 S^{<,>}(v,u)\,, \tag{A.10}$$

$$(i\gamma^0 S^{t}(u,v))^\dagger = i\gamma^0 S^{\bar{t}}(v,u)\,. \tag{A.11}$$

We are mainly interested in situations where the environment changes slowly when compared to internal quantum fluctuations of the fields. To separate these two regimes we define the relative coordinate $r = u - v$ and the absolute coordinate $X = (u + v)/2$. We then perform a so called Wigner transformation, a Fourier transformation in r to obtain

$$S(k,X) = \int \frac{d^4 r}{(2\pi)^4} e^{-ikr} S(X + r/2, X - r/2)\,. \tag{A.12}$$

In Wigner space the hermiticity properties are particularly simple:

$$(i\gamma^0 S^{<,>}(k,X))^\dagger = i\gamma^0 S^{<,>}(k,X)\,, \tag{A.13}$$

$$(i\gamma^0 S^{t}(k,X))^\dagger = i\gamma^0 S^{\bar{t}}(k,X)\,. \tag{A.14}$$

We also define the hermitian and anti-hermitian parts of the retarded and advanced Greens functions as

$$S_h = \frac{1}{2}(S^r + S^a)\,, \tag{A.15}$$

$$S_a = \frac{i}{2}(S^r - S^a) = \frac{i}{2}(S^> - S^<) \equiv \mathcal{A}\,. \tag{A.16}$$

The latter expression is also called the spectral function. Due to the fermionic nature of the Greens functions the hermiticity properties read $S_h^\dagger = \gamma^0 S_h \gamma^0$ and similar for $\mathcal{A}$.

A.1.2 Fermion Equations of Motion

The Dyson-Schwinger equations for the massless fermion propagator is

$$(i\partial\!\!\!/_u) i S^{ab}(u,v) = a\delta_{ab} i\delta^4(u-v) + \sum_c \int d^4 w \Sigma^{ac}(u,w) i S^{cb}(w,v) \tag{A.17}$$

where the self energies are obtained from the 2PI effective action:

$$i\Sigma^{ab}(u,v) = ab \frac{\delta \Gamma_2}{\delta S^{ba}(v,u)}\,. \tag{A.18}$$

After a Wigner transformation in $(u-v)$ and a leading order gradient expansion one obtains for the spectral and statistical components:

$$\left(\not{k} - \frac{i}{2}\not{\partial} - \Sigma^{r,a}\right) S^{r,a} + \frac{i}{2}\left\{\Sigma^{r,a}, S^{r,a}\right\}_{pb} = 1\,, \tag{A.19}$$

$$\left(\not{k} + \frac{i}{2}\not{\partial} - \Sigma_h\right) S^{<,>} - \Sigma^{<,>} S_h = \frac{1}{2}\left(\Sigma^{>} S^{<} - \Sigma^{<} S^{>}\right). \tag{A.20}$$

A more coherent form of eqn. (A.19) in an expansion in gradients is

$$\left(\not{k} - \Sigma^{r,a}\right) S^{r,a} - \frac{i}{2}\left\{\not{k} - \Sigma^{r,a}, S^{r,a}\right\}_{pb} = 1\,. \tag{A.21}$$

This form allows for a straightforward solution up to second order in gradients, since $\{A, 1/A\}_{pb}$ is zero, i.e. first order gradient equation is solved by the zeroth order solution. Thus,

$$S^{r,a} = \frac{1}{\not{k} - \Sigma^{r,a}} \tag{A.22}$$

$$= \frac{1}{\Omega \pm i\Sigma_a} \tag{A.23}$$

where we defined $\Omega = \not{k} - \Sigma_h$ and $\Sigma_{h,a}$ are the hermitian and anti-hermitian components of the self-energies analogeous to (A.15,A.16). Now the spectral function is obtained by taking the imaginary part of (A.22). To this end, we first square the denominator to make it scalar, and then multiply with the complex conjugate to make it real. One obtains

$$S^{r,a} = \frac{(\Omega \pm i\Sigma_a)(\Omega^2 - \Sigma^2 \mp i\Gamma)}{(\Omega^2 - \Sigma^2)^2 + \Gamma^2}\,, \tag{A.24}$$

$$\mathcal{A} = \frac{\Omega\Gamma - \Sigma_a(\Omega^2 - \Sigma_a^2)}{(\Omega^2 - \Sigma^2)^2 + \Gamma^2}\,, \tag{A.25}$$

$$S_h = \frac{\Omega(\Omega^2 - \Sigma_a^2) + \Sigma_a\Gamma}{(\Omega^2 - \Sigma^2)^2 + \Gamma^2}\,, \tag{A.26}$$

and we define $\Gamma = \{\Omega, \Sigma_a\}$. For spatial homogeneous systems only the time derivative is nonzero. Adding to equation (A.20) its hermitian conjugate, we obtain

$$i\gamma^0\partial_0 S^{<,>} + \left[\Omega\gamma^0, \gamma^0 S^{<,>}\right] - \left[\Sigma^{<,>}\gamma^0, \gamma^0 S_h\right] = C + C^\dagger\,, \tag{A.27}$$

.In the single flavor case the oscillator term vanishes since $S^{<,>}$ is proportional to $\not{k}$ to leading order. The same reasoning also allows us to neglect the term involving S_h, and since $C^\dagger = C$ here we obtain

$$\frac{d}{dt} i\gamma^0 S^{<,>}(k) = \Sigma^{>}(k) S^{<}(k) - \Sigma^{<}(k) S^{>}(k)\,. \tag{A.28}$$

Since the theory is chirally invariant, this equation decomposes into separate equations for left and right handed modes.

A.1.3 Spin decomposition

The fermionic propagators can be decomposed into 16 components with definite transformation properties under the Lorentz group using the known Dirac bilinear forms:

$$iS = s_S + \gamma_5 s_P + \gamma_\mu s_V^\mu + \gamma_\mu\gamma_5 s_A^\mu + \frac{1}{2}\sigma_{\mu\nu} s_T^{\mu\nu} \tag{A.29}$$

where $\sigma_{\mu\nu} = [\gamma_\mu, \gamma_\nu]$ and the 16 components are independent complex two point functions. Symmetries can be used to reduce the number of independent functions. Our problem features spatial homogeneity and chiral symmetry. The latter implies that the scalar, pseudo-scalar and all tensorial components vanish since they do not anticommute with γ_5. Spatial homogeneity on the other hand implies that the vector and pseudo-vector functions can be decomposed as

$$\gamma_\mu s_V^\mu = \gamma_0 s_V^0 - \vec{\gamma}\hat{k} s_V \tag{A.30}$$

with $\hat{k} = \vec{k}/k$ and similarly for the axial-vector components. This reduces the problem to four independent propagators.

It turns out to be more convenient to decompose the vector and axial vector components into helicity eigenstates. In the Dirac basis the helicity operator is given by

$$\Lambda(\vec{k}) = \gamma_5\gamma_0(\vec{\gamma}\cdot\hat{\vec{k}})\,. \tag{A.31}$$

Using that $\Lambda(1 \pm \Lambda) = \pm(1 \pm \Lambda)$ and multiplying by γ^0 we can thus write

$$i\gamma^0 S_\ell^{<,>} = \frac{1}{2}\sum_{h=\pm}\left[g_{h0}^{<,>}(\mathbb{1} + h\hat{\vec{k}}\cdot\gamma_5\gamma_0\vec{\gamma}) + g_{h3}^{<,>}(\gamma_5 + h\hat{\vec{k}}\cdot\gamma_0\vec{\gamma})\right] \tag{A.32}$$

$$= \frac{1}{2}\sum_{h=\pm}\left[g_{h0}^{<,>}P_h + g_{h3}^{<,>}\gamma_5 P_h\right], \tag{A.33}$$

where $P_h = 1/2(1 + h\Lambda)$ is the projector on positive and negative helicities. The coefficient functions g_{h0}, g_{h3} are linear combinations of the $s_{V(A)}^{(0)}$ that mix the vector and axial components. Since the chiral projectors $P_{L,R}$ commute with P_h we can also go to a chiral helicity basis where

$$i\gamma^0 S_\ell^{<,>} = \frac{1}{2}\sum_{h=\pm}\left[g_{h,L}P_h P_L + g_{h,R}P_h P_R\right], \tag{A.34}$$

with $g_{hL,R} = g_{h0} \pm g_{h3}$.

A.1.4 (Free) Fermionic Equilibrium Solutions

Without interactions or external forces, the Green's Functions satisfy the free Dirac equation

$$(i\partial\!\!\!/_u - m)iS^{t,\bar{t}}(u,v) = \pm i\delta^4(u-v) \tag{A.35}$$
$$(i\partial\!\!\!/_u - m)iS^{<,>}(u,v) = 0\,. \tag{A.36}$$

In equilibrium S only depends on the relative coordinate $u-v$. Performing a Fourier transformation with respect to that coordinate we obtain

$$(k\!\!\!/ - m)iS^{t,\bar{t}}(k) = i \tag{A.37}$$
$$(k\!\!\!/ - m)iS^{<,>}(k) = 0\,. \tag{A.38}$$

Furthermore in equilibrium the KMS condition

$$iS^{>}(k) = -e^{\beta k_0} iS^{<}(k) \tag{A.39}$$

is satisfied. The Dirac equation is solved by an ansatz of the form

$$iS^{<}(k) = 2\pi(k\!\!\!/ + m)G^{<}(k) = 2\pi(k\!\!\!/ + m)\delta(k^2 - m^2)F^{<}(\vec{k})\,, \tag{A.40}$$

where $F^{<}$ is a yet to be determined scalar functions. The KMS kondition then implies that

$$iS^{>}(k) = 2\pi(k\!\!\!/ + m)G^{<}(k) = 2\pi(k\!\!\!/ + m)\delta(k^2 - m^2)(-e^{\beta k_0}F^{<}(\vec{k}))\,, \tag{A.41}$$

where $k_0 = \sqrt{\vec{k}^2 + m^2}$. This can be re-written in a more standard form by defining

$$f(\vec{k}) = \frac{1}{e^{\beta k_0} + 1} \tag{A.42}$$

and setting $F^{<}(\vec{k}) = -f(\vec{k})$. Observing that

$$\frac{e^{\beta k_0}}{e^{\beta k_0}+1} = \frac{e^{\beta k_0}+1-1}{e^{\beta k_0}+1} = 1 - f(\vec{k}) \tag{A.43}$$

we finally arrive at the known results for the fermionic equilibrium Green's functions:

$$iS^{<}(k) = -2\pi(k\!\!\!/ + m)\delta(k^2 - m^2)f(\vec{k})\,, \tag{A.44}$$
$$iS^{>}(k) = 2\pi(k\!\!\!/ + m)\delta(k^2 - m^2)(1 - f(\vec{k}))\,. \tag{A.45}$$

Out of equilibrium we need to be able to distinguish between particle and anti-particle degrees of freedom. This is discussed in the next section.

A.1.5 Close to Equilibrium Forms

Using the quasi-particle approximation, the spectral function has the solution

$$A(k) = \frac{1}{2}(iS^{>}(k,t) - iS^{<}(k,t)) = \pi(\not{k} + m)\mathrm{sign}(k_0)\delta(k^2 - m^2)\,, \tag{A.46}$$

where we neglect possible finite width effects. The normalization is fixed by the spectral sum rule

$$\int_{-\infty}^{\infty} \frac{dk^0}{\pi}\gamma^0 A(k) = \mathbf{1}\,. \tag{A.47}$$

We now define particle and anti-particle distribution functions as

$$2\theta(k^0)A(k,t)f(k,t) := -\theta(k^0)iS^{<}(k,t)\,, \tag{A.48}$$
$$2\theta(-k^0)A(k,t)\bar{f}(k,t) := \theta(-k^0)iS^{>}(k,t)\,, \tag{A.49}$$

and immediately obtain, using $A = 1/2(iS^{>} - iS^{<})$,

$$iS^{<}(k,t) = 2A(k,t)\left(-\theta(k^0)(f(k,t)) - \theta(-k^0)(1-\bar{f}(k,t))\right), \tag{A.50}$$
$$iS^{>}(k,t) = 2A(k,t)\left(\theta(k^0)(1-f(k,t)) + \theta(-k^0)\bar{f}(k,t)\right). \tag{A.51}$$

Using (A.46) this can be rewritten as

$$iS^{<}(k) = -2\pi(\not{k} + m)\delta(k^2 - m^2)\left(\theta(k^0)(f(k)) - \theta(-k^0)(1-\bar{f}(k))\right), \tag{A.52}$$
$$iS^{>}(k) = -2\pi(\not{k} + m)\delta(k^2 - m^2)\left(-\theta(k^0)(1-f(k)) + \theta(-k^0)\bar{f}(k)\right). \tag{A.53}$$

The explicit time dependence in S and $f, \bar{f}$ has been suppressed. It is also understood that in this approximation, $k_0 = \sqrt{\vec{k}^2 + m^2}$ and therefore the distribution functions depend only on the spatial momenta, i.e. $f(k) = f(\vec{k})$.

A.2 Boltzmann Equations in an Expanding Universe

This appendix contains some supplementary material on the structure of the Boltzmann equations and their numerical implementation.

A.2.1 Physical Quantities in Conformal Coordinates

Starting from a flat expanding (FRW) universe with a scale factor $a(t)$ we introduce conformal time through $d\eta = dt/a(t)$. In this coordinate system the FRW metric simplifies to

$$ds^2 = a^2(\eta)\left(d\eta^2 - dx_i^2\right), \tag{A.54}$$

which shows that the flat FRW model is conformal to Minkowski. It follows that results derived in quantum field theory in flat space can easily be transferred to an expanding spacetime using a simple set of transformation rules, namely by replacing

$$\mathbf{k} \longrightarrow \mathbf{k}_{com}\,, \tag{A.55}$$

$$T \longrightarrow T_{com}\,, \tag{A.56}$$

$$t \longrightarrow \eta\,, \tag{A.57}$$

$$M \longrightarrow a(\eta)M\,. \tag{A.58}$$

Furthermore $f(\mathbf{k}_{com})$ and n are to be understood as comoving phase-space densities and number densities respectively.

In a radiation dominated Universe we can further use

$$a(\eta) = a_R\eta\,, \tag{A.59}$$

and

$$T = \frac{T_{com}}{a(\eta)} = \frac{1}{a(\eta)}\sqrt{\frac{a_R M_{pl}}{2}}\left(\frac{45}{g_*\pi^3}\right)^{1/4} \tag{A.60}$$

where $M_{pl} = 1.22 \cdot 10^{19}$GeV is the Planck mass and $g_* = 106.75$ is the number of relativistic degrees of freedom. Note in particular that the comoving temperature is a constant. We further introduce the variable $z = M_1/T$ that is proportional to η, and

$$z = \frac{M_1 a_R}{T_{com}}\eta\,, \qquad \eta = \frac{T_{com}}{M_1 a_R}z\,. \tag{A.61}$$

For numerical purposes the unknown a_R can be fixed as follows: We require that at $z = 1$ the equilibrium distribution of a particle of mass M_1 agrees with the distribution at $T = M_1$. This is achieved by requiring $T_{com} = M_1$ which fixes a_R as

$$a_R = \sqrt{\frac{4g_*\pi^3}{45}}\frac{M_1^2}{M_{pl}} = 17.15\frac{M_1^2}{M_{pl}}\,. \tag{A.62}$$

We further get the following simple relations:

$$\eta = \frac{1}{a_R}z\,, \qquad a(z) = z\,, \qquad T_{com} = M_1\,, \tag{A.63}$$

$$\frac{d}{d\eta} = a_R\frac{d}{dz}\,, \qquad \frac{d}{dz} = \frac{1}{a_R}\frac{d}{d\eta}\,. \tag{A.64}$$

For the washout term we obtain

$$\frac{d\Delta n_\ell}{dz} = \frac{1}{a_R}W = \frac{1}{17.15}\frac{M_{pl}}{M_1}z^2 \cdot F(z)\Delta n_\ell \tag{A.65}$$

where $F(z)$ is a scalar (i.e. dimensionless) function of z.

This procedure allows us to write down the Boltzmann equations without explicit reference to the Hubble rate H. The whole expansion of the universe is encoded in the variable z. As an example, with the above choices, the equilibrium distribution for the righthanded neutrino takes the simple form

$$f_N^{\rm eq}(\mathbf{k}, z) = \frac{1}{e^{\sqrt{\mathbf{k}^2+z^2}}+1}\,. \tag{A.66}$$

This approach is equivalent to writing down the ordinary equations and then to introduce entropy normalized quantities to absorb the expansion term in the Boltzmann equation.

In general higher order corrections arise from the transformation of the equations of motion to conformal coordinates. These corrections are suppressed by powers of (T/M_{pl}) and are therefore negligible for most leptogenesis scenarios where $T \sim M_1 \ll M_{pl}$.

A.2.2 Solving the flavored evolution equations

In this section, I provide some details on the solution of the Boltzmann equations in the flavored Leptogenesis scenario. The evolution equations are given by

$$\frac{\partial n_{\ell ab}}{\partial \eta} = \sum_c \left[n_{\ell ac}\Xi_{cb} - \Xi_{ac} n_{\ell cb} + W_{ac} n_{\ell cb} + n^\dagger_{\ell ac} W^\dagger_{cb} \right] + 2S_{ab} + \Gamma^{\rm fl}_{\ell ab}\,, \tag{A.67}$$

where

$$n_\ell = \begin{pmatrix} n_{\ell 11} & n_{\ell 12} \\ n^*_{\ell 12} & n_{\ell 22} \end{pmatrix}. \tag{A.68}$$

For a numerical implementation it is useful to work with purely real quantities. Therefore we define $n_{\ell 12} = n_r + \mathrm{i} n_i$, and rewrite our system as a differential equation for the vector $n_\ell = (n_{11}, n_{22}, n_r, n_i)$, where we also dropped the subscript ℓ. An advantage of this decomposition is that the source term is purely real in this basis, so we avoid dealing with complex quantities in the numerical implementation.

Using this decomposition, the washout term can be rewritten as

$$Wn + n^\dagger W^\dagger = \begin{pmatrix} 2W_{11} & 0 & 2W_r & 2W_i \\ 0 & 2W_{22} & 2W_r & 2W_i \\ W_r & W_r & W_{11}+W_{22} & 0 \\ W_i & W_i & 0 & W_{11}+W_{22} \end{pmatrix} \begin{pmatrix} n_{11} \\ n_{22} \\ n_r \\ n_i \end{pmatrix} \tag{A.69}$$

where W_r and W_i denote the real and imaginary parts of W_{12}.

An ansatz for the Ξ matrix in the basis where the charged lepton Yukawas are diagonal is obtained as follows. After factoring out the overall z dependence, the thermal mass matrix for the leptons is given by

$$\varsigma^{\rm fl} = \begin{pmatrix} h_\tau^2 & 0 \\ 0 & 0 \end{pmatrix} + f(z) \begin{pmatrix} |Y_{11}|^2 + Y_{11}^* Y_{12} \\ Y_{11} Y_{12}^* + |Y_{12}|^2 \end{pmatrix} \tag{A.70}$$

where $f(z) = f_0$ for $z \to 0$ and $f(z) = 0$ for $z \gg 1$. Here f_0 is a factor of $1/2$ that accounts for the fact that the righthanded neutrinos are of Majorana type. Introducing $h = h_\tau^2$, $f_1 = f|Y_{11}|^2$ and $f_2 = f|Y_{12}|^2$ the characteristic polynomial for $\varsigma^{\rm fl}$ is

$$(h + f_1 - \lambda)(f_2 - \lambda - f_1 f_2) = 0 \tag{A.71}$$

with eigenvalues

$$2\lambda_{1,2} = h + f_1 + f_2 \pm \sqrt{(h + f_1 + f_2)^2 - 4h f_2}\,. \tag{A.72}$$

The corresponding eigenvectors can then be used to construct the rotation matrix $U(z)$ to obtain expressions for $\Xi(z)$.

Here we discuss the special case where $Y_{11}, Y_{12} \in \mathbb{R}$. Then the rotation matrix can be parametrized as $U(z) = \exp(\mathrm{i}\sigma_2 g(z))$ with an unknown function $g(z)$ that can be determined from $U\varsigma^{\rm fl}U^\dagger = \varsigma_{\rm diag}$. We obtain

$$\tan(2q(z)) = \frac{2Y_{11}Y_{12}f(z)}{h_\tau^2 + f(z)(Y_{11}^2 - Y_{12}^2)} \equiv g(z)\,, \tag{A.73}$$

and $\Xi = i\sigma_2 q'(z)$ with

$$q'(z) = \frac{1}{2}\frac{1}{1 + g(z)^2} g'(z)\,. \tag{A.74}$$

Once $f(z)$ is specified this can be used to implement the dynamical diagonalization of the mass basis as the universe cools down below $T \sim M_1$.

Bibliography

[1] A. Freitas, P. Schwaller and D. Wyler, JHEP **0809**, 013 (2008).

[2] A. Freitas, P. Schwaller and D. Wyler, JHEP **0912**, 027 (2009).

[3] M. Beneke, B. Garbrecht, M. Herranen and P. Schwaller, Nucl. Phys. B **838** (2010) 1.

[4] A. Freitas, P. Schwaller, JHEP **1101** (2011) 022.

[5] M. Beneke, B. Garbrecht, C. Fidler, M. Herranen, P. Schwaller, Nucl. Phys. **B843** (2011) 177-212.

[6] S. L. Glashow, Nucl. Phys. **22** (1961) 579, S. Weinberg, Phys. Rev. Lett. **19** (1967) 1264,
A. Salam, *In the Proceedings of 8th Nobel Symposium, Lerum, Sweden, 19-25 May 1968, pp 367-377.*

[7] F. J. Hasert *et al.* [Gargamelle Neutrino Collaboration], Phys. Lett. B **46** (1973) 138.

[8] G. Arnison *et al.* [UA1 Collaboration], Phys. Lett. B **122** (1983) 103,
M. Banner *et al.* [UA2 Collaboration], Phys. Lett. B **122** (1983) 476.

[9] G. Arnison *et al.* [UA1 Collaboration], Phys. Lett. B **126** (1983) 398,
P. Bagnaia *et al.* [UA2 Collaboration], Phys. Lett. B **129** (1983) 130.

[10] R. Barbieri, A. Pomarol, R. Rattazzi and A. Strumia, Nucl. Phys. B **703** (2004) 127.

[11] P. W. Higgs, Phys. Rev. Lett. **13** (1964) 508,
F. Englert and R. Brout, Phys. Rev. Lett. **13** (1964) 321,
G. S. Guralnik, C. R. Hagen and T. W. B. Kibble, Phys. Rev. Lett. **13**, 585 (1964).

[12] E. C. G. Stueckelberg, Helv. Phys. Acta **11** (1938) 225.

[13] F. Abe *et al.* [CDF Collaboration], Phys. Rev. Lett. **74** (1995) 2626,
S. Abachi *et al.* [D0 Collaboration], Phys. Rev. Lett. **74** (1995) 2632.

[14] A. Denner, Fortsch. Phys. **41** (1993) 307.

[15] A. Strumia and F. Vissani, arXiv:hep-ph/0606054.

[16] A. D. Sakharov, Pisma Zh. Eksp. Teor. Fiz. **5** (1967) 32 [JETP Lett. **5** (1967 SOPUA,34,392-393.1991 UFNAA,161,61-64.1991) 24].

[17] G. Bertone, D. Hooper and J. Silk, Phys. Rept. **405** (2005) 279 [arXiv:hep-ph/0404175].

[18] N. Arkani-Hamed, A. G. Cohen and H. Georgi, Phys. Lett. B **513** (2001) 232.

[19] M. Schmaltz and D. Tucker-Smith, Ann. Rev. Nucl. Part. Sci. **55** (2005) 229.

[20] T. Yangida, in Proceedings of the *"Workshop on the Unified Theory and the Baryon Number in the Universe"*, Tsukuba, Japan, Feb. 13-14, 1979, edited by O. Sawada and A. Sugamoto, KEK report KEK-79-18, p. 95, and *"Horizontal Symmetry And Masses Of Neutrinos"* , Prog. Theor. Phys. **64** (1980) 1103; M. Gell-Mann, P. Ramond and R. Slansky, in *"Supergravity"* (North-Holland, Amsterdam, 1979) *eds.* D. Z. Freedom and P. van Nieuwenhuizen, Print-80-0576 (CERN); see also P. Minkowski, Phys. Lett. B **67**, 421 (1977).

[21] W. Buchmuller and D. Wyler, Phys. Lett. B **521** (2001) 291.

[22] C. Kilic, T. Okui and R. Sundrum, JHEP **1002** (2010) 018 [arXiv:0906.0577 [hep-ph]].

[23] C. Kilic and T. Okui, arXiv:1001.4526 [hep-ph].

[24] Y. Bai and A. Martin, arXiv:1003.3006 [hep-ph].

[25] Y. Bai and R. J. Hill, arXiv:1005.0008 [hep-ph].

[26] M. Cirelli, N. Fornengo and A. Strumia, Nucl. Phys. B **753** (2006) 178.

[27] N. Arkani-Hamed, A. G. Cohen, E. Katz and A. E. Nelson, JHEP **0207**, 034 (2002).

[28] C. Csaki, J. Hubisz, G. D. Kribs, P. Meade and J. Terning, Phys. Rev. D **67**, 115002 (2003);
J. L. Hewett, F. J. Petriello and T. G. Rizzo, JHEP **0310**, 062 (2003);
C. Csaki, J. Hubisz, G. D. Kribs, P. Meade and J. Terning, Phys. Rev. D **68**, 035009 (2003);
W. Kilian and J. Reuter, Phys. Rev. D **70**, 015004 (2004).

[29] J. Wudka, hep-ph/0307339.

[30] H. C. Cheng and I. Low, JHEP **0408**, 061 (2004).

[31] C. T. Hill and R. J. Hill, Phys. Rev. D **75**, 115009 (2007).

[32] C. T. Hill and R. J. Hill, Phys. Rev. D **76**, 115014 (2007).

[33] J. Wess and B. Zumino, Phys. Lett. B **37**, 95 (1971);
E. Witten, Nucl. Phys. B **223**, 422 (1983).

[34] D. Krohn and I. Yavin, JHEP **0806**, 092 (2008).

[35] C. Csaki, J. Heinonen, M. Perelstein and C. Spethmann, arXiv:0804.0622 [hep-ph].

[36] V. Barger, W. Y. Keung and Y. Gao, Phys. Lett. B **655**, 228 (2007).

[37] J. Hubisz and P. Meade, Phys. Rev. D **71**, 035016 (2005).

[38] M. Blanke, A. J. Buras, A. Poschenrieder, S. Recksiegel, C. Tarantino, S. Uhlig and A. Weiler, JHEP **0701**, 066 (2007).

[39] I. Low, JHEP **0410**, 067 (2004).

[40] E. Katz, J. y. Lee, A. E. Nelson and D. G. E. Walker, JHEP **0510** (2005) 088.

[41] A. Pukhov, arXiv:hep-ph/0412191.

[42] A CalcHEP model file for the Littlest Higgs model with broken T-parity `http://www.itp.uzh.ch/~pedro/lht/`.

[43] A. Denner, G. Weiglein and S. Dittmaier, Phys. Lett. B **333** (1994) 420.

[44] R. S. Hundi, B. Mukhopadhyaya and A. Nyffeler, Phys. Lett. B **649**, 280 (2007)

[45] M. S. Carena, J. Hubisz, M. Perelstein and P. Verdier, Phys. Rev. D **75** (2007) 091701.

[46] Vista/Sleuth Global Search for New Physics in 2.0 fb-1 of p-pbar Collisions at sqrt(s)=1.96 TeV,
`http://www-cdf.fnal.gov/physics/exotic/r2a/20080228.vista_sleuth/publicPage.html`

[47] A. Freitas and D. Wyler, JHEP **0611** (2006) 061

[48] A. Belyaev, C. R. Chen, K. Tobe and C. P. Yuan, Phys. Rev. D **74** (2006) 115020

[49] J. Hubisz, S. J. Lee and G. Paz, JHEP **0606**, 041 (2006).

[50] C. R. Chen, K. Tobe and C. P. Yuan, Phys. Lett. B **640** (2006) 263

[51] J. Gasser and H. Leutwyler, Nucl. Phys. B **250**, 517 (1985).

[52] J. F. Donoghue and D. Wyler, Nucl. Phys. B **316**, 289 (1989).

[53] M. J. Savage, M. E. Luke and M. B. Wise, Phys. Lett. B **291** (1992) 481

[54] T. Han, H. E. Logan, B. McElrath and L. T. Wang, Phys. Rev. D **67**, 095004 (2003).

[55] W. Y. Keung, I. Low and J. Shu, arXiv:0806.2864 [hep-ph].

[56] A. Denner, Fortsch. Phys. **41** (1993) 307

[57] N. Arkani-Hamed, A. G. Cohen, E. Katz, A. E. Nelson, T. Gregoire and J. G. Wacker, JHEP **0208**, 021 (2002).

[58] C. Kilic and R. Mahbubani, JHEP **0407**, 013 (2004).

[59] H. C. Cheng and I. Low, JHEP **0309**, 051 (2003).

[60] N. Arkani-Hamed, A. G. Cohen, T. Gregoire and J. G. Wacker, JHEP **0208**, 020 (2002).

[61] S. Chang and J. G. Wacker, Phys. Rev. D **69**, 035002 (2004);
A. Birkedal-Hansen and J. G. Wacker, Phys. Rev. D **69**, 065022 (2004).

[62] C. Csaki, J. Heinonen, M. Perelstein and C. Spethmann, arXiv:0804.0622 [hep-ph].

[63] J. Wess and B. Zumino, Phys. Lett. B **37**, 95 (1971);
E. Witten, Nucl. Phys. B **223**, 422 (1983);
O. Kaymakcalan, S. Rajeev and J. Schechter, Phys. Rev. D **30**, 594 (1984).

[64] C. T. Hill and R. J. Hill, Phys. Rev. D **75**, 115009 (2007);
C. T. Hill and R. J. Hill, Phys. Rev. D **76**, 115014 (2007).

[65] V. Barger, W. Y. Keung and Y. Gao, Phys. Lett. B **655**, 228 (2007);
A. Freitas, P. Schwaller and D. Wyler, JHEP **0809**, 013 (2008).

[66] I. Low, JHEP **0410**, 067 (2004).

[67] H. C. Cheng, I. Low and L. T. Wang, Phys. Rev. D **74**, 055001 (2006).

[68] S. R. Coleman, J. Wess and B. Zumino, Phys. Rev. **177**, 2239 (1969);
C. G. Callan, S. R. Coleman, J. Wess and B. Zumino, Phys. Rev. **177**, 2247 (1969).

[69] J. Hubisz, P. Meade, A. Noble and M. Perelstein, JHEP **0601**, 135 (2006).

[70] M. E. Peskin and T. Takeuchi, Phys. Rev. D **46** 381, (1992).

[71] L. Lavoura and J. P. Silva, Phys. Rev. D **47** 2046, (1993).

[72] J. F. Gunion, H. E. Haber, G. L. Kane and S. Dawson, *The Higgs Hunter's Guide*, (Basic Books, New York, 1990).

[73] C. Amsler *et al.* [Particle Data Group], Phys. Lett. B **667** (2008) 1.

[74] E. Boos *et al.* [CompHEP Collaboration], Nucl. Instrum. Meth. A **534**, 250 (2004).

[75] A. Semenov, Comput. Phys. Commun. **180**, 431 (2009).

[76] J. Hubisz and P. Meade, Phys. Rev. D **71**, 035016 (2005);
A. Freitas and D. Wyler, JHEP **0611**, 061 (2006);
A. Belyaev, C. R. Chen, K. Tobe and C. P. Yuan, Phys. Rev. D **74**, 115020 (2006);
M. S. Carena, J. Hubisz, M. Perelstein and P. Verdier, Phys. Rev. D **75**, 091701 (2007);
D. Choudhury and D. K. Ghosh, JHEP **0708**, 084 (2007).

[77] J. M. Campbell *et al.*, contributed to the *3rd Les Houches Workshop: Physics at TeV Colliders, Les Houches, France, 26 May – 6 Jun 2003* [arXiv:hep-ph/0405302];
W. K. Tung, in *Proceedings of the Workshop on Physics Simulations at High Energy, Madison, Wisconsin, 1986*, ed. V. Barger *et al.* (World Scientific, Singapore, 1986), pp. 601–613.

[78] T. Han, R. Mahbubani, D. G. E. Walker and L. T. E. Wang, JHEP **0905**, 117 (2009).

[79] C. R. Chen, K. Tobe and C. P. Yuan, Phys. Lett. B **640**, 263 (2006).

[80] T. Sjostrand, S. Mrenna and P. Z. Skands, JHEP **0605** (2006) 026 [arXiv:hep-ph/0603175].

[81] J. Conway et. al., http://www.physics.ucdavis.edu/ conway/research/software/pgs/pgs4-general.htm.

[82] The Dzero Collaboration, Dzero Note 5067-CONF.

[83] V. M. Abazov *et al.* [The D0 Collaboration], arXiv:1004.1826 [hep-ex].

[84] The CDF Collaboration, public note, http://www-cdf.fnal.gov/physics/exotic/r2a/20100513.graviton.diphoton/index.html.

[85] J. Alwall *et al.*, JHEP **0709** (2007) 028.

[86] M. Pieri, K. Armour and J. G. Branson, CERN-CMS-NOTE-2006-007.

[87] F. Derue, ATL-COM-PHYS-2005-046.

[88] D. Atwood and S. K. Gupta, arXiv:1006.4370 [hep-ph].

[89] Y. Gao, A. V. Gritsan, Z. Guo, K. Melnikov, M. Schulze and N. V. Tran, Phys. Rev. D **81** (2010) 075022 [arXiv:1001.3396 [hep-ph]].

[90] A. De Rujula, J. Lykken, M. Pierini, C. Rogan and M. Spiropulu, arXiv:1001.5300 [hep-ph].

[91] M. Fukugita and T. Yanagida, Phys. Lett. B **174** (1986) 45.

[92] S. Davidson, E. Nardi and Y. Nir, Phys. Rept. **466** (2008) 105.

[93] D. V. Nanopoulos and S. Weinberg, Phys. Rev. D **20** (1979) 2484.

[94] E. W. Kolb and S. Wolfram, Nucl. Phys. B **172** (1980) 224 [Erratum-ibid. B **195** (1982) 542].

[95] A. D. Sakharov, Pisma Zh. Eksp. Teor. Fiz. **5** (1967) 32 [JETP Lett. **5** (1967 SOPUA,34,392-393.1991 UFNAA,161,61-64.1991) 24].

[96] J. S. Schwinger, J. Math. Phys. **2** (1961) 407.

[97] L. V. Keldysh, Zh. Eksp. Teor. Fiz. **47** (1964) 1515 [Sov. Phys. JETP **20** (1965) 1018].

[98] P. M. Bakshi and K. T. Mahanthappa, J. Math. Phys. **4** (1963) 1.

[99] E. Calzetta and B. L. Hu, Phys. Rev. D **37** (1988) 2878.

[100] W. Buchmüller and S. Fredenhagen, Phys. Lett. B **483** (2000) 217.

[101] A. De Simone and A. Riotto, JCAP **0708** (2007) 002.

[102] A. Anisimov, W. Buchmüller, M. Drewes and S. Mendizabal, arXiv:1001.3856 [hep-ph].

[103] M. Garny, A. Hohenegger, A. Kartavtsev and M. Lindner, Phys. Rev. D **80** (2009) 125027.

[104] M. Garny, A. Hohenegger, A. Kartavtsev and M. Lindner, arXiv:0911.4122 [hep-ph].

[105] L. Covi, N. Rius, E. Roulet and F. Vissani, Phys. Rev. D **57** (1998) 93.

[106] G. F. Giudice, A. Notari, M. Raidal, A. Riotto and A. Strumia, Nucl. Phys. B **685** (2004) 89.

[107] A. Basboll and S. Hannestad, JCAP **0701** (2007) 003.

[108] F. Hahn-Woernle, M. Plümacher and Y. Y. Y. Wong, JCAP **0908** (2009) 028.

[109] T. Prokopec, M. G. Schmidt and S. Weinstock, Annals Phys. **314** (2004) 208.

[110] T. Prokopec, M. G. Schmidt and S. Weinstock, Annals Phys. **314** (2004) 267.

[111] B. Garbrecht and T. Konstandin, Phys. Rev. D **79** (2009) 085003.

[112] A. Pilaftsis, Phys. Rev. D **56** (1997) 5431.

[113] W. Buchmüller, P. Di Bari and M. Plümacher, Annals Phys. **315** (2005) 305.

[114] T. Endoh, T. Morozumi and Z. h. Xiong, Prog. Theor. Phys. **111** (2004) 123.

[115] A. Pilaftsis and T. E. J. Underwood, Phys. Rev. D **72** (2005) 113001.

[116] JCAP **0604**, 004 (2006).

[117] E. Nardi, Y. Nir, E. Roulet and J. Racker, JHEP **0601**, 164 (2006).

[118] M. Flanz, E. A. Paschos and U. Sarkar, Phys. Lett. B **345** (1995) 248 [Erratum-ibid. B **382** (1996) 447].

[119] A. Pilaftsis and T. E. J. Underwood, Nucl. Phys. B **692** (2004) 303.

[120] V. Cirigliano, C. Lee, M. J. Ramsey-Musolf and S. Tulin, arXiv:0912.3523 [hep-ph].

[121] M. Garny, A. Hohenegger and A. Kartavtsev, arXiv:1002.0331 [hep-ph].

[122] A. Denner, H. Eck, O. Hahn and J. Kublbeck, Phys. Lett. B **291** (1992) 278.

[123] A. De Simone and A. Riotto, JCAP **0702** (2007) 005.

[124] P. B. Arnold, G. D. Moore and L. G. Yaffe, JHEP **0011** (2000) 001.

[125] T. Konstandin, T. Prokopec and M. G. Schmidt, Nucl. Phys. B **716**, 373 (2005).

[126] T. Konstandin, T. Prokopec, M. G. Schmidt and M. Seco, Nucl. Phys. B **738** (2006) 1.

[127] M. Joyce, T. Prokopec and N. Turok, Phys. Rev. D **53** (1996) 2930.

[128] S. Blanchet, P. Di Bari and G. G. Raffelt, JCAP **0703** (2007) 012.

[129] W. Buchmüller and M. Plümacher, Phys. Lett. B **511** (2001) 74.

[130] E. Nardi, Y. Nir, J. Racker and E. Roulet, JHEP **0601**, 068 (2006).

[131] M. Le Bellac, *Thermal Field Theory*, Cambridge University Press 1996.

[132] U. Kraemmer and A. Rebhan, Rept. Prog. Phys. **67** (2004) 351.

[133] H. A. Weldon, "Effective Fermion Masses Of Order Gt In High Temperature Gauge Theories With Exact Chiral Invariance," Phys. Rev. D **26** (1982) 2789.